MAY 2021

Ph.D. in Civil Engineering

NECİP ALTAY EREN

REPUBLIC OF TURKEY

GAZİANTEP UNIVERSITY

GRADUATE SCHOOL OF NATURAL & APPLIED SCIENCES

BEHAVIOR OF GEOPOLYMER CONCRETE UNDER IMPACT

Ph.D. THESIS

IN

CIVIL ENGINEERING

BY

NECİP ALTAY EREN

MAY 2021

BEHAVIOR OF GEOPOLYMER CONCRETE UNDER IMPACT

Ph.D. Thesis

in

Civil Engineering

Gaziantep University

Supervisor

Prof. Dr. Abdülkadir ÇEVİK

Co-Supervisor

Asst. Prof. Dr. Anıl NİŞ

by

Necip Altay EREN

May 2021

©2021[Necip Altay EREN]

I hereby declare that all information in this document has been obtained and presented in accordance with academic rules and ethical conduct. I also declare that, as required by these rules and conduct, I have fully cited and referenced all material and results that are not original to this work.

Necip Altay EREN

ABSTRACT

BEHAVIOR OF GEOPOLYMER CONCRETE UNDER IMPACT

EREN, Necip Altay
Ph.D. in Civil Engineering
Supervisor: Prof. Dr. Abdülkadir ÇEVİK
Co-Supervisor: Asst. Prof. Dr. Anıl NİŞ
May 2021
224 pages

This study investigates the properties of self-compacted geopolymer concrete (SCGC) obtained by ground granulated blast furnace slag (GGBFS) as binder in both the fresh and hardened states under the combined addiction of nano-silica (NS), steel fibers (SFs) and recycled tyre rubbers (RTR). While eighteen different mixtures were used in the experimental study, a total of thirty-six beam specimens were produced for the study. Those eighteen mixtures of SCGC contained different percentages of NS (0% and 2%) and different percentages of SFs (0%, 0.5% and 1%) and different percentages of RTR (0%, 10% and 15%). 100% GGBFS with a fixed alkaline activator-to-binder ratio of 0.5 was used as a binder to prepare the SCGC mixes. A blend of sodium-silicate (Na_2SiO_3) solution and sodium hydroxide (NaOH) solutions with a ratio of 2.5 has been chosen as an alkaline activator. The fresh and hardened states concrete tests including slump, flow ability, workability and compressive, impact and flexural strengths were realized in the study. Experimental results were examined in detail to determine the influence of important factors on mechanical performance of SCGC. Furthermore, correlations among the empirical data were evaluated to explore the relations between the hardened and fresh states properties of SCGC. Experimental results showed that the combined use of NS and SFs affected the fresh state properties adversely, while it improved the impact and flexural properties of the SCGC samples considerably. Moreover, the influence of NS was predominant regarding the fresh state performance and compressive strength, while the effect of SFs were superior regarding flexural and impact strength. Moreover, incorporating of RTR influenced the fresh state properties reversely, while the effect of SFs with RTR was superior regarding flexural and impact strength.

Keywords: Self-Compacting Geopolymer Concrete (SCGC), Fresh State Properties of Geopolymer Concrete, Nano-Silica, Recycled Tyre Rubber, Steel Fiber, Impact Strength and Flexural Strength.

ÖZET

GEOPOLİMER BETONUN ÇARPMA DAVRANIŞI

EREN, Necip Altay
Doktora Tezi, İnşaat Mühendisliği
Danışman: Prof. Dr. Abdülkadir ÇEVİK
İkinci Danışman: Dr. Öğr. Üyesi Anıl NİŞ
Mayıs 2021
224 sayfa

Bu çalışma çelik fiber, nano silika ve lastik kauçuk fiberin kombine ya da ayrı ayrı kullanılarak hem taze hem de sertleştirilmiş halde kendiliğinden yerleşen geopolimer betonların (KYGB) özelliklerini araştırmıştır. Çalışmada farklı oranlarda nano-silika (%0 ve %2), çelik fiberler (%0, %0.5 ve %1) ve lastik kauçuk fiberler (%0, %10 ve %15) içeren on sekiz adet farklı karışım ve toplamda otuz altı adet KYGB'lar üretilmiştir. KYGB'ların üretimi sırasında %100 öğütülmüş granüle yüksek fırın cürufu ve 0.5 oranında sabit alkali aktivatör bağlayıcı ile kullanılmıştır. Ayrıca, alkali aktivatör karışımı olarak sodyum-silikat (Na_2SiO_3) ve sodyum- hidroksit çözeltisinin (NaOH) oranı 2.5 alınmıştır. Bu çalışmada, üretilen taze ve sertleşmiş geopolimer betonlar üzerinde çökme hunisi, beton akıcılığı, işlene bilirlik, basınç dayanımı, darbe dayanımı ve eğilme çekme dayanımı testleri yapılmıştır. Yapılan bu deneylerin sonuçları KYGB'ların mekanik performansları üzerinde önemli etkileri olan faktörleri belirlemek için detaylı olarak incelenmiştir. Ayrıca, taze ve sertleşmiş geopolimer betonların özellikleri arasındaki ilişkileri belirlemek için yapılan deneylerden elde edilen veriler arasındaki bağlantılar belirlenmiştir. Deneysel çalışmalar göstermiştir ki; geopolimer beton karışımlarında nano-silika ve çelik fiberlerin birlikte kullanılması taze KYGB'nun özelliklerini olumsuz etkilemiş olmasına rağmen KYGB'nun darbe dayanım ve eğilme çekme dayanım performanslarını önemli ölçüde arttırmıştır. Bunlara ek olarak, çelik fiberler KYGB'ların darbe dayanımı ve eğilme çekme dayanımı özellikleri üzerinde oldukça etkili iken, nano-silika taze KYGB'ların özellikleri ve basınç dayanımı üzerinde baskın etkileri vardır. Ayrıca, KYGB karışımlarında çelik fiberlerle beraber lastik kauçuk lastik fiberlerin kullanılmasıyla darbe dayanımı ve eğilme çekme dayanımı üzerinde daha olumlu etkilerken, sadece lastik kauçuk fiberlerin KYGB karışımlarında kullanıldığı zaman taze KYGB'ların özellikleri üzerinde olumsuz etkilemiştir.

Anahtar Kelimeler: Kendiliğinden Yerleşen Geopolimer Beton (KYGB), Taze KYGB Özellikleri, Nano-Silika, Lastik Kauçuk Fiber, Çelik Fiber, Darbe Dayanımı ve Eğilme Çekme Dayanımı.

"Dedicated to my family"

ACKNOWLEDGEMENTS

I would like to thank my supervisor, Prof. Dr. Abdülkadir ÇEVİK, for his guidance and support throughout the study. I am thankful for his encouragement and motivation.

I would like to thank also Accoc. Prof. Dr. Mehmet Eren GÜLŞAN, Asst. Prof .Dr. Anıl NİŞ, Ph.D. Radhwan Alzeebaree and Ph.D. Alaa Mohammedameen for their support.

I would like to express my love and gratitude to my family for their support, always best wishes.

This study was supported by Gaziantep University Scientific Research Project Goverining Unit (BAPYB). Project Number: MF.DT.17.06

TABLE OF CONTENTS

Page

ABSTRACT ..... **v**

ÖZET ..... **vi**

ACKNOWLEDGEMENTS ..... **viii**

TABLE OF CONTENTS ..... **ix**

LIST OF TABLES ..... **xiii**

LIST OF FIGURES ..... **xiv**

LIST OF SYMBOLS ..... **xvii**

LIST OF ABBREVIATIONS ..... **xviii**

CHAPTER I: INTRODUCTION **1**

1.1. Introduction 1

1.2. Geopolymer Concrete 5

1.3. Superplasticizer 7

1.4. Self-Compacting Geopolymer Concrete 8

1.5. Nano-Silica 8

1.6. Steel Fiber 10

1.7. Recycled Tyre Rubber 12

1.8. Blast Furnace Slag 14

1.9. The Fresh State Tests of Self-Compacting Geopolymer Concrete 16

1.9.1. Slump Flow Test 17

1.9.2. L-Box Test 17

1.9.3. V-Funnel Test 17

1.9.4. Slump Flow Time (T_{50}) 17

1.10. The Hardened State Tests of Self-Compacting Geopolymer Concrete 17

1.10.1. Compressive Strength Test 17

1.10.2. Split Tensile Strength Test 18

1.10.3. Flexural Tensile Strength Test 18

1.10.4. Modulus of Elasticity Test 19

1.10.4. Drop-Weight Test 19
1.10.4.1. Force Sensor 23
1.10.4.2. Accelerometer 23
1.10.4.3. Connection Cable 25
1.10.4.4. Spring-Loaded Linear Potentiometer 25
1.10.4.5. Data Logger 25
CHAPTER II: LITERATURE REVIEW 27
2.1. General 27
2.2. Nano-Silica 28
2.3. Steel Fiber 30
2.4. Fresh State Properties of Geopolymer Concrete 31
2.5. Mechanical Properties of Geopolymer Concrete 33
2.5.1. Compressive Strength 33
2.5.2. Bond Strength 34
2.5.3. Fracture Property 34
2.5.4. Effect of Nano-Silica on Bond Strength of SCGC 35
2.6. Effect of Nano-Silica on Mechanical Properties of SCGC 35
2.6.1. Effect of NS on Compressive Strength of SCGC 36
2.7. Effect of SF on Mechanical Properties of SCGC 38
2.7.1. Effect of SF on Compressive Strength of SCGC 38
2.7.2. Effect of SF on Fracture Property of SCGC 40
2.8. Self-Compacting Rubberized Concrete (SCRC) 42
2.8.1. Properties of Rubberized Concrete 43
2.8.2. Fresh Rubberized Concrete Properties 43
2.8.2.1. Workability of Rubberized Concrete 43
2.8.3. Hardened Rubberized Concrete Properties 44
2.8.3.1. Compressive Strength of Rubberized Concrete 44
2.8.3.2. Flexural Tensile Strength of Rubberized Concrete 45
2.8.3.3. Modulus of Elasticity of Rubberized Concrete 47
2.8.4. The Combined Effect of NS and SF on Properties of SCGC 47
2.9. Impact Test 49

CHAPTER III: EXPERIMENTAL STUDY **52**
3.1. Materials 52
3.1.1. Binder 52
3.1.2. Ground Granulated Blast Furnace Slag (GGBFS) 52
3.1.3. Nano-Silica (NS) 53
3.1.4. Steel Fiber (SF) 53
3.1.5. Recycled Tire Rubber (RTR) 54
3.1.6. Aggregates 55
3.1.7. Super plasticizer (SP) 55
3.1.8. Alkaline Solution 57
3.2. Concrete Mix Design and Mixing Procedure 58
3.3. Fresh State Tests 62
3.4. Curing of the SCGC Specimens 63
3.5. Hardened State Tests 63
3.5.1. Compressive Strength 63
3.5.2. Splitting Tensile Strength 65
3.5.3. Flexural Tensile Strength 67
3.5.4. Modulus of Elasticity 77
3.5.5. Drop-Weight Test (Impact Resistance) 77
3.5.5.1. Force Sensor 79
3.5.5.2. Accelerometer 80
3.5.5.3. Connection Cable 82
3.5.5.4. Spring-Loaded Linear Potentiometer 83
3.5.5.5. Data Logger 85
CHAPTER IV: CONCLUSIONS **86**
4.1. Results and Discussions 86
4.1.1. Fresh State Test Results and Performance of SCGC Specimens 86
4.1.1.1. Effects of SFs, NS and RTR on the Slump Flow Values 88
4.1.1.2. Effects of SFs, NS and RTR on the Slump Flow Time (T_{50}) 90
4.1.1.3. Effects of SFs, NS and RTR on the V-Funnel Flow Time 92
4.1.1.4. Effects of SFs and NS on the L-Box Height Ratio 94
4.1.2. Hardened State Test Results and Performance of SCGC Specimens 96
4.1.2.1. Compressive Strength of SCGC Specimens 97

4.1.2.2. Modulus of Elasticity of SCGC Specimens 99
4.1.2.3. Splitting Tensile Strength of SCGC Specimens 101
4.1.2.4. Flexural Strength of SCGC Specimens 103
4.1.2.5. Failure Modes of the Flexural Specimens 107
4.1.2.6. Relationship and Correlation Between Hardened and Fresh Properties of SCGC 113
4.1.2.7. Scanning Electron Microscopy (SEM) Analysis 121
4.1.2.8. Results of the Drop-Weight Tests 126
4.2. Impact Energy 178
4.3. Conclusions 181
REFERENCES 187
APPENDIX-1 205
CIRRICULUM VITAE (CV) 224

LIST OF TABLES

Page

Table 2.1 The limits of fresh state tests of concrete as per EFNARC (2002) 32

Table 3.1 Chemical & physical characteristic of NS and GGBFS 53

Table 3.2 The aspect ratio and geometrical characteristic of SF 54

Table 3.3 The sieve analysis & physical properties of RTR 55

Table 3.4 The sieve analysis & physical properties of aggregates 55

Table 3.5 Technical properties of MasterGlenium-RMC-303 superplasticizer ... 56

Table 3.6 Technical properties of NaOH-sodium hydroxide 57

Table 3.7 Component of SCGC mixes 61

Table 3.8 EFNARC specification and classification of fresh properties of SCGC mixtures 62

Table 3.9 The technical properties of model ICP 200C20 force sensor 80

Table 3.10 The technical properties of 352C03 model accelerometer 82

Table 3.11 The technical properties of spring-loaded linear potentiometer 84

Table 3.12 The technical properties of EPA 100 84

Table 3.13 The technical properties of NI 9230 with BNC data logger 85

Table 4.1 The fresh state test results of SCGC specimens 87

Table 4.2 The hardened state test results of SCGC specimens 97

Table 4.3 Drop-weight tests results 138

Table 4.4 Impact energy of each beam specimen 180

LIST OF FIGURES

Page

Figure 1.1 Nano-silica sample 10
Figure 1.2 Steel fiber sample..... 11
Figure-1.3 RTR samples 14
Figure 1.4 Sample of GGBFS 16
Figure 1.5 Split tensile strength test 18
Figure 1.6 Sample of data source for accelerometer 24
Figure 3.1 GGBFS used in the study 52
Figure 3.2 NS used in the study 53
Figure 3.3 SFs used in the study 54
Figure 3.4 RTR used in the study..... 54
Figure 3.5 Coarse and Fine Aggregates used in the study 55
Figure 3.6 MasterGlenium-RMC-303 superplasticizer..... 56
Figure 3.7 Sodium silicate-Na2SiO3 and sodium hydroxide-NaOH 58
Figure 3.8 Preparation of alkali activator and SCGC specimens with NS production procedure 59
Figure 3.9 Preparation of alkali activator and SCGC specimens with RTR production procedure 59
Figure 3.10 SCGC production..... 60
Figure 3.11 Molds used in the study and after casting of SCGC mixtures 60
Figure 3.12 Produced SCGC beam specimens..... 61
Figure 3.13 Compressive strength test machine..... 63
Figure 3.14 Compressive strength tests of SCGC..... 65
Figure 3.15 Splitting tensile strength tests of SCGC 66
Figure 3.16 Flexural tensile strength tests machine 68
Figure 3.17 Flexural strength tests of SCGC beams 70
Figure 3.18 The results of SCGC beam specimen flexural strength tests..... 76
Figure 3.19 The modulus of elasticity tests machine 77

Figure 3.20 Drop-weight test machine 78
Figure 3.21 The schematic representation of drop-weight test machine 78
Figure 3.22 The measurement of crack widths using the crack width gauge instrument 78
Figure 3.23 ICP 200C20 force sensor 79
Figure 3.24 The force sensor in the experiment setup 79
Figure 3.25 ICP 352C03 accelerometer 81
Figure 3.26 The accelerometer in the experiment setup 81
Figure 3.27 Accelerometer mounting configurations and their effects on high-frequency 81
Figure 3.28 The low noise coaxial cable in the experiment setup 83
Figure 3.29 Spring-loaded linear potentiometer used in the study 83
Figure 3.30 Measuring & control device of spring-loaded linear potentiometer used in the study 83
Figure 3.31 Spring loaded linear potentiometers mounted on beam specimen. 84
Figure 3.32 NI 9230 with BNC data logger. 85
Figure 4.1 The results of slump flow tests 89
Figure 4.2 The effect of SFs, NS and recycled tyre rubber (RTR) on the slump flow results 90
Figure 4.3 The results of T_{50} slump flow time tests 91
Figure 4.4 The effect of SFs, NS and recycled tyre rubber (RTR) on the T_{50} flow duration. 91
Figure 4.5 The results of V-funnel flow time tests. 93
Figure 4.6 The effects of NS, SFs and RTR on V-funnel time and T50 flow time vs V-funnel flow time relationships of NS, SFs and RTR. 94
Figure 4.7 The results of L-box tests 95
Figure 4.8 The effect of NS, SFs and RTR on the L-box height ratio 96
Figure 4.9 The results of compressive strength 99
Figure 4.10 The effects of NS, SFs and RTR on the compressive strength 99
Figure 4.11 The modulus of elasticity test results 100
Figure 4.12 The effects of NS, SFs and RTR on the modulus of elasticity 101
Figure 4.13 The results of splitting tensile strength tests 103

Figure 4.14 The effects of NS, SFs and RTR on the splitting tensile strength. 103
Figure 4.15 The results of flexural tensile strength tests. 106
Figure 4.16 Force-displacement relationships of SCGC..... 107
Figure 4.17 Relationships between volume fractions and flexural tensile strength of SCGC 107
Figure 4.18 Failure mode of SCGC beam specimens with/out NS and SFs..... 110
Figure 4.19 Failure mode of rubberized SCGC beam specimens with/out SF_1.... 113
Figure 4.20 Correlation between the fresh properties of specimens with/out NS and SFs..... 114
Figure 4.21 Correlation between the hardened and fresh properties of SCGC.... .116
Figure 4.22 Correlation between the hardened performances of SCGC..... 117
Figure 4.23 Correlation between the fresh properties of specimens with RTR and with/out SF_1 119
Figure 4.24 Correlation between the hardened and fresh properties of rubberized SCGC..... 120
Figure 4.25 Correlation between the hardened performances of rubberized SCGC..... 121
Figure 4.26 SEM images of SCGC with/out NS with different scales 124
Figure 4.27 SEM images of rubberized SCGC specimens with different scales..... 126
Figure 4.28 The first drop moment and failure mode of each beam specimen..... 137
Figure 4.29 Effects of NS, effects of SFs volume fraction and effects of SFs aspect ratio..... 174
Figure 4.30 Effects of RTR volume fraction, effects of RTR aspect ratio and effects of SF_1 176
Figure 4.31 Average displacement vs time relations of each SCGC beam specimen..... 178
Figure 4.32 Ratio on impact energy over GB 180
Figure 4.33 Relations between SFs volume fraction & types and drop number & impact energy 180
Figure A.1 Crack propagation of flexural strength test..... 215
Figure A.2 Crack propagation of drop-weight test 223

LIST OF SYMBOLS

E	Energy
m	Impactor Weight
g	Gravitational Acceleration
N	Drop Number
P	Force
A	Area

LIST OF ABBREVIATIONS

GC	Geopolymer Concrete
SCGC	Self-Compacted Geopolymer Concrete
GGBFS	Ground Granulated Blast Furnace Slag
NS	Nano-Silica
SF	Steel Fiber
RTR	Recycled Tyre Rubber
OPC	Ordinary Portland Cement
SP	Superplasticizer
SCC	Self-Compacting Concrete
SAA	Specific Surface Area
RC	Rubberized Concrete
SCRC	Self-Compacting Rubberized Concrete
SFSCC	Steel Fibrous Self-Compacted Concrete
FCR	Fine Crumb Rubber
CCR	Coarse Crumb Rubber
TCR	Tyre Crumb Rubber
BFS	Blast Furnace Slag
LVDT	Linear Variable Displacement Transducers
ITZ	Interfacial Transition Zone

CHAPTER 1

INTRODUCTION

1.1 Introduction

Concrete is the second most usage material in the World after water [1] and is widely used as a construction material. Because, concrete has versatility, high strength, mold ability and numerous other characteristics, huge amounts of concrete have been used broadly and increasingly day by day in the construction industry for five decades and the traditional concrete usage has been spread. Cement is generally employed as the major binder to bind course and fine aggregates for concrete production [1]. A very high temperature is required during cement production, in other words requiring large amounts of energy. Moreover, the cement production process releases a substantial quantity of greenhouse gases (carbon dioxide (CO_2), etc.) to the atmosphere owing to decarbonization of limestone. So, cement releases nearly 1 ton CO_2 for each ton of Ordinary Portland Cement (OPC) during the OPC production [2]. Portland cement production contributes globally 5-7% of entire universal CO_2 releases [3]. OPC is gotten from the limestone deterioration which needs to consumption of huge amounts of energy. CO_2 is released as a result of fuel burning and limestone putrefaction. Analysis on the emissions showed that there is a frightening ratio between the manufacture of cement and CO_2 emissions (54% through calcination and 46% through the burning of fuels) [4]. It is predicted that the annual global cement production will be nearly 4.38 billion tons in 2050 with 5% rise per year [5]. Furthermore, a huge amount of rocks and minerals are consumed in the production of cement and this may lead to diminishing the rocks and minerals in any day [6]. For many years ago, the cement utilization as a binder of concrete has been examined by a lot specialists to protect the environment from pollution [7]. To reduce CO_2 emissions, eco-friendly materials are required in the construction industry, so new alternative materials are researched. One of the alternative materials is Geopolymer Concrete (GC) for construction industry.

GC is a novel combination that does not require the existence of OPC as a binder. Moreover, it is an environmentally friendly binding material and alternative to OPC. The production of GC requires less energy than OPC. Since, it is found that GC releases CO_2 less than OPC by approximately 6 times. This is because of the low calcification temperature in the GC [8]. Henceforth, some of supplementary cementitious materials are used in place of portland cement such as GGBFS, metakaolin, silica-fume, fly ash (FA), etc. These materials include large quantity of silicon and aluminum is activated with chemical compounds such as sodium hydroxide (NaOH) and sodium silicate (Na_2SiO_3) alkaline liquids to form the geopolymer binder [8]. The utilize of GC is not only limited to its contribution to reducing the emissions of CO_2 but also to the consumption of industrial waste and by-products, thus contributing to the transformation of harmful material into useful building materials [9]. Moreover, GC generally has very good mechanical properties such as high early strength, good resistance to acids and sulfates, and low shrinkage and creep [10-11].

In the concrete technology, a novel idea and one of the latest developments is self-compacting geopolymer concrete (SCGC) which does not need vibration for putting and placing [12]. Self-compacting concrete (SCC) was firstly produced in Japan between the end of 1980s and early 1990s. If fresh SCC is compared with fresh traditional concrete, it has better workability, better followability in reinforced zones and less segregation properties. Moreover, it has the capacity to self-compacting under its own weight without vibration and segregation [13].

During the production of SCGC, superplasticizers are used to increase the workability of concrete thus, improvement casting operation, easy placement in congested reinforcing bars, improvement the unification around the reinforced and bonding with the reinforcement, and a faster rate of casting, thus reducing the total cost [14]. It is accepted that the high volume paste in SCC mixtures aid to decline the internal friction between the fine aggregate particles and improve the workability, but a well grain size distribution is now very significant. In SCGC, the primary functions of superplasticizer (SP) are absorption in binding grains, moving a negative effect to them which repulse each other and distributed mixture [15]. This improves the fresh and hardened properties of SCGC, providing great workability and better

performance, thus improving the microstructure of SCGC and achieving better comprehensive strength [15].

Recently, nano-technological materials have been started using in the applications of concrete industry, because nano-technological materials have an important effect on the concrete properties**.** One of the most used nano-materials in concrete industry is nano-silica (NS). It has a high pozzolanic tincture and the capability to collaborate with the free lime during hydration to form C-S-H gel. Thus, it gives the mechanical strength, impermeability, durability properties of concrete [16]. Owing to the larger specific surface area (SAA), the concrete with NS has a better sticky property than the concrete without NS and this causes that the concrete inclusion NS has a better permeability resistance [17]. The studies on cement or concrete show that if a small amount NS is used in concrete, it improves significantly the mechanical properties of concrete [18].

Steel fiber (SF) is another technological material. It has utilized to enhance the mechanical performance of concrete since the last decades. Concrete ruptures generally depends on the composition of crack on account of the loading influences. Temprature changes, dampless and loads lead to microscopic cracks on the coarse aggregate surface of concrete mortar. Also, they cause the increase of crack propagation and spread over the concrete body [19]. Since, SF is used in concrete, it causes that mechanical properties of concrete improves especially flexural strength, impact, fracture toughness, thermal shock and resistance to fatigue. As proportion of SF in concrete increases splitting tensile strength, compressive strength and modulus of rupture results of concrete get higher [20].

The interest in research on the usage of rubber in concrete and the properties of rubberized concrete (RC) has been increasing in the last two decades. RC can be described as fine and/or coarse aggregates in traditional strength concrete. Studies on the self-compacting rubberized concrete (SCRC) have been increased since recently. Moreover, crumb rubber can be replaced in high proportional instead of natural sand without the need for pretreatment of aggregate in SCRC [13] and 64mm crumb rubber aggregate can be used up to 180 kg/m^3 in SCRC by weight as long as getting receivable fresh and hardened properties according to the specification used [21]. The mechanical behavior of SCRC is unusual, because it does not match with

traditional empirical relation of modulus of elasticity with compressive strength. Furthermore, concrete strain capacity and ductility considerably increases when rubber aggregates are added in concrete [22].

The researches of together influences of NS, SF/TR and SFs on the fresh and hardened states properties of SCGC are few and scarce. This led us to study and investigate the effect of this materials on eco-friendly alkali activated GGBFS blends in both fresh and hardened states so as to determine the optimum quantity of each material in the SCGC. The primary target of this study is to determine and investigate the combined effect of NS, SF/RTR and SF when added in varying proportions to the slag based SCGC on fresh state and mechanical performance of SCGC. All the specimens are compared with each other as well as with the control specimens to present the difference and find out the most appropriate ratios of these parameters in this unique type of concrete. This research contributes the support efforts to reduce the utilizing of cement as a binding material and thus diminish the liberation of CO_2 in the ambiance as well as contributing to the use of useless industrial by-products waste tire rubber and converting them into useful materials, thus production an eco-friendly concrete.

This research aimed to determine the impact behaviors of concrete structures and, impact resistance and energy absorption capacities of concrete structures. In literature, there is little research on the effect of dynamic loads on the structure and structure elements. Impact loads are also among these dynamic loads. Impact loads are important according to the intended use of the structures [22]. Throughout any impact incident, structure must absorb a lot amount of energy in a short time. So, some damages to the structure can occur such as cracks or breaks. They are depends on the energy absorption capacity of the structures [23]. Moreover, among the loads affecting concrete structures, the least known behavior loading is impact loading [24] and static methods do not use to estimate the behavior concrete structures under impact loads [23]. Although studies are limited on the impact behavior of concrete, the number of studies using the drop-weight test to investigate the impact behavior of concrete has increased in recent years [25].

1.2 Geopolymer Concrete (GC)

Concrete is the most utilized construction material in our country and the world. Only water consumes more than concrete, the annual production amount reached approximately 13 billion tons and it continues to be used increasingly in the construction industry. It is easy to produce, safe, high strength, easy to form, economical and has many different characteristics, so it is preferred to use in construction industry. Therefore, the development and use of conventional concrete (cemented concrete) is increasing rapidly [26].

Especially preferred cement type in traditional concrete production is Ordinary Portland Cement (OPC). During the production of OPC, a very high amount of energy and temperature is needed to break down the gypsum. Used gypsum causes a large amount of carbon-dioxide (CO_2) emission. Therefore, CO_2 emits during the production of OPC [27]. The production of OPC is caused by 5-7% of CO_2 emission in the World [28]. Emission analysis has shown that CO_2 emission is 54% during cement production and 46% is from consumption of fossil fuels [29]. Researches have shown that the production of OPC increases by 5% every year and is expected to reach 4.38 billion tons by 2050 [30]. In addition, during the production of concrete, large amounts of rocks are used as aggregate, therefore rocks will be depleted [31]. For a long time, many experts have been criticized for the usage of cement as a binder in concrete due to environmental pollution [32].

$$5CaCO3 + 2SiO2 \rightarrow (3CaO.SiO2)\ (2CaO.SiO2) + 5CO2 \text{ [33]}$$

Recently, the alternatives construction materials have been looked to conserve the natural resources and to minimize the environmental exhausting [34]. OPC is the most usage construction material all over the world [34]. The production of OPC is the big problem, because during OPC production process, significant amount energy is consumed and substantial amount of CO_2 etc. is released in to the atmosphere, owing to the decarbonization of limestone and the combustion of fossil fuels. [35]. Therefore, for the future of mankind and cement industry, the high amount of required energy and the undesirable effects of CO_2 on the atmosphere are substantial issues. So, new eco-friendly materials should be used as an alternative of OPC to take away environmental concerns. An eco-friendly concrete has recently investigated to use as an alternative to OPC [36, 37]. This alternative material is GC.

The materials formed by changing the crystal and chemical structures of natural minerals by different methods are called Geopolymer [38]. It is obtained from powder cementitious binders that can be dissolved partially or completely by water with chemical activators instead of cement [39]. GC has received significant interest due to the considerable reduction in both the requirement of natural resources and the amount of carbon dioxide-CO_2 emissions. Moreover, GC also utilizes to produce advanced construction materials using a by-product alumina-silicate composition [37]. So, the GC is discovered to be the better alternative for reducing the global warming, as it may lead to significantly reduce the CO_2 emissions caused by cement industries [40].

GC is a kind of concrete which symbolizes a lot of different inorganic materials. GC uses binder materials such as fly-ash (FA) or slag which containing high amount of Alumina (Al) and Silica (Si). These materials are utilized to eliminate the expenditures, improve the workability, flowability, and mechanical performance of the matrix [41–44]. GGBFS and FA exhibits favorable contributions to the mechanical characteristic of the concrete, economy, and eco-friendly environment materials [45,46].

Those materials react with alkali solution such as NaOH or KOH and Na_2SiO_3 or K_2SiO_3 and obtains a gel that binds the coarse and fine aggregates. In GC, the alkaline solution that react with Si and Al contented FA or slag is used instead of water to bind concrete matrix. The polymerization process is a considerably quick chemical reaction under alkali circumstances on Al-Si minerals. In GC, cementitious materials such as FA or slag are used instead of cement. FA has low calcium content, but slag has high calcium content. Generally, the NaOH is present in solid form as pellets and flakes [47]. These solid pellets are dissolved in water to obtain a NaOH solution with the necessary concentration. The concentration of NaOH solution can be obtained in different molar. In a solution, the mass of NaOH solids changes according to the concentration of the solution. For example, 40 gram of NaOH solids per liter of the water are used to obtain 1 molar NaOH solution, so 12x40=480 gram of NaOH solids per liter of the water are used for 12 molar NaOH solution, 40 gram is the NaOH molecular weight. After NaOH solids are mixed with water, NaOH solution must be leaved 24 hours to obtain NaOH solution prior to use and also if it overruns 36 hours, NaOH solution turns into semi-solid liquid state. Thus the

solution must be utilized within this time. Moreover, Na_2SiO_3 is usually existent in liquid (gel) form and is also known as liquid glass or water glass. Commonly, alkaline activators can be prepared by mixing of NaOH solution and Na_2SiO_3 solution at the room temperature. After the solutions are mixed together, those start to react each other known as polymerization. During polymerization, large amount of heat is released so it is leaved for almost 24 hours to obtain alkaline activator as binder [47].

GC has important benefits over traditional concrete. GC is more eco-friendly and less CO_2 emission. Moreover, it's full curing occurs faster and it acquires its full strength more rapidly, and it has higher tensile and compressive strength. It is also more resistance to fire and corrosion, and is less shrinkage than traditional concrete. Further, it is much more long lasting than traditional concrete and requires less maintenance so obtains saving large amount of money. GC are structures that can survive for thousands of years, for example, it has been found to be used in structures made by the Romans. So, it is safely last for hundreds of years as traditional concrete is last for tens of years [47].

1.3 Superplasticizer (SP)

They are called plasticizers for additives that decrease the amount of water used in the concrete mixture by 5% to 11%, and superplasticizers for additives that decrease over 12% [48]. Superplasticizers are chemical additives that reduce the proportion of water used in the concrete mixture at the same time without changing the proportions of the concrete and increase the precipitation and spread of the concrete [49]. They provide perfect wetting of materials in concrete and so, concrete strength increases [50]. Their contents usually contain melamine and naphthalene sulfonate [51]. Today, they are also known as "superplasticizer" or "hiperplasticizer" [52]. Superplasticizers are expensive additives [53], however, it is a necessary material for self-compacting concrete. Superplasticizers are preferred because they affect the workability and quality of concrete (cost, time etc.) when used in concrete. The superplasticizer improves the workability of concrete, so the casting of concrete is easier and faster, it is easily placed between cramped reinforcements, it increases the bond and joint between reinforcement and concrete, and reduces the total cost [54].

The main functions of the superplasticizer in GC eliminate the negative effects of the grains by absorbing the superplasticizer, such as sweeping back each other and distributing the mixture. Since it enhances the fresh and hardened performance of concrete, the concrete mix has better workability and very good concrete performance. It also improves the microstructure of GC and results in better compressive strength results [55]. In addition, super plasticizers reduce sweating and decomposition, slow the increase of hydration temperature and increase resistance to external influences such as freeze-thaw [56].

1.4 Self-Compacting Geopolymer Concrete (SCGC)

Self-compacting concrete (SCC) is a novel type of concrete that can consolidate by its own weight without needing any external or internal mechanical vibration to fill the formwork [57]. In addition, the resistance to bleeding and segregation without loss of stability is one of the most significant interests in the utilization of SCC. The researchers have been investigated the fresh and hardened state performance of SCC since the 1990s when it was used in the structure industry [58–60]. It has been revealed that the binder content of 500–600 kg/m^3 is required to realize the SCC requirements by related guidelines/standards [61].

The poor tensile strength and ductility of SCC led to the use of SF to avoid this drawback [62]. The post-cracking, ductility and toughness of the concrete improved with the addition of SF [45, 63]. In addition, steel fibrous self-compacted concretes (SFSCC) offer more acceptable cost to benefit ratios with respect to non-fibrous self-compacted concretes [64]. The SF content and SF aspect ratio are considered as a main factor on the design procedure and optimization technique to produce the SCC mixes [65–67]. Researchers considered 1% as an optimal amount of SF for the majority of structures and economic considerations [68].

1.5 Nano-Silica (NS)

Although the use of binder materials in the construction industry dates back to very old times, cement binders used today can be considered as new technology. The newest materials used in this technology are micro-scale. Nano-technological materials are used in many fields. Nanotechnology refers to the nanometer (nm) size that equals one billionth of a meter. Therefore, the usage of nano-metric materials in the concrete industry has a big potential for the development of concrete technology.

As can be seen in the figure-1.1, it is one of the nano-metric materials used in concrete technology. Since the surface area of NS is much larger than silica fume, pozzolanic activity of NS is more than silica fume. Since NS has a very fine particle structure, the large amount of water in the cement paste mixture is depleted early owing to the high pozzolanic activity of NS, causing the cement paste to harden very quickly and to form a porous structure due to the formation of the gel very quickly. This causes high early strength of the mixture and low final strength. All these events are caused by the excessive pozzolanic activity of NS. When NS is used in 0.15-0.20% of the weight, it remarkably increases the final strength of concrete. Today, studies to investigate the effects of nanotechnology in concrete and cement have focused on the effects of nanoparticles used in mixtures on the properties of concrete and the hydration reaction. In addition, the permeability of nano-material concretes is low and the concrete with low permeability has high sulfate resistance [69].

Recently, the fact that nano-technological materials significantly increase the properties of concrete has improved the construction industry. Nano silica is one of the most preferred nano materials because it increases the mechanical performances, impermeability and durability of concrete. The ability of NS to increase these properties is due to its high pozzolanic structure. This pozzolanic structure reacts with free lime during hydration, causing the formation of C-S-H (calcium-silicate-hydrate) gel [70]. In this way, the durability, strength and impermeability of the concrete are increased. Owing to the large special surface area of NS, the surface area of NS concretes is larger than that of non-NS concretes; even concretes with NS have better permeability resistance [71]. According to the literature, studies on cement or concrete have shown that even if a small amount of NS is added to a mixture, the mechanical properties of cementitious materials improve [72].

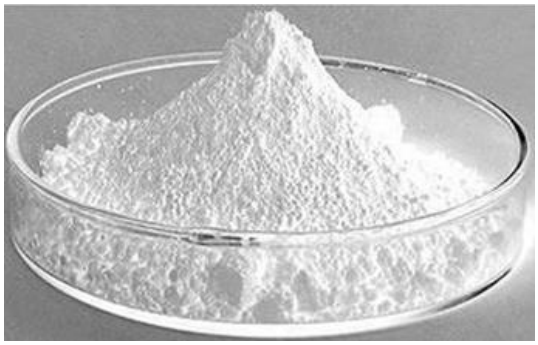


Figure 1.1 Nano-silica sample [73]

Recently, researchers have been investigated the utilization of nano-silica (NS) material in concrete industry [74–78]. The concrete quality primarily depends on the properties of the ITZ between aggregate and cement paste. The obtained findings indicated that the use of NS enhanced the microstructure and the finer hydrated phases (C–S–H gel) through influence of anti-Ca(OH)2-leaching, and as a result, nano-filler enhanced the cement paste due to the high pozzolanic characteristic of NS [77,79]. As well as, the utilization of NS reduced the overall permeability due to the enhanced mechanical and durability properties of concrete [75, 80– 83].

1.6 Steel Fiber (SF)

SFs are used in concrete mix as shown in the figure-1.2. These SFs are found dispersedly and discontinuously in concrete mixtures. SFs significantly reduce crack formation in concrete and increase the toughness, fatigue, impact and tensile strength of concrete. Therefore, it is possible to obtain concretes with high ductility. In addition, the shear strength of concretes with SFs is considerably higher than those without SFs. The SFs in the concrete mixture prevent the formation of many capillary cracks that may occur in the concrete matrix due to pressure and tensile loads until it reaches its tensile strength level. Similarly, due to using SFs in concrete, the cement matrix that holds these fibers together makes stress transfer. Thus, capillary cracks that may occur in cement paste are prevented [84]. Concrete mixtures with SFs continue to carry, although they reach their carrying capacity. In other words, since the concrete containing SF has a high ductility feature after the first break occurs during load carrying, the fracture energies of concretes with SF are high [84]. The slenderness ratio of these fiber types used in concrete varies between 50 and 100, and the volume fraction of SFs in the concrete mix varies between 0.5% and 2.5%. If SFs are used more than these rates in the concrete mixture, it has been observed that there are lumps in the mixture and the mixture does not show homogeneous distribution, so the concrete strength is lower than the normal concrete strength [84].

The slenderness ratio and amount of the SFs used in the concrete mixture affect the properties of concrete. In addition, the homogeneous distribution of the SFs used during the mixture and the extent to which this distribution can be preserved after the mixing process, directly influences the properties of the concrete [84].

In the literature there are many studies on the use of SF in concrete mix and the influence of SFs on the mechanical properties of concrete. Especially the use of SF in the concrete increases the weak tensile strength of concrete and prevents the formation of most of the capillary cracks that will occur on the concrete under service loads [85].

SF mixed concrete is a composite material. Load bearing capacity of concrete mixtures with SF is equivalent to the load bearing capacity of reinforced concrete. If SFs use with in the mesh or reinforced concrete, this can provide better crack control. Although SF applications in concrete mixes are increasing day by day, SF increases the load bearing capacity of concrete and saves considerable time and cost. In addition, since it provides a versatile, homogeneous concrete reinforcement, it prevents the concrete from breaking, bending, increases crack resistance, toughness, energy absorbability, fatigue strength, shear strength and provides high resistance to impact loads [86].



Figure 1.2 Steel fiber sample [87]

SFs are utilized to enhance the mechanical performances of concrete. Under the influence of loading, the breaking of the concrete largely depends on the crack structure. Due to temperature changes and humidity on the surface of coarse aggregates occur micro cracks in the mortar. Also, cracks that occur due to continuous loading spread over the concrete. Therefore, using SF in concrete improves some mechanical properties such as fracture strength, bending strength, impact resistance, heat shock and fatigue resistance. In addition, adding different amounts of SFs to concrete significantly increases split-tensile strength, compressive strength and modulus of rupture [88].

The inclusion of SF improved the compressive strength and this enhancement depends on the SF content and aspect ratio [89]. The improvement of compressive

strength due to the presence the SF may become 20% as compared to the compressive strength of specimens without SF [90, 91]. However, the incorporation of SF can improve the splitting tensile strength much more than the compressive strength and the improvement in the tensile strength can reach up to 98% depending on the amount of SF [91]. The addition of SF also improved the drying shrinkage through bridging the micro cracks created by the restrained shrinkage [92,93]. Furthermore, the addition of SF has superior improvement on the flexural strength, propagation of cracks, post failure ductility, and toughness [94]. Also, the SF increased the energy absorption and the compressive ductility at early age [95].

1.7 Recycled Tyre Rubber (RTR)

Currently, a serious environmental problem emerges in the world due to the massive quantity of waste tyre materials. The billions of tyres in the world are buried and/or throw away to the global environment, which results in an obvious environmental threat to the world, especially in the regions where huge amounts of tyres are produced. The oil that includes toxic and soluble components [96] emerges during the burning procedure of the waste tyres, which pollutes both soil and water [97]. The tyre landfilling also considered to be a significant ecological threat since waste tyre disposal areas reduced biodiversity due to the toxic and soluble components of the tyres [98].

In addition, the less available landfill area and the increased cost of accumulation and transportation of waste tyres also considered to be the main problem for the waste tyre disposal. Researchers expected that the number of waste tyres will increase up to about 5000 million in 2030 if the number of motor vehicles increased to 1200 million [98], which will cause serious environmental pollution. It was reported that the vehicle number in China was 240 million, and the accumulative automobile tyre number was 648 million, and almost 14.58 million tons of waste tyres were produced in 2018 [99]. Therefore, it becomes crucial importance of recycling such a big number of waste tyres for the possible utilization in the construction industry. The reuse of the waste tyres becomes one of the best solutions for both economy and the cleaner environment. In addition, the utilization of recycled rubbers may decrease the dependency on the natural aggregates, resulting in more sustainable constructions [100].

The utilization of tyre chips and crumb rubbers as recycled rubbers in concrete takes great attention to improve low deformation capacity, poor tensile strengths, and energy absorption capacity [101,102]. However, the tyre rubber replacement ratio should be lower than 20% to prevent a destructive effect on the mechanical strength of the rubberized concrete [103]. The slump of the rubberized concrete was found to be reduced with an increase in the rubber amount [104]. Another significant problem for the rubberized concrete is the early cracking because of the lack of the adequate bond between rubbers and concrete matrix, hence rubberized concrete has been limited to the non-structural applications [100,105].

Nowadays, with the development of technology, developments in concrete technology have also occurred. Conventional concrete has high compressive strength, low flexural and tensile strengths. With the advances in concrete technology, the increase in the flexural and tensile strengths of concrete and they have made it inevitable to use concrete in some areas because this technology is economical. In addition, the toughness performance and load carrying capacity of conventional concrete weaken after events such as fatigue, impact, abrasion, cracking and cavitation that may occur in the structure of the concrete. Intense efforts continue to improve these properties of concrete. These studies focus on fiber concretes, ferro concretes, vacuum concretes and waste tyre rubber concretes. There are studies in the literature on the using of waste tyre rubber in concrete instead of aggregate. These studies generally showed that waste tyre rubber decreases the compressive strength of concrete but improves the flexibility and toughness properties of concrete [106].

Recent studies have been experimental studies on self-compacting waste tyre rubber concretes. In these studies, as shown in figure-1.3 crumb rubbers obtain from the waste tyres , which can be converted into coarse crumb, fine crumb and fiber form in different sizes, also 64mm of tyre rubbers are used instead of aggregate in concrete mixtures up to 180kg/m^3. In terms of mechanical behavior, although the tensile capacity and ductility properties have increased significantly, some unusual behaviors such as elastic modulus that do not comply with current literature have been identified [107].



Fine Crumb Rubber (FCR) **Coarse Crumb Rubber (CCR)** **Tyre Crumb Rubber (TCR)**

Figure 1.3 RTR samples [108]

1.8 Blast Furnace Slag (BFS)

One of the most used concrete additives is Blast Furnace Slag (BFS). It is a material whose effect is known on the durability and strength of concrete. BFS is obtained from iron ore composed of iron oxide compounds. There are different types of iron oxide in nature. Apart from iron oxide, small amounts of silica and clay can be found in iron ore. In order to obtain iron from iron ore, furnaces called "blast furnaces" are used, the iron oxide in the iron ore turns into iron under the effect of the heat. The molten state iron accumulates at the bottom of the furnace. Materials such as Si and Al accumulate in the content of the slag just above this molten iron. This molten slag accumulated on the iron is around 1500-1600 ° C when it is removed from the furnace and when it is cooled very quickly by different methods, the slag gains an amorphous structure. Therefore, granulated slag like coarse sand is obtained and the slag shows a pozzolanic feature. This slag is called Ground Granulated Blast Furnace Slag (GGBFS). At least 66% of the GGBFS's mass consists of calcium oxide, magnesium oxide and silicon dioxide. In addition, some of the remaining part consists of aluminum oxide. According to TS EN 197-S; [(calcium oxide + magnesium oxide) / silicon oxide] ratio by mass should not be greater than 1.0 [69].

As it is difficult to store BFS, which is one of the industrial waste materials, its use in the concrete industry is important both economically and in terms of environmental protection. When the GGBFS is used in concrete mix, smaller and less voids occur in the inner structure of the concrete. Therefore, it has been determined that it strengthens the bond between aggregate and cement and improves the durability of concrete [69].

If the BFS is cooled slowly in air, the grains will be crystalline, if they are cooled quickly in water, the slag particles will be glassy. This glassy slag is called granulated blast furnace slag. In addition, slag has binding feature due to the presence of some calcium oxide (CaO) in the structure of the slag. However, this binding feature is not very strong. The main strong binding property of slag occurs by reacting with calcium-hydroxide (CH) in alkaline environments. Also, as the ambient temperature increases, reactions between slag and CH take place earlier. The temperature of the environment, the chemical structure of the slag (amorphous structure) and the fineness of the slag grains affect the activity and binding properties of GGBFS [69].

In addition to its binding feature, it has been determined that when used in concrete mixture, BFS increases the durability and resistance of concrete against sulfate effect. In addition, no negative changes were observed in the concrete structure against sulfate effect in concretes containing GGBFS. Also, it has been determined that the finer the slag particles used in the concrete mixture, the lower the porosity of the concrete, thus increasing the resistance of the concrete against chemicals [69].

Researches have shown that as the amount of BFS in the concrete mixture increases, the resistance of concrete against sulfate effect also increases. In the study by Li and Zhao, it has been determined that mixtures with BFS show the best resistance performance against sulfate effect of concrete [69].

Many studies have been shown that the early age strength of cementitious concrete samples containing slag in its mixture is lower than the cement concrete samples without slag in its mixture, but the cementitious concrete samples containing slag at later ages are generally higher than the slag-free cement concrete samples [69].

As seen in the example in Figure-1.5, it is used primarily because it has more positive effects on the environment since it causes less CO_2 and harmful gas emission as there is less amount of cement in BFS cements [109].



Figure 1.4 Sample of GGBFS [110]

The use of BFS in the concrete mixture increases the workability of fresh concrete, flowability, the hardening time, bleeding, and reduces water amount, the cavity structure and the hydration temperature. In addition, it increases the final strength of hardened concrete, its resistance to sulfate, its tensile strength and reduces its early strength, permeability, thermal cracks, creep-shrinkage, and corrosion [109].

1.9 The Fresh State Properties Tests of SCGC

Immediately after the concrete mixing process, various tests should be performed in the fresh state concrete mixture without any segregation and / or bleeding in order to determine the workability, flow time and transition capability measurements in fresh state for SCGC. The fresh state tests; L-box test, V-funnel test, slump flow time (T_{50}), and slump flow tests were carried out to satisfy the criteria of the passing ability and flowability of the SCGC mixtures according to EFNARC committee [14]. The flowability and viscosity of SCGC mixes were measured by slump flow and V-funnel tests, whilst the passing ability was measured via the L-box test.

1.9.1 Slump Flow Test

Slump flow test is the one of tests to be done to determine the properties of fresh state concrete. Slump flow value is a sensitive test used to define the flowability of a fresh state concrete mixture in free conditions. So, it is applied to specify for all SCC mixes as a primary control that the fresh concrete consistency is suitable for specification.

1.9.2 L-Box Test

L-box test is used to measure the passing ability of the fresh concrete to flow through narrow opening and confined places like areas of congested reinforcement without loss of segregation and homogeneity. The L-box height ratio values of the current study are presented in EFNARC.

1.9.3 V-Funnel Test

V-funnel test is utilized to determine the flowability (filling ability) of the fresh concrete and V-funnel flow time is the time that fresh concrete passes through the V-funnel opening. In addition, the viscosity classifications according to EFNARC.

1.9.4 Slump Flow Time (T_{50})

T_{50} time is the flow time for the fresh concrete mixture to reach 50 cm in diameter according to the slump flow table of EFNARC. During slump flow test, the information about bleeding, uniformity and segregation resistance of concrete mixture is obtained from the measurement of T_{50} time and/or through the visual observations [20]. Slump flow is classified into three classes in EFNARC; a range of applications and the lower and upper limits of typical slump-flow classes are given in EFNARC.

1.10 The Hardened State Properties Tests of SCGC

The hardened tests of SCGC were carried out to determine the mechanical performance and impact resistance of SCGC.

1.10.1 Compressive Strength Test

The compressive strength of a material is the ability of the material to resist breaking under the influence of pressure loads. The most considerable mechanical property required in concrete materials is compressive strength. Because concrete is the highest value of the mechanical properties of a material, it is in correlation with all the properties of the concrete material, that is, the higher the quality of the materials used in the production of concrete, the higher the concrete strength result and also the compressive strength test is utilized to determine the concrete class. Compressive strength test is done on cube or cylinder samples. The values of these compressive strength tests are calculated according to ASTM C39.

$$f'_c = P/A \quad (1.1)$$

f'c is compressive strength values of specimen (MPa), P is specimen's maximum load before breaking (kN) and A is specimen cross-sectional area (mm^2).

1.10.2 Split Tensile Strength Test

This test is also known as the "Brazilian Splitting Test" and it is utilized to determine the tensile strength of the cylindrical hardened concrete samples as shown in Figure 1.6. It was first proposed by Carnerio and Barcellas in 1953. n this experimental method, although it is mostly applied on cylindrical concrete samples used in pressure tests, it can also be applied on concrete cube samples. This test is carried out by placing the cylindrical concrete sample horizontally between the press machine as shown in Figure-1.6 and applying pressure loading in vertical direction to the plates placed both below and above the cylindrical concrete samples [111].

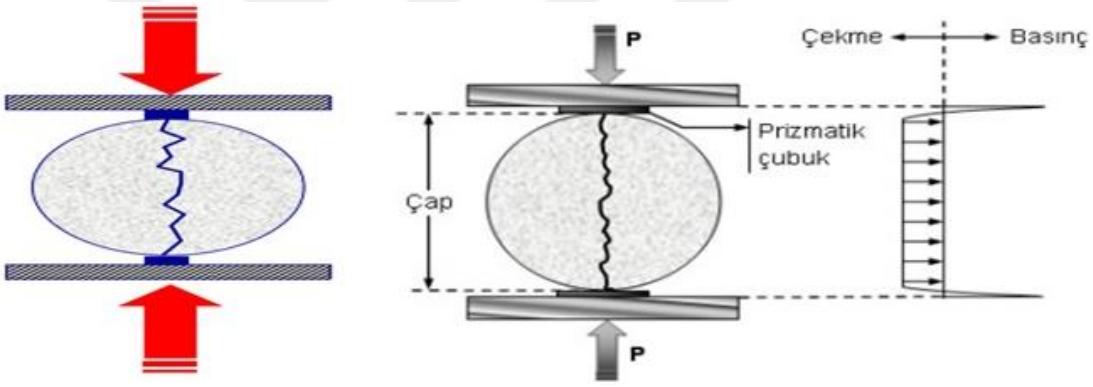


Figure 1.5 Split tensile strength test [111]

1.10.3 Flexural Tensile Strength Test

Flexural strength test is performed to determine the tensile strength of the outer surface of any material, design data related to the strength of the material and to determine the bending strength properties of the material [112]. Flexural strength test is also known as modulus of shear or flexural strength [113].

Bending moments occur on structural elements bearing transverse loads such as beams and slabs. So, this situation reveals the necessity to determine the bending strength and mechanical properties of concrete, especially for buildings, roads, bridges, dams and many structures made of concrete. Because the thickness, size and

distance between the support points of the building element are determined according to the bending resistance [113].

In order to determine this property of concrete, it can be determined by applying loads from three or four points to cylindrical or prismatic specimens. This feature is determined by applying the load until the material breaks by establishing these test mechanisms [113].

1.10.4 Modulus of Elasticity Test

The modulus of elasticity is the measure of the elastic deformation of the material under force. The elasticity modulus of concrete can be determined by performing a compressive strength test on a cylinder concrete sample. During the test, the load-strain data of the sample are taken and analyzed. After the test, stress-strain graph (load-deflection graph) is obtained from which the modulus of elasticity of concrete is determined [114].

1.10.5 Drop-Weight Test

In recent years, there has been increased the studies on the effects and behavior of the impact events on the structures in the world and in our country and increasing the studies on the performance of the structures against impact loads. Therefore, studies and experimental methods on material properties related to impact resistance have started to become importance. In literature, there is not much research on the effects of dynamic loads on structures and structural elements. Impact loads are also among these dynamic effects. Impact loads are important according to the intended use of the structure. During any impact event, the structure absorbs a large amount of energy in a short time. It is the components, additives and material ratios in the structure material that affect the impact strength of the structures. In addition to the studies on this subject in the literature, one of the most applied methods to determine the impact strength of the structure is the drop-weight test method.

Impact loads can generally be classified as low speed or high speed, but there is no clear distinction between these two types of impact loads in the studies. However, some of the studies suggested that low-speed impact should be expressed as low-speed impact to impacts with velocities up to 10 m/s depending on the rigidity of the structure, material properties and the mass of the impactor [115,116]. Generally, low

speed impacts are impacts that cause deformations in the internal structure of the material at the time of impact. At low- speed impact, the structure has sufficient reaction time to impact and therefore the structure can elastically absorb more impact energy. In high speed impact, a very small area is damaged because the reaction time of the structure against impact effect is not sufficient [115]. Although speed and energy values are used to determine the type of impact, classification can be made according to the damage done by the impact on the structure. Low-speed impacts are impacts that cause breaks in the structure, separation of layers in composite structures and rupture of fibers. High velocity impacts are impacts in which the object impact the structure completely affects the structure [116].

External loads such as bending, compression and tension affect concrete structures or structural elements during their service life. Therefore, more durable concrete structures are needed to improve the service life and durability of concrete structures and structure elements and to reduce the effects of these external loads on the structure. Recently, it has been determined that the bending, compressive and tensile strengths of concrete structural elements as well as the strength of these structures against impact loads should also be taken into account [117].

There are many methods applied to determine the impact strength of concrete structures. High velocity bullet impact and drop-weight tests are applied to determine the strength and energy absorption capacity of concrete and reinforced concrete structural members under impact loads [117].

The impact resistance of concrete structure elements is defined as the resistance shows against dynamic loads acting suddenly and repeatedly on concrete structure elements. Impact strength must be very high in concrete water structures, industrial structures, airport runways, piles, railway sleepers, military structures, nuclear structures and concrete structures exposed to explosive substances [117].

The resistance of conventional concrete to impact loads is very low, and cracks formed under these impact loads in concrete develop in an uncontrolled manner. As a result of these cracks, it causes losses in the performance of the concrete. Therefore, studies on improving this weakening feature of concrete have increased [117].

Many test methods can be used to produce impact load effects on the structure. In addition, there is no standard and / or test method accepted by any country, institution or researcher on this subject to determine the behavior of composite materials against impact loads. Therefore, it creates problems when comparing the results obtained from different impact tests on composite materials. Despite these negative situations, Drop-Weight Tests, Charpy & Izod Tests and Ballistic Tests are used today to determine the impact strength of composite materials [116].

In the Charpy and Izod impact test method, a pendulum is dropped on a notched test specimen from a certain height and subjected to impact. After the pendulum impacts the sample, the ascent height of the pendulum rises is determined and the difference between the energy of the pendulum at the height at which it is released and the energy of the pendulum at the height it exits after impacting the sample is the measure of the impact energy absorbed by the sample. If the lower the height that the pendulum rises after impact the sample, the higher the impact energy absorbed by the sample or the resistance of the material to impact or the toughness of the material [116].

Drop-Weight Test method is preferred for impact tests for composite materials in recent years. The most important reason for choosing this test method is that test variables can be determined more easily and test results can be analyzed much more easily. Some of these devices can record the load, acceleration and deformations on the sample at the time of impact. The results obtained with these devices can be converted into load-time, acceleration-time and impact energy-time data. With these data, relationships can be established between the values such as the load on the structure and the absorbed impact energy and the fractures in the structure [116].

Impact tests on composite materials have shown that the mechanical properties of composite materials against impact loads affect the impact test method, the structure of the impactor, the speed and mass of the impactor, the structure of the specimen and how the specimen is supported. For these reasons, it is necessary to pay attention to these issues in the impact tests made to determine the impact properties of the composite material [116].

In the drop-weight test method, the vertical weight is dropped by means of pipes or rails that guide the falling weight during fall. By knowing the height and weight of

the impactor on the device, the impact energy can be calculated [118]. In the impact test, the amount of energy absorbed by the material at the moment of breaking, impact energy is determined. This amount of impact energy detected is a measure of the material's toughness, brittleness and ductility [119].

Impact tests have shown that; brittle materials have low toughness as they can withstand small deformations. The temperature of the materials also affect the impact energy of the material. Generally, materials with low temperatures have low impact energy. For this reason, when choosing the material, the behavior of the material is important, such as at what temperature the material break as ductile or brittle, how much energy the material absorbs while breaking, and how much fracture energy is [120].

The force that occurs as a result of two or more objects colliding with each other in a short time is called impact. This force, which occurs in a short time on the structure, generally has more effect on the structure than the lower forces applied on the structure for a longer time. This effect varies according to the velocity of the objects at the moment of collision and the mass of the objects. Generally, during a completely inelastic collision, the structure can deform and this deformation absorbs all or part of the impact energy [118]. During this energy absorption, cracks and breaks can occur in the material. Every material has the capacity to absorb impact energy. In drop-weight test applications, this energy absorption capacity (impact energy) is found by the following formula:

Energy absorption capacity= impactor weight x impactor height x drop number [121]

$$E=mgh \times N \tag{1.2}$$

where E is energy (J), m is impactor weight (kg), g is gravitational acceleration (m/s^2) and N is drop number. Loss in testing is negligible.

In this study, some devices were used to obtain data on acceleration-time, load-time, load-displacement relationships during the drop-weight tests. The selection of these devices has been selected in accordance with the literature. Measuring devices used during the drop-weight drop tests carried out in this project [20]:

- Force Sensor
- Accelerometer
- Connection Cable
- Spring-Loaded Linear Potentiometer
- Data Logger

1.10.4.1 Force Sensor

Force sensors are sensing sensors with different geometries and mounting styles used to measure stresses, action-reaction forces on the structure in test setups or industrial works. These sensors are generally not easily damaged and are assembled according to the application of force. This transformation takes place with the help of sensors mounted on the structure connected to force sensor.

The force sensor device performs the conversion event indirectly in two steps. Mechanically perceived force causes changes in the shape of the force sensor. The sensor measures the shape change as an electrical signal. Because the voltage alters the effective electrical resistance of the wire [122].

1.10.4.2 Accelerometer

Acceleration refers to the change in velocity with time. When an impact load is applied to an object with mass, the object moves under the effect of this force. This movement varies depending on the force and time. This change refers to acceleration. The acceleration is expressed in units of m/s^2, ft/s^2 and g. Devices used to measure and record this change are called accelerometers. Accelerometers are a kind of sensor. These are the acceleration data types seen in Figure-1.7. Accelerometers are used to record these types of data [22].

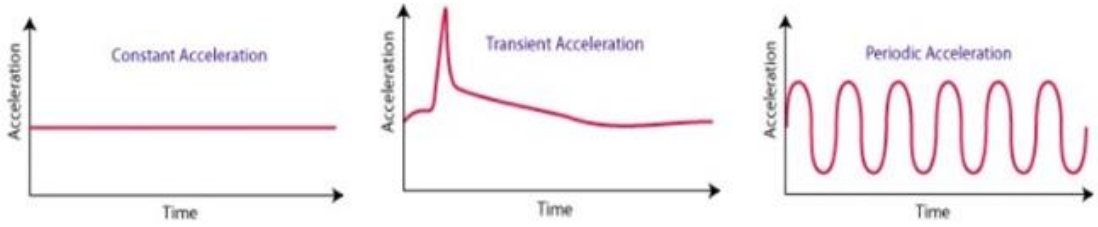


Figure 1.6 Samples of data source for accelerometer [22]

Accelerometers are devices that are used effectively in many areas. It is important to choose a suitable accelerometer for the purpose it will be used for. Accelerometers work in different ways [123].

Accelerometers are classified into two groups according to their purpose of use and types of source data [22]. These are;

- Piezoelectric Accelerometer
- Capacitive Accelerometer

Accelerometers are called piezoelectric accelerometers because they use piezoelectric materials in sensors. Microscopic crystals contained in piezoelectric accelerometers measure the acceleration of the force applied by the formation of electron movement between the two polars separated ends at the moment when the impact force is applied to the object and records the data [22]. This electron movement creates a voltage difference and an electric charge that can be measured on the object. There is a relationship between this electric charge and the charges applied to the object or dynamic effects, and data about the acceleration on the object can be obtained thanks to this electric charge. Quartz is the most commonly used piezoelectric natural material in sensors. In addition, materials such as polycrystalline and piezo-ceramic are produced and used in this type of sensors. Piezoelectric sensors are used to measure motions with non-zero acceleration values rather than measuring constant acceleration movements such as atmospheric pressure or gravity. Since there is no time-dependent change in constant acceleration movements, only the first moment signal value comes to the data sources as the source value. Therefore, piezoelectric sensors do not take measurements. These type of sensors are used to measure the change data of movements such as pressure and acceleration that change with time [22].

Other accelerometer sensors are capacitive accelerometers. Capacitive accelerometers are used to measure data with low frequency and constant acceleration. In this type of accelerometer, two plates with a certain initial position undergo a change in position due to movement, so it perceives the position change between these two plates as a linear signal [22].

The type of accelerometer used in drop-weight tests in the literature is piezoelectric accelerometers. To get the most accurate data from the piezoelectric accelerometer, it is mounted on a concrete sample with a brass cap. While determining the places where the accelerometers will be mounted on the concrete sample, attention should be paid to the maximum high sensitivity-high frequency relationship, and it is necessary to be very careful that there is no gap between the accelerometers and the concrete sample.

1.10.4.3 Connection Cable

Low Noise Coaxial Cables were used in the transmission of data between force sensor and data logger and between accelerometer and data logger used in drop-weight reduction tests in the literature. The cable provides lossless transfer of all high and low signal data between -90 °C and 260 ^{o}C temperatures [22].

1.10.4.4 Spring-Loaded Linear Potentiometer

In the literature, two symmetrical spring-loaded linear potentiometer were used to measure the beam deformations that will occur during drop-weight tests. Potentiometers are mounted on the beam using a connection apparatus. Potentiometers should be mounted symmetrically from the middle of the beam to the right and left sides of the sample [22].

1.10.4.5 Data Logger

Data Logger is a devise that is used to transfer the data taken from potentiometer, accelerometer, force sensor etc. to the computer. They are generally manufactured with multi-channel. According to the literature, two types data loggers were used in the experimental study. One of them was static type data logger was used to transfer the data taken from spring-loaded linear potentiometers to the computer. Another was dynamic type collector was used to transfer the data taken from accelerometers and force sensor to the computer [22].

CHAPTER 2

LITERATURE REVIEW

This chapter offers the history and recent development of self-compacting geopolymer concrete, nanoparticles, steel fiber, tyre rubber, effect of nano-silica, tyre rubber and steel fiber on fresh state, mechanical behavior and behavior under impact loading of self-compacting geopolymer concrete.

2.1 General

Geopolymer concrete (GPC) can show a considerable role in the state of environmental issues and sustainability. Approximately 5% of global CO_2 emissions creates from the cement production (OPC). According to Lawrance (Lawrance 1988) approximately 1 tone of CO_2 produces to atmosphere as a result of the manufacture of the 1 tone of OPC. In addition, other by-product cementitious material like slag (GGBFS) has been revealed to emit less greenhouse emissions than the manufacture of conventional OPC up to 80% (Roy and Idorn, 1982) and up to 80%-90% less greenhouse gas emissions emit in the manufacture of FA (Duxson et al., 2007). Therefore, a 100% replacement of Portland cement with FA or slag would considerably decrease the CO_2 emission of concrete manufacture. Previous researches conducted by (Davidovits, 1991; Rangan, 2010; Collins and Sanjayan, 1998) indicated that the development of new binders alternative to traditional cements commonly recognized as geopolymer can be found by the alkaline activation of various industrial by-products cementitious materials like FA and GGBFS. Geopolymer concretes are described by their low CO_2 emission and good mechanical performance.

In the late eighties, the specification of SCC for special preparations was realized by Japan. Their research represents a considerable technological advancement which lead to obtain a better quality of concrete, increased productivity, and improved the working medium on site (Zhu, 2003). SCC is featured by high flowability under its own weight such that it does not need any external or internal vibration to fill the

formwork and it can be pumped over long distances (Phan, et al., 2006). In SCC production, coarse aggregate amount is limited and mineral and chemical additives are generally used in the concrete mixtures. Some studies have been noticed in the literature on the usage of mineral additives to improve the properties of SCC (Zhu, 2003; Gesoğlu and Özbay, 2007). Gesoğlu and Özbay (Gesoğlu and Özbay, 2007) demonstrated that replacing fly ash with OPC improves the slump flow time, slump flow diameter, L-box height ratio, V-funnel flow time, and viscosity of SCC, while increasing the start and final set times of SCC. Consequently, the presence of very fine mineral additives in the components of the SCC, it has a very strict microstructure, never, the degradation behavior in SCC is till now fragile (Bignozzi and Sandrolini, 2006). SCC is a new idea and one of the latest developments in concrete technology for placement and placement that does not need vibration (Reddy and Kumar, 2017).

There is a lack of research in the literature regarding the use of waste tires in SCGC production. Though there are rare researches on the performance of slag based SCGC, there is a limited study on the mechanical performance of SCGC at ambient environment.

2.2 Nano-Silica

In 2004, the first industrial-scale use of nano-silica in cementitious composites was recognized. Brian Green who is a member of the US Army Corps of Engineers was a pioneer regarding use of nano-silica in order to build up a rock matching grout for military applications. His work emerged out of issues relating with segregation of grouts included of heavy weight aggregates especially hematite. The nano-silica was added to the heavy weight grout mixture as a viscosity-modifying agent. It increased the thickness of the grout mixture, guaranteeing the steady and universal suspension of the hematite aggregate while the grout was in a plastic state. The viscosity-modifying agent used was in the form of an ultra-fine shapeless colloidal silica or nano silica with a particle distribution ranging between 3 and 100 nm. Green discovered that the nano-silica not just upgraded the suspension of hematite and prevention of segregation but also improved the density and strength of the grout (Green, 2008).

It has been shown that the performance of NS regarding development of early strength comes from the large specific surface area (SSA) of free silica (Said and Zeidan, 2009). Similar to class-F fly-ash, the free silica provided by the NS combines with calcium hydroxide in the hydrating cementitious matrix to produce more C-S-H. Because of the smaller size of the NS particles, there is a greater total SSA of free silica which is available for faster pozzolanic reaction leading to increase in the strength at early ages and durability of concrete (Nazari and Riahi, 2011). In spite of the ever growing of the popularity of NS in concrete and composites of cement, a profound concept of the impact of NS is required in both the academic and construction fields to provide the industry confidence in this unique technology. At the present nano-technology was presented in the applications of civil engineering. It is one of the most promising fields of science. From this point on specialists in the field of concrete are studying NS as a new admixture. It has a very high ratio of amorphous silica very large SSA and tiny dimensions (Fallah and Nematzadeh, 2017).

Nano-silica is a silica-dioxide (SiO_2) nano-particle non-natural manufactured of porous and strictly aspheric particles with great possible advantages. The size of nano-particles is extremely small and about one per thousand of the cement particles size (Silica-Fume Association, 2005). It is a crystal composition produced in detail as sand, quartz and numerous other minerals. According to nano-silica composition particles are distributed by two levels in particles: S-type nano-SiO_2 (spherical particles) and P-type nano-SiO_2 (porous particles). P-type nano-SiO_2 poses much greater surface area compared with the other type of nano-SiO_2 (US Research nano-materials, 2015). P-type nano-SiO_2 has a few nano-porous with the pore ratio of 0.611ml/g. The size of NS particles ranges from 15 to 20 nm. NS is one of the best nominees to be utilized as an alternative material to Portland cement. It is well known that utilizing mineral replacement like nano-silica will develop the durability and strength of concrete, owing to the high dense fine particles, the larger surface area and the high SiO_2 content. Nano-silica is more selected than silica-fume because the size of NS particle is smaller than the size of silica-fume with a larger surface area. The fineness of NS particles affects the cement paste or mortar properties, where the pore size increases with increasing the fineness; this will result in increasing the pozzolanic reaction.

2.3 Steel Fiber (SF)

The geopolymer concrete has many benefits such as high mechanical properties, high resistance to fire and low creep and shrinkage as compared with OPC, but it is brittle and has low tensile and flexural strength (Farhan et al., 2018). Researchers explored adding of different kinds of fibers such as steel fiber in GPC to decrease its brittleness by the development of tensile and flexural strengths, energy absorption capabilities and fracture toughness of GPC (Farhan et al., 2018). Also, SF improves the load capacity, curbs the crack growth rate and width of the cracks; this is due to adding of SF in GPC, resulting in higher friction and higher clamping pressure (Shaikh, 2013; Ranjbar et al., 2016). The addition of SF increases the symmetry and homogeneity of concrete which increases its ductility. When the SF used in the concrete is randomly distributed, they curb the cracking mechanism and restrict the spread of the cracks, thus increasing ductility and strength of concrete (Wafa and Ashour, 1992). For structural applications, SF should be utilized mostly as an auxiliary reinforcement (ACI Committee 1988). The usage of the hooked-end steel fiber (HESF) and crimped round SF with dissimilar rates in the same concrete mix have affected the compressive and split tensile strengths (Vairagade and Kene, 2013). The effectiveness of SF in GPC depends on many factors comprising the volume fraction (V_f), SF geometry, aspect ratio (l/d) and tensile strength of SF (Aydın, 2013).

In general, l/d of SF utilized in concrete varies from 50 to 100 (Yazıcı et al., 2007). Likelihood of varied distribution of fibers in the concrete mix increases by increasing l/d. Moreover, volume fraction strikingly influences the workability of concrete. The best V_f values in mixtures of concrete are 0.5% to 2.5% by volume of concrete (Bentur and Mindness, 1990; Gambhir, 1986). When the ratio of SF in concrete exceeds 2%, it can improve ductility, as well as enhance the fracture toughness, strain hardening and some other mechanical properties of the concrete (Li, 1998). There are many shapes of SF available including hooked straight, crimped, twisted, single and collated (Soufeiani et al., 2016). The disadvantages of SF are that it reduces the workability and accelerated stiffening of concrete. Thus, increasing the conctruction labors and time because this requires more vibration to make the concrete workable. As well as increasing the dead load (Li, 2011). SF reinforcement

concrete can be classified based on its fiber volume percentage as follows (Behbahani et al., 2013);

*The very low volume fraction of SF (less than 1% per volume of concrete) which are used to control plastic shrinkage and as pavement reinforcement.

*The moderate volume fraction of SF (1% to 2% per volume of concrete) which have the ability to improve flexural toughness, impact resistance and further mechanical property of concrete.

*The high volume fraction of SF (more than 2% per volume of concrete) used for special applications like blast resistance structures.

In the class of high V_f, SF has an exceptional mechanical property and can be utilized without continuous reinforcement, nevertheless these composite materials are often used in highly specialized applications due to processing difficulty and high cost (Behbahani et al., 2013). SF cannot be used as the main reinforcement in reinforced and prestressed structural members, because it does not improve the flexural strength and it is discontinuous and randomly distributed throughout the concrete matrix. Therefore, the reinforcing performance of SF is inferior to the reinforcing bar and considerably more expensive than the conventional rods (Balaguru and Shah, 1992). Many types of SF are available as reinforcement. But mostly round SF is broadly used in engineering applications. Generally, the SF used in concrete as reinforcement has a diameter ranging in between 5-500mm specific gravity 7.8, modulus of elasticity 200GPa, failure 3-4% and tensile strength 1 to 3 GPa. Flexural strength and ultimate flexural strength are obtained through the using SF of short (6.4 to 63.5mm) and small diameters (0.15 to 0.91mm) (Mahadik et al., 2014).

2.4 Fresh State Properties of Geopolymer Concrete

Workability is the easiness of working with the fresh concrete for handing, placing, compacting and finishing. The geopolymer concrete has a viscous nature causing problems in the compaction; therefore SCGC has been invented. The high slump in geopolymer concrete means reducing stickiness and thus increasing workability (Deb et al., 2014). The workability depends on superplasticizers and the kind of alkaline activators (Nematollahi and Sanjayan, 2014). The extra water increases the

workability about 200% but decreases other properties about 27%. The workability increases about 115% by adding. Admixture, however, reduce other properties by 25% (Aliabdo et al., 2016). Generally, the GPC mixtures demonstrated more cohesion than the OPC mixtures, due to the ingrained difference in the flow of the geopolymer matrix and the traditional concrete matrix (Khale and Chaudhary, 2007). Workability may be a very important concern for a fresh FA-based GPC due to its extreme viscosity. Therefore, the use of superplasticizers should be studied in practice. A large increase in resistance causes a decrease in workability of GPC with an enormous amount of GGBFS and less sodium-silicate to sodium-hydroxide ratio (Deb et al., 2014). The design of concrete requirements depends on several factors including segregation resistance, passing ability and filling ability. For this, the coarse aggregate size should not override 20 mm many fresh state test such as slump flow time (T_{50}), slump flow, L-box, J-ring, V-funnel and U-box are utilized to determine the passing ability and flowability of concrete. Table-2.1 shows their limits according to EFNARC guidelines.

Table 2.1 The limits of fresh state tests of concrete as per EFNARC (2002)

Test	Unit	Minimum Value	Maximum Value
Slump Flow	mm	650	800
T_{50} - Slump Flow	sec	2	5
J - Ring	mm	0	10
V - Funnel	sec	6	12
L–Box (H_2/H_1)	mm	0.8	1.0
U–Box (H_2-H_1)	mm	0	30

Nuruddin et al. (2011) explored the influences of superplasticizer and sodium-hydroxide alkaline solution on the workability of SCGC by using different ratios of superplasticizer (3,4,5,6,7%) according to EFNARC (2002). They used a different molarity of Na_2SiO_3 and NaOH solution (8,10,12,14) M with remaining the ratios of other materials constant for all mixtures. In their experimental work, dry low-calcium FA (class F) as per ASTM C618 was utilized. Their results were satisfactory according to EFNARC requirements. Increase in molarity from 8 to 14 led to reduction the workability and low SP content (3, 4 and 5%) was poor in results of

passing ability, filling ability and the workability were not meet the requirements of EFNARC.

The use of nano-silica leads to reduce in the workability of concrete due to its great ability to absorb water (because it has very large SSA and their much finer dimensions compared to ordinary cement). The amount of NS above 3% volume content in the high strength concrete mixtures cannot be used when the ratio of water to cement is low, because NS possesses a big water decrease property which counteracts full hydration reaction (Fallah and Nematzadeh, 2017).

Generally, incorporation of fibers makes the SCC less viscous and do not permit the aggregates to move easily, this lead to a decrease in the workability. In addition, high V_f of SF decreases the workability to values lower than those allowed in EFNARC (Khaloo et al., 2014). The slump values are from 65mm to 100mm for the fresh GPC, while it is between 28.2mm and 27.5mm for GPC with SF (Sunilkumar and Amol, 2015).

Abdullah et al. (2017) conducted a practical experiment to demonstrate the influence of SF on the workability of GPC from FA and alkaline solution. They presented that the workability values of the GPC specimens without HESF was 100mm while the workability values of HESF specimens with ratios of 1,3,5 and 7% by weight were between 30mm to 60mm.

2.5 Mechanical Properties of Geopolymer Concrete

2.5.1 Compressive Strength

Compressive strength is a fundamental characteristical of concrete depends on some factors like w/c ratio, the strength of cement and cementitious material, quality of concrete and quality control during concrete production, coarse aggregate size and curing. The strength increases as the curing time and temperature increase. It can be obtained about 40MPa to 50MPa when the curing temperature is between 60^{o}C to 90^{o}C for a period ranging from 24 to 72 hours. Further, the compressive strength of GPC also depends on the smoothness of FA particles (smaller than 43 nm) (Van Chanh et al., 2008). Where the strength increases by increasing the smoothness of FA particles. The concentration of silicon is important to determine the strength of alkali activator. Thus, the existence of dissolved silicon in the water solution of

sodium-silicate clearly contributes to increasing of reaction velocity, therefore this lead to the increase compressive strength (Komljenovic et al., 2010). Maximum compressive strength was in the FA/GGBFS-based GPC with 30% GGBFS. Nevertheless, adding of 50% GGBFS is likely to decrease the strength at 28 days (Wardhono et al., 2017).

2.5.2 Bond Strength

The bonding between the reinforcement bar and the concrete is an important characteristic of the structures of concrete which must be taken into account. Bonding stress acts at the interface of reinforcing steel bars and surrounding concrete and allows transferring of tensile stress from the bars into the concrete and vice versa, because of the adhesion between the bar and concrete (Doguparti, 2015). There are two types of bonding anchorage bond and flexural bond. Chemically, the geopolymer binder differs from the cement Portland binder. Therefore, studying the bonding between the reinforcement bars is very important to know the bonding strength between GPC and bar (Sarker, 2010).

2.5.3 Fracture Property

The fracture mechanism is defined as the occurrence of failure and its spread through the structure. From a physical point of view, it is defined as separating the material into two or more parts, when enough stress is applied at the atomic level to break down the bonds that combine the atoms together. There are several reasons for fracture failure comprising, uncertainty in the loading impact of environment, the defects of materials and design and defects in construction and maintenance (Alyhya, 2016). Concrete is a brittle material having strength over 100 MPa may produce by conventional materials (Balaguru et al., 1992). Precipitation, shrinkage and thermal movement are major causes of cracks in non-structural sections, whereas it occurs due to excessive tensile stress in structural sections (Olek et al., 2004).

Fibers are a natural or synthetic substance that is significantly longer than it’s wide. It is utilized to improve the properties of concrete, such as compressive, flexural, toughness, ductility of post-failure and crack control. Currently, SF is utilized to develop the fracture behavior of concrete. It possesses higher fracture energy than normal concrete (Peng et al., 2006). Since the binder in GPC is quite different from

that available in OPC, thus the interaction between each of the geopolymer and aggregate needs to be studied. Therefore, it is essential to explore the fracture parameters of GPC to comprehend its failure behavior.

2.5.4 Effect of NS on Bond Strength of SCGC

Improving the interfacial transition zone between aggregates and mortar as well as between aggregates and steel bars are the best ways to enhance concrete bond strength. It is clear that utilizing deformed bars can extremely improve the concrete bars bond strength. There are three essential mechanisms that define the bond strength between the ribs adjacent to the reinforcing bar. These mechanisms are the bearing stresses against the faces of ribs (mechanical interlock), shear stresses, because of the adherence throughout the surface of the bar and the friction between bumps of bars and the surrounding concrete. Lately, those ways were done by using pozzolanic materials like nano-silica. Many properties were not studied sufficiently well such as the bond strength of NS concrete. The best proportion of NS to increase the bond strength of 12 mm bars is 3% by weight, the improvement in bond strength reached 38.5% as compared to the same mixture without NS (Serag et al., 2017).

Adak et al. (2017) proved that using 6% of NS in the FA-based GPC (curing at room temperature 25^{o}C) gives better bond strength than those are free from the NS (at heat curing 60^{o}C, 48h.) and conventional cement concrete (at water curing) for both mild and deformed steel bars.

2.6 Effect of NS on Mechanical Properties of SCGC

Nano-materials have excellent physical, chemical and mechanical properties that lead to a development of more effective materials than ones which are currently available. Currently, the nano-structured material technology increasing at an amazing quickness and will be applied widely with numerous materials (Li et al., 2004).

One of the most utilized nano-materials is nano-silica; it has more pozzolanic nature which gives strength, durability and impermeability to concrete. Ultra-fine particles of NS stop the voids of C-S-H structure which afford more homogenous spreading of hydrated products, which improves the strength and the durability of cement

composites (Gopinath et al., 2012). Nano-silica is being effectively used to reinforce geopolymer matrices to enhance the mechanical properties; it works to increase the reactions of the geopolymer and also to fill the voids. NS was added to high-calcium FA-based GPC cured at ambient temperature to decrease the setting time and improve shear strength (Phoo-ngernkham et al., 2014). It is utilized in self-curing GPC in order to enhance the mechanical properties of metakaolin based GPC when the curing temperature is 20^{o}C (Pacheco-Torgal et al., 2011). Furthermore, strenuous efforts have been made to use NS in alkali-activated materials as alternatives to Portland cement to reduce the negative environmental influences of the cement industry. The use of nano-silica in cement composites has two vital problems that must be studied well; one of these problems is the non-distribution of particles regularly in the concrete mixture. Some researchers showed that the proper ratio of NS should be small (1-5 wt %) to prevent agglomeration of particles through blending (Al-Amoudi et al., 2004; Qing et al., 2007). However, others researchers have shown that the properties of concrete may be enhanced with dosages up to roughly 10 wt% if these particles are distributed positively in the initial cementitious mixture (Al-Amoudi et al., 2004; Ji, 2005; Cwirzen, 2010). The other problem related to the usage of nano-silica in concrete is the high surface area that characterizes it which leads to an increase its need for water and thus decrease the liquidity of concrete (Cwirzen, 2010; Qing et al., 2006).

2.6.1 Effect of NS on Compressive Strength of SCGC

There is limited literature available for the effect of NS on the compressive strength of GPC perhaps the most prominent are:

Adak et al. (2014) conducted a Practical experiment to research the effect of adding different proportions of NS in low-calcium FA-based geopolymer mortar using various molar concentrations. They adopted four various ratios of NS addition (0,4,6,8 and 10% by mass). The results displayed that addition of 6% NA in geopolymer mortar improved the compressive strength at 28 days when cured at ambient temperature.

Deb et al., (2015) have tested the effect of NS on GPC using low-calcium FA (class F) and blended with GGBFS and OPC in small percentages to hurry the curing at

ambient temperature. In their experimental work, average particles diameter of FA (15 nm), rate about 3% of the binder and sodium-hydroxide (8M) and sodium-silicate were used. Several mixtures were taken in different proportions; every mix contained the same proportion of alkaline solution (40%) with a ratio of sodium-silicate to sodium-hydroxide of 2.0. Size of cube samples 50x50x50mm^3 was cast and compacted by a vibrator. The samples were cured at 20±2^{o}C (room temperature) and at a relative humidity of 70±10%. They found that the compressive strength of ambient cured geopolymer specimens improved with addition of NS at early ages. Furthermore, adding NS up to a dosage of 2% has led to increasing the compressive strength.

Gao et al. (2015) studied the influences of NS on compressive strength of eco-friendly alkali activated GGBFS/FA mixtures. In their study, many samples with dissimilar NS content (0,1,2,3%) and slag/fly-ash ratios (70/30 and 30/70) were taken. The samples were tested at the ages of 3, 7 and 28 days respectively. The average of compressive strength was calculated for every six specimens. Researchers have found that increasing NS content up to 2% has benefited the compressive strength at curing ages of 3, 7 and 28 days, this percentage has set higher compressive strength with higher slag content. While that, NS content higher than 2% showed a negative influence.

Naskar and Chakraborty (2016) explored the influences of different ratios of NS in low-calcium FA-based GPC. They used the aggregate as a dry saturated surface and $NaOH/Na_2SiO_3$ as a solution of 16M. At firstly, they cured the specimens for 48 hours and then treated at 60^{o}C for 48 hours. After that, it stored in the air until the testing. They determined the compressive strength of GPC for all mixtures without and with an addition of NS at 7 and 28 days. By casting the normal cubes specimens of size 150x150x150mm. GPC specimens presented nearly 80% of the compressive strength at 7 days, but 28 days the strength appeared to be reduced. Also, the addition of 3% and 6% did not offer satisfactory compressive strength at 7 and 28 days.

Nano-silica can be utilized to overcome the problem of heat curing of FA-based GPC and gives excellent mechanical properties in this regard. Adak et al. (2017) have added 6% NS in FA-based GPC specimens and compared with two other specimens. One of which was geopolymer without NS and the other was a normal specimen

containing OPC. After 24 hours of casting, NS modified geopolymer concrete samples were eliminated from the mold and cured at ambient temperature (27±2^{o}C). While the GPC samples without NS were cured at 60^{o}C for 48 hours with an oven. Further, these samples were reserved at ambient temperature till testing. The results displayed that the samples containing NS had higher compressive strength than others at different ages.

Assaedi et al. (2015) studied the effects of mixing procedures on mechanical properties of low-calcium FA (class F)-based GPC matrices containing NS by using the dry and the wet mixing methods for preparing geopolymer process. They used a blend of NaOH (purity 98% and 8M) and Na_2SiO_3 grade D as an alkaline activator. The ratio of alkaline solution to FA and Na_2SiO_3 to NaOH was 0.75 and 2.5 respectively. For dry-mix process, NS (dia. 18-25nm) was first added to the FA at the dosages of 0, 0.5, 1.0, 2.0 and 3.0% by weight and was dry-mixed for 5 min. to create the wet mix paste similar mixtures were prepared, but NS was added to the alkaline at first. After casting, all specimens were enclosed with nylon packaging and cured at 80^{o}C for 24 hours in a furnace before demold. Then, they were placed under ambient conditions for 28 days. The two methods were compared. In the dry-mixing method, results showed that addition of 1% NS has improved the compressive strength by 28%.

Phoo-ngernkham et al. (2014) explored the influence of NS on GPC using FA as a binder, they concluded that increasing NS content led to a diminution setting time and improvement of mechanical properties. Also, they found by microstructure analysis that NS content up to 2% densities the matrix and increase the reaction product, but higher NS content showed negative effects.

2.7 Effect of SF on Mechanical Properties of SCGC

2.7.1 Effect of SF on Compressive Strength of SCGC

Ramkumar et al. (2015) used two mixes of geopolymer based on 50% GGBFS so that each mixture contains either crimped stainless SF or crimped mild SF, they compared it with the same mixture but without SF to demonstrate the influence of SF on GPC. SF had an aspect ratio of 60. They mixed the three materials with the dry state and then added the alkaline solution composed of Na_2SiO_3 and NaOH. The

researchers concluded that the compressive strength increased by 2.25% when adding SF and was higher than the control mixture by 20%.

Sivakumar et al. (2014) have used glued SF with length of 35mm and diameter of 0.5mm having l/d of 70 at various V_f of 0.5, 1.0 and 1.5% in the GGBFS-based GPC activated by 12M of NaOH. A special invented stream room was used by them to curing the samples at 75^oC for 6 hours. The results displayed that the percentage of binder to the total aggregate of 0.3 and fine aggregate to coarse aggregate of 0.8 with 1.5% volume fraction of SF has obtained a maximum compressive strength of 54.77 MPa.

Yuvaraj and Srinivasan (2016) investigated the compressive strength of GPC. In their specimens, GGBFS was utilized as a binder with the addition of NaOH and Na_2SiO_3 as an alkaline solution. They used HESF of 60mm and 30mm length together in the specimens. They have observed that the specimen which consisted of 60% of 30mm and 40% of 60mm SF have given a maximum compressive strength (41.2 MPa) and they also concluded that shorter SF showed greater compressive strength.

Bernal et al. (2006) investigated the performance of GPC incorporating GGBFS as a binder and reinforced with SF. Their results showed that using of SF in the matrix decreased the compressive strength at early ages.

Ganesan et al. (2013) carried out a study on the influence of SF on the mechanical properties of low-calcium FA-based GPC. In their study, different volume fractions of crimped SF having l/d of 66mm and ultimate tensile strength of 800 MPa were utilized. They reported that utilization of crimped SF in GPC slightly improves the compressive strength. Especially at 1% where this ratio gave the greatest compressive strength compared to other ratios.

Bernal et al. (2010) conducted a practical experiment on the influence of SF on the mechanical properties of GGBFS-based GPC and concluded that the use of SF reduced the compressive strength.

Sayyad & Patankar (2013) studied the effect of crimped SF on low-calcium FA-based GPC activated by alkaline solutions ($NaOH+Na_2SiO_3$) with the solution to FA proportion of 0.35. They used a crimped SF having l/d of 50 with V_f of 0 to 0.5% at

an interval of 0.1% by mass. They concluded that the wet and dry densities of GPC composites increased with increase in SF content constantly. Abdullah et al. (2017) used the HESF in GPC using FA as a binder mixed with the alkaline activators. In their study, different amount of HESF 1, 3, 5 and 7% by weight were for preparing GPC; all the specimens were cured at ambient temperature until testing. The results revealed that the compressive strength of GPC increased as the HESF increase. The maximum compressive strength gotten was about 87.83 MPa at the 14^{th} day.

2.7.2 Effect of SF on Fracture Property of SCGC

Due to the brittle, low tensile strength and strain capacity of GPC, fibers are used to increase the tensile strength and improve post-cracking behavior of the material where the fibers bind the slots of cracks (Gopalaratnam and Shah, 1987; Guerrero and Naaman, 2000). The idea of insertion fibers as reinforcement in GPC is presented to improve the properties of GPC such as durability, flexural strength and fracture toughness. Several types of fibers such as steel, synthetic and glass were used as reinforcement in GPC (Vijai et al., 2010). The main object of using fibers is to contain the cracks and improve the fracture toughness of the brittle matrix by working to scale the micro cracks in the matrix. At the prefacing of micro cracking, the bridging activity of fibers blocks the opening and development of cracks. This activity raises the demand for energy to propagate the cracks (Dias and Thaumaturgo, 2005; Reis, 2006; Reis, 2007). Specific studies have been done to investigate the effect of SF on the fracture properties of GPC including.

Ding and Bai (2018) studied the fracture energy, fracture toughness and flexural strength parameters of the GGBFS-based GPC containing SF using three volume fractions of 1.0, 1.5 and 2.0%, and compared the specimens with others without SF through conducting three-point bending (TPB) test. The experimental results showed that the addition of SF meaningfully increased the fracture energy and fracture toughness. The fracture energy achieved the largest value when the volume content of fiber was 1.5%. A rough correlation between the residual flexural strength and equivalent was also noted.

Deepa et al. (2013) conducted an experiment to define the fracture parameters of fiber reinforced geopolymer concrete (M30 grade) and they compared the results

with that of conventional fiber reinforced concrete of the same grade using TPB test on notched prisms 100x100x500mm^3 with an effective span of 400mm and notch depth to beam depth percentage of 0.4 (notch depth=40mm). In GPC, cement was completely substituted by low-calcium FA. A blend of Na_2SiO_3 and NaOH solution was selected as the alkaline solution. According to the results, the fracture energy of GPC was more than Portland cement concrete by 80%. GPC also exhibited 10-40% more fracture toughness than the conventional concrete. The increase in fiber content has led to increasing the fracture energy and fracture toughness of both GPC and normal concrete. Fiber reinforced geopolymer concrete specimens exhibited 10-40% more fracture energy than reinforced concrete specimens.

Bernal et al. (2010) made a comparison between specimens of Colombian alkaline concrete based on alkali-activated GGBFS and specimens OPC type-1 in terms of the impact of incorporation SF on its fracture toughness properties using TPB test with a loading rate of 3 mm/s. In their study, the alkali-activation has been completed with a water glass solution of Na_2SiO_3 with a chemical composition of 32.4% SiO_2, 13.5% Na_2O and 54.1% of water and a solution modulus (M_s=SiO_2/Na_2O) of 2.4. The results revealed that the flexural toughness value of alkali-activated GGBFS was three times greater than the OPC at early ages of curing in both notched and continuous specimens.

Dahake and Charkha (2016) studied the effect of several types and aspect ratios of SF at a constant volume fraction of 2.5% by the weight of cement on flexural strength of SCC specimens by using beams of 150x150x700mm depending on one mix design with strength of 35 MPa (normal concrete). The result revealed that the flexural strength has enhanced with the addition of SF. The reason for this is that the fibers arrests micro cracks in the concrete.

2.8 Self-Compacting Rubberized Concrete (SCRC)

The waste rubber is an important part of the world's solid waste management problem and this problem continues to increase. The use of waste rubber at SCC can be seen as a positive step forward. For example, around 30 million waste tyres are produced each year in the UK, while around 1 billion waste tyres is produced each year worldwide. About half of these can be recycled, exported and stored or

stockpiled for illegal disposal. Since 2006, the European Union's Landfill Directive has banned the disposal of most waste tires as landfill material. As a result, if no alternative is found to dispose of these waste tyres in landfills, their disposal costs will increase and problems with illegal dumping or insufficient storage will continue to increase. It has the potential to cause fire risk and major environmental problems in illegal dumps due to waste tyres. In the last two decades, the use of waste tires as construction material, especially in concrete and asphalt mixtures, has gained importance in research as an alternative use for the consumption of this environmentally friendly waste material. (Airey and Collop, 2004; Ei-dieb and Abdelw, 2001; Eldin, 1993; Ganjian, Khorami and Maghsoudi, 2009). Using waste tyre rubber in SCC can contribute to reducing environmental problems. (Topçu and Bilir, 2009).

SCC, a special concrete material, is produced that has similar compression properties and does not require vibration / compression by adding superplasticizer to fresh concrete (Okamura, 1995). This new technology is increasingly being used in the construction industry to produce better quality, safer and eco-friendly concrete. Over the past 20 years, researches on SCC has made significant progress in improving the design, properties, manufacture and durability of SCC mixes. Among its many advantages, SCC with a similar water/cement ratio tends to be slightly stronger compared to ordinary concrete. The reason for this is that an interface with better adherence and less void structure between aggregate and cement mortar and the mixture does not need more vibration/compression. (Ahmadi et al., 2007).

The compressive and flexural strength of SCC was found higher than ordinary concrete. (B.1999-Turatsinze and Garros, 2008; Arshad Umar, 2011; Pons GE, Proust S., 2003; Domone, 2007).

The higher tensile strength of SCC is due to the increased homogeneity of SCC and the less voided microstructure of SCC. (Coppola, Cerulli and Salvioni, 2004; Turcy et al., 2006). The characteristic strength of SCC is at least equal to the strength of ordinary concrete and has a similar strength for the same quality concrete (Goodier, 2003). Since the water/cement ratio is low in SCC mixtures, the compressive

strength is generally between 40 MPa and 100 MPa. Tensile strength can equally be compared to ordinary concrete (Goodier, 2003).

However, previous researches have shown that although SCC appears to be a promising development in the concrete industry, it has a higher shrinkage crack than ordinary concrete. Turcy et al. (2006) stated that the shrinkage of SCC was 10-50% greater than the portland concrete. This is because SCC increases paste volume, which increases shrinkage in the mix. This is because it increases the volume of paste, which increases shrinkage in the SCC mix (Qadi et al., 2009). At the same time, other studies noticed that the shrinkage of SCC is similar to ordinary concrete with the same compressive strength. (B.1999; Pons GE, Proust S., 2003).

2.8.1 Properties of Rubberized Concrete

One of the possible methods of using waste tyre rubber is to replace natural aggregates in the concrete mix.

2.8.2 Fresh Rubberized Concrete Properties

2.8.2.1 Workability of Rubberized Concrete

Fresh concrete is a concrete in a plastic state that can take the shape of any formwork. One hundred percent compression of fresh concrete is a significant parameter to ensure maximum strength of concrete. A concrete with high workability property can provide full compaction. The workability of concrete is the state how easily concrete can be mixed, placed and compacted. Holmes, Browne and Montague (2014) observed a decrease in the workability of concrete according to the increase in the quality and amount of crumb rubber used in the concrete mix. The reduction may be due to reduced adherence between rubber and other materials in the concrete mix. This decreasing may be due to reduced adherence between rubber and other materials in the concrete mix. Dong, Huang, and Shu (2013) reported that concrete workability decreases as the amount of rubber increases in the concrete mix. Youssef et al. (2014) stated that the workability of the waste tyre rubber-containing concrete mixture can be improved by using the appropriate amount of superplasticizer (1-3% by weight of cement). Bravo and De Brito (2012) explained that concrete mix containing mechanically ground waste rubber aggregate had a lower slump rate than those without it. Pacheco-Torgal, Ding and Jalali (2012) reported that when coarse

crumb rubber were used up to 15% by volume instead of partially coarse aggregate in the concrete mix, the slump of the concrete mix increased, but decreased above 15%. When fine crumb rubber was used instead of fine aggregate, the slump reduced of up to 15%, but showed uneven values above 15%.

2.8.3 Hardened Rubberized Concrete Properties

2.8.3.1 Compressive Strength of Rubberized Concrete

Ganjian, Khorami and Maghsoudi (2009) reported the reasons for the decrease in the compressive strength of rubberized concrete. (a) Aggregates shall be surrounded by cement mortar including rubber particles. This cement mortar would be much softer than rubber-free mortar. This causes rapid cracking around rubber parts during loading and rapid deterioration of samples. (b) The bond between cement mortar and aggregates is stronger than the bond between rubber particles and cement mortar. This can cause cracks due to the fact that the stresses that occur on the structure are not evenly distributed. (c) Compressive strength depends on the mechanical and physical properties of the materials used in the concrete mixture. If some of the materials in the concrete mix are rubber, it causes a decrease in the compressive strength of the concrete. (d) Owing to the low specific gravity of rubber and its weak bond with other concrete materials, the rubber tends to move upward during vibration of the structure, resulting in a greater amount of rubber in the upper layer of the structure. This kind of mixture causes a decrease in the compressive strength of concrete samples that are not homogeneous.

Al-Akhras and Smadi (2004) researched the properties of concrete mortars containing rubber ash. An increase was observed in the compressive strength of concrete, in which rubber ash was used instead of fine aggregate up to 10% in its mixture. The use of 14, 21, 29 and 45% rubber ash in the concrete mixture increased the compressive strength of the concrete on the 90th day by 2.5, 5, 7.5 and 10%, respectively. Gesoglu et al. (2014) stated that rubber has a negative effect on the compressive strength of permeable concrete due to the movement of rubber in the concrete. As the amount of rubber in the concrete mixture increases, the decrease in the compressive strength of the concrete increases. It has been observed that there is a maximum decrease in the compressive strength of concrete samples containing a mixture of crumb rubber and rubber chips. Holmes, Browne, and Montague (2014)

stated that by using crumb rubber up to 20% of the amount of aggregate instead of aggregate in the concrete mix, significant decreases in the compressive strength of concrete can be prevented. Ganjian, Khorami and Maghsoudi (2009) reported that since crumb rubber is used instead of aggregates, the compressive strength of concrete is 10-23% and the compressive strength is reduced by 20-40% since rubber ash is used instead of cement. Dong, Huang and Shu (2013) investigated the properties of rubber concrete, which is uncoated rubber in the concrete mix and coated rubber with a silane coupling agent. It has been stated that the compressive strength of the coated rubber concrete is significantly increased, as an improved interface is formed around the rubber particles due to chemical bonding. Hereaaguluchi and Panesar (2014) stated that significant improvements were observed in the compressive and tensile strength of batons containing rubber and silica fumes in their mixtures. Youssef et al. (2014) stated that there is no significant effect on the compressive strength of concretes in which crumb rubber is used instead of 3.5% mineral aggregates in its mixture. Concrete with untreated rubber in its mixture increased the compressive strength of concrete with untreated rubber by 15% in 28 days compared to concrete with treated rubber and NaOH.

2.8.3.2 Flexural Tensile Strength of Rubberized Concrete

Ganjian, Khorami, and Maghsoudi (2009) stated that the use of partially rubber chips instead of coarse aggregates in the mixture showed a decrease of 37% in the flexural strength of concrete, and a 29% decrease in the use of partially rubber ash instead of cement in the mixture. Su et al. (2015) observed that when 20% fine aggregate and rubber aggregate were replaced in the mixture, there was a 12.8% reduction in the bending strength of concrete. It was stated that the smaller the size of the rubber particles in the concrete mixture, the lower the loss in the strength of the concrete. This may be due to the fact that rubber parts increase the compactness of the concrete, reducing the voids in the internal structure due to the small rubber particles filling the voids and thus reducing the possibility of breaking the concrete. Aiello and Leuzzi (2010) observed that when waste rubber particles are used instead of coarse and fine aggregates in the mixture, there are more losses in the bending strength of concrete. Elchalakani (2015) explained that adding silica fume to the mixture and decreasing the water / cement ratio increased the flexural strength of rubberized concrete. Since the silica fume increases the interface transition zone

bond of the concrete, the decrease in the strength of high strength rubberized concrete was less than that of normal strength concrete. Gupta, Chaudhary and Sharma (2014) stated that as the amount of rubber ash increases in the mixture, the bending strength of concrete decreases, and the flexural strength of concrete containing 10% rubber ash and varying proportions of rubber fibers increases as the amount of rubber fiber (aspect ratio 8-10) increases. Yılmaz and Değirmenci (2009) stated that the bending strength of concretes using up to 20% rubber (in fiber form) in the mixture is higher than the control samples. The bending strength of concrete decreases if the amount of rubber in its mixture is between 20-30%. The samples with rubber fibers showed deformation without complete dispersion, while control samples showed brittle deformation and split into two pieces shortly after cracks formed on the samples. Ganesan, Bharati Raj, and Shashikala (2013) observed an increase in flexural strength of SCC as the amount of rubber in SCC mix increased. It was stated that when the rubber content in the mixture was 15% and 20%, the bending strength of the concrete was 15% and 9% higher than the bending strength of the control samples, respectively. Segre and Joekes (2000) studied on the flexural strength of concrete containing imported rubber and NaOH treated rubber in the concrete mix. The bending strength of concrete samples in both cases was stated to be higher than the control samples. Al-Akhras and Smadi (2004) investigated the properties of concrete with rubber ash. It has been reported that there is an increase in the bending strength of concrete when rubber ash is used instead of fine aggregates up to 10% in the mixture. Concretes with 2.5%, 5, 7.5 and 10% rubber ash in their mixture, respectively, the increases in 28-day curing compared to the control mixture are 12, 27, 32 and 43%, respectively.

2.8.3.3 Modulus of Elasticity of Rubberized Concrete

Gesoglu and Guneyisi (2011) observed that the changes in compressive strength and in the modulus of elasticity were similar. With the addition of rubber into the concrete mix, the compressive strength of the concrete decreased and the elasticity module of the concrete was similarly reduced. As the amount of rubber in the concrete mixture increases, the paste amount of the concrete decreases, which has caused a significant decrease in the elastic modulus of the concrete. Ganjian, Khorami and Maghsoudi (2009) stated that when using 5-10% chipped rubber instead of aggregate in the mixture, 17-25% decrease in the elastic modulus of the

concrete and 18-36% decrease in the elastic modulus of the concrete when using 5-10% powder rubber instead of aggregate in the mixture.

Dong, Huang, and Shu (2013) investigated the properties of concrete containing uncoated rubber and concrete containing rubber coated with a silane coupling agent. It has been stated that the rubberized concrete module is lower than the control sample. As the amount of rubber in the concrete mix increases, the concrete's modulus decreases. Coated rubber concrete has a higher modulus than uncoated rubber concrete because coated rubber has a stronger chemical bond in the mixture. Pelisser et al. (2011) stated that concrete with rubber in its mixture has less hardness than the control sample. It was noticed that the average decrease in the elastic modulus of the concrete containing rubber in its mixture was 49% less than the decrease in the compressive strength of the concrete

2.8.4 The Combined Effect of NS and SF on Properties of SCGC

Currently, crumb rubbers are used as a composition of cement concrete. According to previous studies: many features of concrete greatly improve after adding crumb rubbers. However, crumb rubberized concrete applications are limited due to low tensile and compressive strengths. For the possibility of improving these properties. Wang et al. (2018) have carried out a laboratory experiment by adding NS and SF by different percentage to this type of concrete. They concluded that the compressive and splitting tensile strength of crumb rubber concrete enhanced by using NS and SF as additives.

Ozakca et al. (2018) conducted a laboratory experiment to investigate the sectional effect of SF and NS on the compressive strength of alkali-activated GGBFS/FA concrete combined cold-bonded FA aggregate. The researchers relied on both NS having SSA of 170-230 m^2/g and HESF with a yield strength 1500 N/mm, young modulus=200 GPa, density=7850 kg/m^3, length=30mm and l/d=54.55. They used 0.2% of NS together with different percentages of SF (0.5, 1.0 and 1.5%). The specimens were cured at ambient temperature. They have found that the incorporation of SF did not markedly improve the compressive strength expect when utilized with NS. The maximum compressive strength of 40-56 MPa was reached at the combined use of 1% SF and 2% NS.

The researchers have noted that when adding SF and NS to the SCC, a reverse effect occurred in the workability, so they have increased the proportion of SP to keep within the limits of specifications. They also noted that the combined effect of 4% NS with 1.5% SF have given a better effect on hardened properties. As compared with the other used ratios in their experiment (Gorgis et al., 2016). Elboghdadi et al. (2015) also explored the combined effect of NS and SF on the mechanical performance of concrete. In their study, NS with a particle size of 9 to 20 nm as part cement replacement by 1, 1.5, 2 and 4, and 0.45, 0.9 and 1.35% was used with HESF made of low-carbon steel wire having a length of 30 mm and a diameter of 0.8 mm. The samples were reserved at ambient condition for 24 hours then they were demoded and saved in 22-25^{o}C water until testing. The results presented that the optimum ratios of NS and SF were 2 and 0.9% respectively, this ratio led to improving the elastic modulus about 94%. The flexural strength improved about 88% for specimens of 2% NS and 1.35% SF, compared to specimens without NS and SF.

Zhang et al. (2014) have used two methods according to ASTM C1018 and DBV-1998, respectively, by utilizing of TPB test to calculate the flexural toughness of the concrete with high performance containing FA, NS and SF. They observed that the utilizing of SF in concrete had an important development in flexural toughness values (15, 110, 120, 130) and coefficient of variation of the flexural capacity of concrete containing 15% FA and 5% NA.

2.9 Impact Test

Soe et al. (2013) investigated the behavior of elements prepared with a cement-based composite mixture designed with PVA and steel fibers, for which they aim to have better strength and energy absorption ability under high-speed impact loads (ballistic impact test). In this context, panels with dimensions of 300 mm * 170 mm * 50 mm were produced and the different materials and amounts of the mixtures were used in the mixtures. As the amount of PVA and steel fiber in the concrete mixture increased, the energy absorption ability of the sample and its resistance to impact loads increased. In the sample prepared with hybrid ECC mixture, micro-scale crack development was observed in a wide area except for local impact damage. It was observed that as the amount of PVA and steel fiber in the concrete mixture increased, there was less crack formation on the sample.

Radnic´ et al. (2015) studied that firstly, traditional two-sided reinforced concrete slab and the one that is reinforced with carbon fiber polymers were experimentally tested. In this experimental study, hammer weight and drop height are variable. In the experimental study, the impactor with 4,208 kg was dropped from 1, 2, 3, 4 and 5 meters, respectively. Then the elements were tested by dropping the 1,621 kg impactor from 1,2,3,4,5,6,7 and 8 meters, respectively. Before this impact test, the element under the same conditions was subjected to flexural test. Given the force at the moment of collapse in flexural strength test, the measured impact force is approximately twice this during impact test. The slab stiffness is greatly affected by the magnitude of the impact force. Repeated drops reduce the stiffness of the previous one each time. Accordingly, although the height of the drop increases, the measured impact force decreases. As a results of the tests, only the bearing capacity of the carbon fiber reinforced slab has increased compared to conventional concrete slab.

Doo-Yeol Yoo et al. (2015) examined the effects of reinforcement ratio on bending effect in concrete reinforced with high performance steel fibers. In this context, they manufactured 4 beams and subjected them to an impact test in the drop-weight test setup. The impactor height is constant in all tests. The moment of impact kinetic energy and speed are 4.2 kj and 5.6 m/s, respectively. In addition, numerical modeling was performed using nonlinear analysis methods. The increase in the ratio of reinforcement has increased the impact resistance performance of the samples. With the increase in the reinforcement ratio, the maximum and permanent deformations in the beam decreased. With the increase in the reinforcement ratio, there was a decrease in the maximum crack width that occurred in the tests performed with constant impactor height.

Zhan et al. (2015) investigated the behavior of reinforced concrete beams under high velocity impact. Impact Tests were performed using flexural strength test and drop-weight test. They obtained data on impact load, beam midpoint displacement, crack profile and strain during the tests. In this context, they produced 6 beams with shear reinforcement. Experimental elements were produced according to two different concrete classes. The impact test was carried out using the drop-weight test setup.

The impactor weight was 33.6 kgf and the drop heights were different. The flexural strength tests result; the stiffness and load carrying capacity of beam increase with the increase of reinforcement ratio and concrete strength and the maximum deformation decreased. Even if the stress or strain rate in the beam increases, the bearing capacity does not increase when the bending load capacity of the beam reaches the point where it cannot increase for a certain drop mass. The impulse resulting from the impact is directly proportional to the momentum of the colliding masses, and this situation changes with the bearing of the falling weight by the beam or the bounce. The maximum and permanent deformation impact energy is almost directly proportional to the impact energy and this proportion can be calculated empirically using the inverse of the flexural strength capacity of the beam.

Ivañez et.al (2014) investigated analytically and empirically the behavior of composite sandwich beam against low speed impact load. The prepared analytical models were compared with the experimentally obtained data. When the dimensionless global stiffness is decreased, the maximum impact force decreases, however the collision time increases. When dimensionless global stiffness is increased, the maximum impact force and collision time tend to reach a stable point. Increasing the initial velocity in the drop significantly increases the maximum impact force and there is a linear regression relationship. However, the collision time remains constant around a certain value.

Xu et al. (2010) examined the behavior of normal, lightweight and PVB (Polyvinyl Butyral) aggregate resin beam concrete specimens containing PVA fibers under impact loads under the ASTM E23 standard Charpy Impact test. In this context, different mixed elements have been produced and tested. However, the impact energies were calculated theoretically and compared with the test results. PVB-PVA mixed composite mixture has higher energy absorption capability than conventional concrete and lightweight concrete. The reason for this is that PVB, when used as aggregate, has a very high surface bond energy with the cement matrix. PVB is a hydroxyl group material and intermolecular hydrogen bonds can be established in the mixture. The addition of small volumes of PVA fibers to the mixture increased the impact resistance and energy absorption ability of beam samples and energy absorption ability. In this way, its resistance to impact loads and energy absorption

capability is higher than normal concrete and light concrete. the improvement in impact energy and the formation of the multiple crack mechanism show that the strength of the bond between the surfaces between PVB and PVA is very high in the PVB composite mixture reinforced with PVA, compared to normal concrete and light concrete.

CHAPTER 3
EXPERIMENTAL STUDY

The main purpose of the experimental study was to estimate the impact resistance or energy absorption capacity of SCGC specimens with SFs, NS and RTR. Also, their splitting tensile strength, flexural tensile strength, compressive strength and modulus of elasticity were determined.

3.1 Materials

3.1.1 Binder

The industrial waste material GGBFS was used as a binder to produce the SCGC mixes. GGBFS with a specific surface area and specific gravity of 418 m^2/kg and 2.79 kg/m^3 respectively, was utilized in the study. The chemical compositions and physical characteristic of GGBFS were shown in the Table 3.1.

3.1.2 Ground Granulated Blast Furnace Slag (GGBFS)

Slag is a by-product of iron production in iron and steel plants. After the BFS is cooled very rapidly and form to the granule, it is GGBFS is obtained. The obtained GGBFS can be used by adding it to cement or adding it separately in the concrete mix. GGBFS does not have binding feature alone, but when used together with Portland cement in concrete mix, GGBFS gains binding feature. Since it contributes positively to the physical and mechanical properties of both fresh and hardened concrete, GGBFS has been used within the scope of this study, as shown in Figure 3.1 below and the technical characteristics and chemical components of which are given in Table 3.1.



Figure 3.1 GGBFS used in the study

3.1.3 Nano-Silica (NS)

In this study, one of the materials used to produce the SCGC mixes was NS. NS is highly pozzolanic material containing very fine particles which is smaller than the particles of cement about one thousand times. The specific surface area and specific gravity of NS were 150000 kg/m^2 and 2.2 g/cm^3 respectively. The amount of NS was used as 2 % by weight of the GGBFS material. The pH value of NS in 4% dispersion was in the range of 3.7 and 4.7 and the particle size was 14 nm. The NS was replacement by the weight of GGBFS. NS used in this experimental study was manufactured by AEROSIL (domestic USA-CHEMTREC), (domestic Canada-CANUTEC) which is shown in Figure 3.2. In the Table 3.1, the chemical compositions and physical characteristic of NS were presented.



Figure 3.2 NS used in the study

Table 3.1 Chemical & physical characteristic of NS and GGBFS

Component	CaO	SiO_2	Al_2O_3	Fe_2O_3	MgO	SO_3	K_2O	Na_2O	LOI	SG	BF (m^2/kg)
NS (%)	-	99.8	-	-	-	-	-	-	<1.00	2.20	-
GGBFS (%)	34.12	36.40	11.39	1.69	10.30	0.49	3.63	0.35	1.64	2.79	418

3.1.4 Steel Fiber (SF)

The most advantage of concrete as structure material is that it has high mechanical performances. Concrete, a semi-brittle material, has a high compressive strength but a very low tensile strength. Therefore, SF with high tensile strength is added to the concrete in order to increase the tensile strength of the concrete. Moreover, these SF not only increase the tensile strength of concrete, but also contribute to the mechanical properties of concrete such as ductility and toughness. In this study, two types of the hooked-end SF were used at 0%, 0.5% and 1% as shown in the Figure 3.3. These SFs were Dramix 60/80 and Kemerix 30/40 hooked-end which were commercially available and Table 3.2 shows the aspect ratio and geometrical characteristic of SFs.



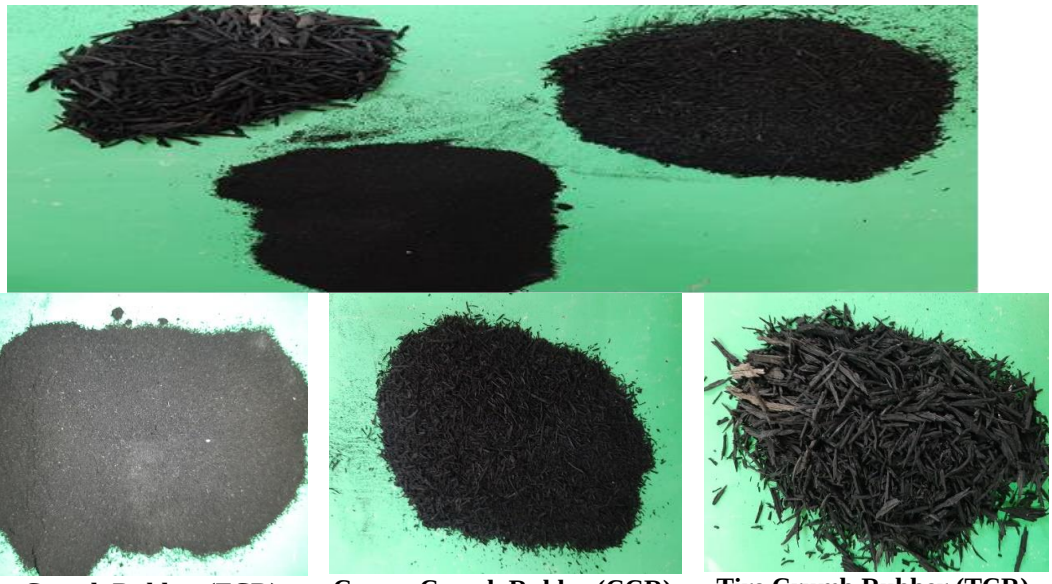
Figure 3.3 SFs used in the study

Table 3.2 The aspect ratio and geometrical characteristic of SF

Designation of Steel Fiber	Diameter (mm)	Length (mm)	Aspect Ratio
SF_1	0.75	30	40
SF_2	0.75	60	80

3.1.5 Recycled Tyre Rubber (RTR)

In the study, the three types of RTR materials were used as shown in the Figure 3.4 and were replaced with aggregates. These were fine crumb rubber (FCR), coarse crumb rubber (CCR) and tire crumb rubber (TCR). Moreover, these were replaced with 10% and 15% of coarse aggregates and, 10% and 15% of crumb rubber (CR) was replaced with coarse and fine aggregates. Moreover, coarse crumb rubber (CCR) and fine crumb rubber (FCR) replaced by equal proportions of 5% and 5% or 7.5% and 7.5% in the production of rubberized SCGC, respectively. Table 3.3 presents the physical properties and the sieve analysis of RTR.



Fine Crumb Rubber (FCR) **Coarse Crumb Rubber(CCR)** **Tire Crumb Rubber (TCR)**

Figure 3.4 RTR used in the study

Table 3.3 The sieve analysis & physical properties of RTR

Sieve Size (mm)	16	8	4	2	1	0.5	0.25	Fineness Modules	Specific Gravity	Absorption (%)
Coarse Crumb Rubber	12.2	21.8	33.5	81.7	100	100	100	2.23	0.83	2.2
Fine Crumb Rubber	11.1	47.4	86.3	100	100	100	100	1.97	0.48	1.8
Tyre Crumb Rubber	5.3	9.6	24.6	53.8	89.6	100	100	3.88	1.02	2.9

3.1.6 Aggregates

The coarse aggregate utilized in this study was the crushed limestone whose grain size is between 5 and 11 mm as shown in the Figure 3.5. As the fine aggregate, the crushed sand was used whose grain size is smaller than 4 mm as shown in the Figure 3.5. The crushed limestone coarse and fine aggregates were achieved from the original source utilized to produce the SCGC mixes. Table 3.4 presents the physical properties and the sieve analysis of aggregates.



Figure 3.5 Coarse and fine aggregates used in the study

Table 3.4 The sieve analysis & physical properties of aggregates

Sieve Size (mm)	16	8	4	2	1	0.5	0.25	Fineness Modules	Specific Gravity	Absorption (%)
Fine Aggregate	100	100	100	67.3	39.9	28.4	16.4	2.57	2.45	1.5
Coarse Aggregate	100	31.5	1	0.5	0.5	0.5	0.4	5.66	2.72	2.4

3.1.7 Superplasticizer (SP)

Superplasticizer is a chemical addmixture used to prevent the separation of concrete and to increase flowbility of fresh concrete without changing the mechanical properties of fresh concrete. In addition, when these chemical addmixtures are used in concrete mixture, they contribute to the reduction of the water/cement ratio without any adverse effect of the workability of fresh concrete. In this study,

commercially available MasterGlenium-RMC-303 superplasticizer was used, whose technical properties are given in Table 3.5 and as seen in Figure 3.6. Poly-carboxylates ether shown in Figure 3.6 with the specific gravity of 1.1 kg/m^3 and density of 1.095 g/cm^3 was utilized in this research as a superplasticizer.

Table 3.5 Technical properties of MasterGlenium-RMC-303 superplasticizer [124]

Structure of the Material	Modified Polycarboxylic Ether Based
Appearance	Green
Specific gravity @ 20°C	1.023-1.063 kg/litre
pH-value	5 - 8
Alkali content (%)	≤ 3.00 (by mass)
Chloride content (%)	≤ 0.10 (by mass)
Corrosion behaviour	Contains only components according to BS EN 934-1:2008



Figure 3.6 MasterGlenium-RMC-303 superplasticizer

Advantages [124]

- MasterGlenium-RMC-303 is used in the concrete mix during the production of structural elements in the concrete industry, allowing the concrete to gain self-compacting concrete property (slump 60-70 cm) and optimize the concrete.
- MasterGlenium-RMC-303 has been developed especially for hot weather conditions.
- MasterGlenium-RMC-303 improves concrete's early and final compressive strength, tensile strength, adherence to steel and impermeability properties more than conventional superplasticizers containing naphthalene and melamine sulfonate.
- MasterGlenium-RMC-303 improves the carbonation of concrete, its resistance to chlorine ion, its resistance to chemicals, its mechanical properties such as shrinkage and creep.

- MasterGlenium-RMC-303 allows concrete production at low water/cement ratio.
- MasterGlenium-RMC-303 reduces the production, casting, setting and curing times of concrete and also minimizes the energy required for production by reducing the temperature of the concrete, thus providing maximum economic efficiency.

3.1.8 Alkaline Solution

The alkaline activator was prepared by mixing of NaOH solution and Na_2SiO_3 solution at the room temperature. These alkaline activator was made ready 24 hours before using in SCGC mixtures. The Na_2SiO_3 solution was commercially available with components ratio (SiO_2: 29.4, water: 55.9% and Na_2O: 13.7% by mass) and was obtained from a local supplier (ZAG Kimya). The NaOH was present in solid form as pellets [125]. The NaOH pellets were got from KOSFLAKE Company and technical properties of NaOH as shown in the Table 3.6. These solid pellets were dissolved in water to obtain a NaOH solution with the necessary concentration. The NaOH had 97-98% purity. In the study, the molarity of NaOH was designed as 12M (molar) because, according to many researcher the best performance of SCGC is obtained at the 12M NaOH solution [126]. Initially, NaOH solution was prepared dissolving NaOH pellets in water. After a while, Na_2SiO_3 solution and NaOH solution were blended. This process was carried out 24 hours before casting, since the prepared alkaline activator solution should be used within 24-36 hours after mixing. Na_2SiO_3 to NaOH ratio was 2.5 in the experimental. This ratio was generally selected between 1.5 and 2.5 due to economic reasons [127]. The prepared sodium-silicate is shown in the Figure 3.7 a,b and sodium-hydroxide is shown in the Figure 3.7 c,d.

Table 3.6 Technical properties of NaOH-sodium hydroxide [128]

Chemical Name	Sodium Hydroxide
Chemical Formula	NaOH
Molecular Weight	39.9971 gr/mol
Color	Beyaz Sıvı
Density	2.1 gr/cm^3
Melting Point	318^oC
Boiling Point	1390^oC



Figure 3.7 (a) & (b) Sodium silicate-Na_2SiO_3, (c) & (d) Sodium hydroxide-NaOH

3.2 Concrete Mix Design and Mixing Procedure

In this study, fully eighteen (18) SCGC mixes were designed and total thirty-six (36) beam specimens were produced in two series as shown in the Table 3.7. For the first series, the SCGC samples with NS (0 and 2%) the SF_1 (Kemerix 30/40), and SF_2 (Dramix 60/80) were utilized with ratios of 0, 0.5 and 1%. For the second series, the SCGC samples with SF_1 (0 and 1%) and RTR (CCR, FCR and TCR) (0, 10 and 15%) were produced. CCR represents coarse crumb rubber, FCR represents fine crumb rubber and TCR represents tyre crumb rubber. This experimental study consisted of all mixes of SCGC with a constant binder content of 500 kg/m^3; all mixes contained slag for each mixture and the alkali activator/binder ratio was kept constant for all mixes as shown in Table 3.7. The study is to determine the combined and individual effects of SFs, NS and RTR on the hardened and fresh states performance of SCGC mixtures.

To achieve the SCGC mixes, the mixing sequence was as following; both aggregates under saturated surface dry condition, GGBFS and NS were firstly mixed in dry state for 2.5 minutes. The prepared alkaline solution was added, then SP and extra-water were added in 1 minute to the dry mix and kept mixing simultaneously and thereafter

they were swiftly mixed for 2 minutes. After that, if mixture contained SFs (SF_1 or SF_2) or RTR (CCR or FCR or TCR), SFs was added to the mixture. Subsequently, the mixture was further mixed for extra 3 minutes to confirm uniformity and homogeneity of SCGCs mixes. The complete mixing procedure is shown in the Figure 3.8.a and Figure 3.8.b, and SCGC production is shown in the Figure 3.9. Moreover, molds of all specimens before and after casting are shown in the Figure 3.10 a and b respectively. Moreover, produced SCGC beam specimens are shown in the Figure 3.11.

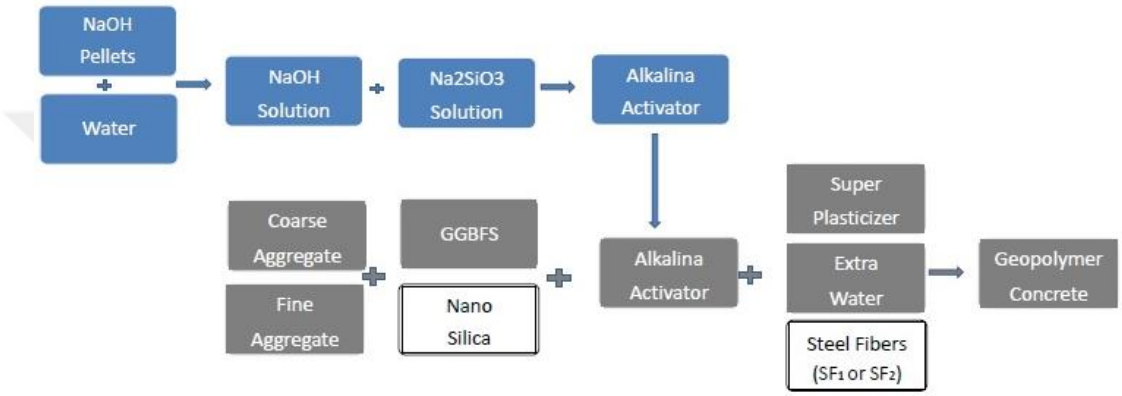


Figure 3.8 Preparation of alkali activator and SCGC specimens with NS production procedure

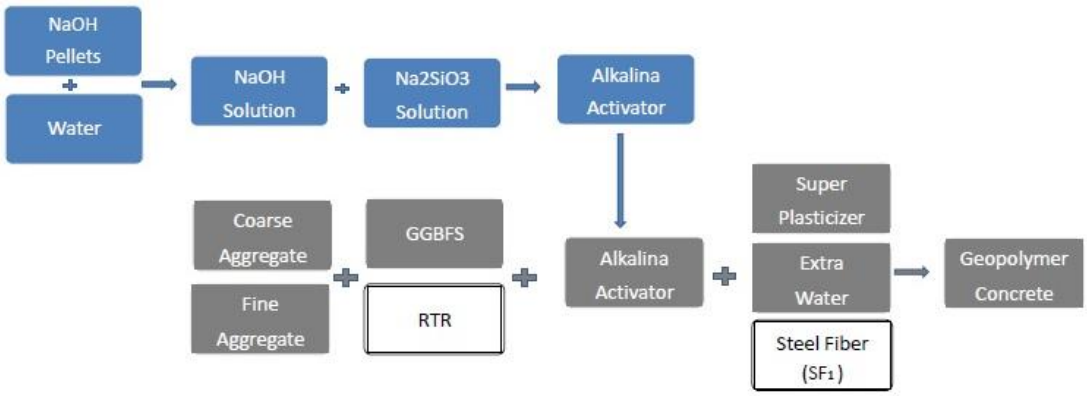


Figure 3.9 Preparation of alkali activator and SCGC specimens with RTR production procedure



Figure 3.10 SCGC production



(a)



(b)

Figure 3.11 (a) Molds used in the study and (b) After casting of SCGC mixes



Figure 3.12 Produced SCGC beam specimens

Table 3.7 Component of SCGC mixes

Mixture	Binder	GGBFS	NS	SF	Fine Agg.	Coarse Agg.	Na_2SO_3 +NaOH	Molarity	SP	Ekstra Water
	kg/m³	kg/m³	kg/m³	kg/m³	kg/m³	kg/m³	kg/m³		%	%
GB	500	500	0	0	860.07	738.12	250	12	7	10
GB-SF_1/0.5	500	500	0	39.2	860.07	738.12	250	12	7	10
GB-SF_1/1.0	500	500	0	78.4	860.07	738.12	250	12	7	10
GB-SF_2/0.5	500	500	0	39.2	860.07	738.12	250	12	7	10
GB-SF_2/1.0	500	500	0	78.4	860.07	738.12	250	12	7	10
GBN	500	490	10	0	858.49	736.76	250	12	7	10
GBN-SF_1/0.5	500	490	10	39.2	858.49	736.76	250	12	7	10
GBN-SF_1/1.0	500	490	10	78.4	858.49	736.76	250	12	7	10
GBN-SF_2/0.5	500	490	10	39.2	858.49	736.76	250	12	7	10
GBN-SF_2/1.0	500	490	10	78.4	858.49	736.76	250	12	7	10

Mixture	Binder	GGBFS	SF_1	FCR	CCR	TCR	Fine Agg.	Coarse Agg.	Na_2SO_3 +NaOH	Molarity	SP	Ekstra Water
	kg/m³	kg/m³	kg/m³	kg/m³	kg/m³	kg/m³	kg/m³	kg/m³	kg/m³		%	%
GB-FCR/5.0-CCR/5.0	500	500	0	7.95	10.65	0	780.44	738.12	250	12	7	10
GB-FCR/7.5-CCR/7.5	500	500	0	11.9	15.98	0	700.80	738.12	250	12	7	10
GB-TCR/10	500	500	0	0	0	30.9	621.16	738.12	250	12	7	10
GB-TCR/15	500	500	0	0	0	46.36	541.53	738.12	250	12	7	10
GB-SF_1/1.0-FCR/5.0-CCR/5.0	500	500	78.4	7.95	10.65	0	779.00	736.76	250	12	7	10
GB-SF_1/1.0-FCR/7.5-CCR/7.5	500	500	78.4	11.9	15.98	0	699.51	736.76	250	12	7	10
GB-SF_1/1.0-TCR/10	500	500	78.4	0	0	30.9	620.02	736.76	250	12	7	10
GB-SF_1/1.0-TCR/15	500	500	78.4	0	0	46.36	540.53	736.76	250	12	7	10

The fresh and hardened states mechanical properties, and the impact resistance of SCGC specimens are mainly affected by the amount and type of binder, the amount and ratio of alkaline activator, aggregates, maximum grain size (Dmax), SF volume fraction, SF aspect ratio, NS amount, RTR volume and RTR aspect ratio. According to the previous studies, the ratio of Na_2SiO_3/ NaOH must be in the range of 1.5 to 2.5 for economic reasons [126]. So, this ratio was taken as 2.5 in this study.

3.3 Fresh State Tests

The fresh state tests of SCGC were done immediately after the mixing process for each mixture which controls the requirements of flowability, filling ability and passing ability without separation and/or bleeding. All fresh state properties tests of SCGC mixes were made according to the Europe specification EFNARC committee. Fresh state tests are L-box height ratio, V-funnel flow time, T_{50} slump flow time and slump flow diameter. Slump flow test is the one of tests to be done to determine the properties of fresh state concrete. Slump flow value is a sensitive test used to define the flowability of a fresh state concrete mixture in free conditions. So, it is applied to specify for all SCC mixes as a primary control that the fresh concrete consistency is suitable for specification. T_{50} time is the flow time for the fresh concrete mixture to reach 50 cm in diameter according to the slump flow table of EFNARC. During slump flow test, the information about bleeding, uniformity and segregation resistance of concrete mixture is obtained from the measurement of T_{50} time and/or through the visual observations [14]. Slump flow is classified into three classes in EFNARC; a range of applications and the lower and upper limits of typical slump-flow classes are given in the Table 3.8. V-funnel flow time or T_{50} slump flow time can be utilized to assess the viscosity of the SCC. Moreover, these tests do not specify the direct viscosity, but they specify the rate of flow in term of viscosity. V-funnel test is utilized to determine the filling ability (flowability) of the fresh concrete and V-funnel flow time is the time that fresh concrete passes through the V-funnel opening. In addition, the viscosity classifications according to EFNARC are represented in the Table 3.8 [14]. L-box test is used to measure the passing ability of the fresh concrete to flow through narrow opening and confined places like areas of congested reinforcement without loss of homogeneity and segregation. The L-box height ratio values of the current study are presented in the Table 3.8. Moreover, all fresh test's results are shown in the Table 4.1.

Table 3.8 EFNARC specification and classification of fresh properties of SCGC mixes

Classification of Slump Flow	
Class	Slump flow diameter [mm]
Slump Flow 1	550-650
Slump Flow 2	660-750
Slump Flow 3	760-850
Classification of Viscosity	

Class	T_{50} [sec]	V-funnel time [sec]
VS_1/VF_1	≤ 2	≤ 8
VS_2/VF_2	> 2	9 to 25
Classification of Passing Ability		
PA1	≥ 0.8 with two rebar	
PA2	≥ 0.8 with three rebar	

3.4 Curing of the SCGC Specimens

After the SCGC casted, the specimens were demoded after 24 hours and placed in the laboratory ambient for 28 days of hardened state tests. Three similar specimens were produced for every test and the average of the test results was calculated.

3.5 Hardened State Tests

The hardened tests of SCGC were carried out to determine the effects of SFs, NS, together use of SFs and NS, and TR and together effects of SF_1 and TR on the mechanical performance and impact resistance of SCGC.

3.5.1 Compressive Strength

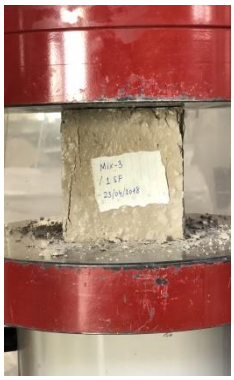
Compressive strength tests were conducted on cubes with dimensions of 100x100x100 mm and the compressive strength testing machine used in the study is shown in the Figure 3.12. The compressive strength values were calculated according to ASTM C39 standard and calculated based on Equation 3.1. Compressive strength test procedure is shown in the Figure 3.13.

$$f_c' = P/A \quad (3.1)$$

where f_c' is the compressive strength of specimens (MPa), P is the maximum load (kN) and A is the cross-sectional area of specimens (mm^2). The results of tests are given in the Table 4.2.



Figure 3.13 Compressive strength test machine



GB



GB-SF_1/0.5



GB-SF_1/1.0



GB-SF_2/0.5



GB-SF_2/1.0



GBN-SF_1/0.5



GBN-SF_1/1.0



GBN-SF_2/0.5



GBN-SF_2/1.0



GBN



GB-FCR/5.0-CCR/5.0



GB-FCR/7.5-CCR/7.5



GB-TCR/10



GB-TCR/15



GB-SF_1/1.0-FCR/5.0-CCR/5.0



GB-SF_1/1.0-FCR/7.5-CCR/7.5



GB-SF_1/1.0-TCR/10 GB-SF_1/1.0-TCR/15

Figure 3.14 Compressive strength tests of SCGC

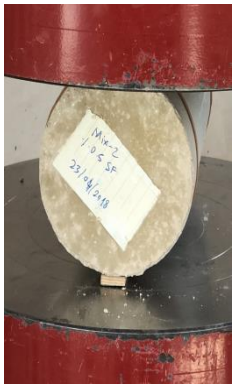
3.5.2 Splitting Tensile Strength

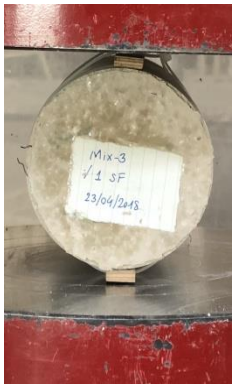
The cylinder specimens of SCGC (Ø100x200mm) were utilized to evaluate the splitting tensile strength according to ASTM C496. Prior to evaluate the splitting tensile strength of SCGC, the cylinder specimens were also tested to measure the modulus of elasticity of SCGC specimens according to ASTM C469. Therefore, the cylinder specimens were capped and levelled with sulfur according to the ASTM C617 before the tests. A compress-meter including a dial gage capable to measure the deformation up to 0.002 mm attached to each cylindrical specimen prior testing. The cylinder specimens thereafter loaded three times to 40% of the compressive strength evaluated from cube specimen for the same mixture. The modulus of elasticity of the specimens were evaluated as the average value of the last two readings and discard the first readings of each cylinder specimen. Three typical specimens were tested for each hardened property. The results of the tests are shown in the Table 4.2.

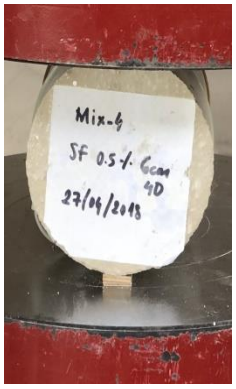
According to ASTM C496 (1994), splitting tensile strength of the concrete is measured by using the cylindrical samples of 100x200 mm at 28 days. The splitting tensile strength is obtained by averaging the results from the three tested cylindrical samples and splitting tensile strength (T) of cylindrical concrete specimens was calculated based on Equation 3.2 and the splitting tensile strength tests of SCGC are shown in the Figure 3.14.

$$T=2p/\Pi ld \qquad (3.2)$$


GB


GB-SF_1/0.5


GB-SF_1/1.0


GB-SF_2/0.5


GB-SF_2/1.0


GBN


GBN-SF_1/0.5


GBN-SF_1/1.0


GBN-SF_1/0.5


GBN-SF_2/1.0


GB-FCR/5.0-CCR/5.0

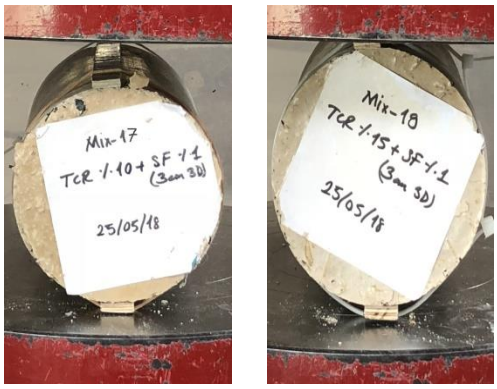

GB-FCR/7.5-CCR/7.5


GB-TCR/10


GB-TCR/15


GB-SF_1/1.0-FCR/5.0-CCR/5.0


GB-SF_1/1.0-FCR/7.5-CCR/7.5



GB-SF_1/1.0-TCR/10 GB-SF_1/1.0-TCR/15

Figure 3.15 Splitting tensile strength tests of SCGC

3.5.3 Flexural Tensile Strength

In order to clarify the influence of SFs, NS and TR on SCGC tensile strength, the four-point flexural tensile strength test were carry out on (100x100x500mm) beam specimens through using of displacement-controlled loading machine. Three linear variable displacement transducers (LVDT) were used to evaluate the deflection and deformation of the beam specimens. The displacement control machine was utilized to investigate the flexural tensile strength; the rate of loading was 0.02 mm/min and the results of the tests are given in the Table 4.2. The test set-up and details of specimen under four-point bending tests are shown in Figure 3.15 and the flexural tensile strength test of SCGC beam specimens are shown in the Figure 3.16, respectively. In this test, the loading rate has relied upon 0.02 mm/min under displacement control. In addition, the results of SCGC beam specimen flexural strength tests are shown in the Figure 3.17.

The net flexural strength (f_{flex}) of all specimens was calculated by the Equation 3.3 [129].

$$F_{flex}=3P_{max}L/2b(d-a)^2 \quad (3.3)$$

where P_{max} is the peak load (N), L is the span length (mm), b is the width of specimen (mm), d is the depth of specimen (mm) and a is the depth of notch (mm).

Fracture energy (G_f) represents the energy amount required to create a crack in the binder paste matrix. Through the three-point bending test and using the Equation 3.4 which is proposed by RILEM, the G_f of the prismatic specimens was calculated.

$$G_f=(w_o+mg\delta_s)/A_{ig} \quad (3.4)$$

where w_o is the area under the load –displacement curve (N-m), m is the mass of beam (kg), g is the acceleration caused by gravity (9.81 m/s^2), δ is the specific displacement (m) and A_{ig} is the area of ligament (m^2).

Moreover, the critical stress intensity factor (K_{IC}) was calculated using Equation 3.5 (Peterson 1980) for each beam specimens:

$$K_{IC}=3P_{max}l/2bd^2 \sqrt{a_o}\,(1.93-3.07A+14.53A^2-25.11A^3+25A^4) \qquad (3.5)$$

where P_{max} is the peak load, l is the span length, b is the width of specimens, d is the depth of specimens, a_o is the depth of notch and A is the ratio of notch depth to specimen depth. Moreover, the test results obtained are given in the Figure 3.15.

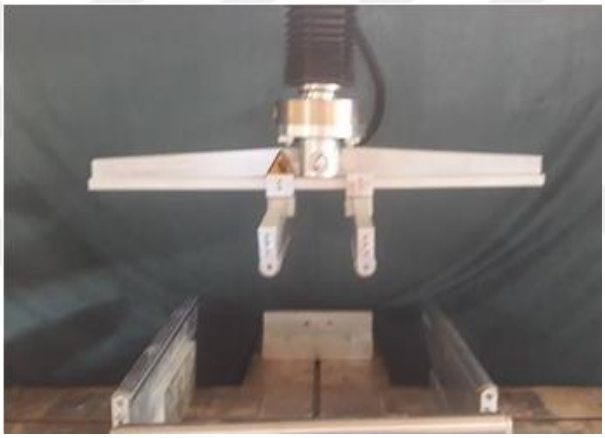
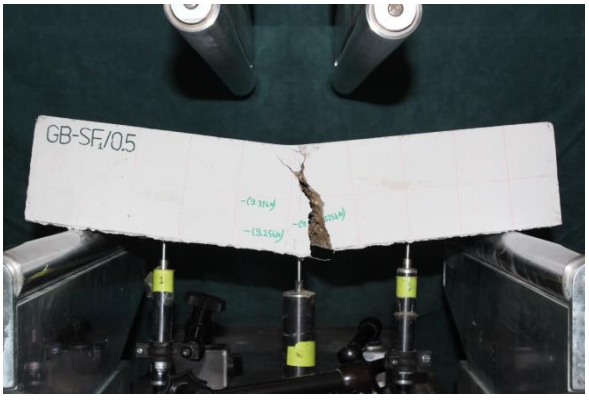


Figure 3.16 Flexural tensile strength tests machine



GB



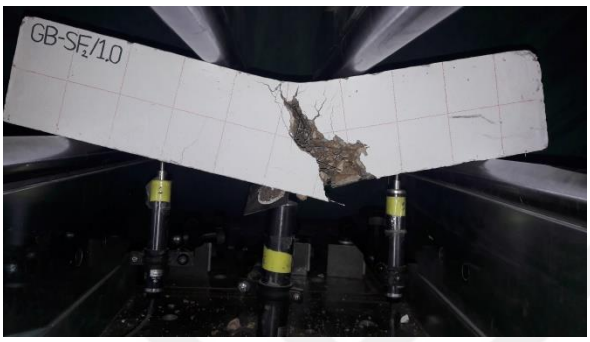
GB-SF_1/0.5



GB-SF$_1$/1.0



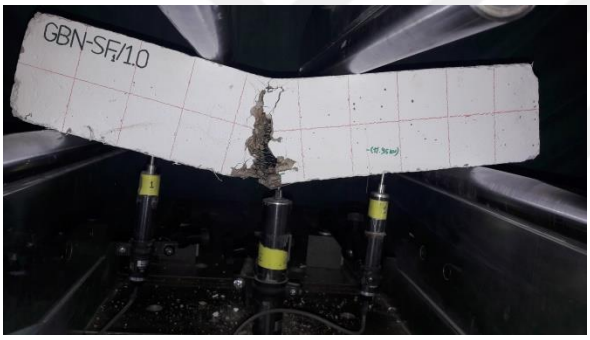
GB-SF$_2$/0.5



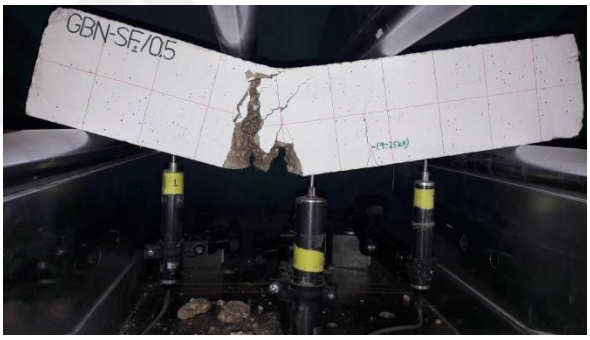
GB-SF$_2$/1.0



GBN-SF$_1$/0.5



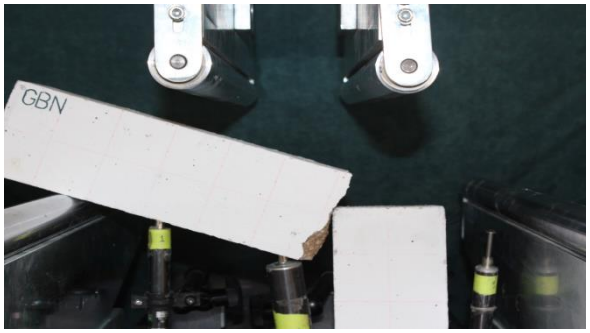
GBN-SF$_1$/1.0



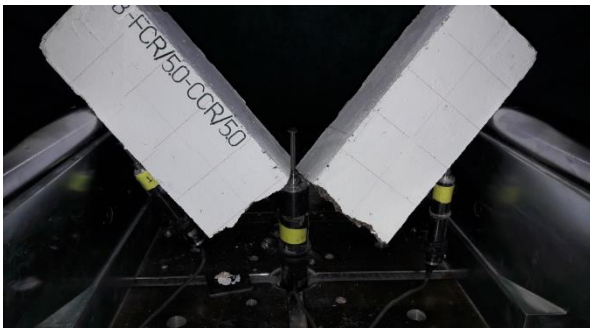
GBN-SF$_2$/0.5



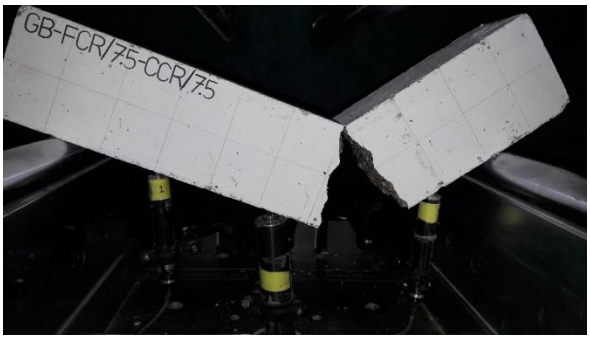
GBN-SF$_2$/1.0



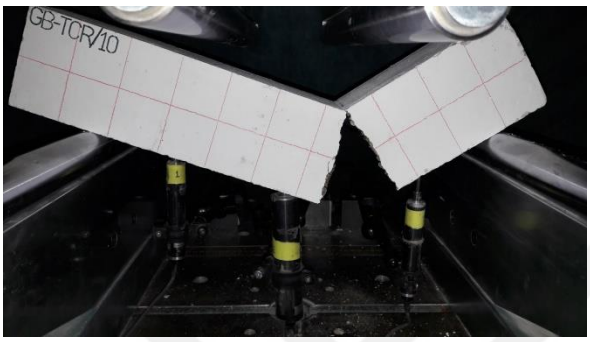
GBN



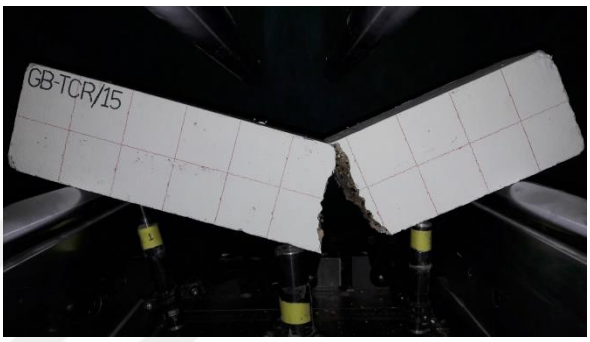
GB-FCR/5.0-CCR/5.0



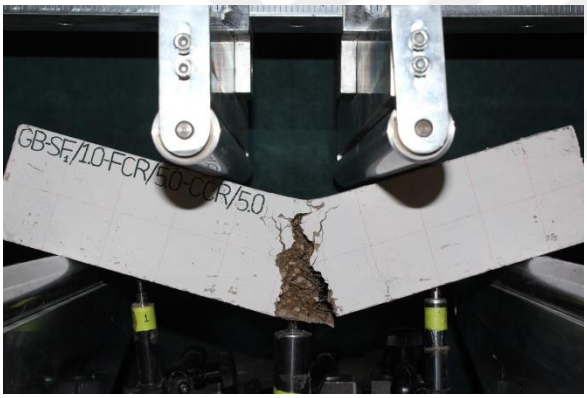
GB-FCR/7.5-CCR/7.5



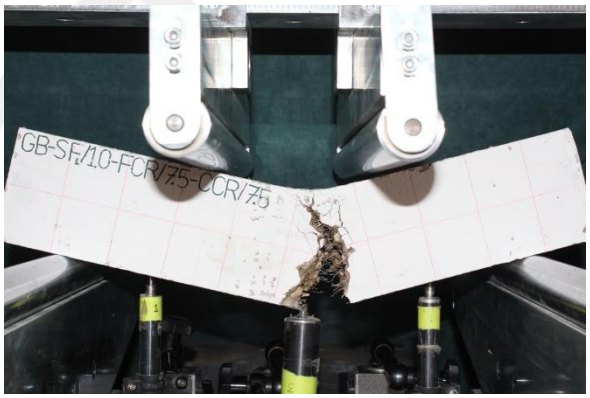
GB-TCR/10



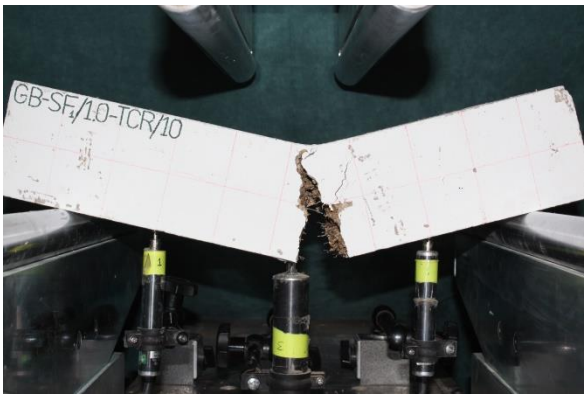
GB-TCR/15



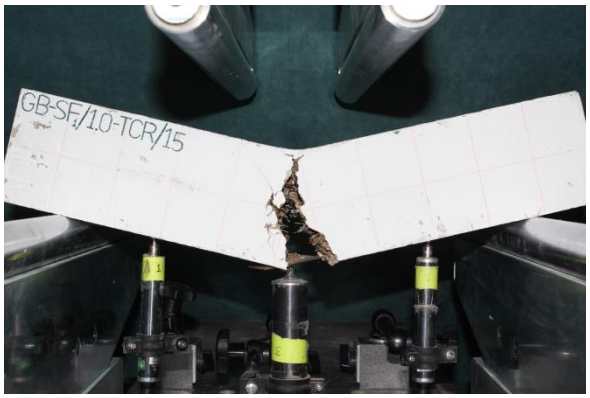
GB-SF$_1$/1.0-FCR/5.0-CCR/5.0



GB-SF$_1$/1.0-FCR/7.5-CCR/7.5

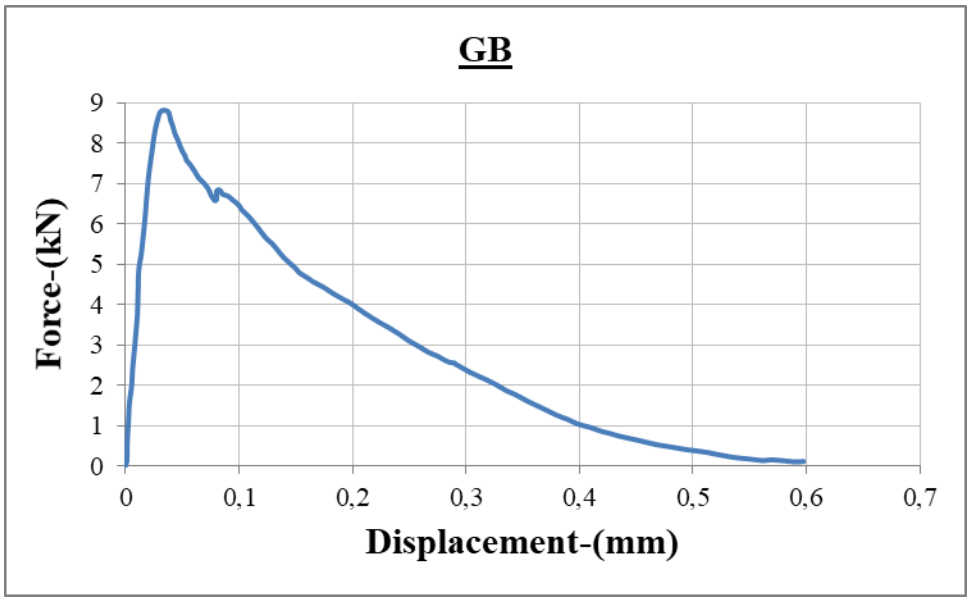


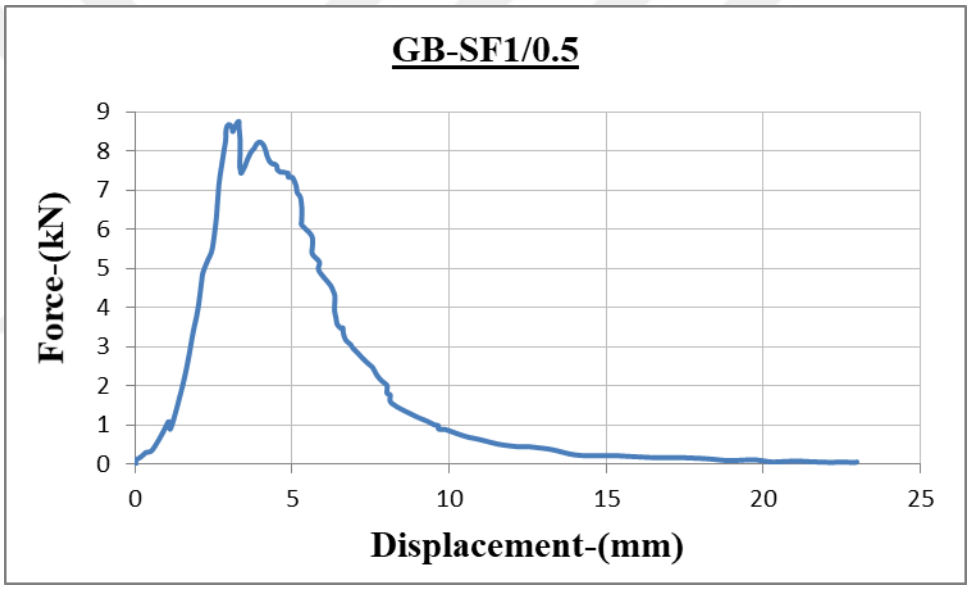
GB-SF$_1$/1.0-TCR/10

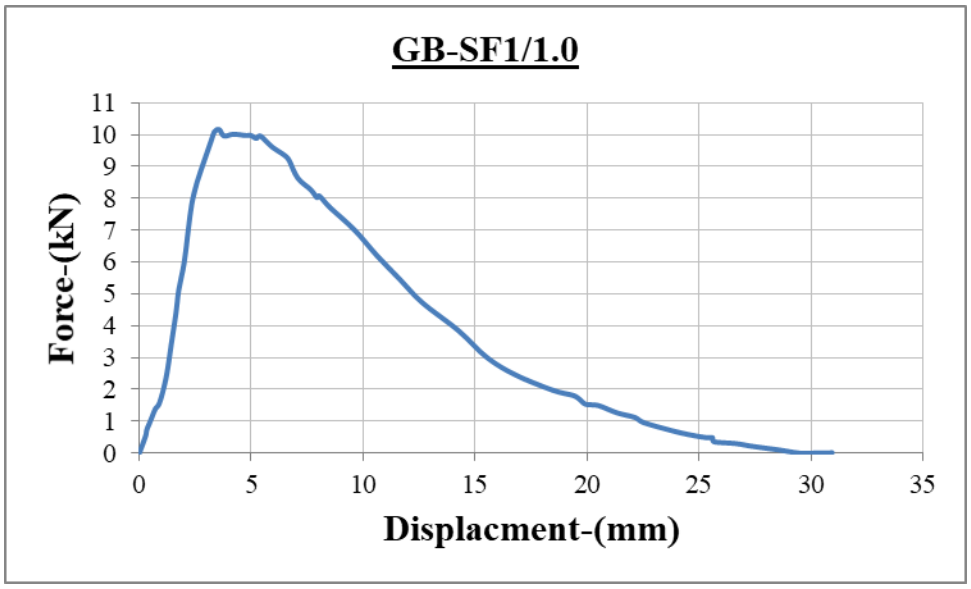


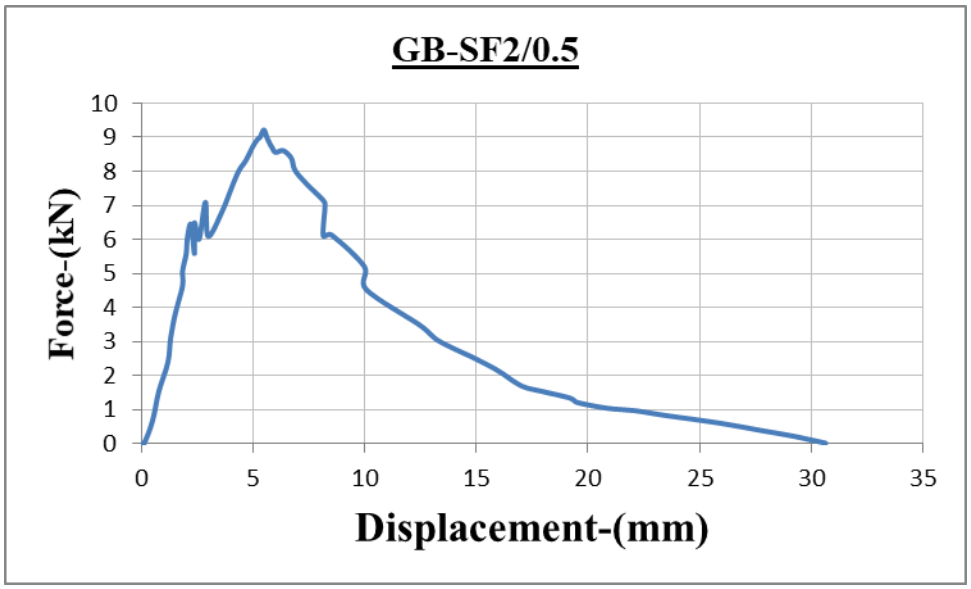
GB-SF$_1$/1.0-TCR/15

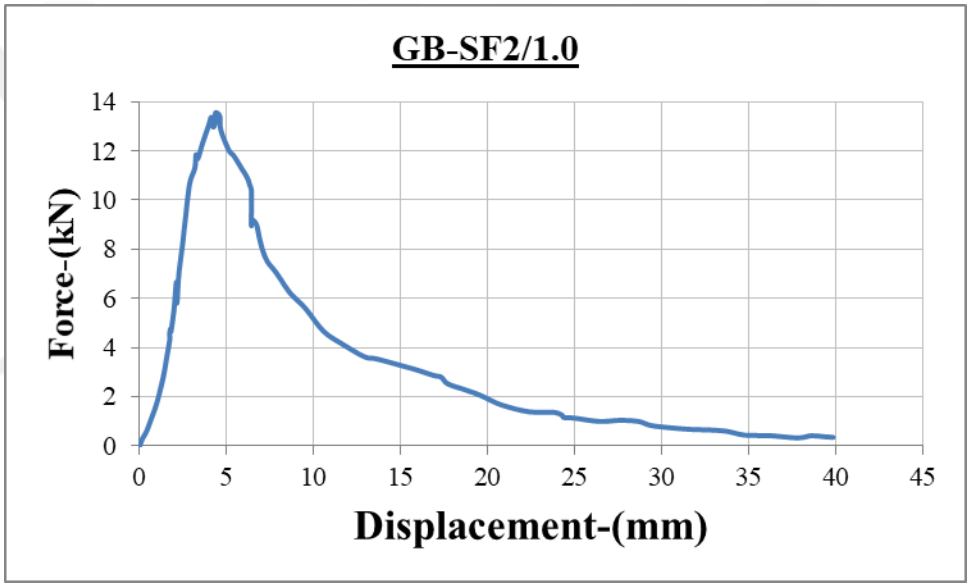
Figure 3.17 Flexural strength tests of SCGC beams

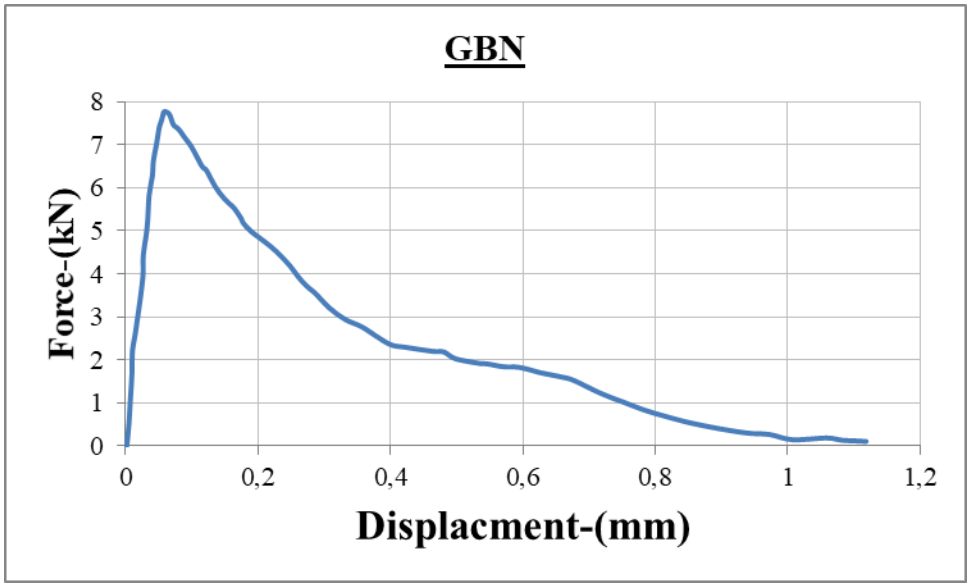

GB
Force-(kN)
Displacement-(mm)
0
1
2
3
4
5
6
7
8
9
0
0,1
0,2
0,3
0,4
0,5
0,6
0,7

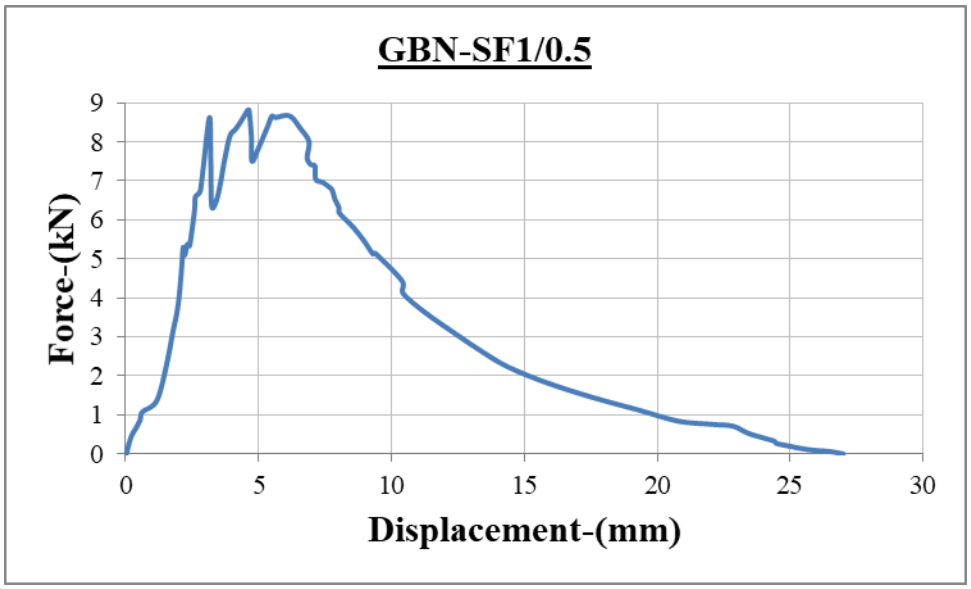

GB-SF1/0.5
Force-(kN)
Displacement-(mm)
0
1
2
3
4
5
6
7
8
9
0
5
10
15
20
25

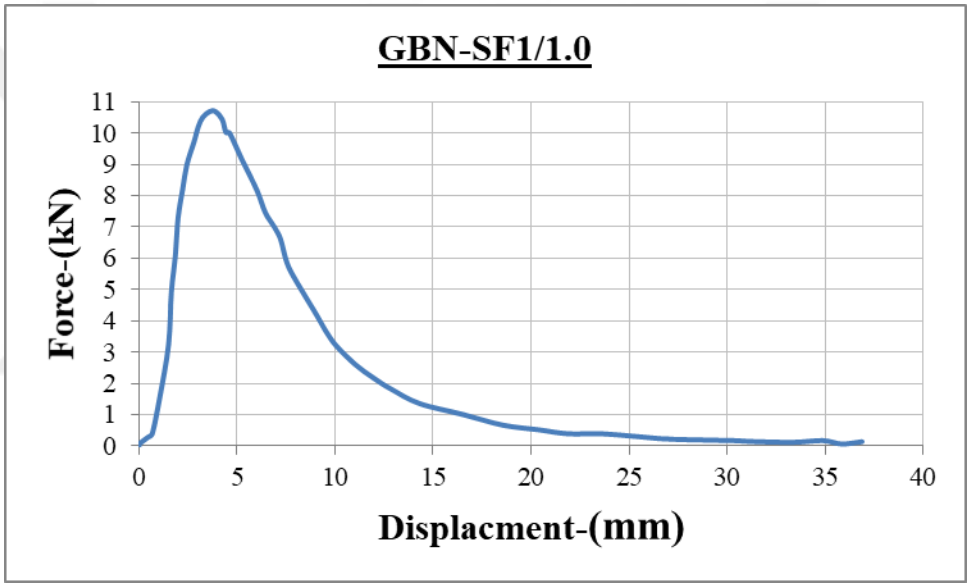

GB-SF1/1.0
Force-(kN)
Displacment-(mm)
0
1
2
3
4
5
6
7
8
9
10
11
0
5
10
15
20
25
30
35

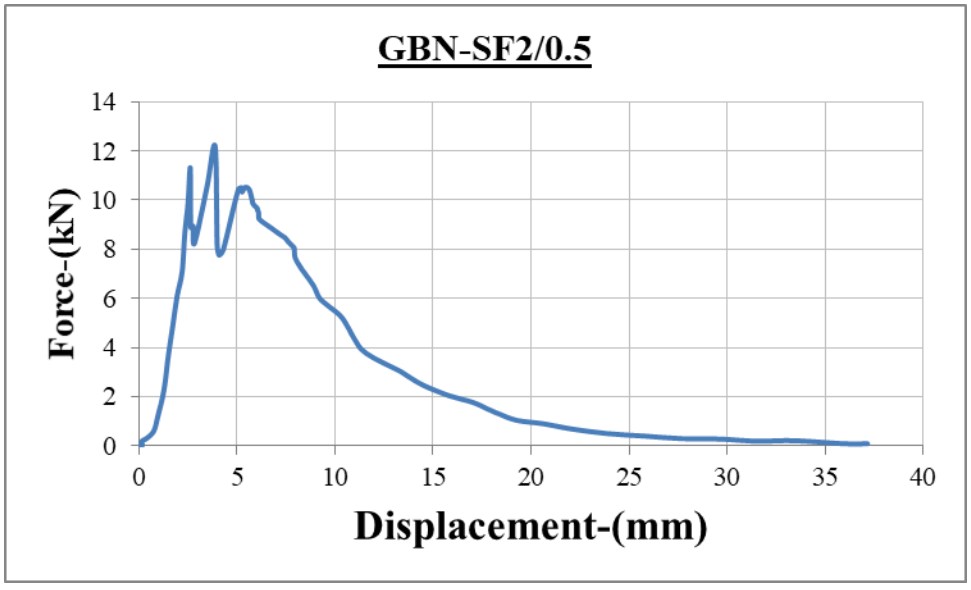

GB-SF2/0.5
Force-(kN)
Displacement-(mm)
0
1
2
3
4
5
6
7
8
9
10
0
5
10
15
20
25
30
35

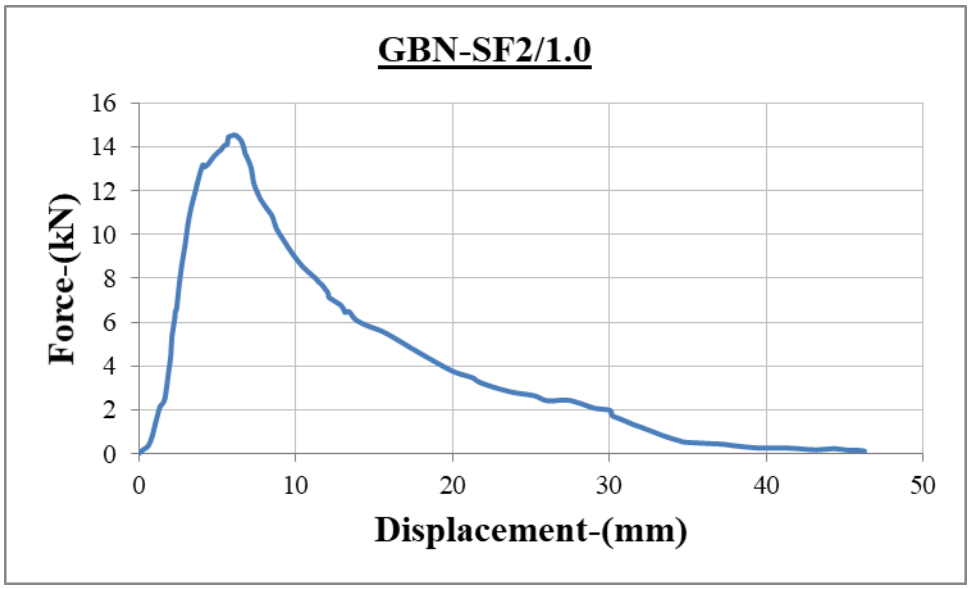

GB-SF2/1.0
Force-(kN)
Displacement-(mm)
0
2
4
6
8
10
12
14
0
5
10
15
20
25
30
35
40
45

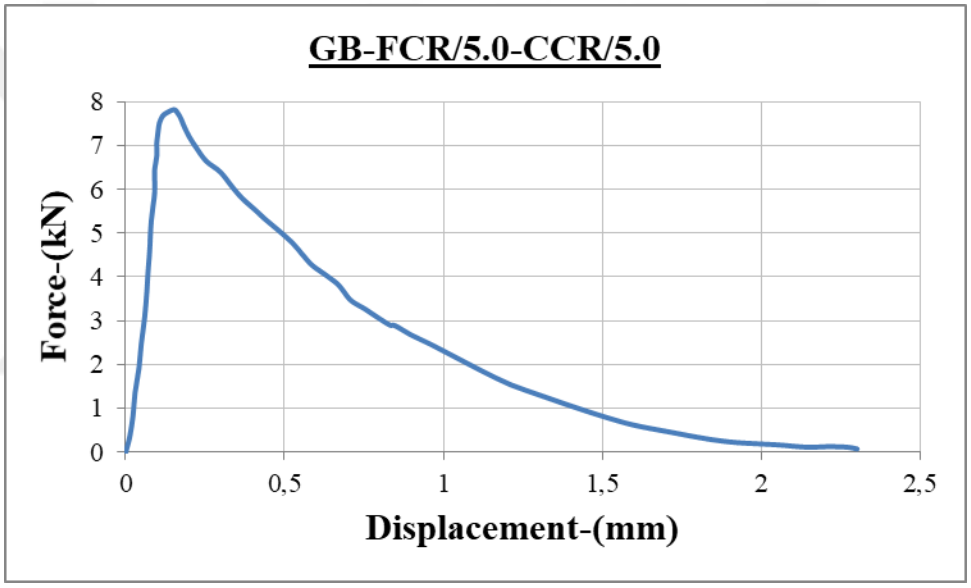

GBN
Force-(kN)
Displacment-(mm)
0
1
2
3
4
5
6
7
8
0
0,2
0,4
0,6
0,8
1
1,2

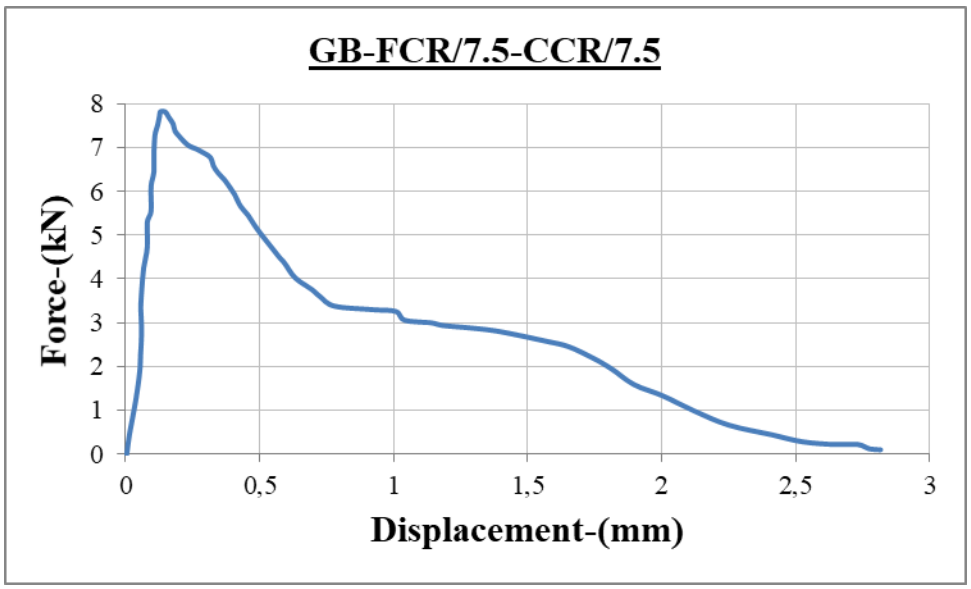

GBN-SF1/0.5
Force-(kN)
Displacement-(mm)
0
1
2
3
4
5
6
7
8
9
0
5
10
15
20
25
30

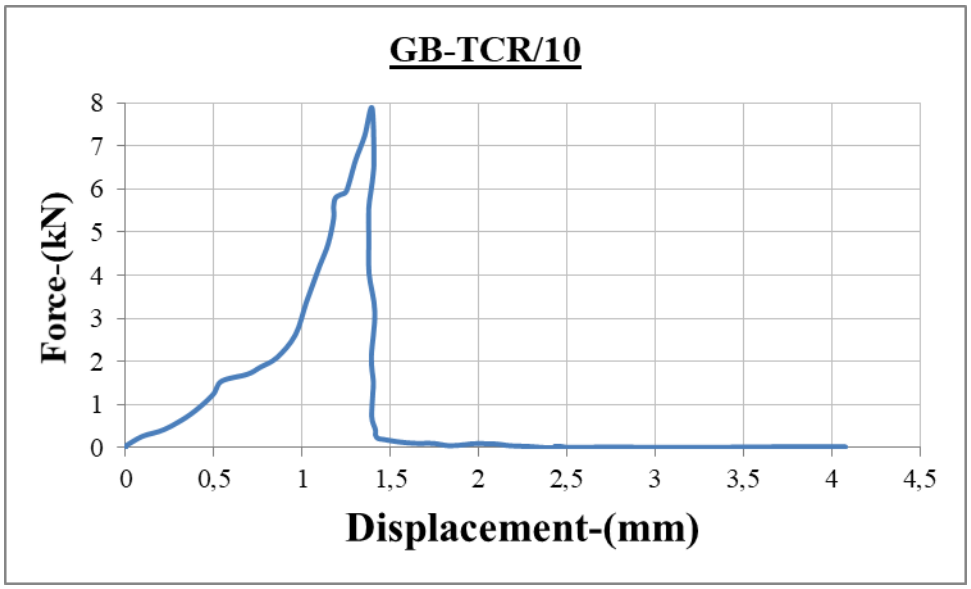

GBN-SF1/1.0
Force-(kN)
Displacment-(mm)
0
1
2
3
4
5
6
7
8
9
10
11
0
5
10
15
20
25
30
35
40

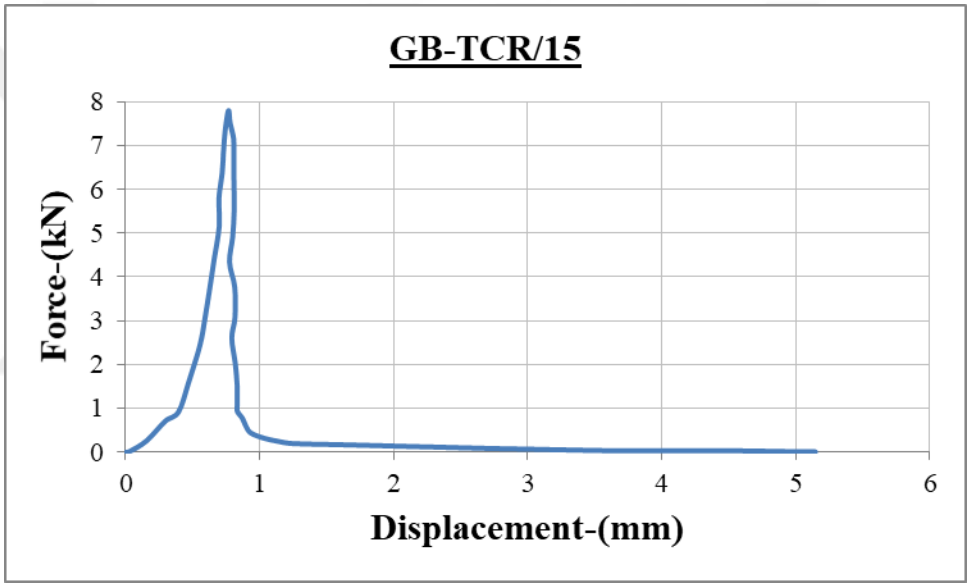

GBN-SF2/0.5
Force-(kN)
Displacement-(mm)
0
2
4
6
8
10
12
14
0
5
10
15
20
25
30
35
40

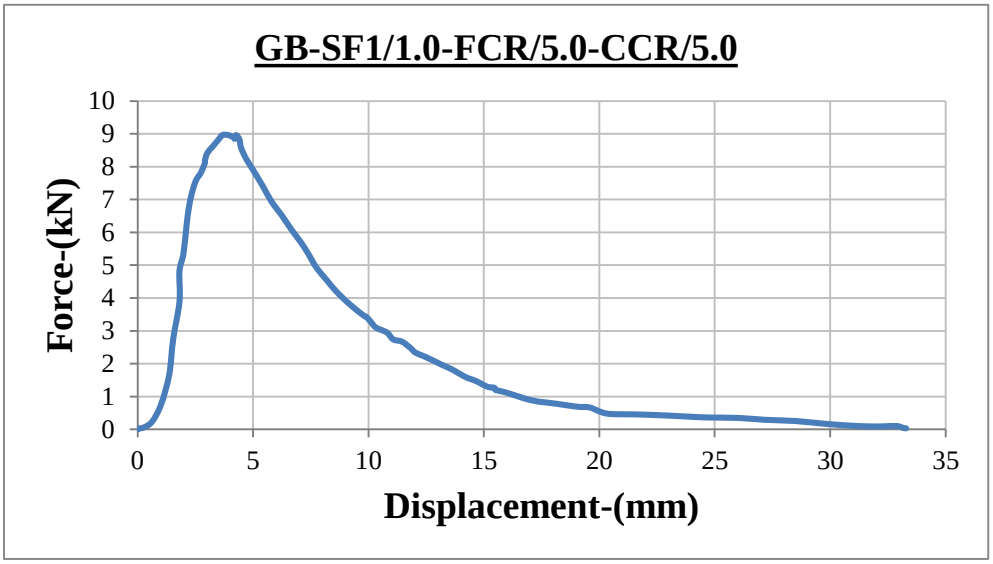

GBN-SF2/1.0
Force-(kN)
16
14
12
10
8
6
4
2
0
0
10
20
30
40
50
Displacement-(mm)

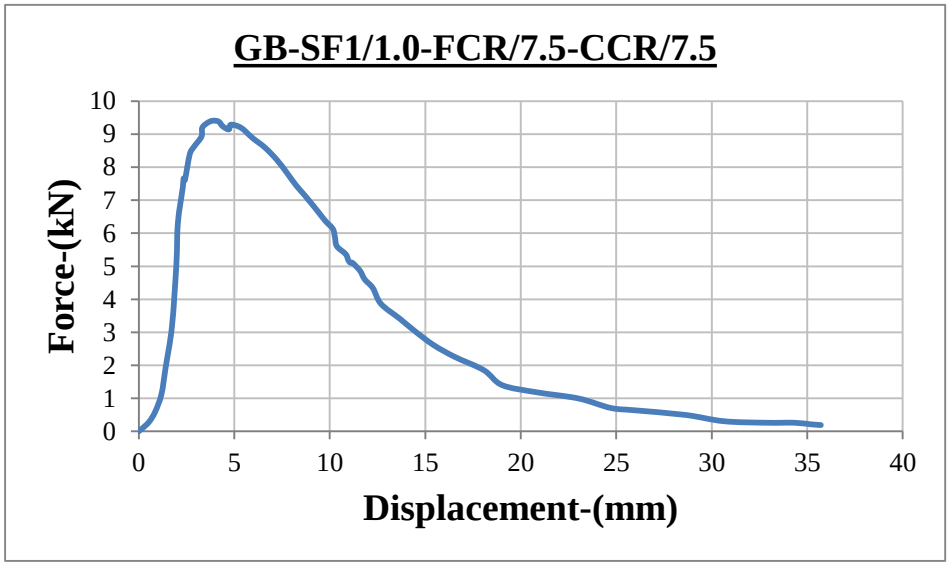

GB-FCR/5.0-CCR/5.0
Force-(kN)
8
7
6
5
4
3
2
1
0
0
0,5
1
1,5
2
2,5
Displacement-(mm)

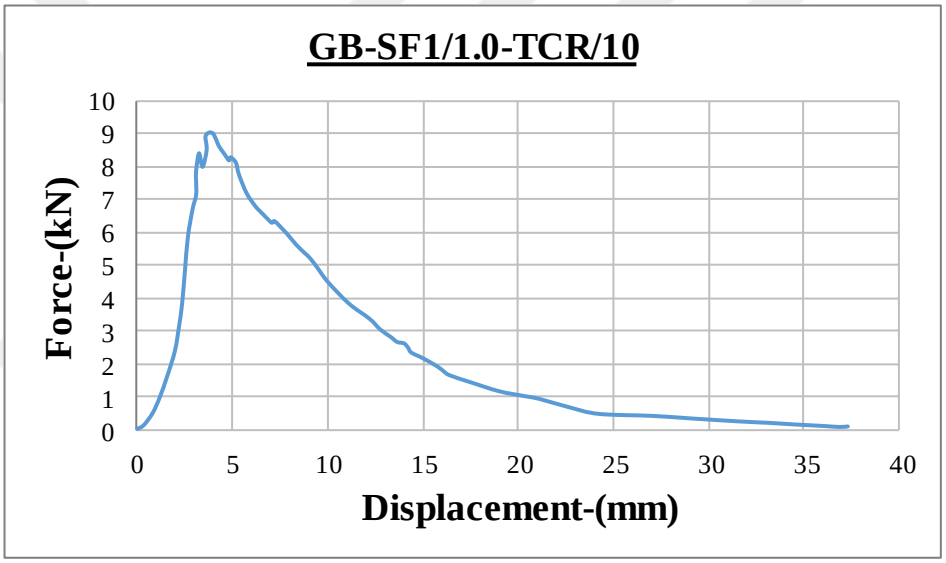

GB-FCR/7.5-CCR/7.5
Force-(kN)
8
7
6
5
4
3
2
1
0
0
0,5
1
1,5
2
2,5
3
Displacement-(mm)


GB-TCR/10
Force-(kN)
Displacement-(mm)
0
1
2
3
4
5
6
7
8
0
0,5
1
1,5
2
2,5
3
3,5
4
4,5


GB-TCR/15
Force-(kN)
Displacement-(mm)
0
1
2
3
4
5
6
7
8
0
1
2
3
4
5
6


GB-SF1/1.0-FCR/5.0-CCR/5.0
Force-(kN)
Displacement-(mm)
0
1
2
3
4
5
6
7
8
9
10
0
5
10
15
20
25
30
35





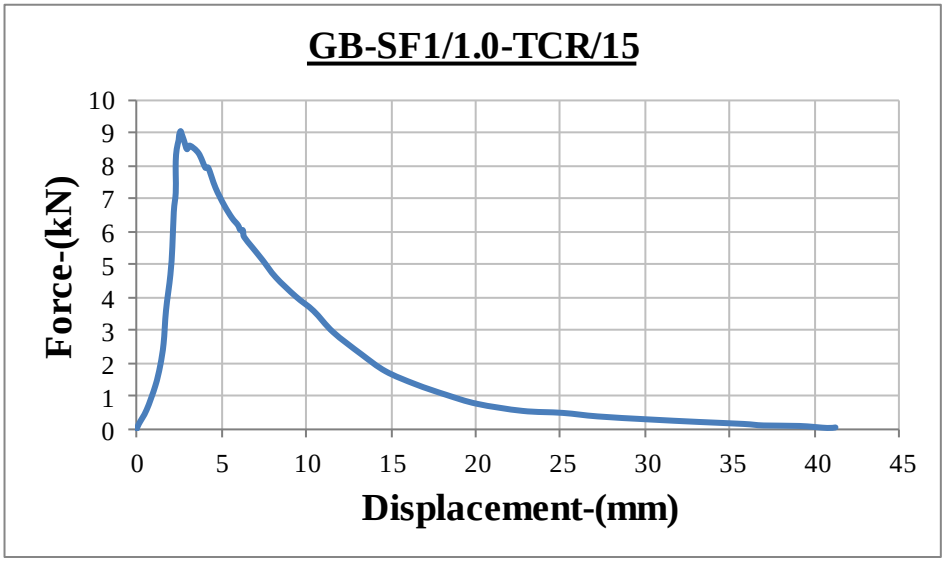


Figure 3.18 The results of SCGC beam specimen flexural strength tests

3.5.4 Modulus of Elasticity (E)

Static modulus of elasticity was determined by the testing of cylinder specimens with a dimension of ϕ100x200 mm according to ASTM C469 (ASTM Designation C 1984). Each of the specimens was fitted with a compress meter containing a dial gage capable of measuring deformation to 0.002 mm as shown in the Figure 3.18 and then loaded three times to 40% of the ultimate load. The ultimate load was determined based on the compressive strength test results for each mix. The first set of readings of each cylinder specimen was discarded and the modulus of elasticity was reported as the average of the second two sets of readings. For each parameter, three specimens were used (ASTM Designation C 1984). The results of the tests are given in the Table 4.2.



Figure 3.19 The modulus of elasticity tests machine

3.5.5 Drop-Weight Test (Impact Resistance)

The drop-weight tests were carried out to determine the impact resistance of SCGC beam specimens in the study. Moreover, the drop-weight test machine used in this study and its schematic representation are shown in the Figure 3.19 and Figure 3.20. The tests were done according to recommendations of ACI Committee 544 and the test is made as repeated impacts to the same point [129]. For each impact event, the data of acceleration-time, force-time, and displacement-time and crack propagation were taken at the same time in this scope of study. In this test, a 28.5kg impactor was released from a height of 100mm on the 100x100x500mm beam specimens. The number of blows that caused the first crack and failure mode of SCGC beam specimens were observed and these number of blows were used to determine the

impact energy of the beam specimens. The impact energy is given in the following Equation 3.6:

$$E_{impact}=m.g.h.N \quad (3.6)$$

where, E_{impact} = impact energy in Joule (J); m = mass of drop hammer = 28.5 kg; g = 9.81m/s^2; h = releasing height of drop hammer = 100 mm; N = number of blows.

Moreover, after each drop, crack widths of all the SCGC beam specimens were measured using the crack width gauge and the propagation of cracks in the SCGC beams were observed. Figure 3.21 show the measurement of crack widths using the crack width gauge instrument.



Figure 3.20 Drop-weight test machine

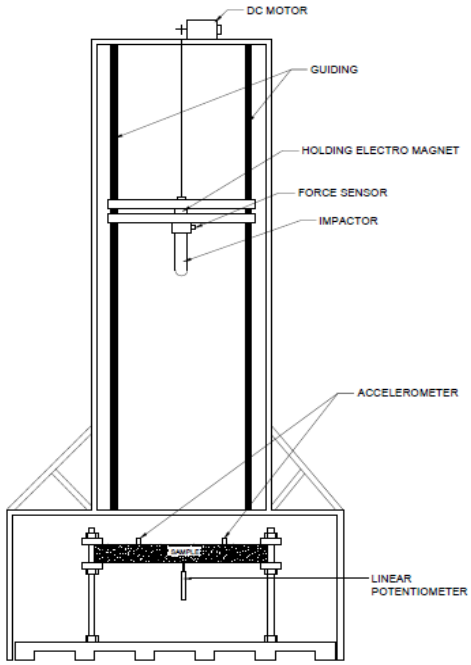


Figure 3.21 The schematic representation of drop-weight test machine



Figure 3.22 The measurement of crack widths using the crack width gauge instrument

In this study, some devices were used to obtain data on acceleration-time, force-time and displacement-time relationships during the drop-weight tests. The selection of these devices has been selected in accordance with the literature. Measuring devices used during the drop-weight drop tests carried out in this study:

- ICP 200C20 Force Sensor
- ICP 352C03 Accelerometer
- Low Noise Coaxial Connection Cable
- LTR 100 Spring-Loaded Linear Potentiometer
- NI 9230 with BNC Data logger

3.5.5.1 Force Sensor

The Force Sensor device used in the experiments of this project is a device converted a force or stress on the structure to an electrical signal. This conversion event takes place with the help of sensors mounted on the structure connected to force sensor as seen in the Figure 3.22. Force is mechanically perceived and it causes changes in the shape of the force sensor. The force sensor measures the shape change as an electrical signal. Because the force alters the effective electrical resistance of the wire.

The force sensor (Model ICP 200C20) with quartz ring produced by PCB Group Company was used in the experimental study as shown in the Figure 3.23.



Figure 3.23 ICP 200C20 force sensor

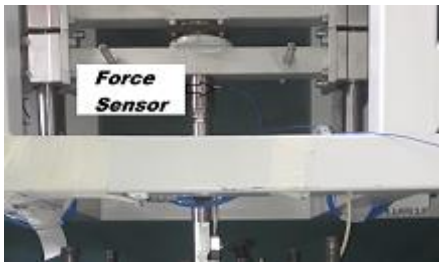


Figure 3.24 The force sensor in the experiment setup

Figure 3.23 shows the force sensor mounted on the impactor. The force sensor must be mounted precisely to detect the incoming signals correctly. In addition, the cable of the force sensor should be installed in a way that does not damage the other devices on the test setup and the connection apparatus of these devices after each

drop. These considerations took into account when mounting the force sensor and during experimental studies. The technical properties of the Model ICP 200C20 force sensor given by the manufacturer are shown in the Table 3.9.

Table 3.9 The technical properties of model ICP 200C20 force sensor [131]

	Units	
PERFORMANCE	**ENGLISH**	**SI**
Sensitivity (±15 %)	*0.25 mV/Ib*	*56.2 mV/kN*
Measurement Range (Compression)	*20000 lb*	*88.96 kN*
Maximum Static Force (Compression)	*30000 lb*	*133.44 kN*
Broadband Resolution (1 to 10000 Hz)	*0.30 lb-rms*	*1.3 N-rms*
Low Frequency Response (-5 %)	*0,0003 Hz*	*0,0003 Hz*
Upper Frequency Limit	*40000 Hz*	*40000 Hz*
Non-Linearity	*≤ 1% FS*	*≤ 1% FS*
ENVIRONMENTAL		
Temperature Range	*-65 to +250 ^{o}F*	*-54 to +121 ^{o}C*
Temperature Coefficient of Sensitivity	*≤0.08 %/^{o}F*	*≤0.144 %/^{o}C*
ELECTRICAL		
Discharge Time Constant (at room	*≥ 2000 sec*	*≥ 2000 sec*
Excitation Voltage	*20 to 30 VDC*	*20 to 30 VDC*
Constant Current Excitation	*2 to 20 mA*	*2 to 20 mA*
Output Impedance	*≤100 Ohm*	*≤100 Ohm*
Output Bias Voltage	*8 to 14 VDC*	*8 to 14 VDC*
Spectral Noise (1 Hz)	*0.039 lb/√Hz*	*0.17 N/√Hz*
Spectral Noise (10 Hz)	*0.012 lb/√Hz*	*0.054 N√Hz*
Spectral Noise (100 Hz)	*0.0034 lb/√Hz*	*0.015 N/√Hz*
Spectral Noise (1000 Hz)	*0.00088 lb/√Hz*	*0.0039 N/√Hz*
Output Polarity (Compression)	*Positive*	*Positive*
PHYSICAL		
Stiffness	*63 lb/μin*	*11 kN/μm*
Size - Diameter	*1.5 in*	*38.1 mm*
Size - Height	*0.5 in*	*12.7 mm*
Weight	*3.1 oz*	*88 gm*
Housing Material	*Stainless Steel*	*Stainless Steel*
Sealing	*Hermetic*	*Hermetic*
Electrical Connector	*10-32 Coaxial Jack*	*10-32 Coaxial Jack*
Electrical Connection Position	*Side*	*Side*
Mounting Thread	*1/4-28 Female*	*Not Applicable*

3.5.5.2 Accelerometer

The piezoelectric accelerometer devices used in drop-weight tests in this project is shown in the Figure 3.24 and they mounted with the brass head on the sample is shown in the Figure 3.25. While the accelerometers mounted on the SCGC samples, the relationship between maximum high sensitivity and high frequency was paid attention. In addition, great care has been taken to ensure that there was no gap

between the accelerometers and the SCGC samples while mounting the accelerometers on the sample. In the experimental studies, two accelerometers with ICP band 352C03 model number produced by PCB Group from piezoelectric accelerometers group were used.



Figure 3.25 ICP 352C03 accelerometer

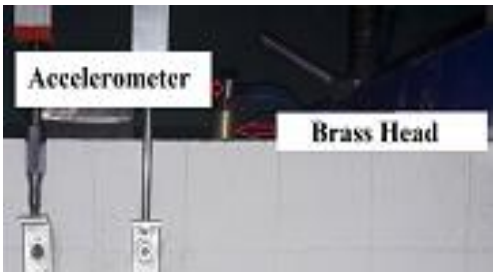


Figure 3.26 The accelerometer in the experiment setup

During the mounting of these piezoelectric accelerometers on SCGC beam specimens, in order to maximize the high sensitivity-high frequency relationship, stud mount method was applied. As shown in the Figure 3.26, this mounting method and connection geometry selection was taken from the experimental data under the technical information tab on the website of the piezoelectric accelerometer manufacturer PCB Group. Moreover, brass heads were mounted between the concrete beam specimens and the accelerometers by screwing into dowel-bearing holes drilled on the SCGC specimen. In addition, the technical properties of the accelerometers used in the experimental study, taken from the installation and operation manual provided by the manufacturer, are given in the Table 3.10.

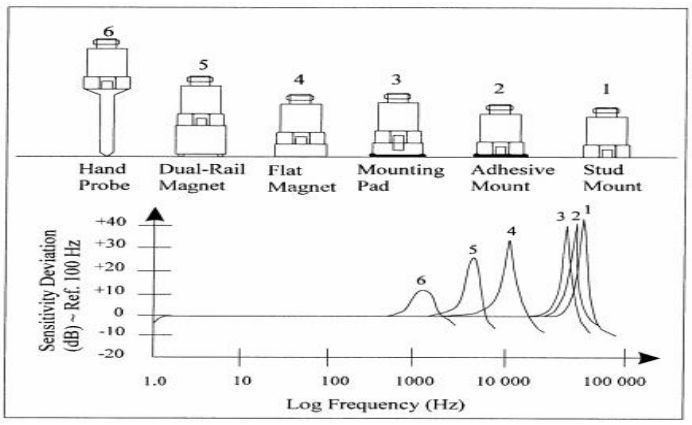


Figure 3.27 Accelerometer mounting configurations and their effects on high-frequency

Table 3.10 The technical properties of 352C03 model accelerometer [131]

	Units	
PERFORMANCE	**ENGLISH**	**SI**
Sensitivity (±10 %)	*10 mV/g*	*1.02 mV/(m/s²)*
Measurement Range	*±500 g pk*	*± 4900 m/s²pk*
Frequency Range (±5 %)	*0.5 to 10000 Hz*	*0.5 to 10000 Hz*
Frequency Range (±10 %)	*0.3 to 15000 Hz*	*0.3 to 15000 Hz*
Resonant Frequency	*≥ 50 kHz*	*≥ 50 kHz*
Broadband Resolution (1 to 10000 Hz)	*0.0005 g rms*	*0,05 m/s²rms*
Non-Linearity	*≤ 1%*	*≤ 1 %*
Transverse Sensitivity	*≤ 5%*	*≤ 5 %*
ENVIRONMENTAL		
Overload Limit (Shock)	*± 5000g pk*	*±49000m/s² pk*
Temperature Range (Operating)	*-65 to +250 °F*	*-54 to +121 °C*
Temperature Response	*See Graph % °F*	*See Graph % °F*
Base Strain Sensitivity	*0.003 g/με*	*0.003 (m/s²)/με*
ELECTRICAL		
Excitation Voltage	*18 to 30 VDC*	*18 to 30 VDC*
Constant Current Excitation	*2 to 20 mA*	*2 to 20 mA*
Output Impedance	*≤100 Ohm*	*≤100 Ohm*
Output Bias Voltage	*7 to 12 VDC*	*7 to 12 VDC*
Discharge Time Constant	*1.0 to 2.5 sec*	*1.0 to 2.5 sec*
Settling Time (within 10% of bias)	*<10 sec*	*<10 sec*
Spectral Noise (1 Hz)	*110 μg/√Hz*	*1080 (μm/sec²)/√Hz*
Spectral Noise (10 Hz)	*25 μg/√Hz*	*245 (μm/sec²)/√Hz*
Spectral Noise (100 Hz)	*8 μg/√Hz*	*78 (μm/sec²)/√Hz*
Spectral Noise (1 kHz)	*4 μg/√Hz*	*390 (μm/sec²)/√Hz*
PHYSICAL		
Size - Height	*0.62 in*	*15.7 mm*
Weight	*0.20 oz*	*5.8 g*
Sensing Element	*Ceramic*	*Ceramic*
Size - Hex	*0.44 in*	*11.2 mm*
Sensing Geometry	*Shear*	*Shear*
Housing Material	*Titanium*	*Titanium*
Sealing	*Hermetic*	*Hermetic*
Electrical Connector	*10-32 Coaxial Jack*	*10-32 Coaxial Jack*
Electrical Connection Position	*Side*	*Side*
Mounting Thread	*10-32 Female*	*10-32 Female*
Mounting Torque	*10 to 20 in-lb*	*113 to 226 N-cm*

3.5.5.3 Connection Cable

Low Noise Coaxial Cables given in the Figure 3.27 were used in the transmission of data between force sensor and data logger, and between accelerometers and data logger used in the experiments of this study. These cables provide lossless transfer of all high and low signal data between -90 °C and 260 °C.



Figure 3.28 The low noise coaxial cable in the experiment setup

3.5.5.4 Spring-Loaded Linear Potentiometer

Two symmetrical spring-loaded linear potentiometer were used to measure the beam deformations that occurred during the drop in drop-weight tests. The spring loaded linear potentiometers used in the study are shown in the Figure 3.28. In the experimental studies, two potentiometers produced by Eskon Sensor Technology were used and their technical properties taken from the website of the producing company are shown in the Table 3.11. In addition, the measuring and control device of these potentiometers is shown in the Figure 3.29 and its technical properties taken from the website of the producing company is given in the Table 3.12. Moreover, the spring-loaded linear potentiometers mounted on the beam using a connection apparatus can be seen in the Figure 3.30. The linear potentiometers were mounted symmetrically in the right and left directions from the middle of the beam.



Figure 3.29 Spring-loaded linear potentiometer used in the study



Figure 3.30 Measuring & control device of spring-loaded linear potentiometer used in the study

Table 3.11 The technical properties of spring-loaded linear potentiometer [132]

Model	*LTR 100*
Electrical Stroke (mm)	*100*
Mechanical Stroke (mm)	*102*
Independent Linearity	*±0,2%*
Repeatability	*0.01 mm*
Max Operating Speed	*5 m/s*
Resistance Element	*Conductive Plastic*
Resistance	*5K, 10K (optional other)*
Output Signal	*4-20 mA (optional 0…20 mA), 0-10V or*
Supply Voltage	*'A' ve 'V' models: 12…30 V_{DC}*
Electrical Connection	*Potentiometric output model: 42V max.* *DIN 43650-C socket or 3 x 0,14 mm2 shielded PVC cable*
Operating Temperature	*-30°C…+100°C*
IP Protection Class	*IP40*
Life	*100 million movements*
Rod Material	*Stainless Steel*
Body Material	*Aluminum*

Table-3.12 The Technical Properties of EPA 100 [132]

Display	*1st Line: 7-segment LED, digit height:7mm* *2nd Line: 7-segment LED, digit height:7mm*
Supply Voltage	*24 $V_{AC/DC}$ 50/60 Hz* *85-265 V_{AC} 50/60 Hz*
Power usage	*9 VA / 2,7 Watt Max*
Sensor Supply Voltage	*Pot: 5 V_{DC} mV/V: 10 V_{DC}* *0-10V: 24 V_{DC} 4-20 mA: 24 V_{DC}* *CANopen: 24 V_{DC}*
Max Sensor Supply Current	*100 mA*
Refresh Rate	*3.5 kHz*
Resolution	*16 bit*
Analogue Inputs	*Potentiometer, 0.5-4.5 V, 0-5 V, 0-10 V, 4- 20 mA, 0-20 mA, 3.33 mV/V, 2mV/V, 2.5mV/V Ratiometric*
Relay Outputs	*2 x 250 V_{AC} 3A Relay*
Serial Communication (Optional)	*RS-232, RS-485, USB, CANopen*
Analogue Outputs (Optional)	*0-10 V, 0-5 V, 0.5- 4.5 V, 4-20 mA, 0-20 mA*
Electrical Connection	*2,5 mm2 Universal Terminal*
Weight	*200 gr*
Operating Temperature	*0 … 50 °C*
Protection Class	*IP60 Front Panel, IP20 Back Panel*

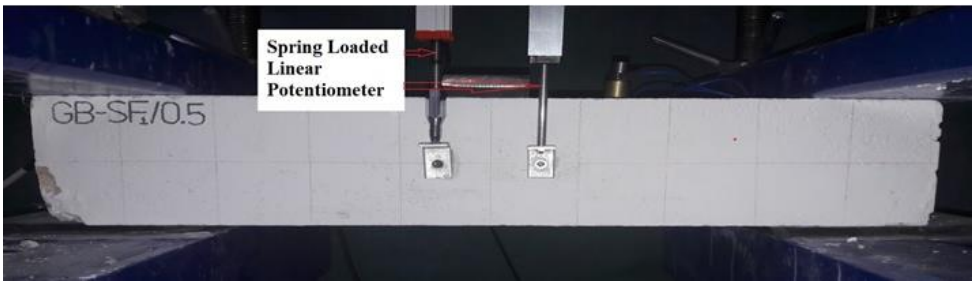


Figure 3.31 Spring loaded linear potentiometers mounted on beam specimen

3.5.5.5 Data Logger

In the study, dynamic type data logger was used to transfer the data taken from accelerometers and force sensor to the computer. NI 9230 with BNC Data logger produced by National Instruments Company was utilized as shown in the Figure 3.31 and its technical properties taken from the website of the producing company is given in the Table 3.13.



Figure 3.32 NI 9230 with BNC data logger

Table 3.13 The technical properties of NI 9230 with BNC data logger [134]

Product Name	*NI 9230*
Signal Ranges	*±30 V*
Channels	*3*
Sample Rate	*12.8 kS/s/ch*
Input Configurations	*IEPE with AC Coupling, AC Coupling, DC Coupling*
Noise at Maximum Sample Rate	*106 µVrms*
Connectivity	*Screw Terminal, BNC*
Isolation Continuous	*60 VDC Ch-Earth*

CHAPTER 4
CONCLUSIONS

4.1 Results and Discussions

4.1.1 Fresh State Test Results and Performance of SCGC Specimens

The results of flowability and passing ability tests of the fresh state SCGC mixes are in accordance with the specifications in EFNARC. The slump flow test results of SCGC mixes were observed to be in the range of EFNARC values and the minimum value was 661 mm which is higher than the minimum slump flow value that is 550 mm given in EFNARC specification. Also, these test results were appropriate with the minimum values (600mm) given in EN 12350-8 standard and that value is less than the minimum values as shown in the Table 3.8 . In addition, segregation and bleeding were not exhibited in the SCGC mixes. The influence of SFs, NS, RTR and using together of them on the flowability and passing ability of fresh state SCGC and each fresh state property are separately investigated and summarized in the following sections.

The fresh state tests' results of the SCGC specimens are given in the Table 4.1. The results of flowability indicated that the minimum flowability of 659 mm was obtained for GB-SF_2/1.0 mixture, which met the minimum flowability requirements of 550 mm according to EFNARC specification [14] and 600 mm according to EN 12350-8 standard [135]. For the L-Box tests, PL value must be higher than 0.8 according to the indicated requirements/specifications and the test results showed that all PL values were obtained higher than 0.8, which satisfied the passing ability requirements criteria of the SCGC mixes. In the V-Funnel test, the maximum discharge duration allowed to be a 15 sec to obtain excellent filling performance [135]. The test results showed that the specimens with non-fibrous and SFs/0.5% almost satisfied this standard. But, the discharge duration of the specimens including SFs/1.0% were obtained to be higher than the standard (15 sec) and the maximum discharge duration of the mixtures was GBN-SF_2/1.0, its discharge duration was

determined as 24 sec. However, the SCGC specimens reinforced with SFs/1.0% was not observed any blocking. For the mixtures high flowability, T_{50} duration of the mixes must be under 6 sec according to the standard [135]. The results showed that T_{50} duration of all SCGC mixes met the criterion of 6 sec, indicating that these all mixes had enough flowability characteristics.

The fresh properties of the second series of the SCGC mixes were also indicated in the Table 4.1. The minimum slump flow value of the mixes was obtained form the GB-SF_1/1.0-TCR/15 mix and it was measured as 657 mm. Acoording to the specifications, this value is higher than the least slump flow values of 550 mm [14] and 600 mm [135]. Also, the highest T_{50} duration among the T_{50} flow time tests was obtained as 4 sec on the GB-SF_1/1.0-TCR/15 mix and all T_{50} values were gotten lower than the maximum standard T_{50} slump flow time of 6 sec [135].

The V-Funnel discharge time of the SCC mixtures should be less 15 sec to obtain superior filling ability according to B.12350-9 EN specification [136]. In the Table 4.1, the results showed that the V-Funnel discharge times were generally obtained to be higher than 15 sec for the SCGC specimens, except GB, GB-SF_1/0.5, GBN, GBN-SF_1/0.5 and GB-FCR/5.0-CCR/5.0 specimens. The highest V-Funnel discharge time was gotten as 24.13 sec on the GB-SF_1/1.0-TCR/15 mix. However, the all rubberized SCGC specimens were not observed any blocking.

The L-Box test results show the pass ability of SCC mixtures and the PL value must be greater than 0.8 to satisfy the pass ability criteria [14,137]. In the Table 4.1, the results of PL were obtained higher than 0.8 that means all SCGC specimens had the adequate passing ability. The fresh state tests' results pointed out that the almost all SCGC mixes have adequate flowability and passing ability.

Table 4.1 The fresh state test results of SCGC specimens

Sample	S-Flow (mm)	L-Box (PL)	V-Funnel (sec)	T_{50} (sec)
GB	741 (±2)	1 (±0)	10.71 (±0.55)	2.46 (±0.04)
GB-SF_1/0.5	707 (±5)	0.96 (±0.02)	14.25 (±0.89)	3.13 (±0.07)
GB-SF_1/1.0	664 (±7)	0.83 (±0.02)	19.91 (±1.19)	3.63 (±0.10)
GB-SF_2/0.5	693 (±6)	0.94 (±0.02)	17.09 (±0.98)	3.37 (±0.09)
GB-SF_2/1.0	659 (±9)	0.81 (±0.03)	23.49 (±1.26)	4.07 (±0.13)
GBN	750 (±1)	1 (±0)	9.25 (±0.46)	2.21 (±0.03)
GBN-SF_1/0.5	720 (±4)	0.97 (±0.01)	13.88 (±0.74)	2.87 (±0.06)
GBN-SF_1/1.0	687 (±6)	0.85 (±0.02)	18.33 (±0.97)	3.59 (±0.08)
GBN-SF_2/0.5	710 (±5)	0.96 (±0.01)	16.62 (±0.88)	3.23 (±0.07)
GBN-SF_2/1.0	661 (±7)	0.82 (±0.02)	22.61 (±1.17)	3.97 (±0.10)
GB-FCR/5.0-CCR/5.0	704 (±4)	0.94 (±0.01)	14.23 (±0.76)	3.25 (±0.06)
GB-FCR/7.5-CCR/7.5	673 (±5)	0.89 (±0.02)	17.93 (±0.82)	3.63 (±0.08)
GB-TCR/10	683 (±4)	0.90 (±0.01)	19.49 (±0.86)	3.47 (±0.08)
GB-TCR/15	667 (±6)	0.84 (±0.02)	22.94 (±0.94)	3.91 (±0.11)
GB-SF_1/1.0-FCR/5.0-CCR/5.0	678 (±6)	0.90 (±0.02)	17.57 (±1.02)	3.37 (±0.11)
GB-SF_1/1.0-FCR/7.5-CCR/7.5	664 (±8)	0.84 (±0.03)	19.97 (±1.15)	3.87 (±0.13)
GB-SF_1/1.0-TCR/10	672 (±8)	0.85 (±0.02)	22.68 (±1.23)	3.73 (±0.12)
GB-SF_1/1.0-TCR/15	657 (±10)	0.80 (±0.03)	24.13 (±1.38)	4.01 (±0.14)

4.1.1.1 Effects of SFs, NS and RTR on Slump Flow Values

The results of slump flow tests are shown in the Figure 4.1. The effects of NS, SFs, RTR and using together of them on the slump flow values of SCGC were shown in the Figure 4.2.a and 4.2.b. The maximum slump flow value (750 mm) was observed in the mix just only with NS. So, the presence of NS in the SCGC mixes improved the slump flow value of the mixes. However, the addition of only SFs in the mixes were reduced the slump flow value from 741mm to 707mm with SF_1/0.5% to 664mm with SF_1/1.0% to 693mm with SF_2/0.5% and to 659mm with SF_2/1.0%. According to the test results, the SFs/1.0% reinforced SCGC specimens showed poor performance. In addition, the slump flow of the SCGC mixes reduced with increasing SFs length and aspect ratios. So, the SCGC mixes with SF_2 indicated slightly less flowability performance than SF_1 reinforced SCGC mixes. Also, when using NS in steel fibrous SCGC mixtures, the slump flow values of the mixtures significantly improved. Consequently, the negative effect of SFs on slump flow can be covered with the incorporation of NS. According to the test results, the minimum slump flow value (659mm) was obtained with the mixtures containing maximum volume fraction of SF (SF_2/1.0%). Moreover, the aspect ratio and amount of SFs in

the SCGC mixtures affect on the slump flow values of the mixtures, namely the slump flow value of the mixtures seriously reduced with increase in the aspect ratio and amount of SFs. Regarding the type and the amount of SFs, the slump flow values were found to be more as the aspect ratio increased and the amount of SFs decreased. Furthermore, the tests results shows that the slump flow value of all SCGC mixes were in the range of slump flow 2 in the classification of EFNARC. This class are compatible for several structural applications (slabs, beams and columns) according to the EFNARC specifications [29]. Consequently, the SCGC mixes are appropriate for the beam members in this study.

Figure 4.2.b shows the slump flow variation of SCGC mixes with the SF_1 and RTR. The results showed that the flowability performance of SCGC mixes reduced with addition of RTR and SF_1. The highest slump flow performance was obtained on the control mix (GB), while the minimum slump flow performance was obtained from the SCGC mix containing SF_1/1.0% and TCR/15% (GB-SF_1/1.0-TCR/15%). It has been found that the slump flows of the mixtures decrease with an increase in RTR replacement ratios. So, the slump flows of the mixes contaning FCR/7.5%-CCR/7.5% and TCR/15% were obtained lower than the mixes containing FCR/5.0%-CCR/5.0% and TCR/10%. A similar result was also obtained in the previous research that the flowability properties reduce with the increase in RTR particles [138]. In addition, the rubberized mixes with bigger sizes rubber (TCR) showed lower flowability performnace than the rubberized mixes with lower sizes rubber (FCR and CCR) under the same replacement ratio. Moreover, the rubberized mixes inclusion of SF_1 decreaced the flowability performance more compared to non-fibrous rubberized mixes. The previous studies were also noticed that the slump flow of rubberized mixes reduced owing to the addition of SF_1/1.0% [139,140].

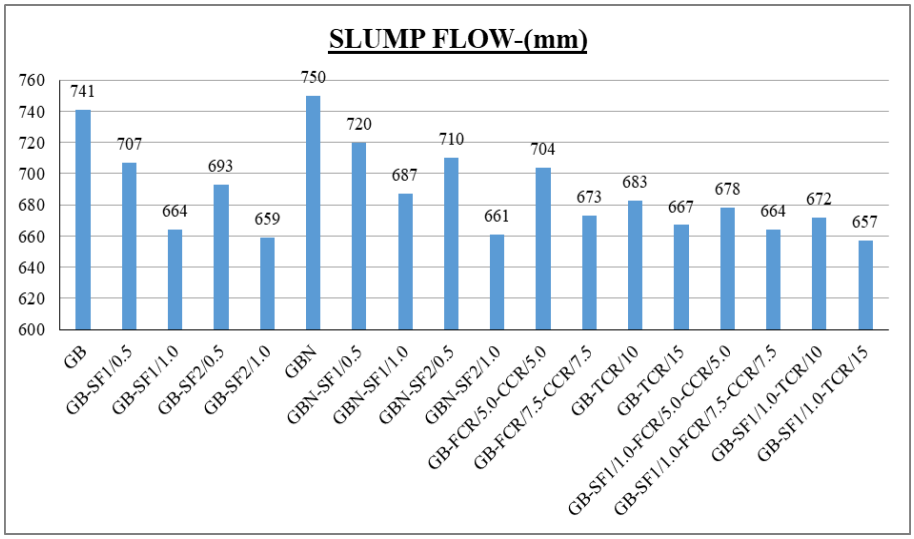
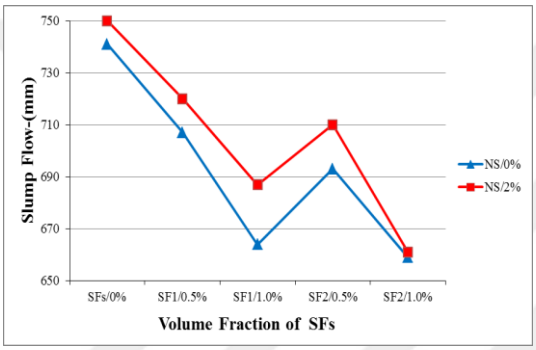
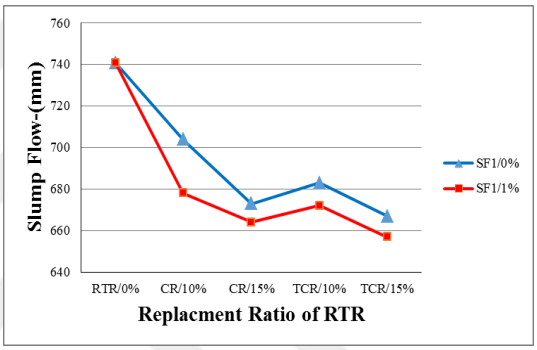


Figure 4.1 The results of slump flow tests



a) The Effects of SFs and NS on the Slump Flow of SCGC Mixes



b) The Effects of SF_1 and RTR on the Slump Flow of SCGC Mixes

Figure 4.2 The effect of SFs, NS and recycled tyre rubber (RTR) on the slump flow results

4.1.1.2 Effects of SFs, NS and RTR on The Slump Flow Time (T_{50})

The results of T_{50} Slump Flow Time tests are given in the Figure 4.3.The effects of NS, SFs, RTR and using together of them on the T_{50} durations are shown in the Figure-4.4.a and 4.4.b. Moreover, T_{50} represents the time measured until the fresh state SCGC touches the 500 mm diameter. According to the Figure-4.4.a, T_{50} durations of the mixes only including SF_1 type with volume fraction of 0%, 0.5% and 1% are 2.46 sec, 3.13 sec, and 3.63 sec, respectively; and 2.46 sec, 3.37 sec, and 4.07 sec, respectively for the mixes including 0%, 0.5% and 1% SF_2 type. Moreover, for the mix only including 0% and 2% NS , the T_{50} durations were 2.46 sec and 2.21 sec, respectively. Hence, it can be deducted that the adding of NS in the mixes improved their T_{50} durations and enhance the flowability of SCGC mixes. The T_{50} duration of GBN-SF_2/1.0 (including SF_2/1% and NS/2%) were increased to 3.97 sec that is less than the value of mix including only GB-SF_2/1.0 (including SF_2/1%). It can be

concluded that the using of NS in the SCGC mixes improve the flowability of mixes. Similar to slump flow test results, the highest T_{50} duration of the SCGC mixes were observed in the mix with only NS (GBN). Also, the flowability of the fibrous mixes with NS are better than the fibrous mixes without NS. Moreover, T_{50} durations in the current study are less than 6 sec so they are compatible with the EN 12350-8 standard [136]. Consequently, T_{50} result of all mixes are in the state to be acceptable according to both EN 12350-8 standard [136] and EFNARC specification [14]. In addition, the T_{50} duration results of the mixes showed that the flowability of SCGC mixes were adversely influenced by the aspect ratio and the increasing amount of SFs; as the volume fraction and aspect ratio of SFs decrease, the T_{50} duration of mixes decrease.

Similar results were obtained with the slump flow values. Figure 4.4.b represents the T_{50} flow times of the rubberized SCGC mixtures with SF_1 and without SF_1. The minimum T_{50} flow time was obtained in the control specimen (GB) without RTR and SF_1, while the maximum T_{50} flow time was achived in the specimens containing TCR/15% and SF_1/1.0% (GB-SF_1/1.0-TCR/15).Similar to the slump flow test results, T_{50} flow time of the SCGC mixes increased as RTR and SF_1 volume ratios increased in the mixes.Also, the delay of the T_{50} flow times of the SCGC mixes with TCR was found to be more than the FCR and CCR based mixes under the

the same replacement ratios as shown in the Figure 4.3.b. Meanwhile, the rubberized mixes addition of 1.0%SF_1 also increased the T_{50} slump flow time of the all rubberized mixes; nevertheless, all rubberized mixes the requirements of minimum slump flow values and maximum T_{50} slump flow times according to the relevant specifications and standards.

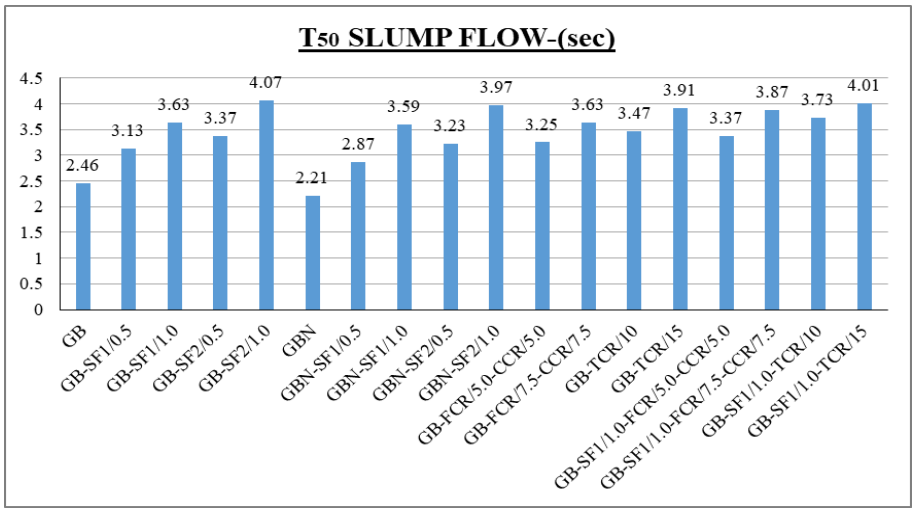
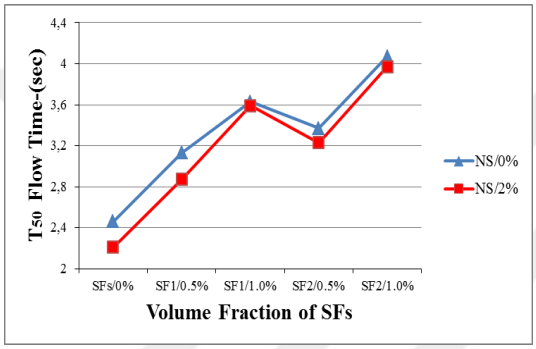
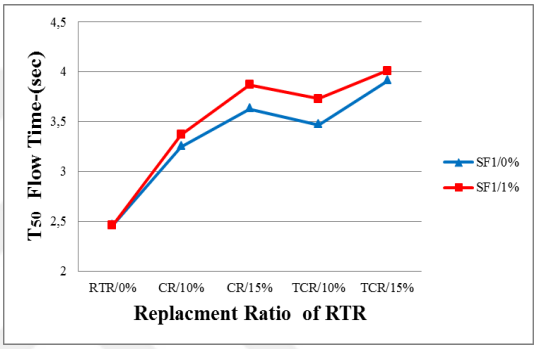


Figure 4.3 The results of T_{50} slump flow time tests



a) Effect of SFs and NS on the T_{50} duration of SCGC mixes



b) Effect of SF_1 and RTR on the T_{50} duration of SCGC mixes

Figure 4.4 The effect of SFs, NS and recycled tyre rubber (RTR) on the T_{50} flow duration

4.1.1.3 Effects of SFs, NS and RTR on V-Funnel Flow Time

The results of V-funnel flow time tests are shown in the Figure 4.5. The V-funnel flow duration is a response of flowability and the viscosity of SCGC mixes. Figure 4.6.a and 4.6.b represents the results of the mixes with SFs, NS and RTR. Similar to the results of the T_{50} duration tests and slump flow test , the discharge time of the mixes with only NS from V-funnel opening showed the lowest results, while the highest discharge time was achieved on specimens without NS and with SF_2/1.0% (GB-SF_2/1.0). The V-funnel flow durations of the mixes only consists of SFs were obtained as 10.71 sec, 14.25 sec, and 19.91 sec for the mixes with 0%, 0.5%, and 1.0% SF_1, respectively; 10.71 sec, 17.09 sec, and 23.49 sec for the mixes with 0%, 0.5%, and 1.0% SF_2, respectively. V-funnel discharge time was also increased with an increase in SFs volume ratio. In addition, specimens with SF_2 showed higher V-Funnel discharge duration than the specimens with SF_1, indicating that longer fibers

and higher aspect ratio caused a decrease in flowability compared to shorter fibers and lower aspect ratio. The similar results that higher aspect ratios for the same fiber volume decreases the flowability of SCC were obtained in the previous study [142]. Moreover, the V-funnel flow durations for the mix just incorporating NS were 10.71 sec (NS/0%) and 9.25 sec (NS/2.0%). As a result, the effects of SFs on the V-funnel flow time were determined to be more than the influence of NS. In addition, the flow time of fibrous mixes for both types of SFs improved with the incorporation of NS. Similarly, the minimum and maximum flow times were the mix with only NS and the mix with just including SF_2/1.0% respectively, as shown in the Figure 4.6.a. On the other hand, the aspect ratio and amount of SFs significantly affected the flow time of mixes. Also, Figure 4.6 indicate that the flow ability times increased with increase in the amount and aspect ratio of SFs.

Figure 4.6.b indicates the V-funnel discharge time of SCGC rubberized mixes. According to the V-Funnel test results, the minimum V-funnel discharge time of the mix without SFs and RTR was obtained, while the highest discharge time was obtained in the mixture including TCR/15% and SF_1/1.0% (GB-SF_1/1.0-TCR/15). So, the V-funnel discharge time of the rubberized mixes increased as the RTR ratio increase in the mixes. The mixes with TCR showed the higher V-funnel flow time than the mixes with FCR and CCR under the same replacement ratios, because longer rubber particles had the worse flowability performance than the shorter rubber particles.

Figure 4.6.c and 4.6.d show the V-funnel discharge duration and T_{50} flow duration relationships stated by EFNARC specifications [14]. According to the results of T_{50} and V-funnel discharge durations, all SCGC mixes of the study were taken part in the region of VS2/VF2 classification. Moreover, the region of VS1/VF1 viscosity classification has a suitable flow for high reinforcements structures according to EFNARC specification. But, this class has insufficient resistance to segregation and bleeding. While VS2/VF2 class has low formwork pressure, it has good resistance to segregation and bleeding. Therefore, the surface finish property of VS2/VF2 class is insufficient and it can disrupt from the stoppage of SCGC mixes flow. The V-funnel results show that the asset of NS increased the discharge flow duration, resistance to the bleeding and segregation. Moreover, the V-funnel flow duration of any SCGC

mix must be lower than 15 sec to obtain an excellent filling ability according to the EN 12350-9 standard [136]. The flow duration of the non-fibrous mixes with and without NS, and the flow duration of the mixes incorporation SF_1/0.5% with and without NS were below the standard limit value (15 sec), except the mixes containing SFs/1.0% and SFs/0.5%. In addition, the flow duration of all SCGC mixes consist of NS were more than the mixes without NS. So, it can be concluded that NS can be used to improve significantly the filling ability of SCGC incorporating SFs.

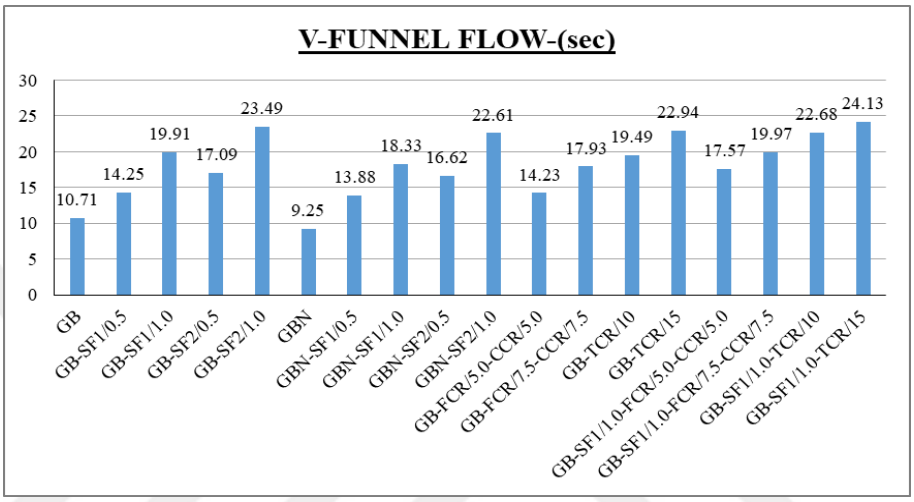
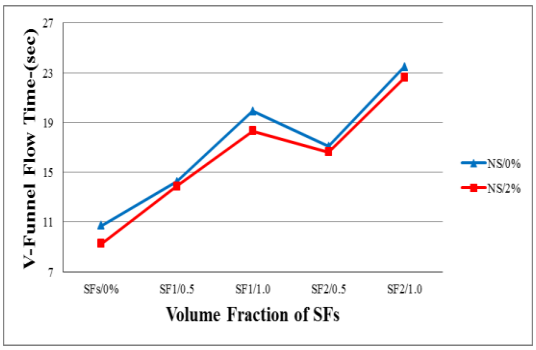
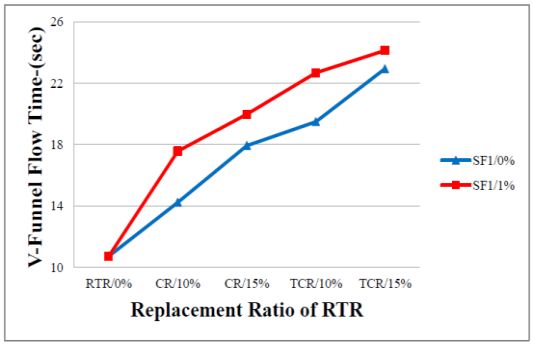


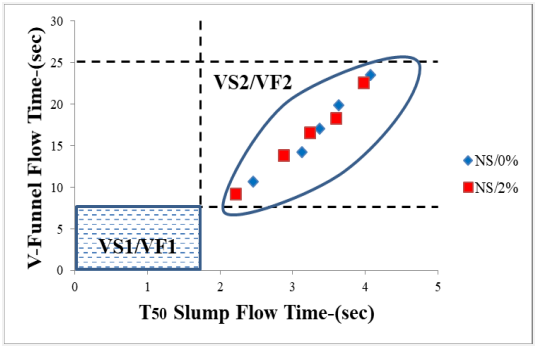
Figure 4.5 The results of V-funnel flow time tests



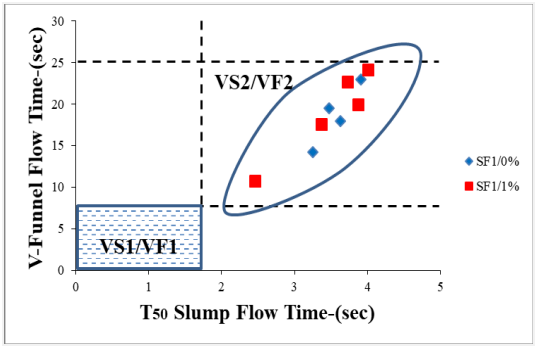
a) The effect of NS and SFs on the V-funnel duration of SCGC mixes



b) The effect of RTR and SF_1 on the V-funnel duration of SCGC mixes



c) T_{50} flow time vs V-funnel flow time Relationships of NS



d) T_{50} flow time vs V-funnel flow time Relationships of Rubberized Mixes

Figure 4.6 The effects of NS, SFs and RTR on V-funnel time and T50 flow time vs V-funnel flow time relationships of NS, SFs and RTR

4.1.1.4 Effects of SFs, NS and RTR on The L-Box Height Ratio

The results of L-box tests are shown in the Figure 4.7. The L-Box test is used to determine the flow ability of SCGC mixes through narrow open channel including three bars (41±1 mm) and it is measured the ratio of H_2/H_1 (the height of the horizontal part of concrete/the height of the vertical part of concrete) after fully flow. In the EN12350-10 standard and EFNARC specification, it is specified that the passing ability ratio (H_2/H_1) through L-Box test must be higher or equal than 0.8 in order to satisfy satisfactory passing ability requisites for SCC mixes [137]. The results of L-Box passing ability test of the mixes with/out NS and/or SFs are shown in the Figure 4.8.a. The mixes of the highest passing ability (1.0) are mixes without SFs. So, it is concluded that the passing ability of SCGC mixes decreased with the addition of SFs; the passing ability for the just fibrous mixes were 1.0, 0.96, and 0.83 for the mixes includes 0%, 0.5% and 1.0% SF_1, respectively; 1.0, 0.94, and 0.81 for the mixes consist of 0%, 0.5% and 1.0% SF_2, respectively. The superior passing ability was obtained in the mixes without SFs, whereas the poorest performance was achieved in the mixes with reinforced SF_2/1.0%. In addition, it was observed that adding NS/2% in the mixes with fibrous the passing ability values of SCGC mixes increased. But, according to the test results, the passing ability of SCGC were adversely affected with increasing the amount of SFs from 0.5% to 1%. It can be concluded that the passing ability requirements of the SCGC mixes couldn't provide, if the amount of SFs is more than 1%. Furthermore, it was noted that the addition of NS in the mixes of SCGC enhanced the passing ability of the fibrous and non-fibrous mixes. Therefore, it can be deductived that the incorporation of NS

recommended for the fibrous SCGC to achieve the better and/or adequate fresh properties of SCGC. The passing ability of the mixtures reduced as SFs volume ratio (Vf) increased. In addition, the higher SFs length and aspect ratio decreased, while the NS addition slightly improved the passing ability of the mixes. The volume and aspect ratio of the SFs decreased, while the addition of NS to the mixes slightly improved the passability of the mixes.

Figure 4.8.b shows the L-Box test results for the rubberized SCGC mixtures. The results showed that all rubberized mixes had higher PL values than the minimum standard PL value of 0.8. The lowest PL value was obtained as 0.8 for the mixes including SF_1/1.0% and TCR/15% (GB-SF_1/1.0-TCR/15), while the maximum PL value was reached as 1 for the mixes without RTR and SF_1 (GB). Similar to other tested fresh state properties, PL value decreased with an increasing RTR ratio and SF_1 inclusion. Also, the FCR and CCR based mixes exhibited higher PL values than the TCR based mixes for the same replacement ratios. All SCGC mixes are an acceptable passing ability as shown in the figure (passing ability $\geq$ 0.8).

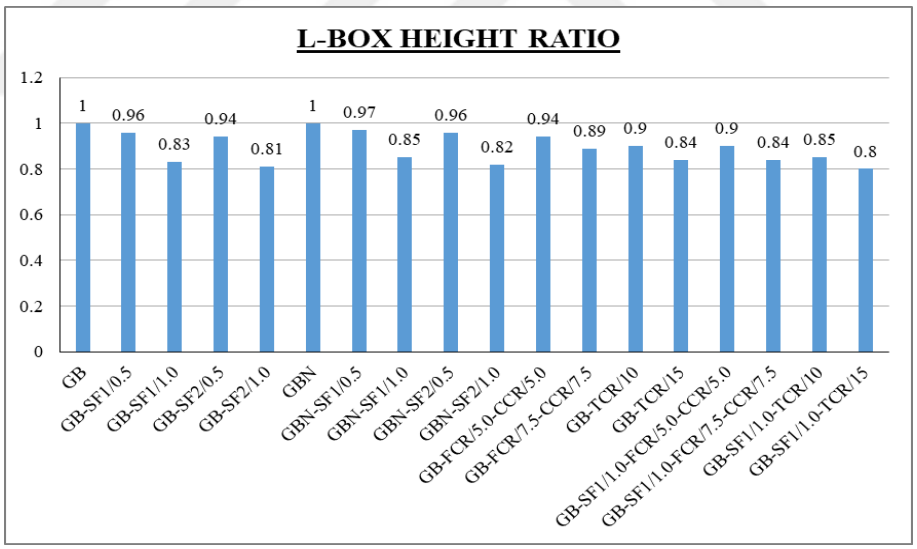
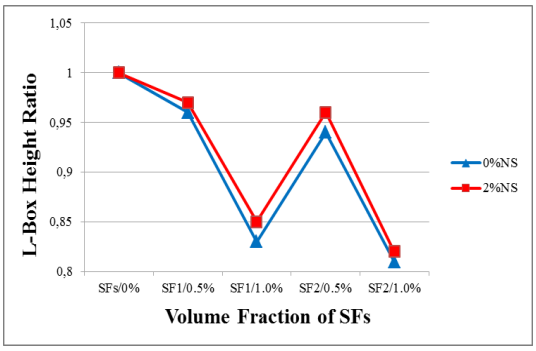
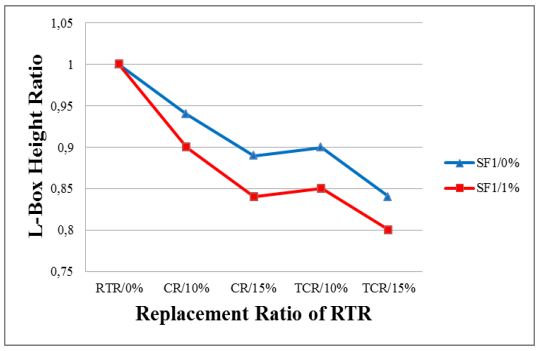


Figure 4.7 The results of L-box tests



a) The variation of the L-box ratio with SFs & NS



b) The effect of SF_1 and RTR on the L-box ratio

Figure 4.8 The effect of NS, SFs and RTR on the L-Box height ratio

Finally, it can be said that according to the the tests' results addition of NS in the mixes improved the passing ability and flowability of slag based SCGC mixes. But, the adding of SFs in the mixes reduce the passing ability and flowability of SCGC. Moreover, the using together SFs and NS in the mixes obtain better the passing ability and flowability properties than the just using SFs. Also, increasing the aspect ratio and amount of SFs in the mixes, the flow ability and passing ability of SCGC are adversely affected. However, it was indicated that all mixes of the study satisfied the passing ability and flowability criteria requirements according to TS EN 12350 standards and EFNARC specifications even for the presence of highest volume fraction (1%) for SFs. Moreover, it was noticed that addition of NS improved the fresh state properties of SCGC mixes and increasing the resistance to bleeding and segregation, and sametime enhance the finishing surface and uniformity. Therefore, it is recommended that NS can be used to obtain the better fresh state properties (the passing ability and flowability) in the SCGC mixes with SFs. The fresh state results indicated that RTR decreased the fresh state properties, and the reduction was found more with the SF inclusions into the rubberized SCGC mixes. Among the RTR, TCR reduced the fresh state performances of mixes more than the FCR and CCR. The results revealed that all rubberized SCGC mixes had adequate flowability and passing ability characteristics based on the related guidelines and standards.

4.1.2 The Hardened State Test Results and Performance of SCGC Specimens

The hardened state test results of the SCGC specimens are shown in the Table 4.2. The results showed that NS addition to the specimens slightly increased the compressive strength, modulus of elasticity, splitting tensile strength, and flexural strength of the samples. Moreover, the mechanical properties of the specimens

increased, as SFs amount and aspect ratio increased. In the case where SF_2 and NS were used together, the sample showed superior improvement in its mechanical performance. The results showed that compressive strength, modulus of elasticity, splitting tensile and flexural strengths decreased, as RTR replacement ratios in the non-fibrous specimens increased. However, the deformation capacity of the specimens including RTR and SF_1/1.0 significantly improved. The inclusion of SF_1 in rubberized samples slightly reduced the compressive strength, while the modulus of elasticity, splitting tensile and flexural tensile strengths slightly increased with the addition of SF_1. It was emphasized that when SFs and RTR are used together, deformation and energy absorption capacities are significantly increased.

Table 4.2 The hardened state test results of SCGC specimens

Specimen	Compressive Strength (MPa)	Modulus of Elasticity (GPa)	Splitting Tensile Strength (MPa)	Maximum Load (kN)	Flexural Strength (MPa)	Drop Number
GB	60.95	20.73	3.43	8.65	3.89	2
GB-SF_1/0.5	64.30	22.15	3.92	8.77	3.94	10
GB-SF_1/1.0	66.93	29.09	4.76	10.25	4.61	41
GB-SF_2/0.5	66.52	24.39	4.36	9.10	4.10	47
GB-SF_2/1.0	69.08	33.11	5.55	13.67	6.15	128
GBN	59.73	20.49	3.29	7.96	3.58	7
GBN-SF_1/0.5	61.41	23.25	4.90	8.86	4.03	25
GBN-SF_1/1.0	62.53	26.65	5.42	10.93	4.92	89
GBN-SF_2/0.5	62.72	23.62	5.62	12.23	5.50	62
GBN-SF_2/1.0	66.12	31.41	6.32	14.67	6.60	289
GB-FCR/5.0-CCR/5.0	52.74	19.17	3.17	7.75	3.49	3
GB-FCR/7.5-CCR/7.5	50.74	18.47	2.97	7.44	3.35	4
GB-TCR/10	53.23	19.52	3.12	8.02	3.61	5
GB-TCR/15	49.31	19.18	3.02	7.75	3.49	6
GB-SF_1/1.0-FCR/5.0-CCR/5.0	55.32	21.97	3.95	9.05	4.07	55
GB-SF_1/1.0-FCR/7.5-CCR/7.5	52.23	22.87	4.61	9.11	4.10	59
GB-SF_1/1.0-TCR/10	56.29	22.26	4.22	9.03	4.06	37
GB-SF_1/1.0-TCR/15	52.85	23.19	4.65	9.13	4.11	52

4.1.2.1 Compressive Strength of SCGC Specimens

The compressive strength results of SCGC specimens in the study are shown in the Figure 4.9 and the effects of SFs, NS and RTR on the compressive strength are given in the Figure 4.10. The results showed that the incorporating of NS in the mixes had no important influence on compressive strength of SCGC specimen as shown in the Figure 4.10.a. So, the compressive strength of SCGC specimens including NS were

little less than the compressive strength of the specimens without NS. These may be owing to the excessive self-dehydration of the specimens including NS as a results of partially unreacted NS particles which causes formation of cracks (weakened the microstructure) and so deteriorate the compressive strength [77,142]. The compressive strength of the specimens including NS were 2% less than without NS. But, the test resuts were shown that presence of SFs in the mixes considerably improved the compressive strength of SCGC specimens. The compressive strength of the mixes were increased more than 5% and 9% for the specimens including 0.5% and SF_1/1.0%, respectively; 9% and 13% for the specimens including 0.5% and 1.0% SF_2, respectively. Previous studies showed that the presence of SF improve the compressive strength of ordinary concrete [143]. Moreover, this compressive strength improvement may be attributed to the improved SFs and matrix bond strength caused by the crack arresting capability of fibers [80]. Hence, it is worth to indicate that the addition of SFs can compensate for the decrease in the compressive strength resulted due to the incorporation of NS. The aspect ratio 40 and 80 of SFs has significant effect on the compressive strength as reported by Bayramov et al. [144]. In the study, the aspect ratio 80 of SF improved the compressive strength of the mixes more than the aspect ratio 40 of SF. According to Mohammadi et al. [145] and Yazıcı et al. [146], the mechanical characteristic of ordinary concrete enhance as the aspect ratio of SF increase. Furthermore, in the SCGC mixes, increasing the amount of SFs from 0.5% to 1.0% improved the compressive strength of the mixes. The highest compressive strength was obtained for longer steel fiber and higher aspect ratio samples without NS (GB-SF_2/1.0). The positive effect of high aspect ratio on compressive strength has also been reported in previous studies [144-146].

The effects of SCGC specimens with RTR on the compressive strength are shown in the Figure 4.10.b. The compressive strength of rubberized SCGC specimens deacreased, as the ratios of RTR increased in the specimens. The reductions in the compressive strengths of the GB-FCR/5.0-CCR/5.0, GB-FCR/7.5-CCR/7.5, GB-TCR/10, and GB-TCR/15 non-fibrous rubberized specimens were 13%, 17%, 13%, and 19% with respect to GB (non-fibrous and non-recycled rubber) specimen, repectively. However, the reductions of compressive strength became 9%, 14%, 8%, and 13% for the GB-SF_1/1.0-FCR/5.0-CCR/5.0, GB-SF1/1.0-FCR/7.5-CCR/7.5, GB-SF_1/1.0-TCR/10, and GB-SF_1/1.0-TCR/15 specimens as compared to GB specimen,

respectively. The compressive strengths increasing of the rubberized specimens were observed with the addition of SF_1/1.0 in the specimens. The results also showed that since close compressive strength values were obtained under the same replacment ratios in TCR and CR samples, the compressive strength was found to be independent from rubber sizes**.**

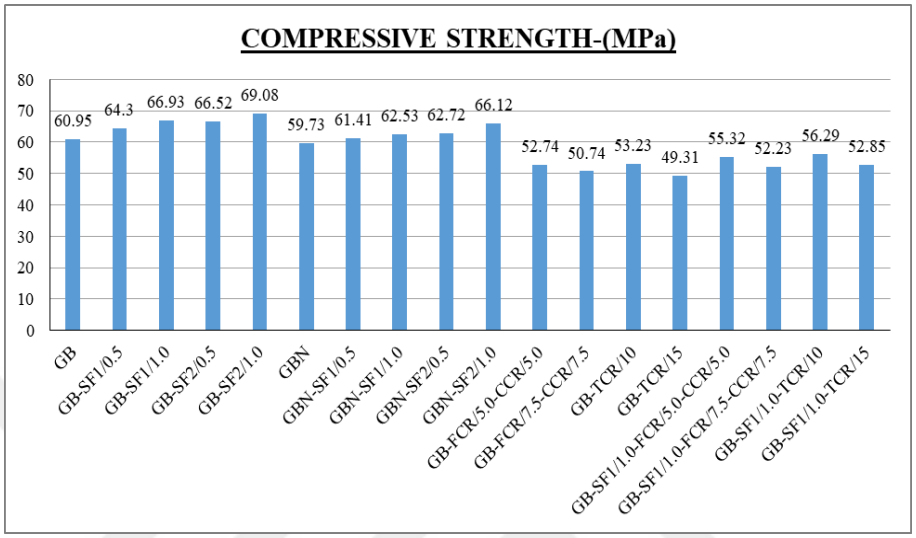
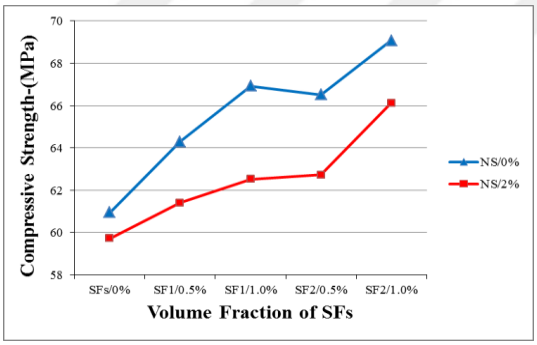
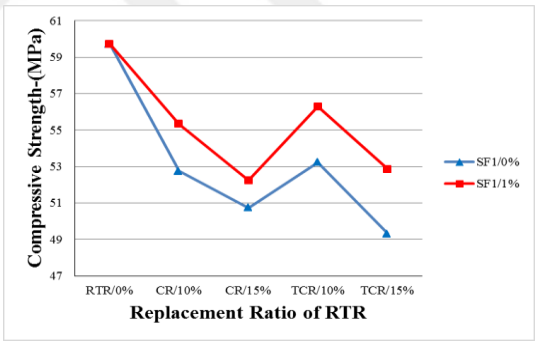


Figure 4.9 The results of compressive strength



a) The effects of SFs and NS on the compressive strength



b) The effects of SF_1 and RTR on the compressive strength

Figure 4.10 The effects of NS, SFs and RTR on the compressive strength

4.1.2.2 Modulus of Elasticity of SCGC Specimens

The results of the modulus of elasticity of the SCGC mixes obtained from the cylindrical specimens in the study are shown in the Figure 4.11 and the effects of SFs, NS and RTR on the modulus of elasticity are given in the Figure 4.12. The results are range from 18.47 to 33.11 GPa for slag based SCGC mixtures. As with the compression strength, the modulus of elasticity of the mixes increased with an increase in the amount and aspect ratio of SFs. So, the highest elasticity modulus was obtained in the GB-SF_2/1.0 specimen, while the lowest elasticity modulus was

obtained in the GBN specimen similar to compressive strength test results. It was found that the NS incorporation decreased the modulus of elasticity, which may be attributed to unreacted NS particles in the matrix. However, the use of NS had no considerable effect on the modulus of elasticity. But, the use of together SFs and NS increased the modulus of elasticity. It can be deducted that the utilize of NS improves the bond strength of SFs with the microstructure of SCGC mixes. In addition, the modulus of elasticity of mixtures with just fibrous are close to each other.

The modulus of elasticity of the non-fibrous specimens decreased with the addition of RTR. The reductions in the modulus of elasticity results due to the RTR were found to be 8%, 11%, 6%, and 7% for the GB-FCR/5.0-CCR/5.0, GB-FCR/7.5-CCR/7.5, GB-TCR/10, and GB-TCR/15 with respect to GB specimen, respectively. However, when SF_1 was added to the rubberized specimens, the modulus of elasticity of the specimens improved, and these improvements were found to be 6%, 10%, 7%, and 12% for the GB-SF_1/1.0-FCR/5.0-CCR/5.0, GB-SF_1/1.0-FCR/7.5-CCR/7.5, GB-SF_1/1.0-TCR/10 and GB-SF_1/1.0-TCR/15 specimens, respectively. The average reductions of the non-fibrous specimens in the modulus of elasticity were found 7% and 9% for the 10% and 15% RTR replacements, whilst the average increasing of the specimens including SF_1 were 7% and 11% for the 10% and 15% RTR replacements, respectively. The addition of SF_1 to the rubberized specimens improved the modulus of elasticity and the improvement was found to be further increased with higher RTR replacements.

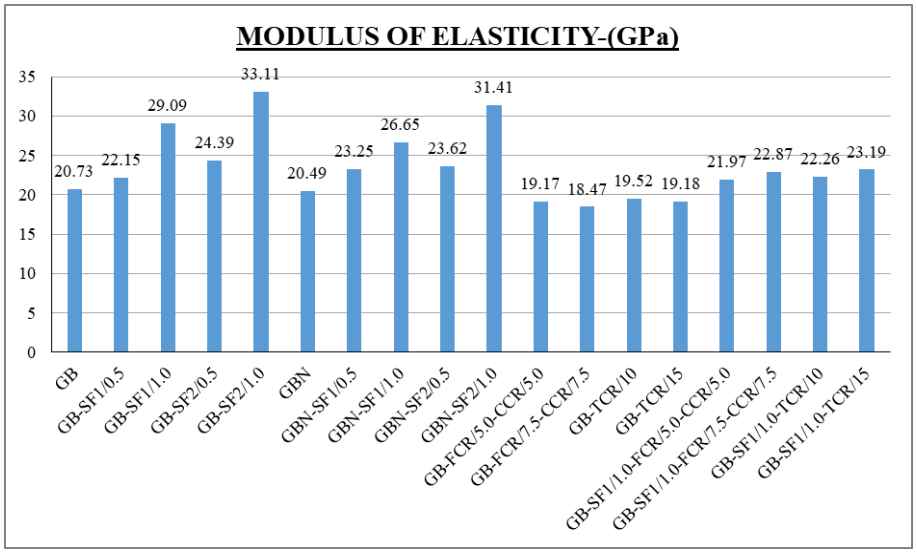
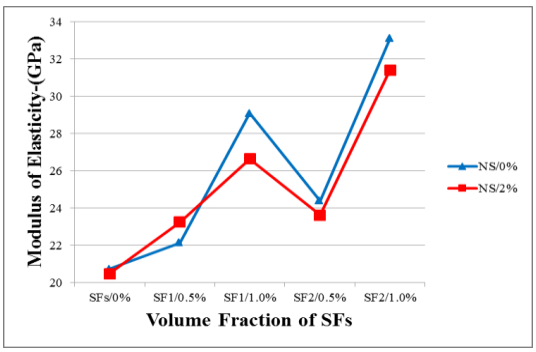
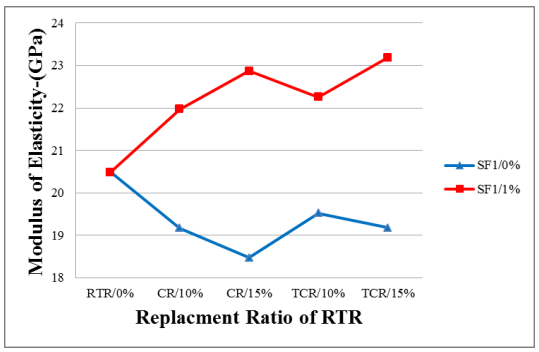


Figure 4.11 The modulus of elasticity test results



a) The effect of SFs and NS on modulus of elasticity



b) The effect of SF_1 and RTR on the modulus of elasticity

Figure 4.12 The effects of NS, SFs and RTR on the modulus of elasticity

Though there are many studies about the modulus of elasticity of ordinary portland concrete containing SF while there are limited or no studies related to the effect of NS on the modulus of elasticity and on bond strength of SCGC specimens. This study highlight the effect of NS incorporation on the modulus of elasticity of the SCGC specimens. Previous studies show that the concrete quality significantly affected the modulus of elasticity, compressive strength, and tensile strength. The addition of NS in the mixes improved the characteristic of the SCGC matrix and enhanced the microfilling influence through high surface area and pozzolanic activity of NS [46,63,80] and the bond strength of the SCGC including SFs were also improved by the NS incorporation. The together influence of SFs and NS on the properties of SCGC was studied by Gulsan et al. [95]; they concluded that the amount of SFs had no substantial effect on compressive strength; but SFs had significant effects on the bending strength and the bond strength of SCGC. In the research, it can be concluded that the use together of SF and NS improve the almost all properties of SCGC.

4.1.2.3 Splitting Tensile Strength of SCGC Specimens

The results of splitting tensile strength tests are given in the Figure 4.13. The effects of NS, SFs and RTR on the splitting tensile strengths results are shown in the Figure 4.14. Moreover, the variation in the splitting tensile strength results of the cylindrical SCGC specimens with/out NS and SFs are shown in the Figure 4.14.a. It can be concluded that the splitting tensile strength of SCGC was improved as the amount and aspect ratio of SFs increased. The splitting tensile strength improvement of volume fraction SFs/1.0% were about 39% and 62% more than non-fibrous and non-NS specimen (GB) at aspect ratio of 40 and 80 respectively. Moreover, the favorable

influence of SFs on the splitting tensile strength was also reported in the earlier studies [147-150]. The splitting tensile strength of the specimens containing the lower amount SFs/0.5% also increased with decreasing rate. However, the use together of NS and SFs significantly improved the splitting tensile strength of SCGC specimens, because they had an intensive microstructure and excellent bond strength between the SFs and matrix of SCGC specimens. The improvement of splitting tensile strength of the SCGC specimens was found to be 58% for GBN-SF_1/1.0 and 84% for GBN-SF_2/1.0 specimens. In addition the amount and aspect ratio of SFs improved the splitting tensile strength of SCGC specimens with/out NS. The obtained results pointed out that the NS/2% utilization also enhanced the splitting tensile strength, but the alone use of NS had no substantial effect on the splitting tensile strength of SCGC. This improvement was found higher for the SFs reinforced specimens with a higher aspect ratio, which may be due to the dense microstructure and excellent bond strength between matrix and SFs in the presence of NS. Previous researces were shown that the concrete including SF has more superior tensile characteristic than the non-fibrous concrete [147]. It was also determined that the utilize of SFs less than 0.5% improved the splitting tensile strength more almost 16–61% than the non-fibrous concrete. Moreover, the use of SFs between 0.5% and 1.0% improved the splitting tensile strength in the range of 19–116% and ıt's use between 1.0% and 2.0% caused an improvement almost 61% and 118%, respectively [148,150].

Figure 4.14.b shows the variation of splitting tensile strength results of the rubberized SCGC specimens. The results indicated that splitting tensile strength of the non-fibrous specimens slightly decreased, as the RTR ratio increased. The reductions of the splitting tensile strength of the rubberized SCGC specimens were obtained to be 8%, 13%, 9%, and 12% for the GB-FCR/5.0-CCR/5.0, GB-FCR/7.5-CCR/7.5, GB-TCR/10 and GB-TCR/15 compared to GB specimen, respectively**.** However, the splitting tensile strength significantly improved with SF_1 addition to the rubberized specimens and these improvements were found as 15%, 34%, 23%, and 36% for the GB-SF_1/1.0-FCR/5.0-CCR/5.0, GB-SF_1/1.0-FCR/7.5-CCR/7.5, GB-SF_1/1.0-TCR/10, and GB-SF_1/1.0-TCR/15 specimens compared to GB specimen, respectively. The average splitting tensile strength of the non-fibrous specimens decreased were 8% and 12% for the 10% and 15% RTR replacement ratios, whilst

the average splitting tensile strength improvements of the steel fibrous specimens were 19% and 35% for the 10% and 15% RTR replacement ratios compared to GB specimen, respectively. The SF_1 addition to the rubberized specimens improved the splitting tensile strength with further RTR replacements (15%). The results also pointed out that similar the splitting tensile strength values were obtained in the specimens with FCR, CCR and TCR under the same replacement ratios.

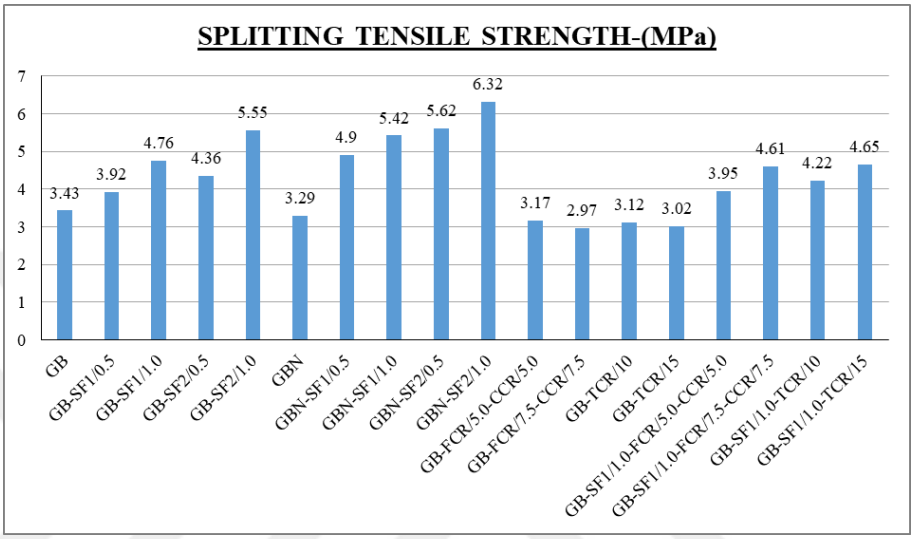
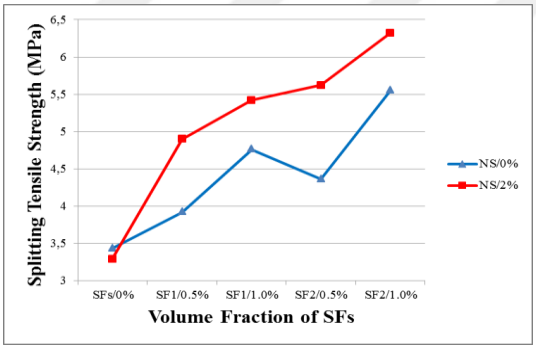
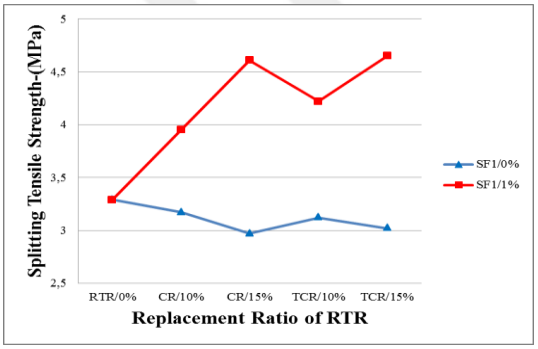


Figure 4.13 The results of splitting tensile strength tests



a) The effects of SFs and NS on the splitting tensile strength



b) The effects of SF_1 and RTR on the splitting tensile strength

Figure 4.14 The effects of NS, SFs and RTR on the splitting tensile strenght

4.1.2.4 Flexural Tensile Strength of SCGC Specimens

The results of flexural tensile strength tests are shown in the Figure 4.15. Moreover, under bending loads the force-displacement relation curves and the results of SCGC specimens are shown in the Figure 4.16. In the beginning of loading, a linear slope was detected until the creation of the first crack for all SCGC specimens and then strain relaxation was shown until the failure of specimens. In an other saying, a linear slope up to the first crack in the pre-peak zone and then strain softening in the post-

peak zone observed during four-point bending tests for all specimens. The load-displacement relation curves of the non-fibrous specimens exhibited similar performance and they also had almost similar values of the flexural tensile strength regardless of NS content as shown in the Figure 4.16.a. In addition, a sharp decrease in the post-peak zone was observed for the NS including specimens as shown in the Figure 4.16.b compared to specimens without NS as shown in the Figure 4.16.c for the steel fibrous specimens. Moreover, the specimens containing volume fraction SFs/1.0% had the higher residual flexural tensile strengths and less load relaxations than the specimens without NS as represented in the Figure 4.16.c. Figure 4.16.b shows the together effects of SFs and NS on the flexural tensile strength. It was shown that adding NS to SCGC samples with the same SFs volume fraction improved the flexural tensile strength of SCGC specimens. The specimens incorporation of NS improved the microstructure of specimens and enforced the bond strength between SFs and matrix, so the flexural tensile strength of the specimens increased. So, the flexural tensile strengths of the NS including specimens were found to be higher than the specimens without NS. A similar result was also obtained for the 50% fly ash and 50% slag based AAC specimens in the earlier investigation [95]. On the other hand, the specimens including SF_2 (higher aspect ratio) exhibited the higher flexural tensile strength than the specimens including SF_1 (lower aspect ratio). Kayali used the SF in the production of OPC; they investigated that the major effect of SF on the concrete was the increase of tensile strain capacity [99]. In the study of Nanni [100], It was also reported that the tensile strength can be significantly improved with the presence of SF owing to the crack bridging property of the fibers. Generally, the material properties of the matrix and the fiber characteristics such as tensile strength, aspect ratio, geometry and orientation affect the bond strength, the crack propagation and the flexural tensile strength of the concrete. Mohammadi et al. [145] made a study on the plain and steel fiber reinforced concrete and SFs were used different aspect ratio in the study. For the same amount of SFs, the tensile strength and fracture toughness of the specimens just including longer SF (SF_2) were higher than the specimens just including shorter SF (SF_1). Moreover, different hooked end SFs has aspect ratios of 45, 65, and 80 were studied by Yazıcı et al.[146]. The SF with aspect ratios of 45 was shorter than the other SFs and SFs with aspect ratios 65 and 80 were in same length. In the study, it was indicated that the mechanical properties of the same length fibrous concrete

improved as the aspect ratio of SF increased from 65 to 80. Moreover, the flexural tensile strength of the specimens including shorter SF was less than the specimens containing other SFs. The best tensile strength performance was obtained from the specimen including SF_2/1.0% and NS (GBN-SF_2/1.0). So, it can be concluded that an excellent bending behavior of SCGC achieve from the combined use of NS and SFs. Relationships between SFs volume fraction and the flexural tensile strength are shown in the Figure 4.17. In addition, the flexural tensile strength performance of specimens with a higher aspect ratio (SF_2) exhibited better performance than the specimens with a lower aspect ratio (SF_1). For the NS including specimens, the post-peak performance of 0.5% steel fibrous specimens with a higher aspect ratio was found to be better than the 1.0% steel fibrous specimens with a lower aspect ratio as shown in the Figure 4.16.b. For the specimens without NS, the flexural strength performance was influenced by the SF ratio, the higher SF ratio the better flexural performance as shown in the Figure 4.16.c. The enhanced flexural performance may be due to the improved interfacial transition zone and higher bond strength between NS particles and SFs, especially for higher aspect ratios. The favorable influences of SF characteristics were found on tensile strength [151,152], flexural strength and failure performance [140], and bond strength [95] in the previous studies. In another study, the effect of different SF aspect ratios was studied, tensile strength and fracture toughness were found high for the specimens with a high SF aspect ratio [74]. In addition, Figure 4.16.b showed that the more toughness and controlled load decrease were observed for the specimens including NS. Meanwhile, for the non-fibrous specimens, similar load-deflection curves were obtained as shown in the Figure 4.16.a, proving that NS utilization becomes significant when it was utilized with SFs in the SCGC specimens.

The results showed that the flexural tensile strength of the non-fibrous specimens was slightly decreased with the RTR additions as shown in the Figure 4.16.d and 4.16.e. The reductions of flexural tensile strength were reached as 10%, 14%, 7%, and 10% for GB-FCR/5.0-CCR/5.0, GB-FCR/7.5-CCR/7.5, GB-TCR/10 and GB-TCR/15 non-fibrous rubberized SCGC specimens with respect to GB specimen, respectively. However, the addition of SF slightly increased the flexural strength of the rubberized SCGC specimens. The flexural tensile strength improvements of 5%, 5%, 4% and 6% were obtained for GB-SF_1/1.0-FCR/5.0-CCR/5.0, GB-SF_1/1.0-

FCR/7.5-CCR/7.5, GB-SF$_1$/1.0-TCR/10 and GB-SF$_1$/1.0-TCR/15 SF rubberized specimens compared to GB specimen, respectively. For non-fibrous specimens, the average flexural tensile strength is 8% and 12% for 10% and 15% RTR replacement ratio, whilst the average flexural tensile strength improvements of SFs specimens were 5% and 6% for 10% and 15% RTR replacements ratio compared to GB specimen, respectively. The similar findings were obtained in the flexural tensile strength results with the splitting stress results.

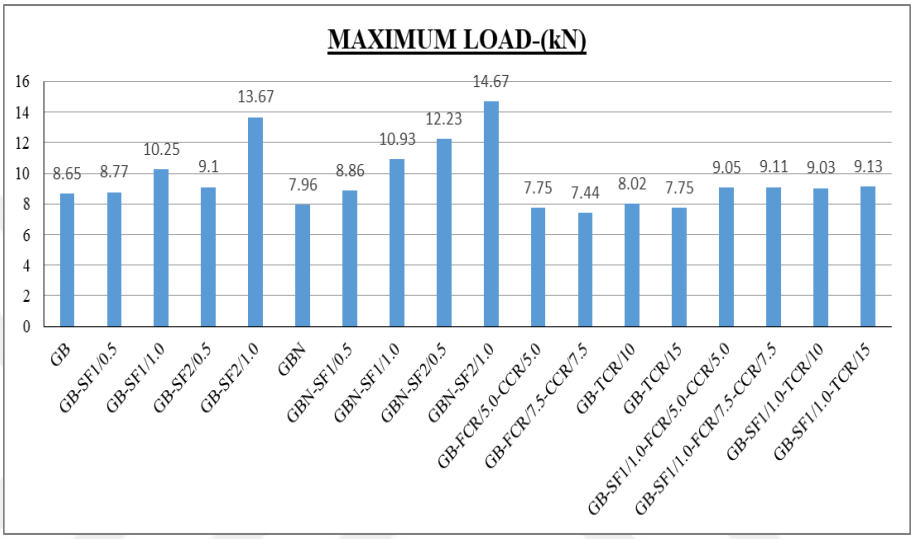
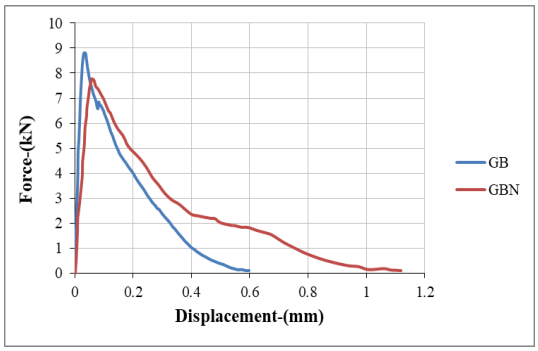
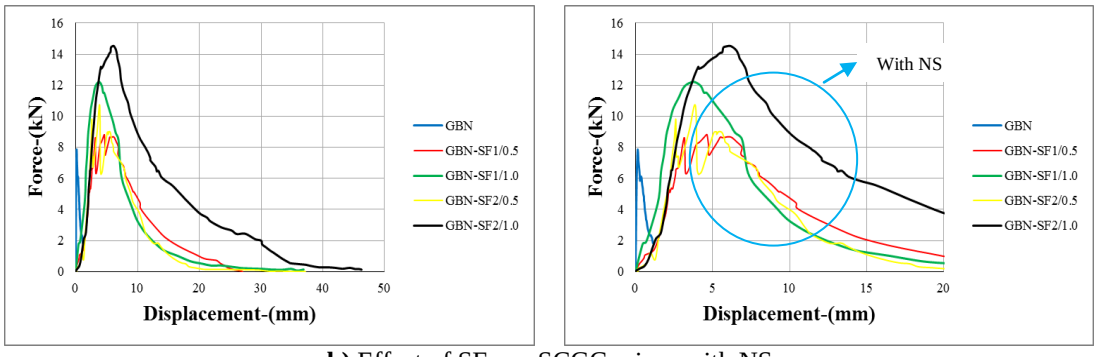


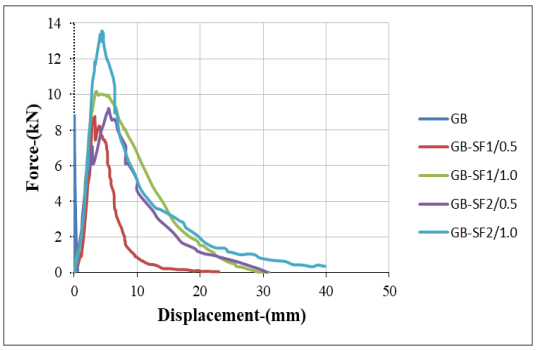
Figure 4.15 The results of flexural tensile strength tests

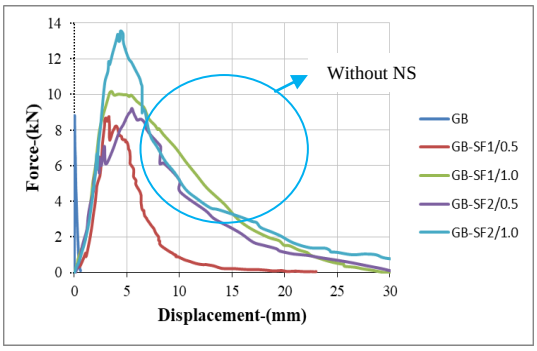


a) Effect of NS on SCGC mixes without SFs

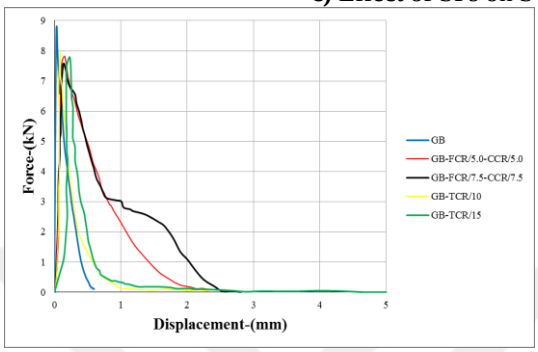


b) Effect of SFs on SCGC mixes with NS

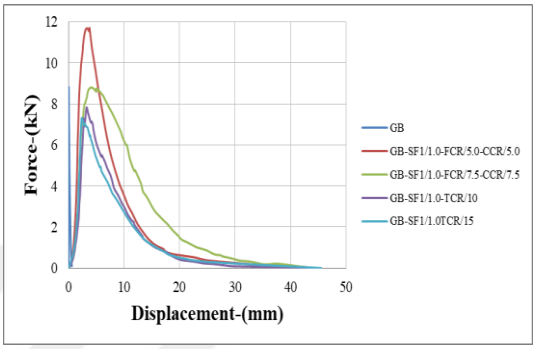




c) Effect of SFs on SCGC mixes without NS

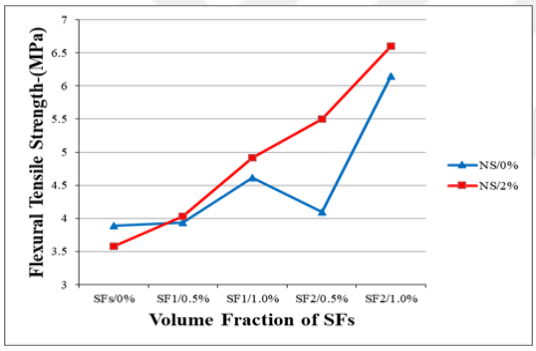


d) Effect of RTR on specimens without SF_1

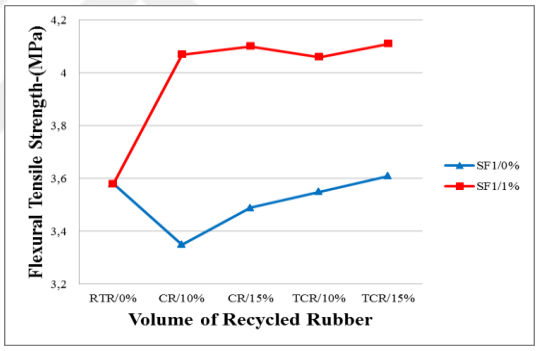


e) Effect of RTR on specimens with SF_1

Figure 4.16 Force-displacement relationships of SCGC



a)Flexural tensile strength vs volume fraction of SFs



b)Flexural tensile strength vs volume fraction of RTR

Figure 4.17 Relationships between volume fractions and flexural tensile strength of SCGC

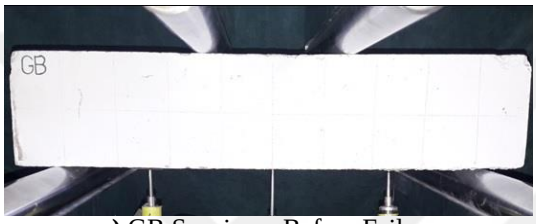
4.1.2.5 Failure Modes of The Flexural Specimens

The cracking pattern at before and after failure of SCGC beam specimens are shown in the Figure 4.18. The results showed that the cracking patterns were affected by the presence of NS and SFs content. The crack arrest capacity of SFs can be represented by the sample thickness/SF length ratio (d/F_L ratio) [140]. The SFs efficiency was increased as the d/F_L ratio decreased and so SFs can arrest more easily the cracks for the lower d/F_L ratios. The specimens including SFs were failed in the flexural-tension mode. The homojen distribution of SFs is substantially specify the pattern of failure. Moreover, it was indicated that the crack pattern was substantially affected with an increase length of SFs. Furhermore, the proportion of SFs have direct

relationship with the type and morphology of cracks. As the volume fraction of SFs increase in the SCGC specimens , they have significant resistance to failure and enhances time of stability. The flexibility and stability time of SCGC specimens was significantly improved with incorporation of SFs/1.0% and their enhancement were better than the specimens including SFs/0.5%. These improvements can easily be figure out from the Figure 4.18 of load-displacement relation. Moreover, the longer SF (SF_2) with high aspect ratio was found better than shorter SF (SF_1) with low aspect ratio, because it has more resistance to failure and the crack propagation. For the GB-SF_1/1.0 specimen, only one major crack of larger dimension occurred in the maximum moment zone (flexure crack) without any hairline crack as shown in the Figure 4.18.e and 4.10.f. The d/F_L of these specimens was 3.33, and SF_1 efficiency was found to be less due to the formation of a single crack with a larger width, which was found parallel to the loading direction.

In addition, the SCGC specimens incorporation of NS have superior effect on the resistance to failure and enhances time of stability especially when it was used together with SFs. The type and pattern failure of the specimens including NS indicated the significant bond enhancement. On the specimens without NS and SF (builds up from plain concrete), shear cracks are occurred, while flexural cracks are occurring due to the addition of SFs/1.0% with/out NS, (builds up from fiber reinforced concrete, content SFs/1.0%). Meanwhile, flexural cracks converted to shear cracks owing to the addition of SFs/1.0%. Moreover, the failure pattern and type of cracks are shown in the Figure 4.18. This is an intermediate propagation of shear flexural crack. The shear failure of beam structures could be reduced through use of SFs incorporated NS. For the GBN-SF_1/1.0 specimen, the main crack was re-formed in the bending zone (flexural crack), but an additional hairline crack of 1mm in size before failure as shown in the Figure 4.18.p. For this case (d/F_L=3.33), low width main failure crack occurred parallel to the loading direction. For the GB-SF_2/1.0 (d/F_L=1.25) specimens, inclined crack (45°) formed around the support not in the middle. In addition, an additional inclined crack appeared with a larger dimension (>1 mm) around the supports. For these specimens with a ratio of 1.25 d/F_L, the failure was because of the flexural-shear type cracks. For the GBN-SF_2/1.0 (d/F_L=1.25) specimen, numerous branching type cracks occurring in the bending zone showing the efficiency of SF and NS, but it was found that the main cracks

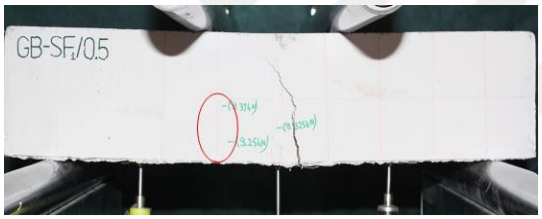
leading to the failure were inclined with a larger crack width in the support zone. Additional multi-inclined hairline cracks were also observed in the bending zone around the support. The main failure crack type was observed as a flexural-shear type crack in specimens with a ratio of 1.25 d/F_L. The inclined and multiple cracks around supports were attributed to the stress transfer between SFs. This stress transfer was found to be greater when the d/F_L ratio was low, since specimens can easily stop cracks, enables stress transfer with long SFs. NS provides improved flexural tensile strength performance by improving the bond strength between matrix and SFs. Moreover, the sudden failure occurred in the middle of samples without NS and SFs as shown in the Figure 4.18.b and 4.18.m.



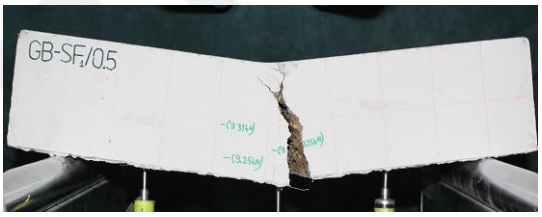
a) GB Specimen Before Failure



b) GB Specimen Failure Mode



c) GB-SF_1/0.5 Specimen Before Failure



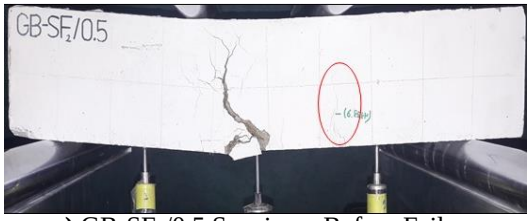
d) GB-SF_1/0.5 Specimen Failure Mode



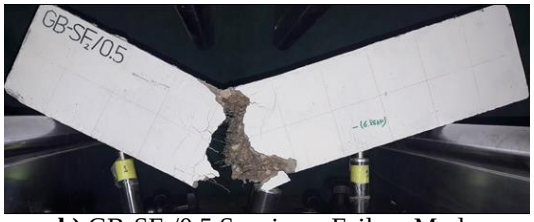
e) GB-SF_1/1.0 Specimen Before Failure



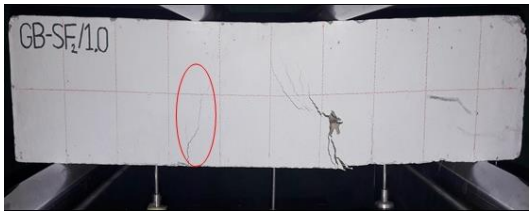
f) GB-SF_1/1.0 Specimen Failure Mode



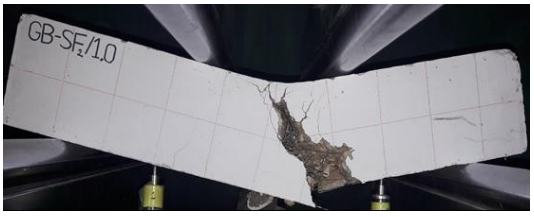
g) GB-SF_2/0.5 Specimen Before Failure



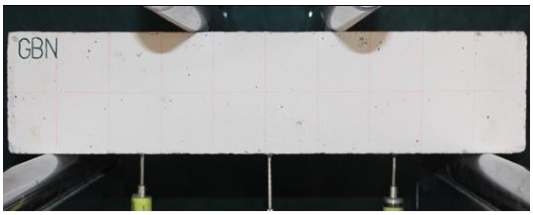
h) GB-SF_2/0.5 Specimen Failure Mode



i) GB-SF_2/1.0 Specimen Before Failure



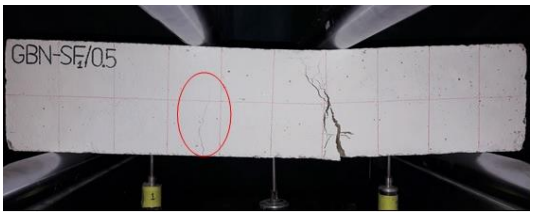
k) GB-SF_2/1.0 Specimen Failure Mode



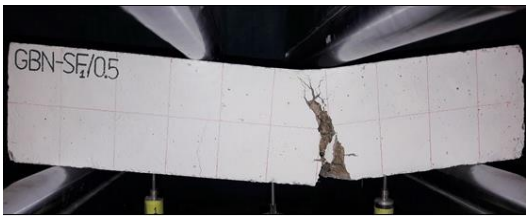
l) GBN Specimen Before Failure



m) GBN Specimen Failure Mode



n) GBN-SF_1/0.5 Specimen Before Failure



o) GBN-SF_1/0.5 Specimen Failure Mode



p) GBN-SF_1/1.0 Specimen Before Failure



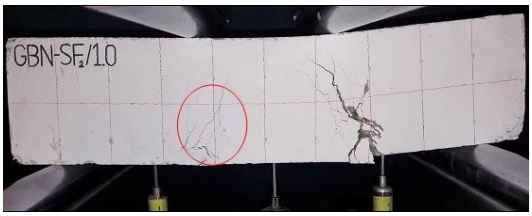
r) GBN-SF_1/1.0 Specimen Failure Mode



s) GBN-SF_2/0.5 Specimen Before Failure



t) GBN-SF_2/0.5 Specimen Failure Mode



u) GBN-SF_2/1.0 Specimen Before Failure

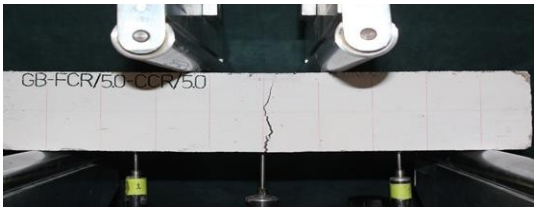


v) GBN-SF_2/1.0 Specimen Failure Mode

Figure 4.18 Failure mode of SCGC beam specimens with/out NS and SFs

The cracking patterns of the rubberized SCGC specimens under four-point loading before failure are shown in the Figure 4.19. The flexural type cracks and flexural failure achieved in the rubberized specimens. For the non-fibrous rubberized samples, a large major crack was observed in the bending region as shown in the Figure 4.19.a, 4.19.e, 4.19.g, except for GB-FCR/7.5-CCR/7.5 specimen as shown in the Figure 4.19.c. For the GB-FCR/7.5-CCR/7.5 specimen, very small extra hairline cracks (≤0.1 mm) was observed in addition to the main flexural crack type. Therefore, low deformation (low toughness) capacity was observed in non-fibrous rubberized specimens as shown in the Figure 4.16.d. For the rubberized specimens

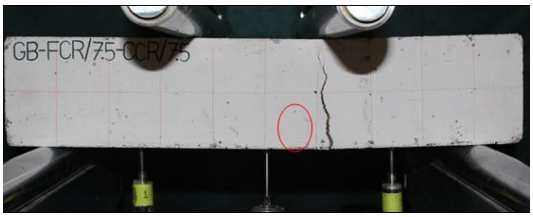
with SF_1, multiple cracks shown as red circles in the Figure 4.19.i, 4.19.l and 4.19.p were observed in the bending zone of the specimens. The obtained cracks stated that stress transfers existed among SFs due to the crack-stopping capability of the hook-end SFs, due to the crack-stopping ability of the hooked-end SFs, which results in improved deformation capacities for the rubberized specimens. When the obtained cracks were examined in detail, a main flexural crack was observed in the FCR/5.0%-CCR/5.0% replaced SF specimen (GB-SF_1/1.0-FCR/5.0-CCR/5.0) in the tension region of the bending zone and branching of this crack occurred in the upper (compression) region of the specimen as shown in the Figure 4.19.i-k, the main crack with a larger size was observed in the tension zone and fracture continued to the failure. However, two additional vertical cracks were also observed, one of which had a greater crack width (> 0.1 mm) with branching in the tension zone as shown in the Figure 19.p. This branched secondary crack caused more deformation (more energy loss) in the specmen, which is an indication of the highest load and deformation capacity in GB-SF_1/1.0-FCR/5.0-CCR/5.0 specimen under flexure. For the GB-SF_1/1.0-FCR/7.5-CCR/7.5 specimen, one main crack and two vertical hairline cracks were obtained and these two cracks were found independent of the main crack and progressed up to half of the specimen. The main flexural crack progressed to fracture with branching in both tension and compression zones as shown in the Figure 4.19.l-m. For the GB-SF_1/1.0-TCR/10, one main crack was observed in the tension region of the bending zone and the cracks reached the main crack in the tension zone. The main flexural crack advanced to the compression zone by branching and caused the specimen to failure as shown in the Figure 4.19.n-o. For the GB-SF_1/1.0-TCR/15 specimen, one main crack and two small hairline cracks were obtained in the tension region of the bending zone and the cracks reached to the main crack in the tension zone. The main flexural crack proceeded to the compression zone with branching and resulted in the failure of the specimens as shown in the Figure 4.19.p-r.



a) GB-FCR/5.0-CCR/5.0 Specimen Before Failure



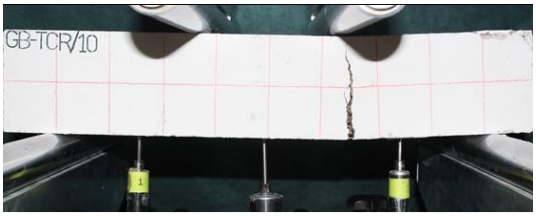
b) GB-FCR/5.0-CCR/5.0 Specimen Failure Mode



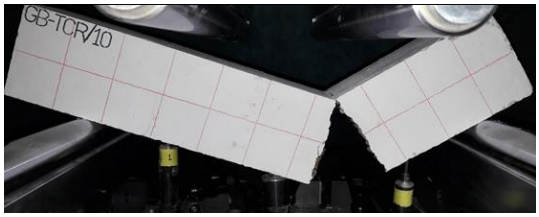
c) GB-FCR/7.5-CCR/7.5 Specimen Before Failure



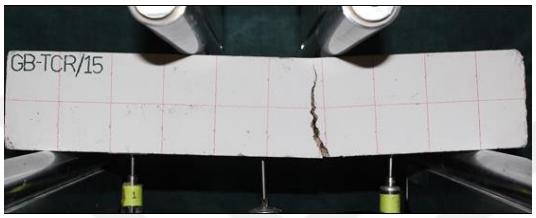
d) GB-FCR/7.5-CCR/7.5 Specimen Failure Mode



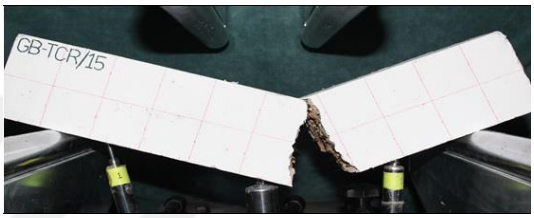
e) GB-TCR/10 Specimen Before Failure



f) GB-TCR/10 Specimen Failure Mode



g) GB-TCR/15 Specimen Before Failure



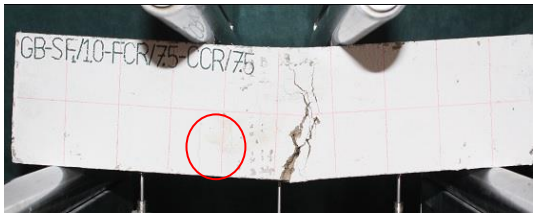
h) GB-TCR/15 Specimen Failure Mode



i) GB-SF_1/1.0-FCR/5.0-CCR/5.0 Specimen Before Failure



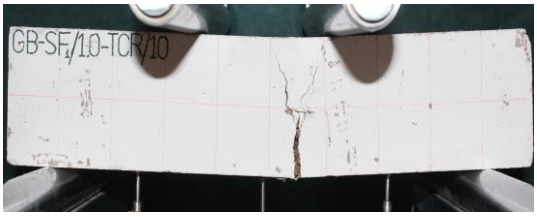
k) GB-SF_1/1.0-FCR/5.0-CCR/5.0 Specimen Failure Mode



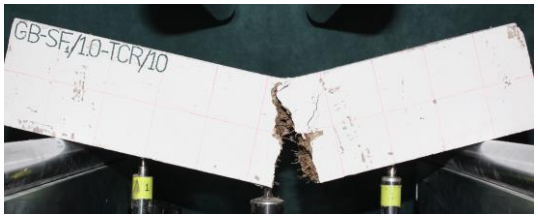
l) GB-SF_1/1.0-FCR/7.5-CCR/7.5 Specimen Before Failure



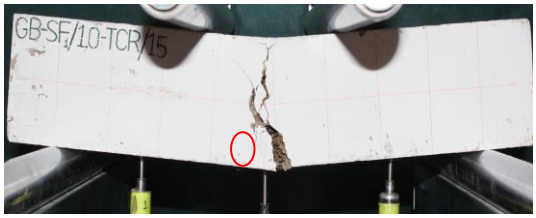
m) GB-SF_1/1.0-FCR/7.5-CCR/7.5 Specimen Failure Mode



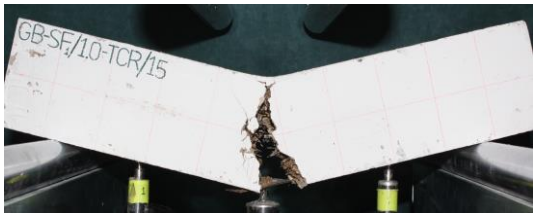
n) GB-SF_1/1.0-TCR/10 Specimen Before Failure



o) GB-SF_1/1.0-TCR/10 Specimen Failure Mode



p) GB-SF_1/1.0-TCR/15 Specimen Before Failure



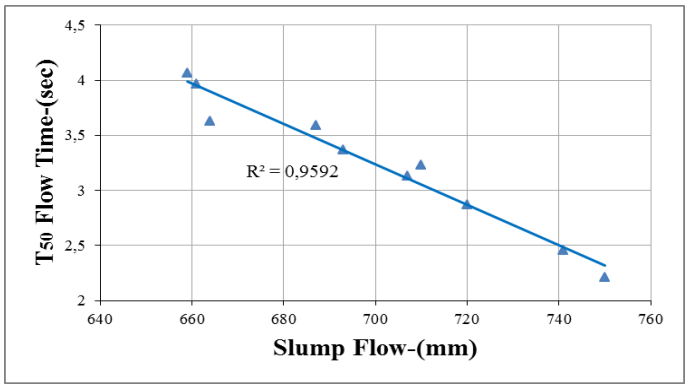
r) GB-SF_1/1.0-TCR/15 Specimen Failure Mode

Figure 4.19 Failure mode of rubberized SCGC beam specimens with/out SF_1

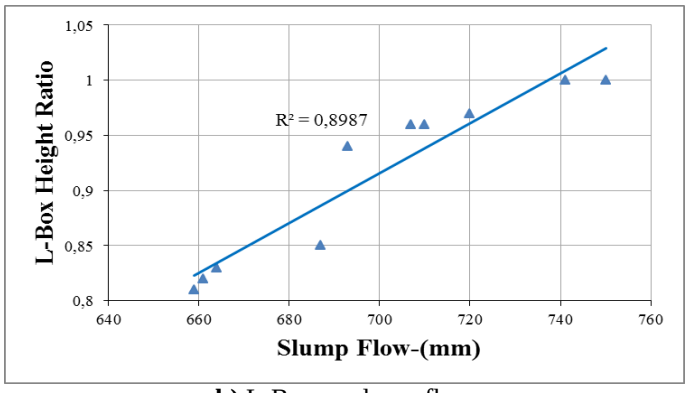
4.1.2.6 Relationship and Correlation Between Hardened and Fresh Properties of SCGC

In order to evaluate the experimental outcomes, it is significant for researcher to find the correlation of the experimental data. Theoretically, the major effect factors of the fresh and mechanical characteristic of concretes are aggregate, water-cement ratio and cementitious binder content. As mentioned earlier, the mechanical characteristic of the concrete significantly influenced by the compressive strength values of concrete. The compressive strength of concretes are also affected by matrix properties. In this study, the relationships between fresh and hardened states properties were investigated. In this study, the effects of SFs, NS and RTR on the properties of SCGC were studied. Therefore, the fresh and hardened states properties of SCGC were also investigated as well as the correlating and relationship between the experimental datas.

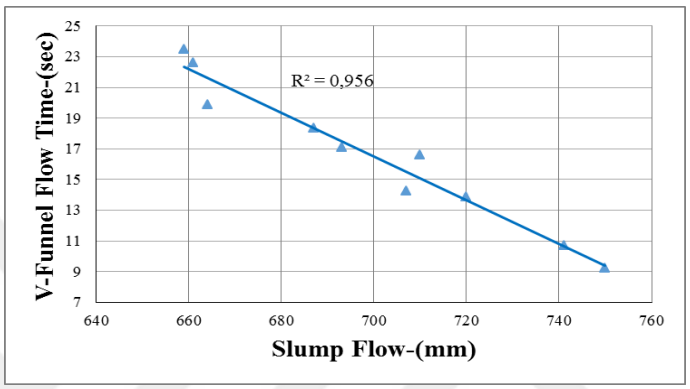
According to the experimental datas, the close relationships were found between V-funnel and slump flow (R^2: 0.9592), L-Box and slump flow (R^2: 0.8987) as well as slump flow and T_{50} time (R^2: 0.956) as shown in the Figure 4.20.a, 4.20.b and 4.20.c, respectively. According to the R^2 values, it can be concluded that there is a excellent correlation between the slump flow and other properties even in the presence of both SFs and NS.



a) T_{50} vs slump flow



b) L-Box vs slump flow

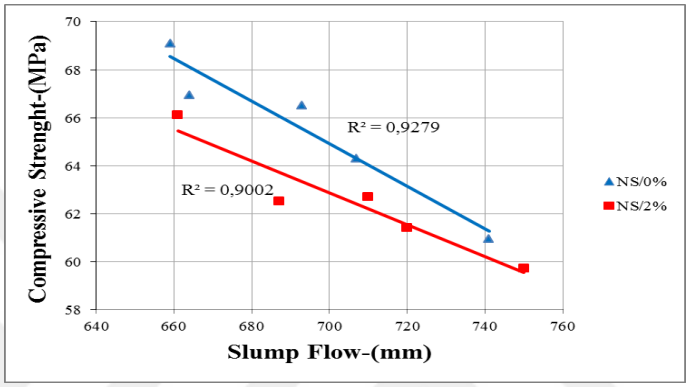


c) V-Funnel vs slump flow

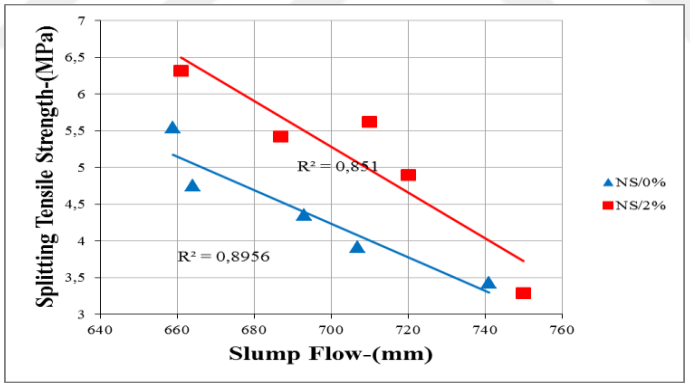
Figure 4.20 Correlation between the fresh properties of specimens with/out NS and SFs

On the other hand, the results also showed that there were close relationships between slump flows and the mechanical properties of SCGC specimens as shown in the Figure 4.21. The results showed that strong relationships were observed between compressive strength-slump flow, splitting tensile strength-slump flow, modulus of elasticity-slump flow, and high relationships between flexure tensile strength-slump flow as shown in the Figure-4.21.a, 4.21.b, 4.21.c and 4.21.d, respectively. The well correlation shows high coefficient (R^2) values which indicate that the slump flow values significantly affected on the mechanical properties of SCGC despite the existance of SFs and NS. Moreover, good relationships presence between the hardened performance of SCGC specimens. The correlation between compressive strength vs modulus of elasticity, compressive strength vs splitting tensile strength, compressive strength vs flexural strength shows high coefficient (R^2) values as shown in the Figure-4.22. Generally, it can be deduced that there are excellent relationship between hardened state and fresh state properties of SCGC despite the incorporation of SFs and NS. In addition, the R^2 results also showed that strong

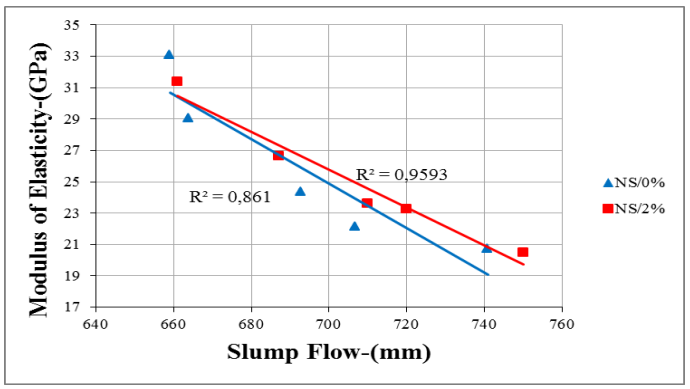
associations were observed in specimens with NS/2% addition compared to specimens without NS. The findings obtained indicated that the mechanical performance is directly related to the slump flow. This may be due to increased SFs orientations in the higher flowability casting directions, resulting in improved mechanical performance. The fresh state properties of the SCGCs had substantial impact on the hardened state properties. Therefore, in order to obtain the superior SCGC specimens have inevitable requirements that are good mechanical and good fresh state properties.



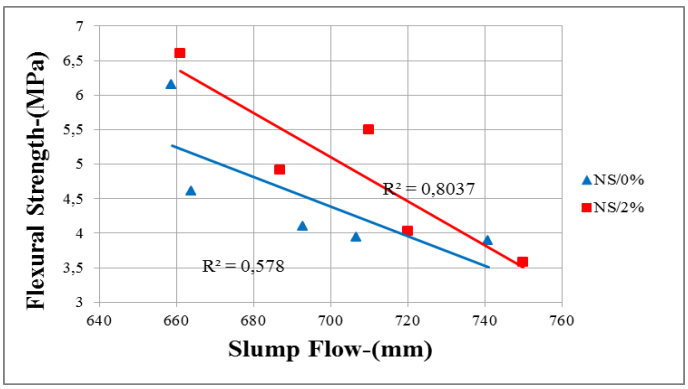
a) Compressive strength vs slump flow



b) Splitting tensile strength vs slump flow

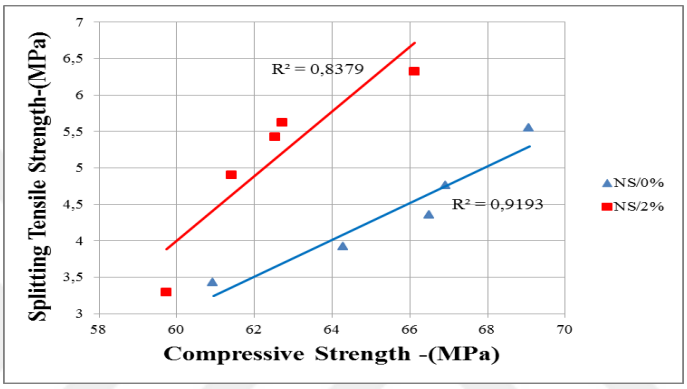


c) Modulus of elasticity vs slump flow

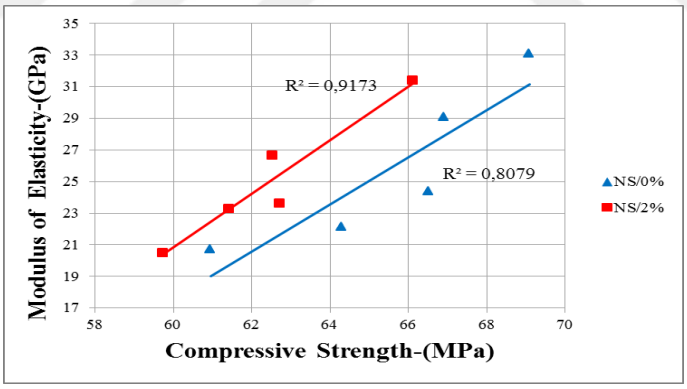


d) Flexural tensile strength vs slump flow

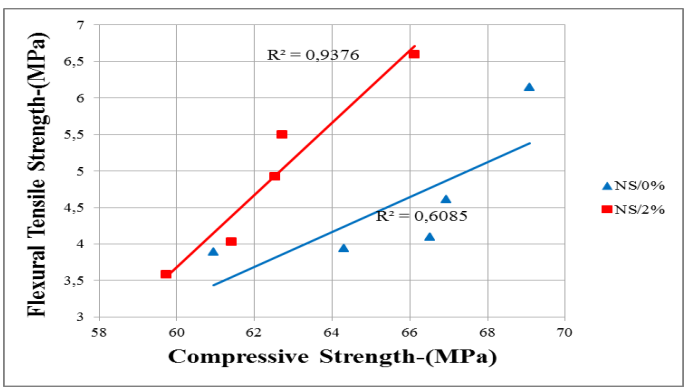
Figure 4.21 Correlation between the hardened and fresh properties of SCGC



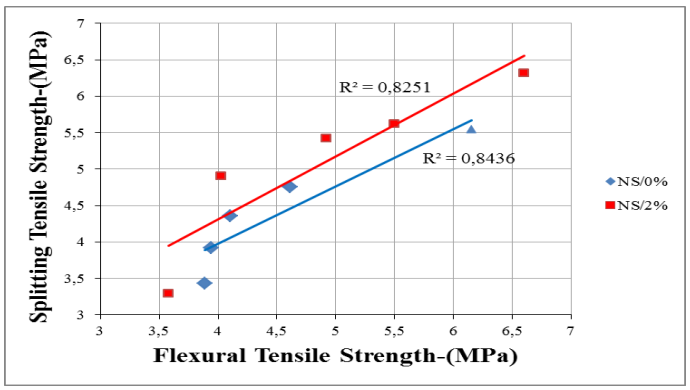
a) Splitting tensile strength vs compressive strength



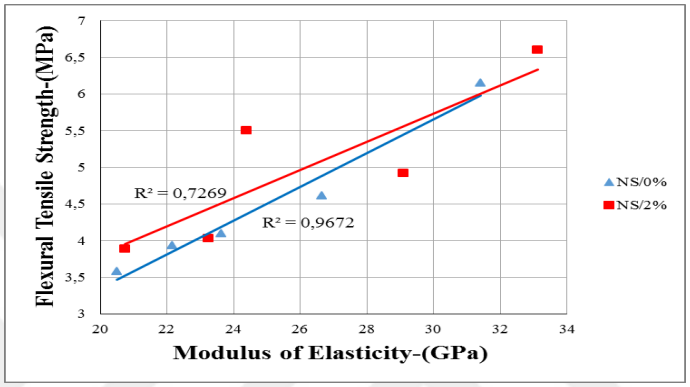
b) Modulus of elasticity vs compressive strength



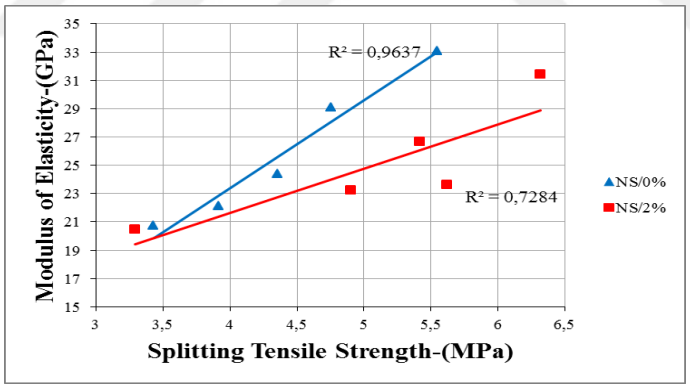
c) Flexural tensile strength vs compressive strength



d) Flexural tensile strength vs splitting tensile strength



e) Flexural tensile strength vs modulus of elasticity

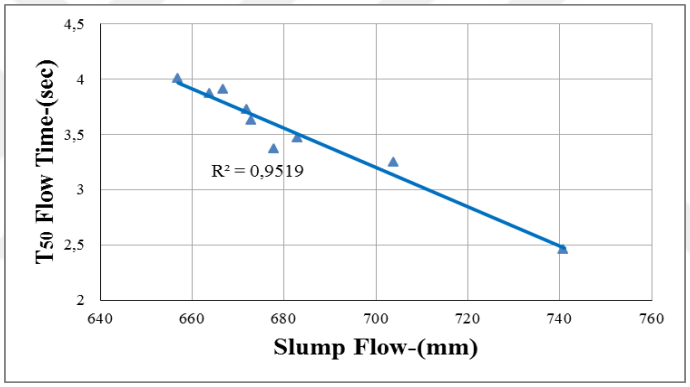


f) Modulus of elasticity vs splitting tensile strength

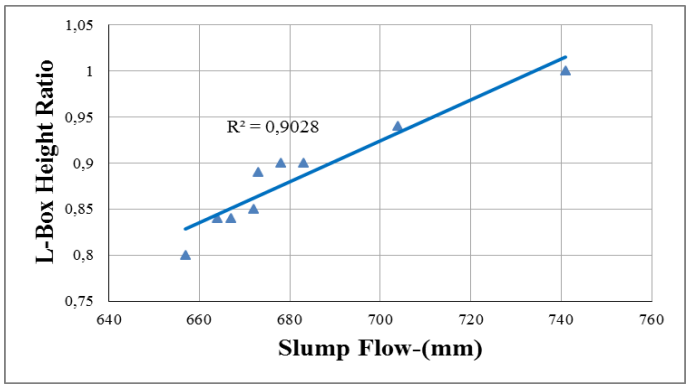
Figure 4.22 Correlation between the hardened performances of SCGC

Within the scope of the research, the combined effects of SF_1 and RTR conjugation on the flowability, passing ability and mechanical properties were investigated using the correlations between experimental data. So, The relationships between the fresh state properties of the rubberized SCGC specimens with/out SF_1 are shown in the Figure 4.23. Moreover, The correlation between fresh and hardened states performances of the rubberized mixes/specimens are shown in the Figure 4.24. In addition, the higher R^2 values indicated a strong correlation between the examined parameters. Furhermore, the results showed that there were close relationships (R^2>0.9) among fresh state properties, hardened state properties, and between fresh

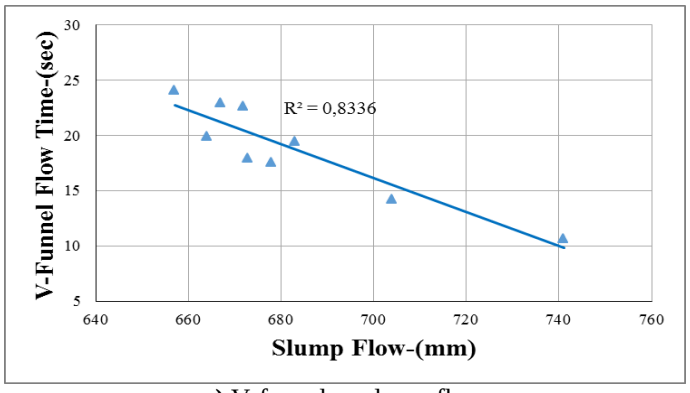
and hardened state properties. In addition, the rubberized specimens with SF showed higher R^2 values than the rubberized specimens without SF_1 as shown in the figure-4.25.



a) T_{50} vs slump flow

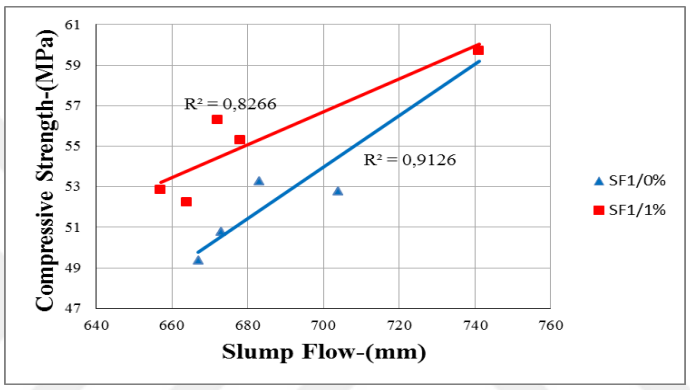


b) L-box vs slump flow

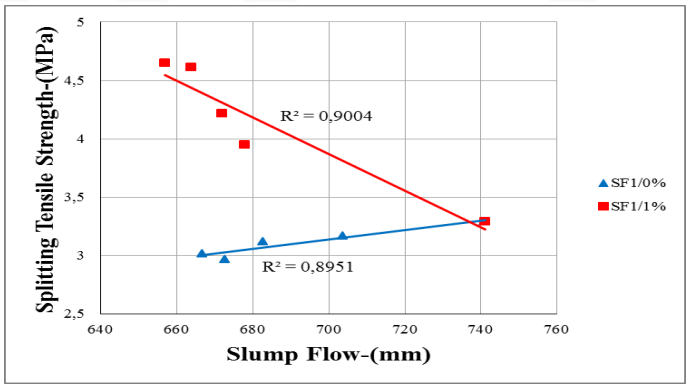


c) V-funnel vs slump flow

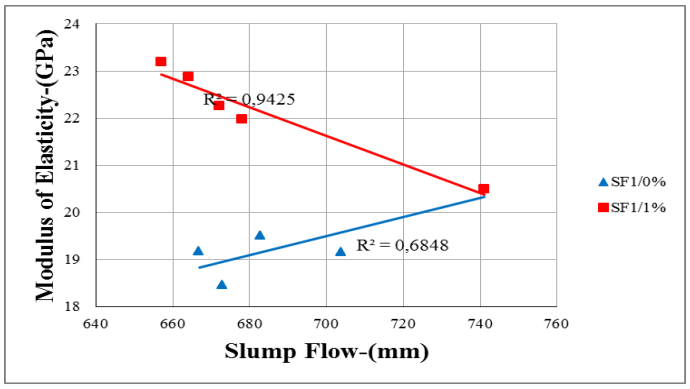
Figure 4.23 Correlation between the fresh properties of specimens with RTR and with/out SF_1



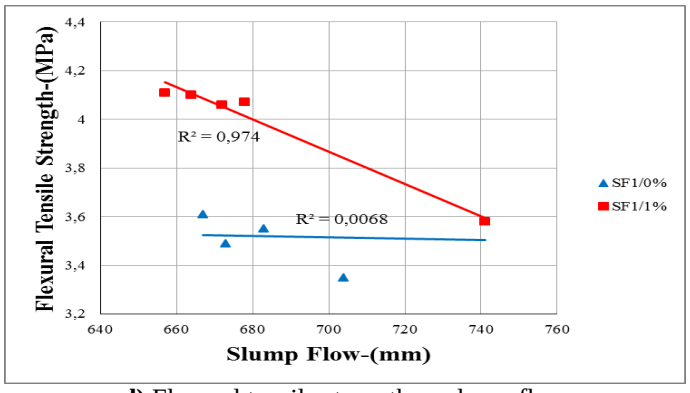
a) Compressive strength vs slump flow



b) Splitting tensile strength vs slump flow

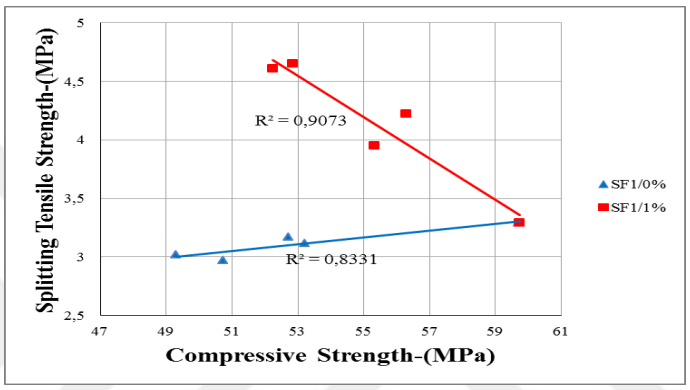


c) Modulus of elasticity vs slump flow

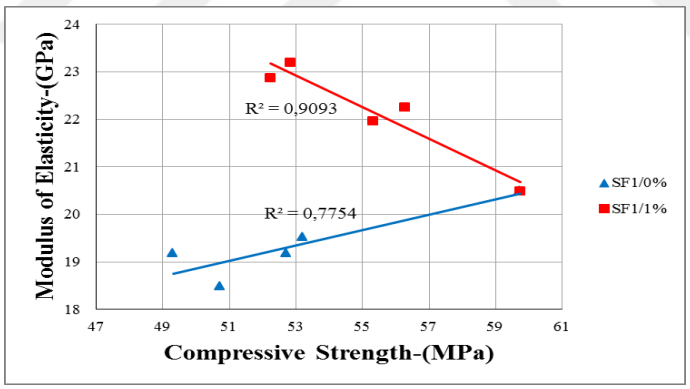


d) Flexural tensile strength vs slump flow

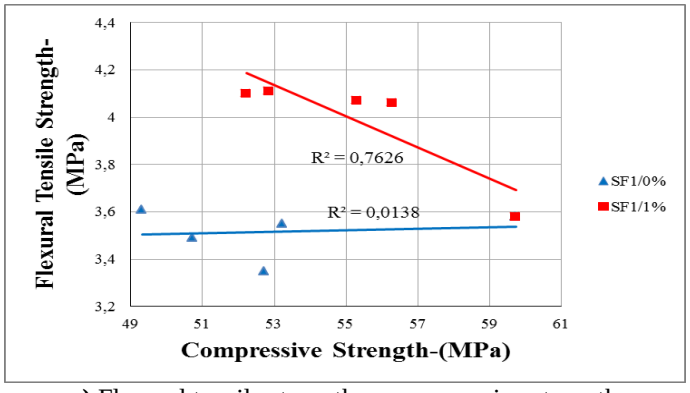
Figure 4.24 Correlation between the hardened and fresh properties of rubberized SCGC



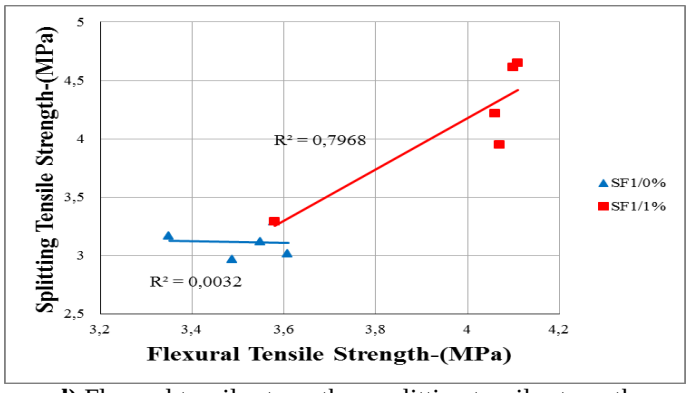
a) Splitting tensile strength vs compressive strength



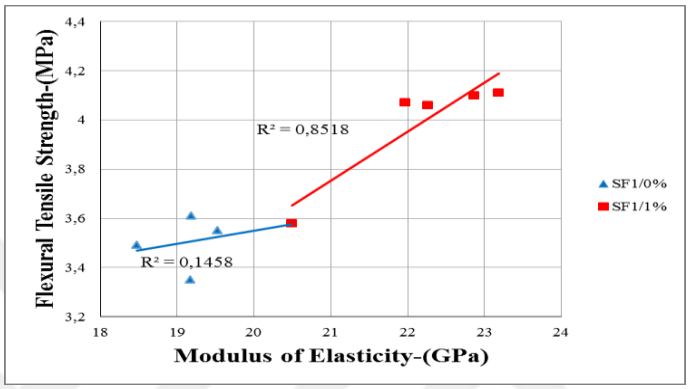
b) Modulus of elasticity vs compressive strength



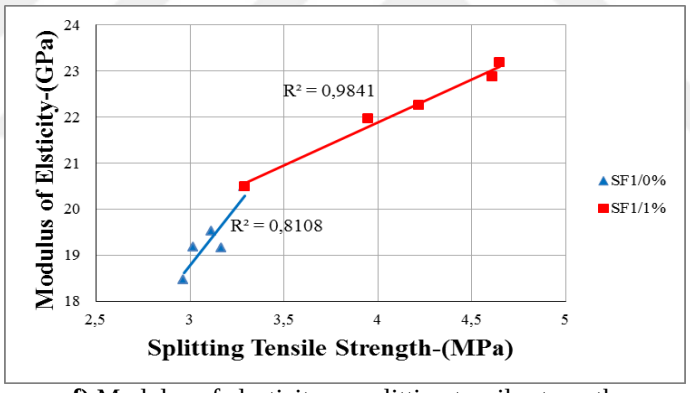
c) Flexural tensile strength vs compressive strength



d) Flexural tensile strength vs splitting tensile strength



e) Flexural tensile strength vs modulus of elasticity



f) Modulus of elasticity vs splitting tensile strength

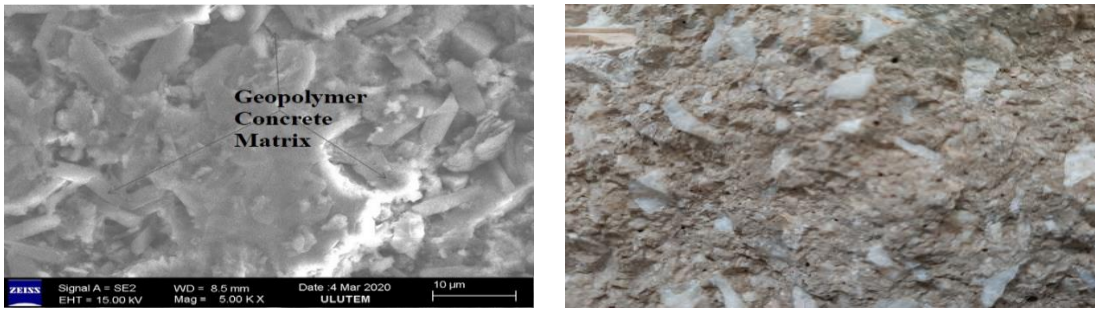
Figure 4.25 Correlation between the hardened performances of rubberized SCGC

4.1.2.7 Scanning Electron Microscopy (SEM) Analysis

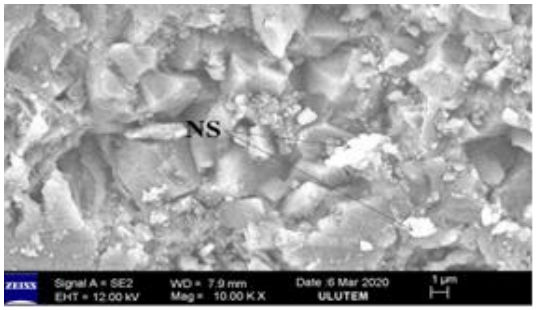
The all SCGC specimens in the study were analyzed in detail through the scanning electron microscopy (SEM) to identify the influence of NS on the interfacial transition zone (ITZ) between the aggregates and matrix. Besides, the effects of NS on the bond strength between SFs and matrix of SCGC was also investigated in micro-scale. As expected, the incorporation of NS improves the micro-structure of concrete denser with low pores and then enforces the bond strength of SCGC specimens [46,95]. SEM photos were taken for each specimen with/out NS and

with/out SFs. Those were taken on sample having dimensions 1 cm thick circular slice prepared by bifurcating perpendicular to sample axis. The samples dimensions for SEM were 1×1×1cm. In order to identify the effect of NS on the micro-structure of SCGC specimens, SEM photos were taken from the control specimen (GB-without NS and SFs) and the specimens with/out NS. The SEM photos of the control specimen and the SCGC specimens including NS and/or SFs are shown in the Figure 4.26. NS via decreasing the pores in the matrix of SCGC make the micro-structure denser. Earlier studies investigated the micro-structure of GC specimen including NS [83]: they investigated that the specimen permeability and water absorption of NS was less the specimen without NS. The SEM photos prove the obtained results; the NS decrease the density of micro void and increase the bond strength between the SFs and the matrix.

The SEM of the rubberized SCGC specimens with/out SF_1 to identify the influences of SF_1 and RTR particles on the microstructure of the specimens as shown in the Figure 4.27. The SEM results showed that the well-distributed paste containing less unreacted slag particles indicating the denser and homogeneous microstructure of the SF_1 reinforced rubberized SCGC specimens. However, wider interconnected macro cracks were observed in the microstructure, which could be attributed to the evaporation of water and self-drying [153] and shrinkage of the reaction products [154]. This can cause improper bonding between the matrix and rubber particles, thus causing a decrease in the mechanical strengths of the rubberized SCGC specimens.

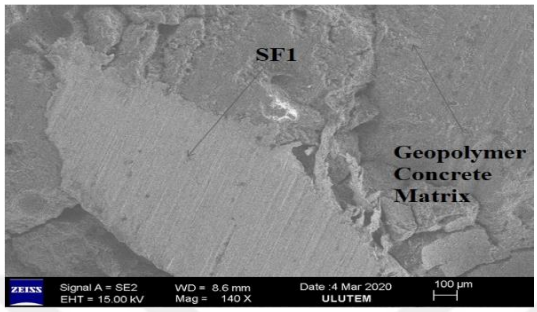


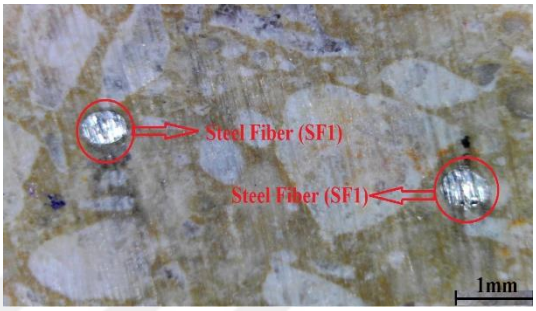
GB



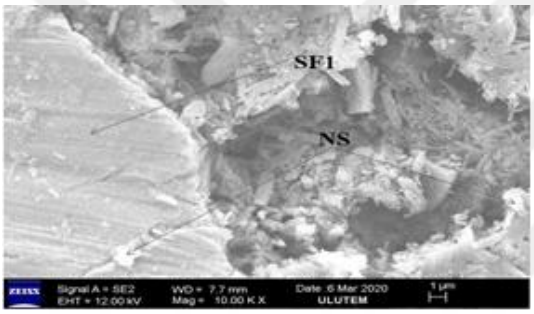


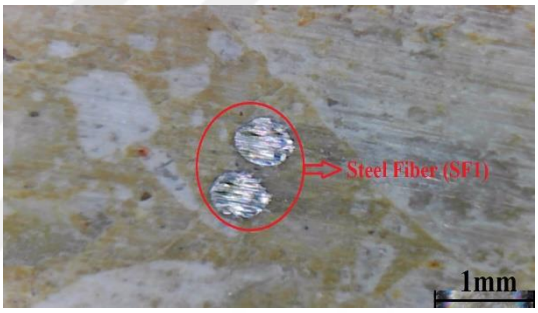
GBN



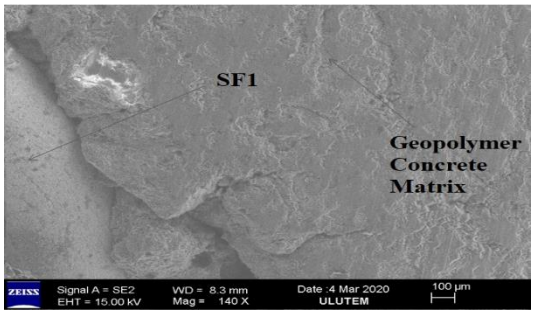


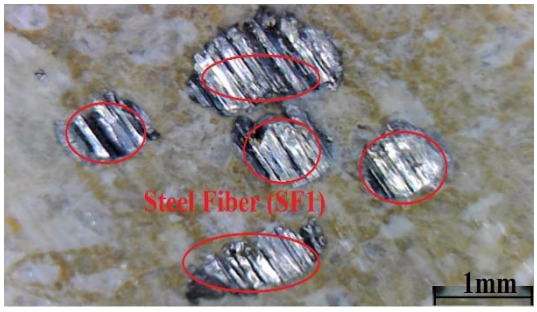
GB-SF$_1$/0.5



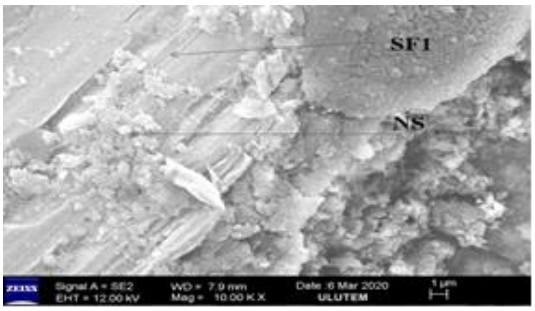


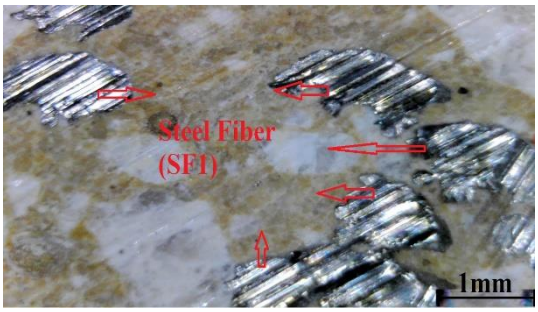
GBN-SF$_1$/0.5



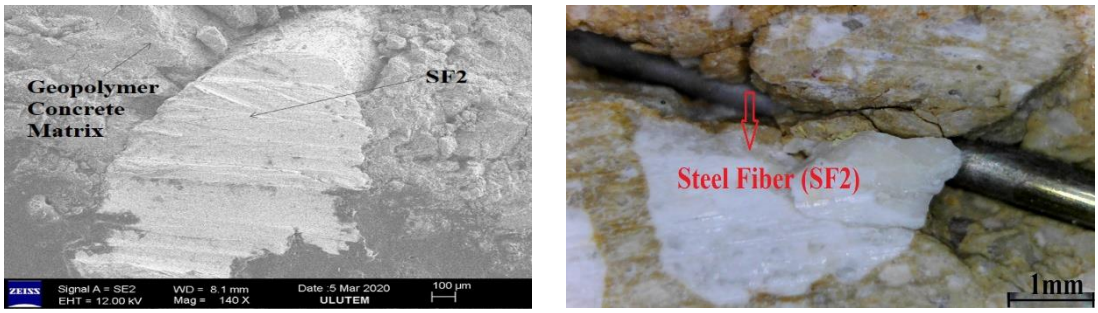


GB-SF$_1$/1.0

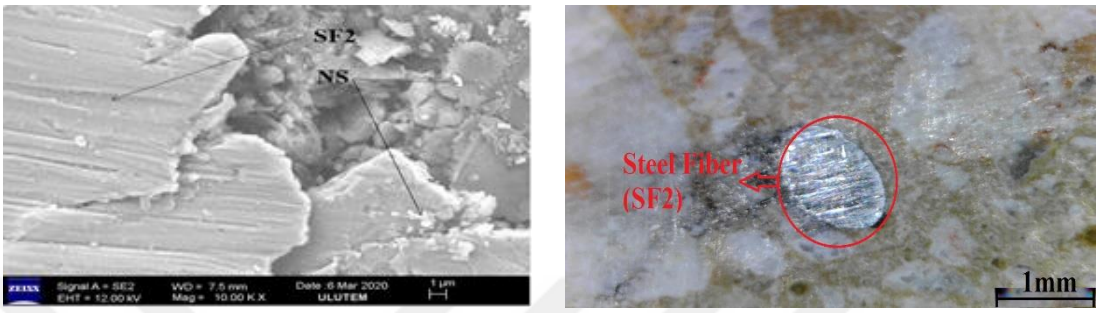




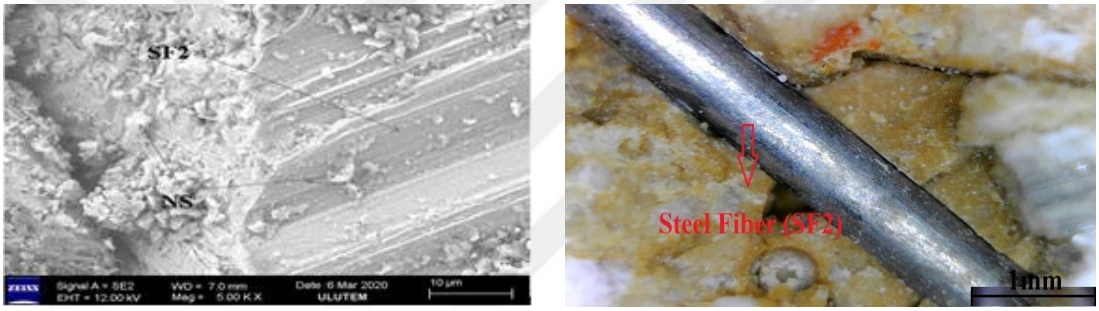
GBN-SF$_1$/1.0



GB-SF$_2$/0.5

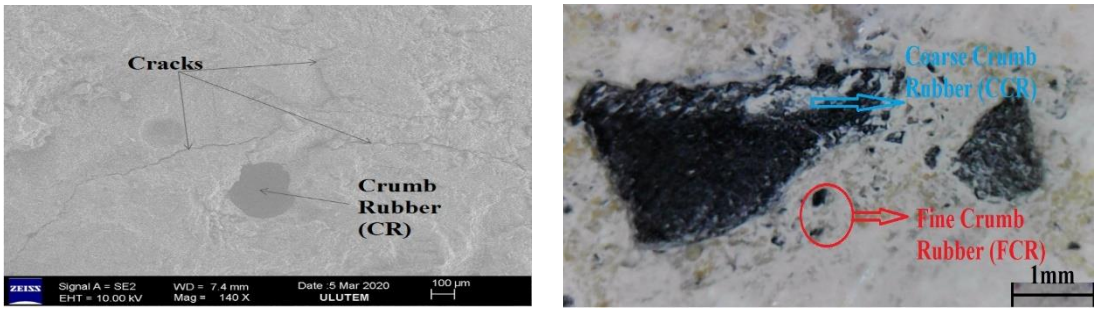


GBN-SF$_2$/0.5

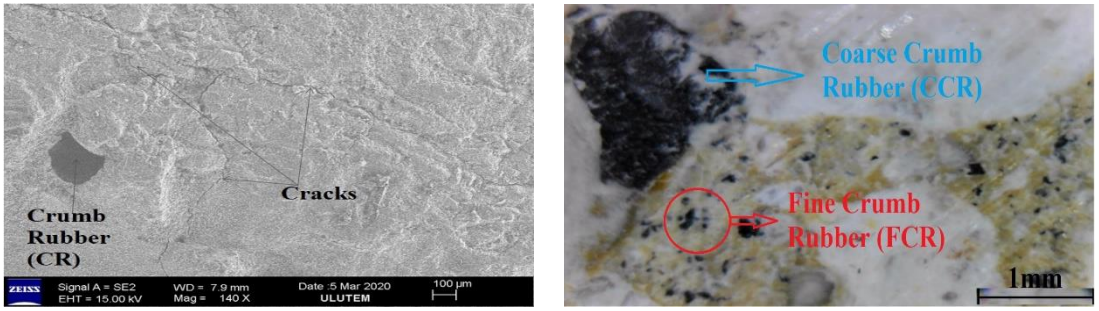


GBN-SF$_2$/1.0

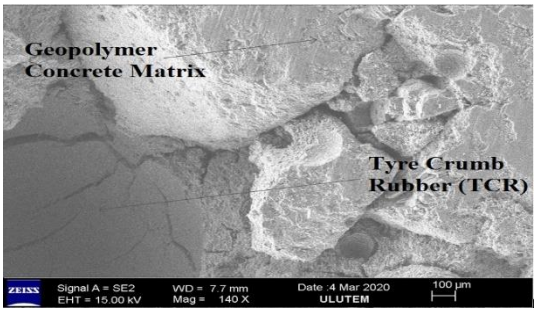
Figure 4.26 SEM images of SCGC with/out NS with different scales



GB-FCR/5.0-CCR/5.0

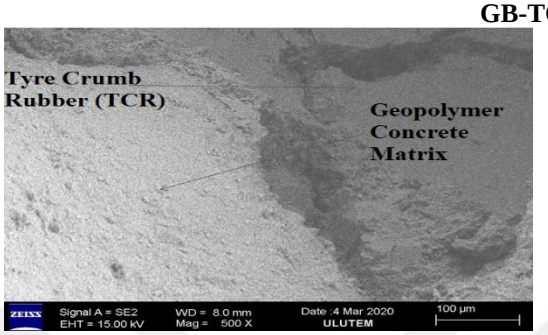


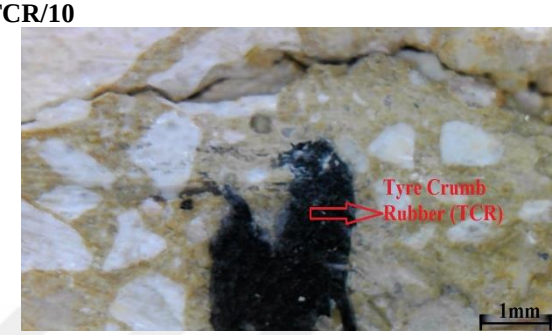
GB-FCR/7.5-CCR/7.5



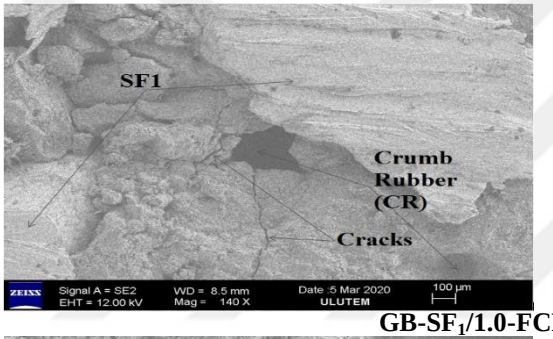


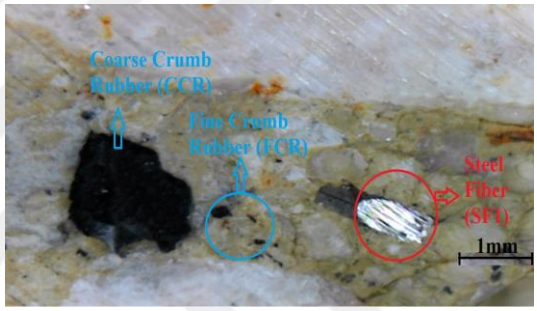
GB-TCR/10



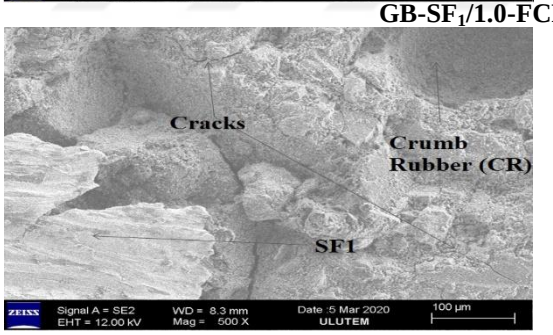


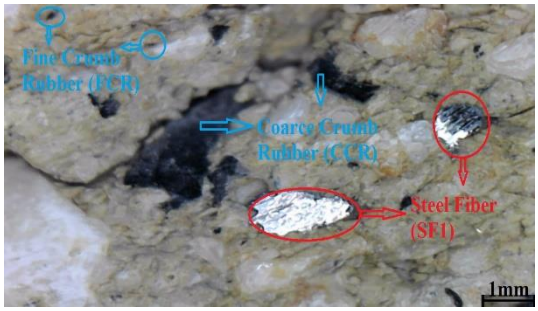
GB-TCR/15



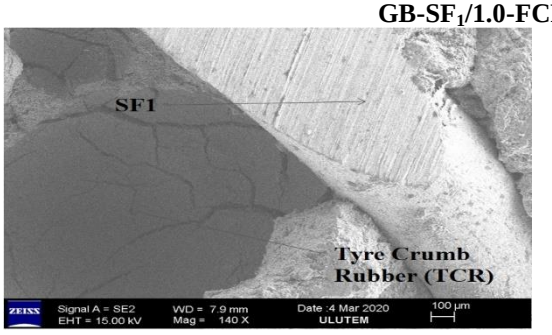


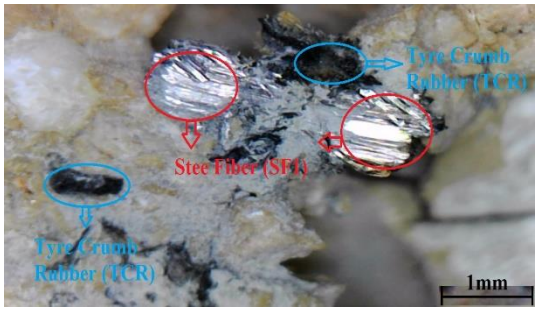
GB-SF$_1$/1.0-FCR/5.0-CCR/5.0



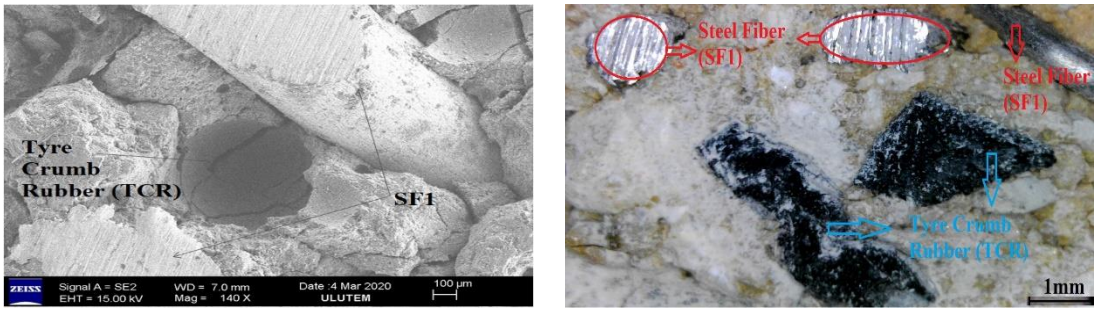


GB-SF$_1$/1.0-FCR/7.5-CCR/7.5





GB-SF$_1$/1.0-TCR/10



GB-SF$_1$/1.0-TCR/15

Figure 4.27 SEM images of rubberized SCGC specimens with different scales

4.1.12.8 Results of The Drop-Weigth Tests

In the study, the following results were obtained. Figure 4.28 shows the first drop moment and failure mode of each specimens and the all data obtained at the moment of each drop are given in the Table 4.3. Moreover, Figure 4.29 indicates the effects of SFs volume fraction, SFs aspect ratio and NS. Furhermore, Figure 4.30 effects of RTR volume fraction, RTR aspect ratio and SF_1. In addition, the average accleration-time relation graph, force-time relation graph, crack width and displacement of the each drop of the SCGC beam specimen are given in the Table 4.4. Moreover, Figure 4.31 shows the average displacement-time relation graph of the first drop of each specimen.

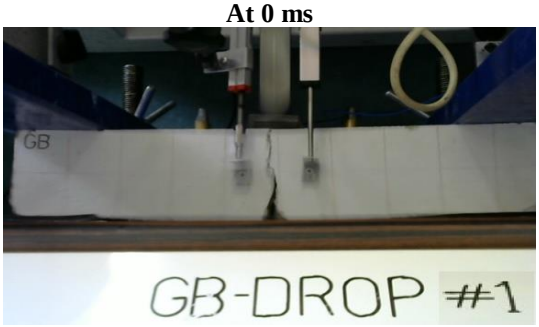
GB



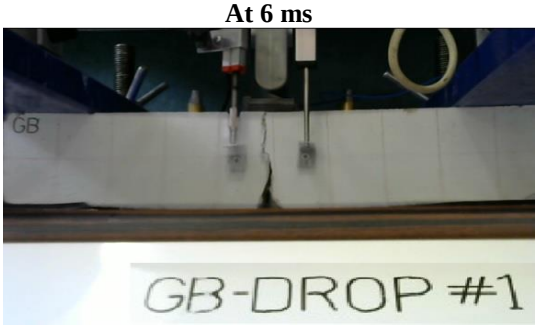
At 0 ms



At 6 ms



At 12 ms



At 18 ms





At 24 ms **Failure Mode**

(a)

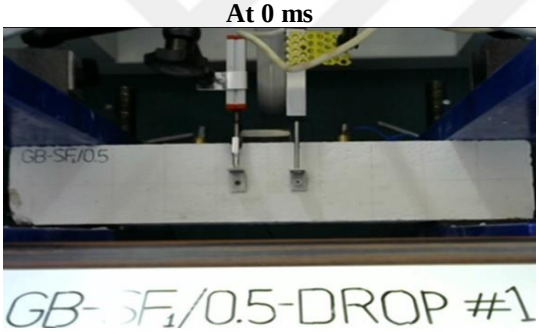
GB-SF$_1$/0.5



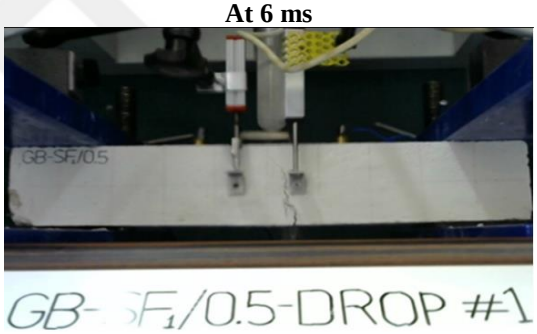
At 0 ms



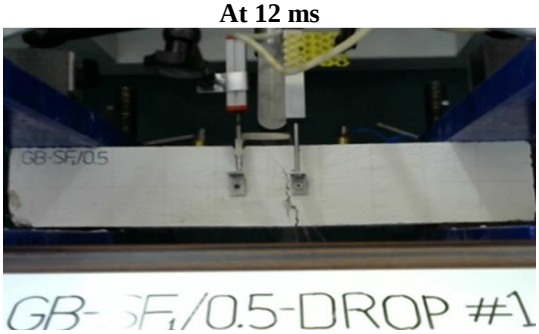
At 6 ms



At 12 ms



At 18 ms



At 24 ms



Failure Mode

(b)

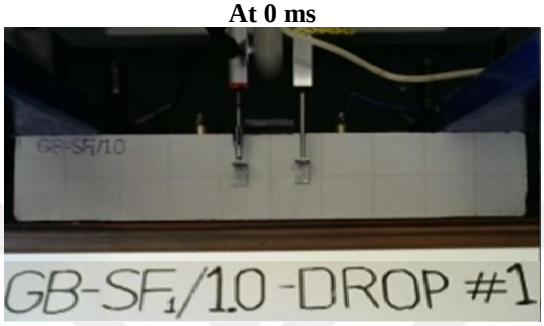
GB-SF$_1$/1.0



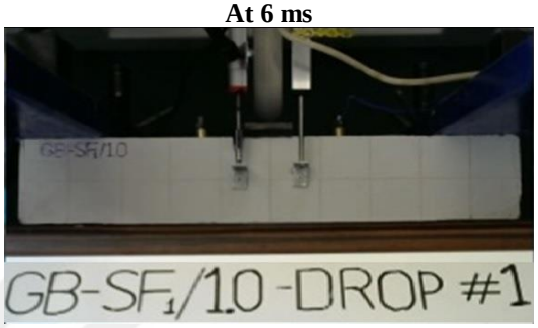
At 0 ms



At 6 ms



At 12 ms



At 18 ms



At 24 ms



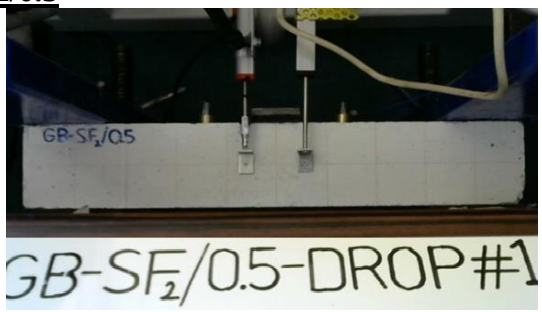
Failure Mode

(c)

GB-SF2/0.5



At 0 ms



At 6 ms



At 12 ms



At 18 ms



At 24 ms



Failure Mode

(d)

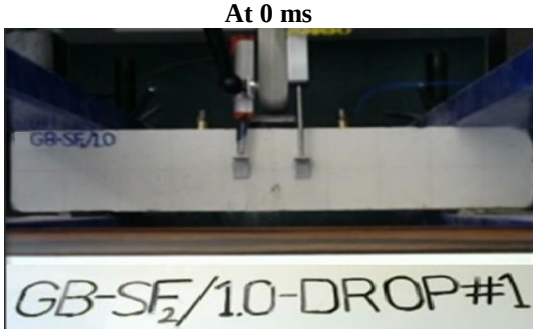
GB-SF$_2$/1.0



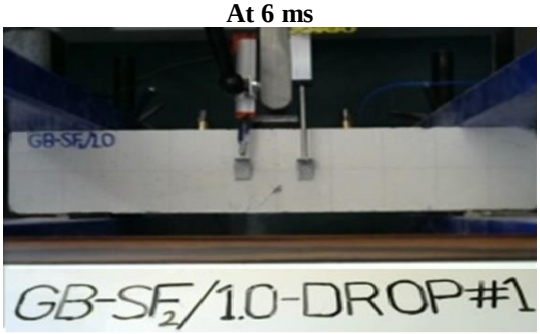
At 0 ms



At 6 ms



At 12 ms



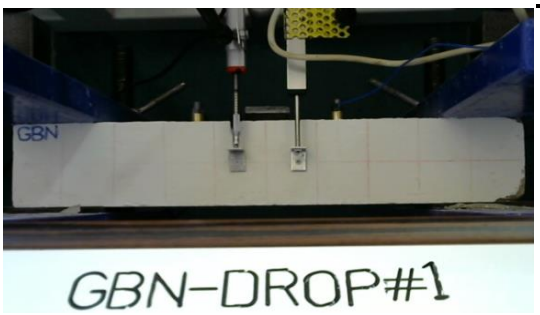
At 18 ms



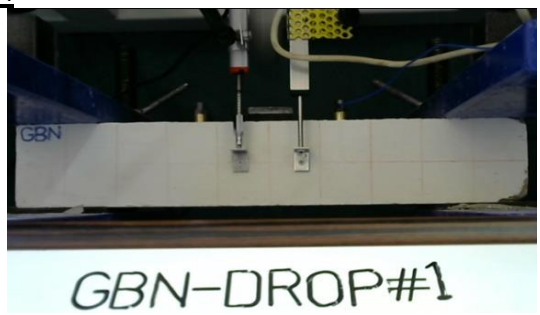
Failure Mode

(e)

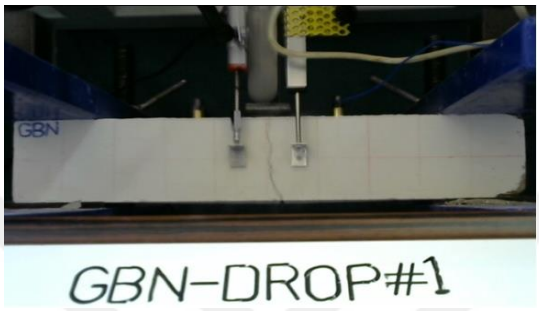
GBN



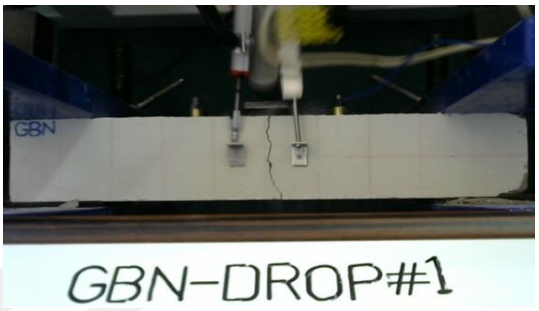
At 0 ms



At 6 ms



At 12 ms



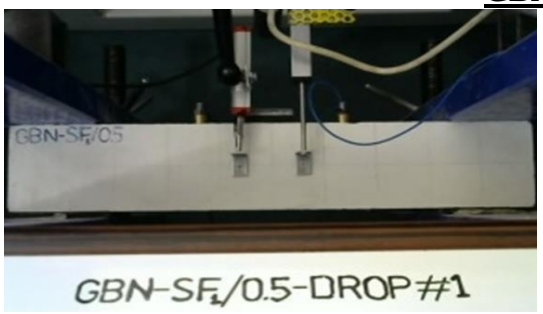
At 18 ms



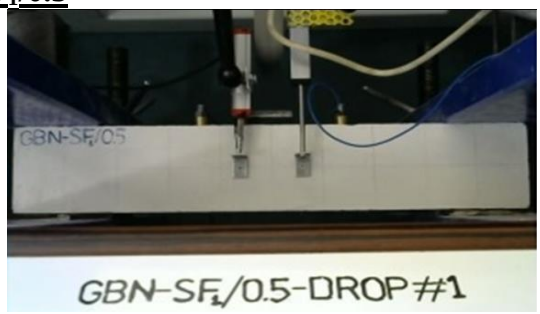
Failure Mode

(f)

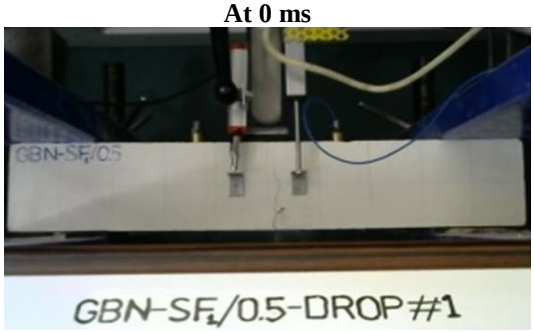
GBN-SF_1/0.5



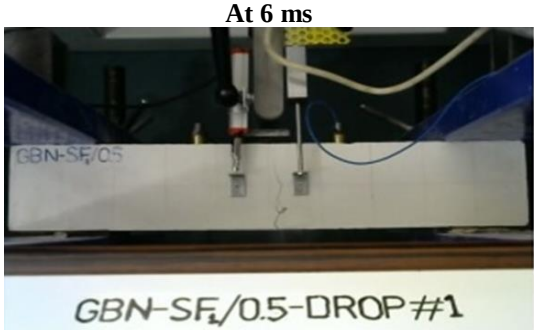
At 0 ms



At 6 ms



At 12 ms



At 18 ms



Failure Mode

(g)

GBN-SF$_1$/1.0



At 0 ms



At 6 ms



At 12 ms



At 18 ms



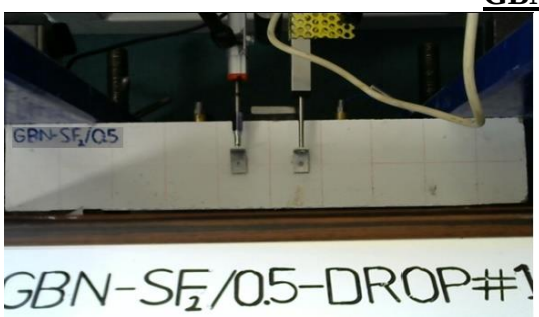
At 24 ms



Failure Mode

(h)

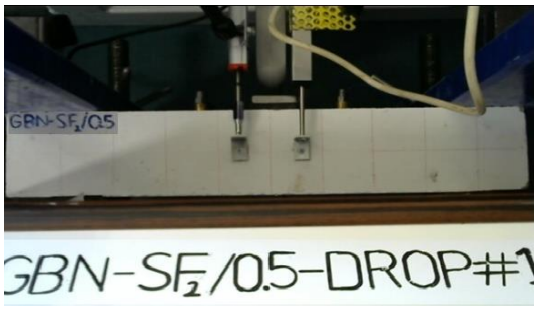
GBN-SF$_2$/0.5



At 0 ms



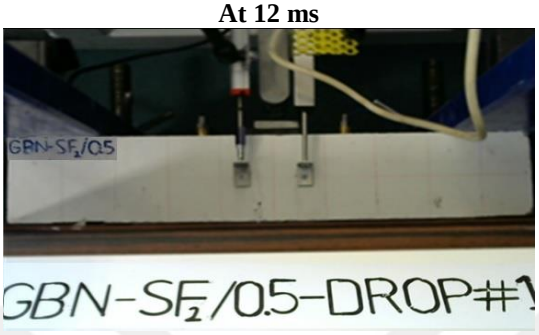
At 6 ms



At 12 ms



At 18 ms



At 24 ms



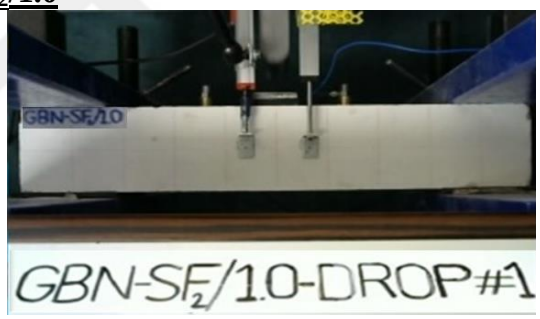
Failure Mode

(i)

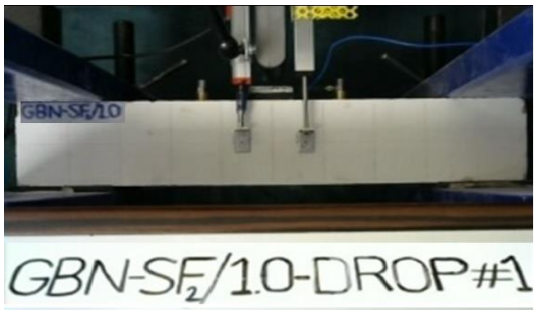
GBN-SF$_2$/1.0



At 0 ms



At 6 ms



At 12 ms



At 18 ms



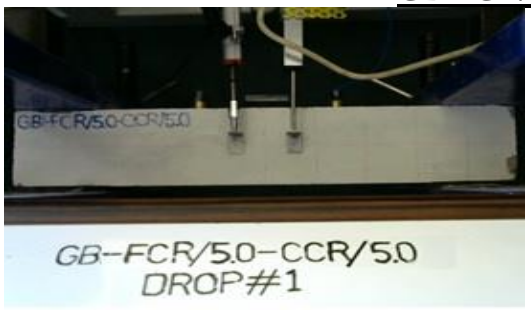
At 24 ms



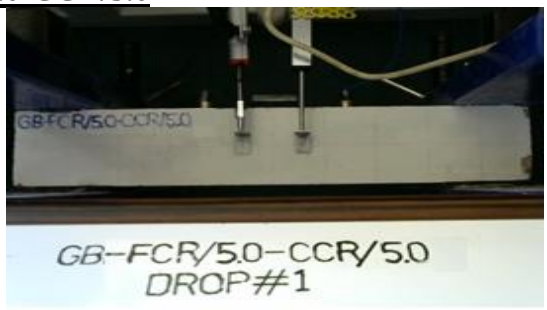
Failure Mode

(j)

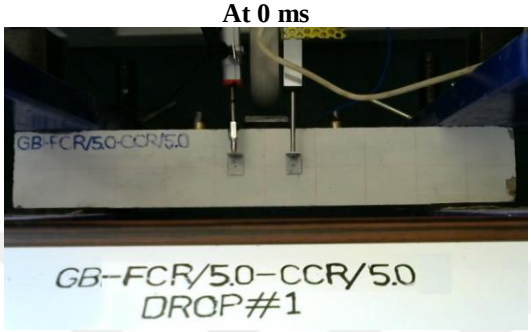
GB-FCR/5.0-CCR/5.0



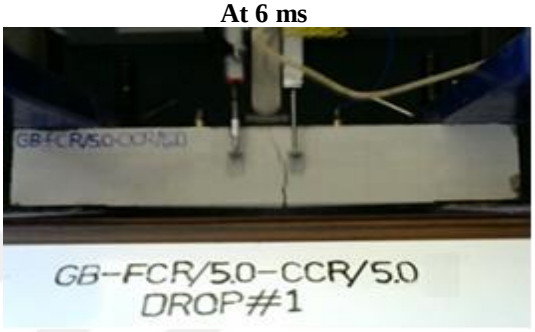
At 0 ms



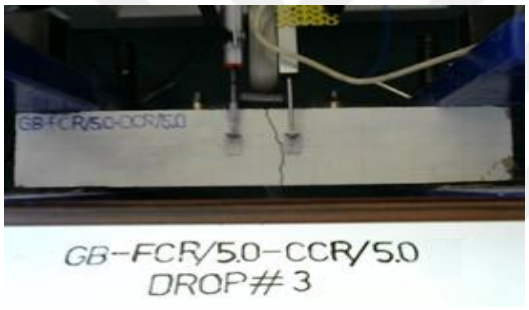
At 6 ms



At 12 ms



At 18 ms



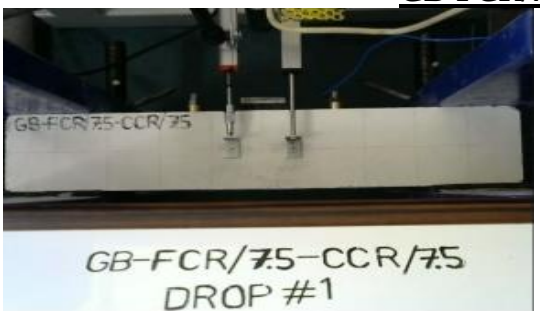
At 24 ms



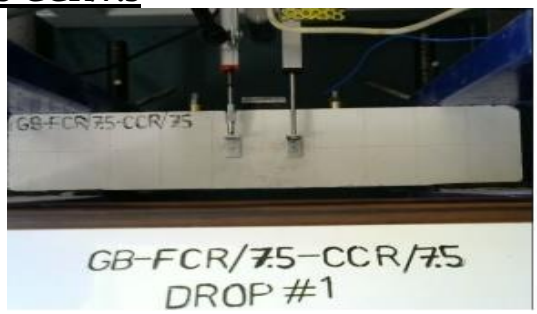
Failure Mode

(k)

GB-FCR/7.5-CCR/7.5

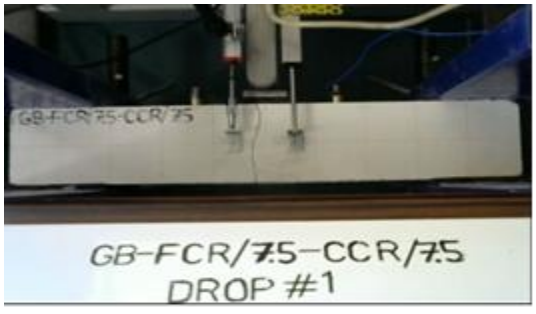


At 0 ms

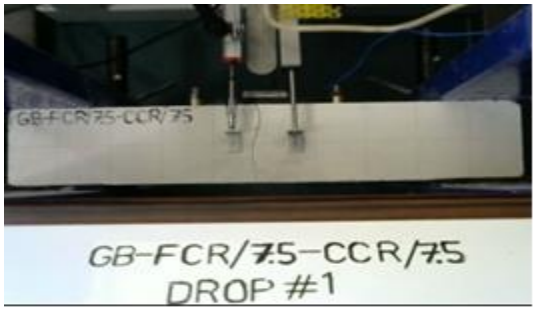


At 6 ms





At 12 ms



At 18 ms



At 24 ms

Failure Mode

(l)

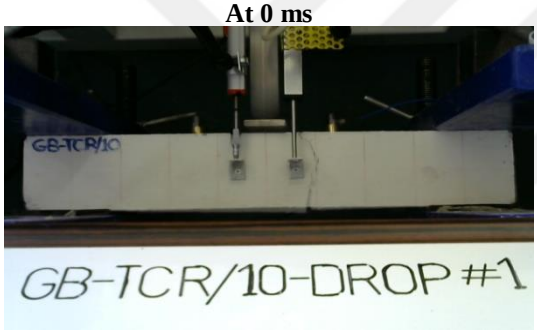
GB-TCR/10



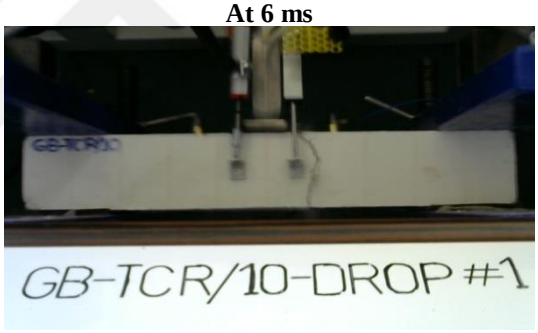
At 0 ms



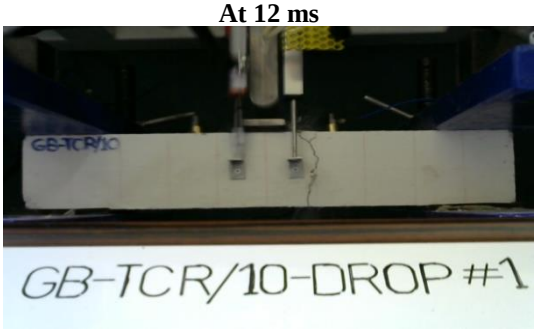
At 6 ms



At 12 ms



At 18 ms



At 24 ms



Failure Mode

(m)

GB-TCR/15



At 0 ms



At 6 ms



At 12 ms



At 18 ms



At 24 ms



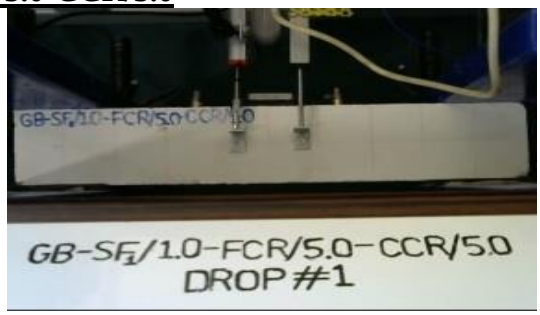
Failure Mode

(n)

GB-SF$_1$/1.0-FCR/5.0-CCR/5.0



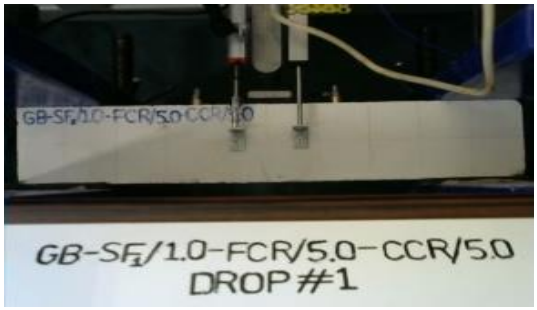
At 0 ms



At 6 ms



At 12 ms



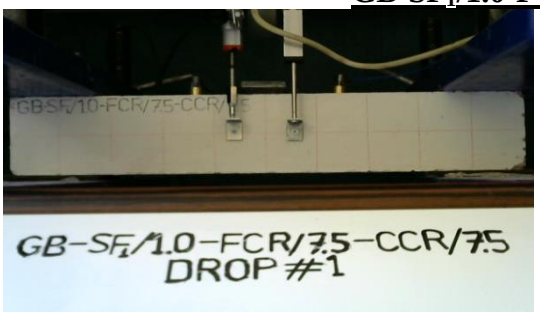
At 18 ms



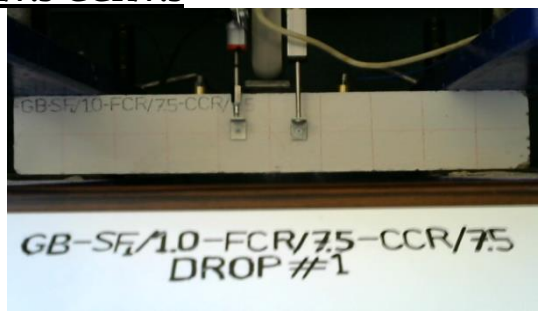
Failure Mode

(o)

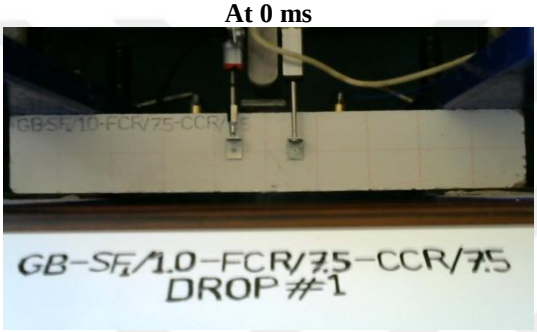
GB-SF$_1$/1.0-FCR/7.5-CCR/7.5



At 0 ms



At 6 ms



At 12 ms



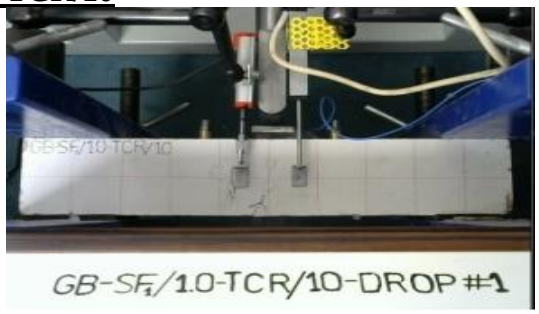
Failure Mode

(p)

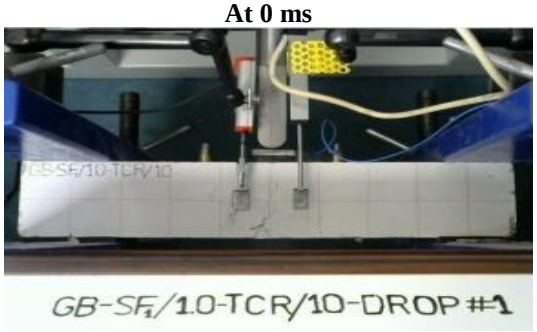
GB-SF$_1$/1.0-TCR/10



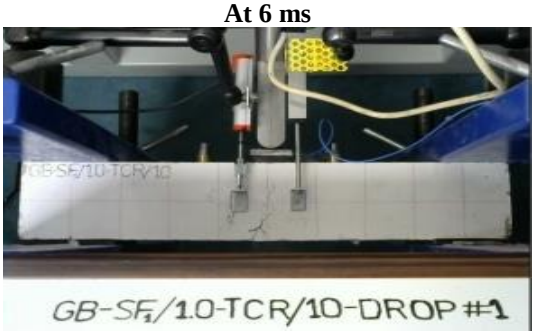
At 0 ms



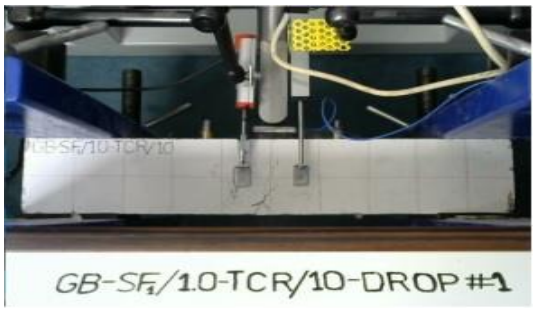
At 6 ms



At 12 ms



At 18 ms





At 24 ms **Failure Mode**

(r)

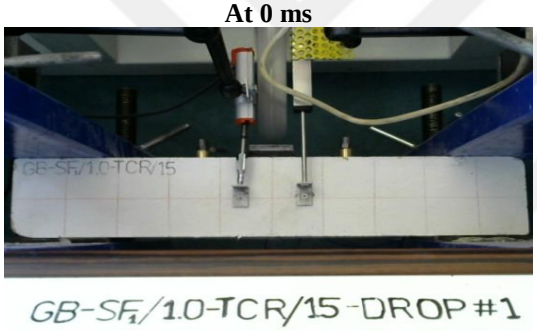
GB-SF$_1$/1.0-TCR/15



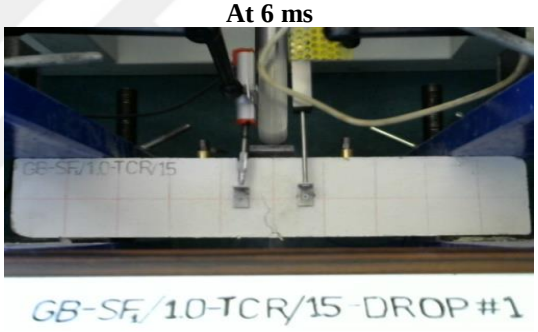
At 0 ms



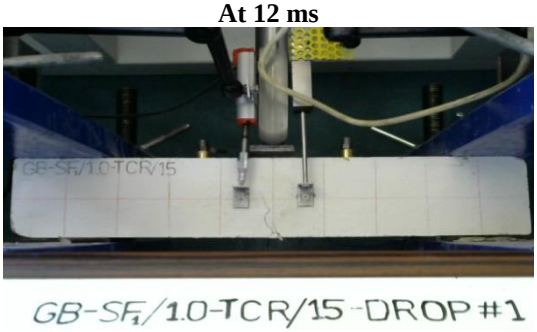
At 6 ms



At 12 ms



At 18 ms



At 24 ms

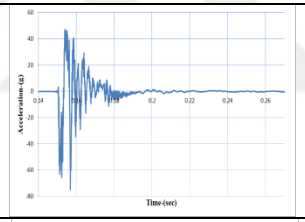
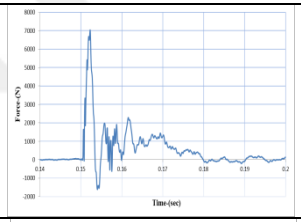
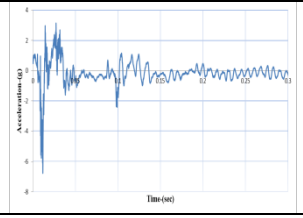
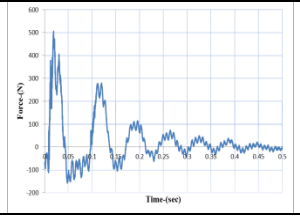


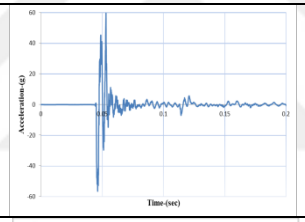
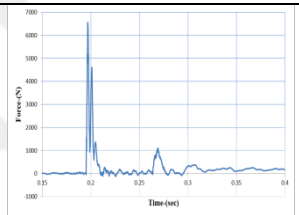
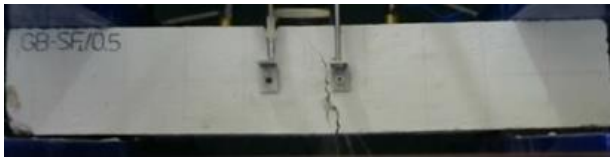
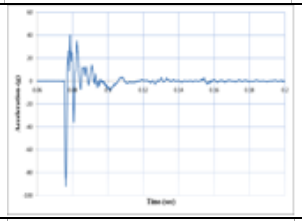
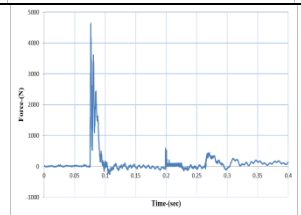
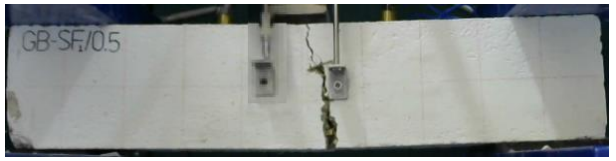
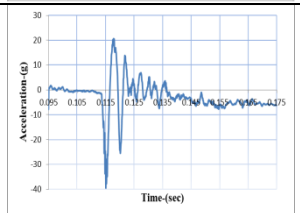
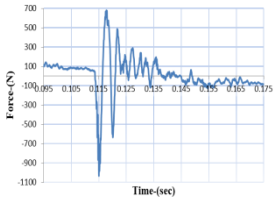
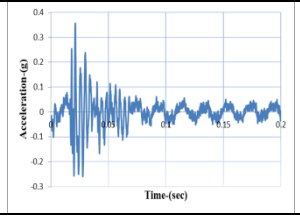
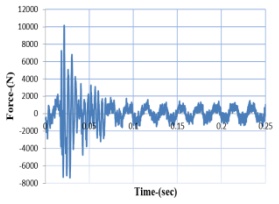
Failure Mode

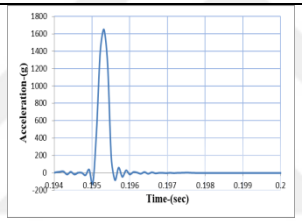
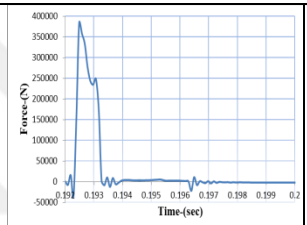
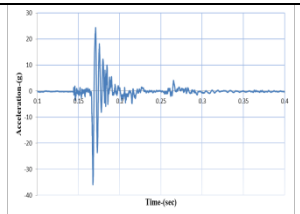
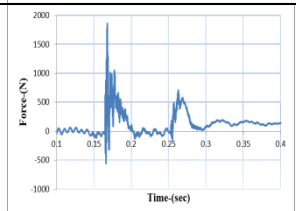
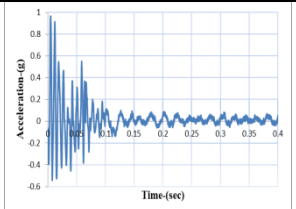
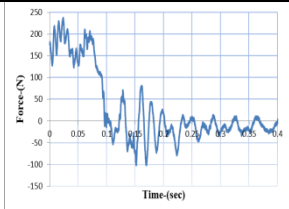
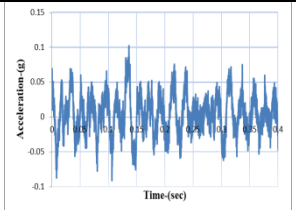
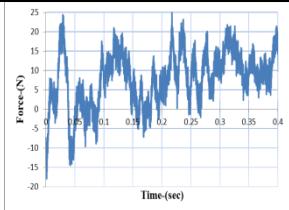
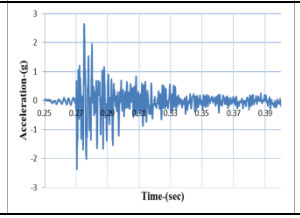
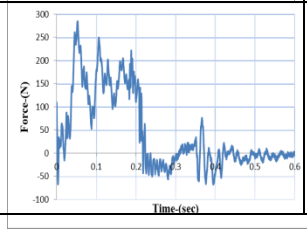
(s)

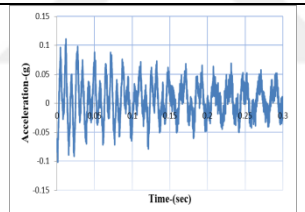
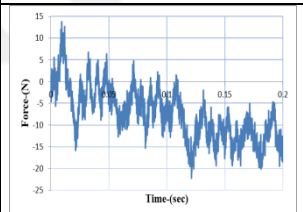
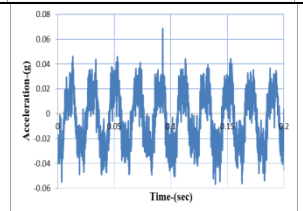
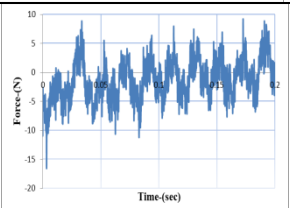
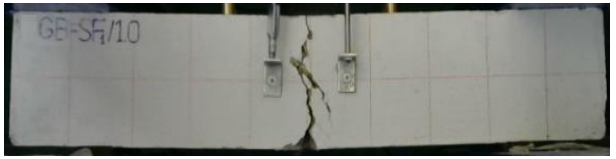
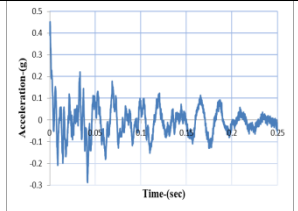
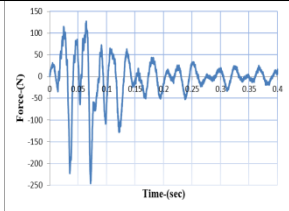
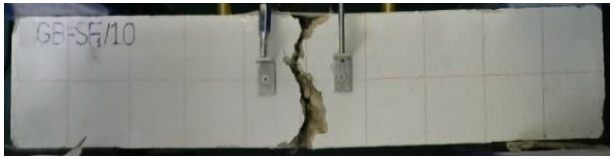
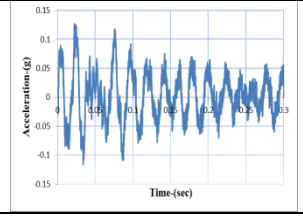
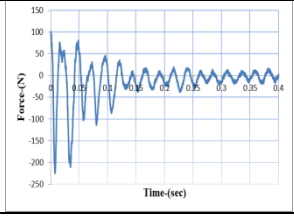
Figure 4.28 The first drop moment and failure mode of each beam specimen

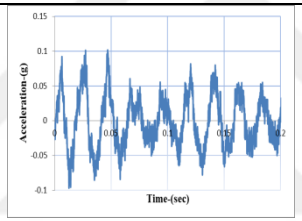
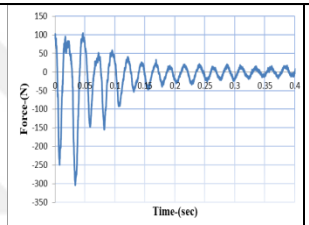
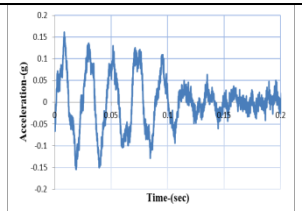
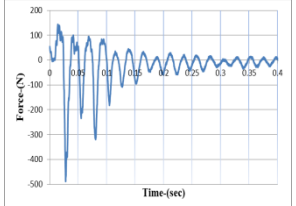
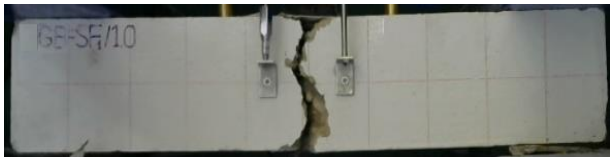
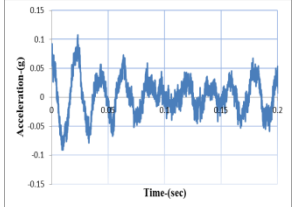
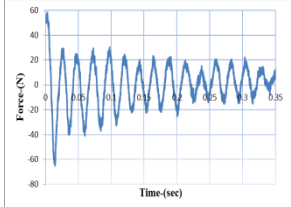
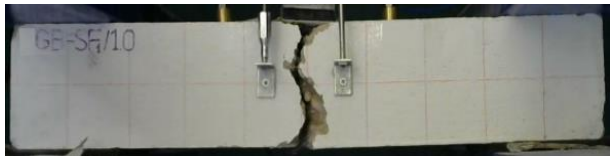
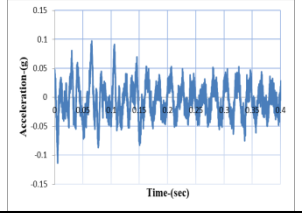
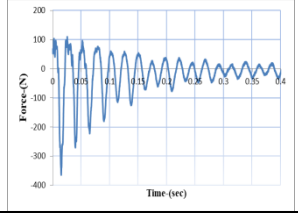
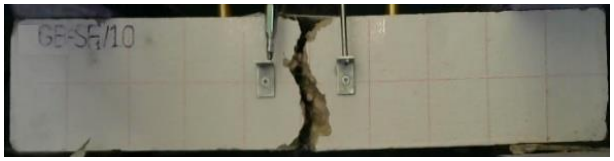
Table 4.3 Drop-weight test results

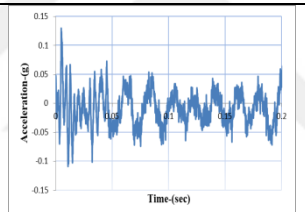
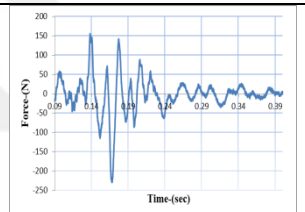
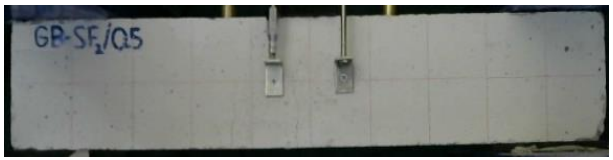
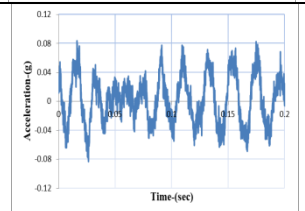
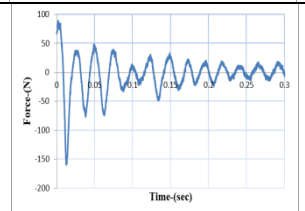
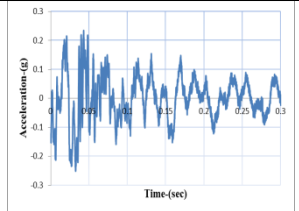
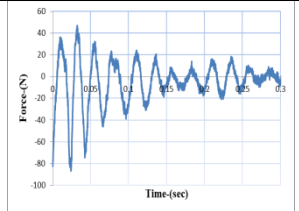
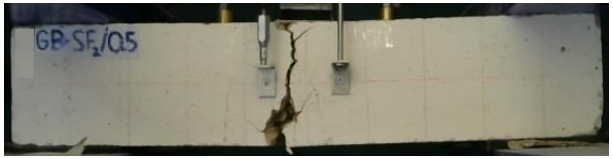
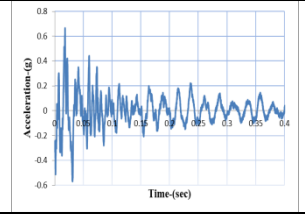
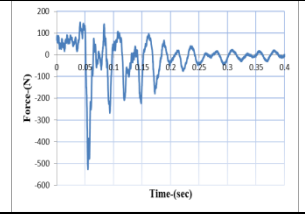
SAMPLE NAME	DROP NUMBER	DISPLACEMENT (mm)	CRACK WIDTH (mm)	AVERAGE ACCELERATION(g)-TIME(sec)	FORCE(N)-TIME(sec)	
GB	1	51.8783	14			
	2	0.0034	18			

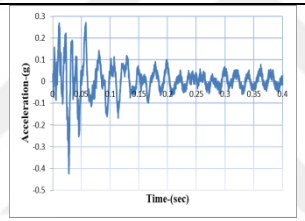
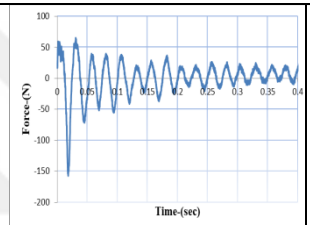
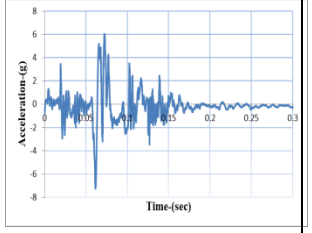
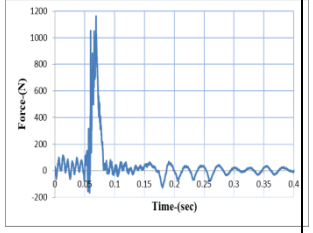
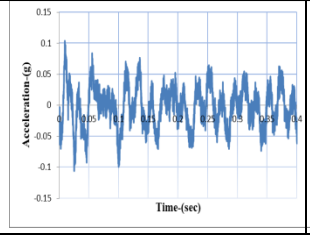
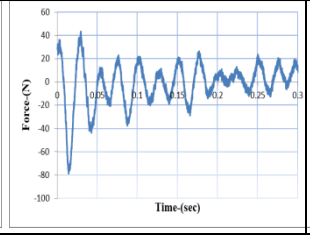
SAMPLE NAME	DROP NUMBER	DISPLACEMENT (mm)	CRACK WIDTH (mm)	AVERAGE ACCELERATION(g)-TIME(sec)	FORCE(N)-TIME(sec)	
GB-SF$_1$/0.5	1	1.2237	0.12			
	2	0.1575	9			
	4	1.0731	11			
	5	1.394	11.8			

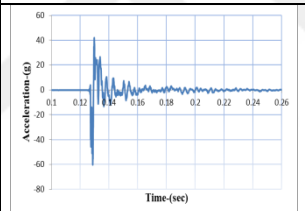
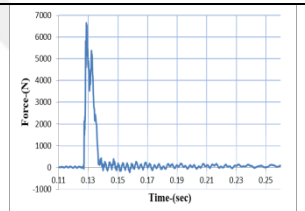
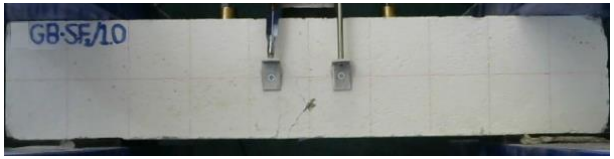
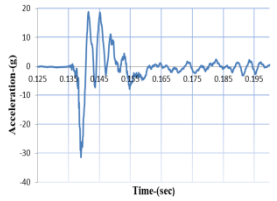
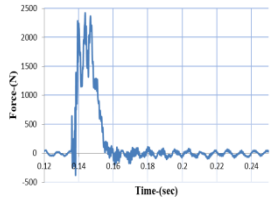
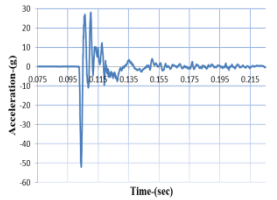
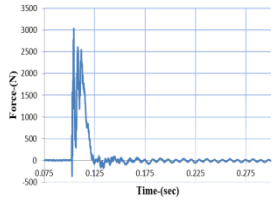
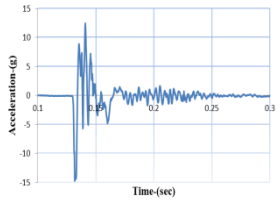
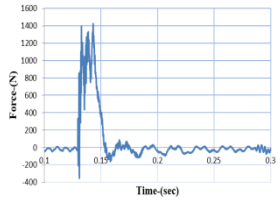
GB-SF$_1$/0.5	6	2.5416	12			
	7	2.910	12			
	8	1.360	12.9			
	9	0.855	12.9			
	10	0.1267	14			

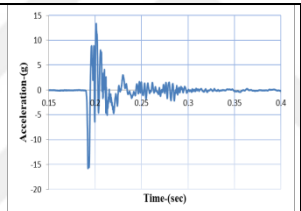
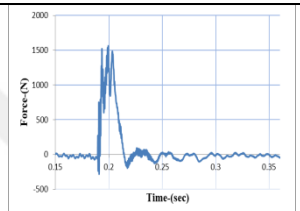
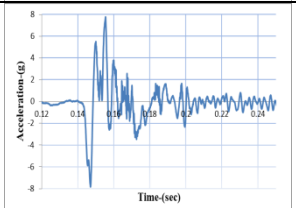
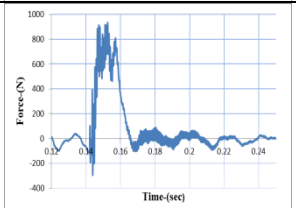
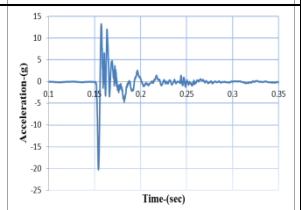
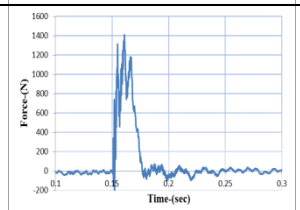
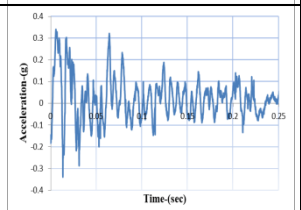
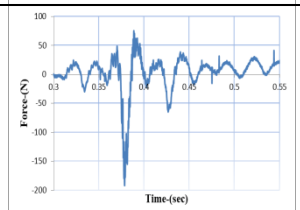
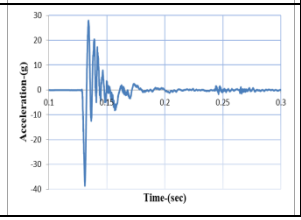
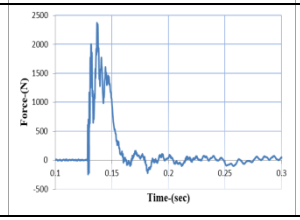
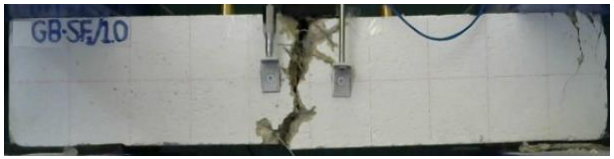
SAMPLE NAME	DROP NUMBER	DISPLACEMENT (mm)	CRACK WIDTH (mm)	AVERAGE ACCELERATION(g)-TIME(sec)	FORCE(N)-TIME(sec)	
GB-SF$_1$/1.0	1	0.0052	0.35			
	7	0.2499	21			
	14	0.017	23			
	19	0.020	24			

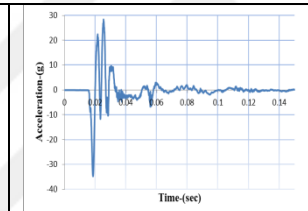
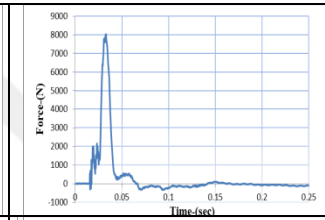
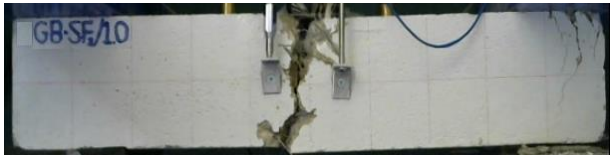
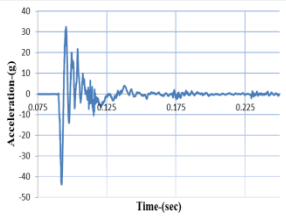
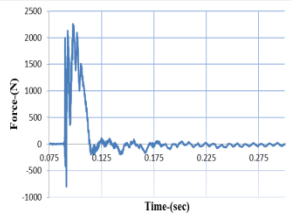
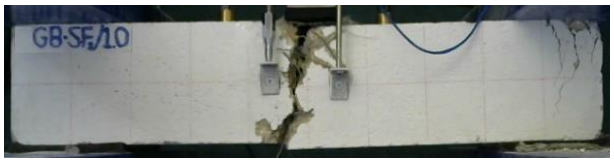
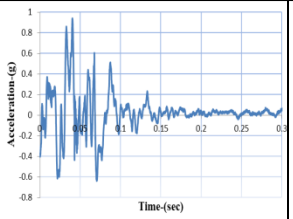
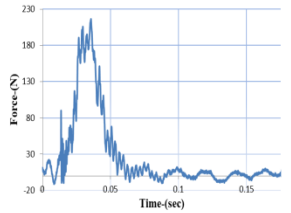
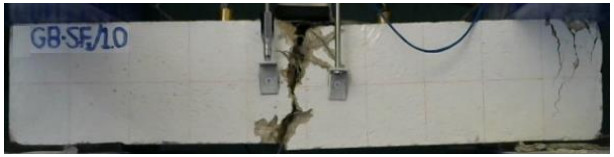
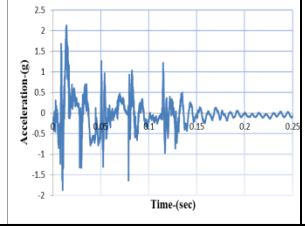
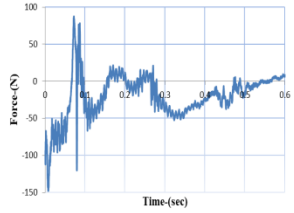
GB-SF$_1$/1.0	26	0.0291	25			
	32	0.027	25			
	37	0.008	25			
	41	0.061	27			

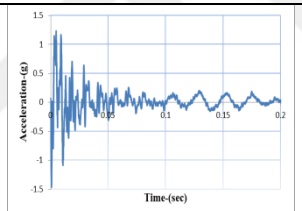
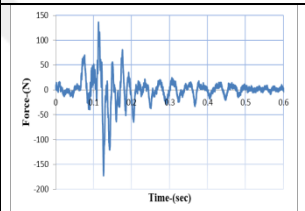
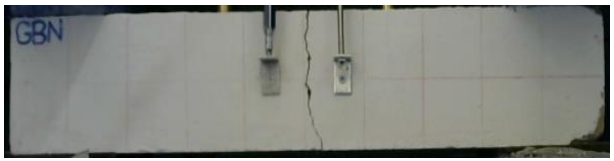
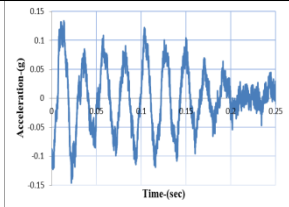
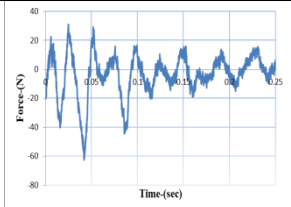
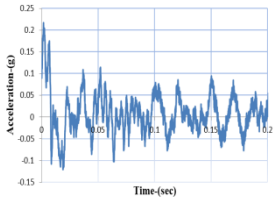
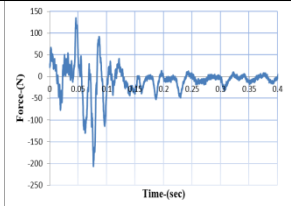
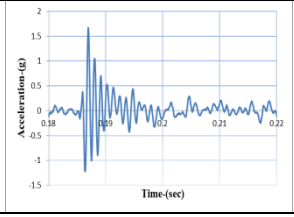
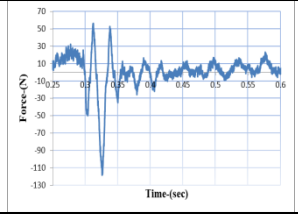
SAMPLE NAME	DROP NUMBER	DISPLACEMENT (mm)	CRACK WIDTH (mm)	AVERAGE ACCELERATION(g)-TIME(sec)	FORCE(N)-TIME(sec)	
GB-SF$_2$/0.5	1	0.3445	0.06			
	14	0.023	9			
	22	0.005	18			
	32	0.013	19			

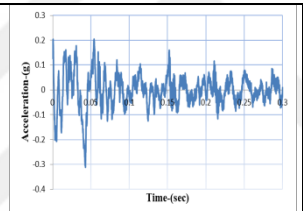
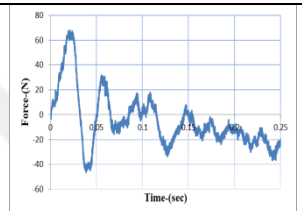
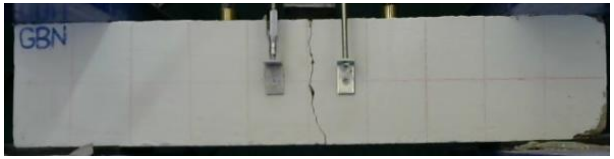
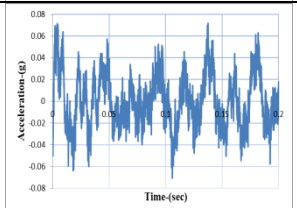
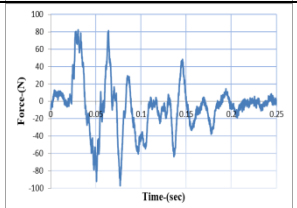
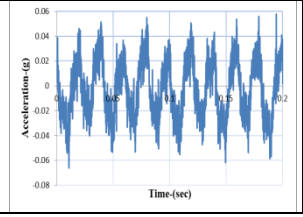
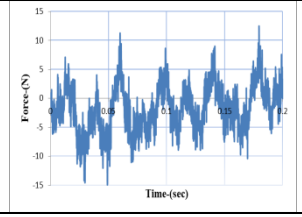
GB-SF$_2$/0.5	37	0.000	31			
	43	0.0309	32			
	47	0.0205	34			

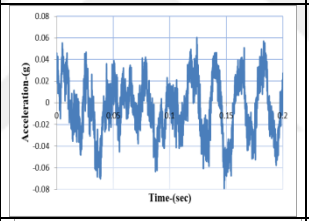
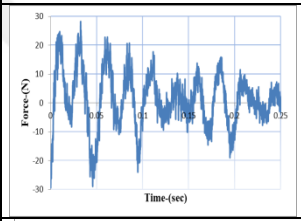
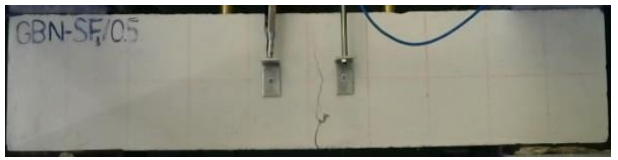
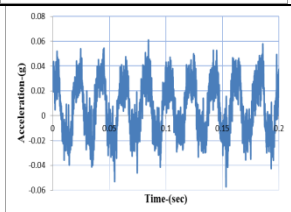
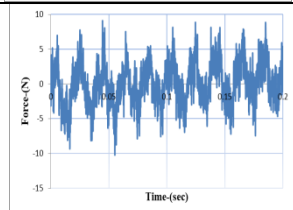
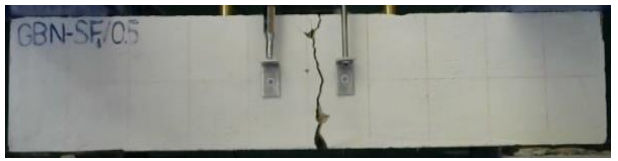
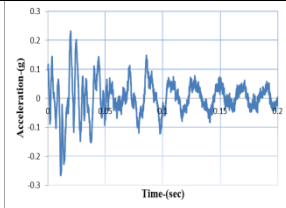
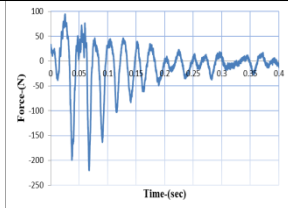
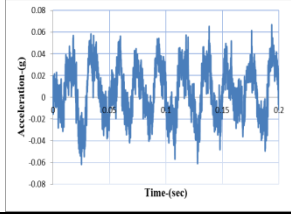
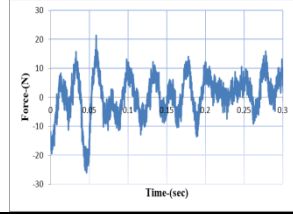
SAMPLE NAME	DROP NUMBER	DISPLACEMET (mm)	CRACK WIDTH (mm)	AVERAGE ACCELERATION(g)-TIME(sec)	FORCE(N)-TIME(sec)	
GB-SF$_2$/1.0	1	0.0394	0.06			
	7	0.0239	11			
	18	0.0294	13			
	29	0.0291	25			

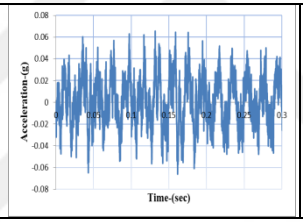
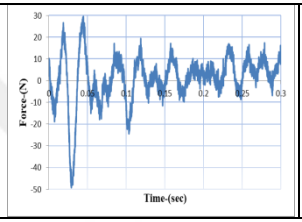
GB-SF$_2$/1.0	37	0.0462	25			
	47	0.0702	26			
	57	0.003	26			
	66	0.0445	26			
	80	0.025	26			

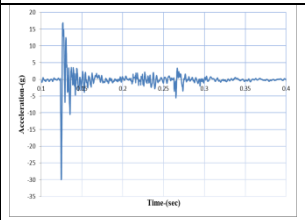
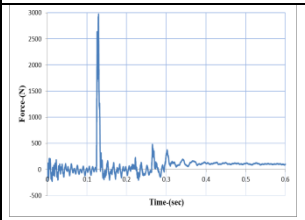
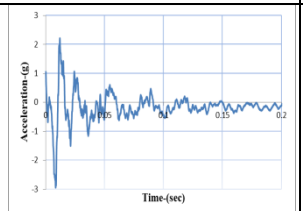
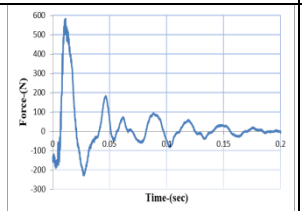
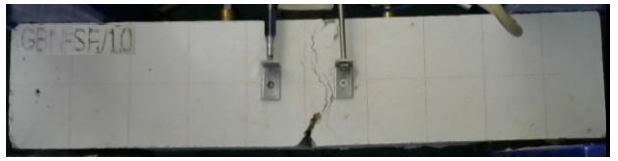
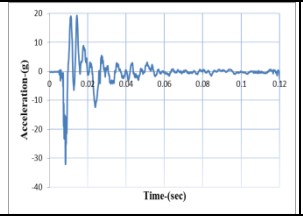
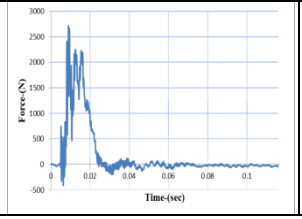
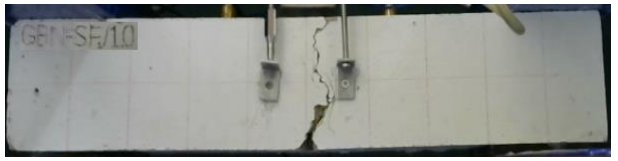
GB-SF$_2$/1.0	90	0.0582	26			
	99	0.010	26			
	107	0.0325	26			
	128	0.024	26			

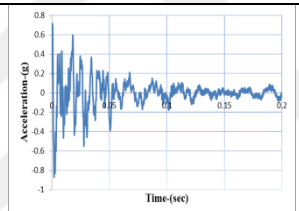
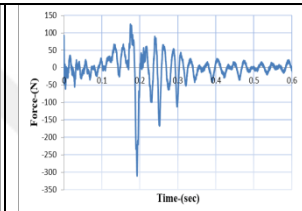
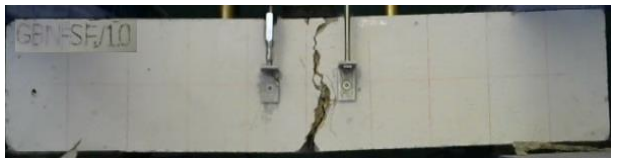
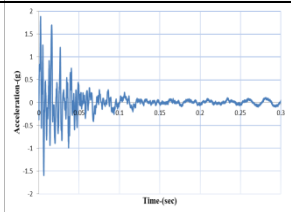
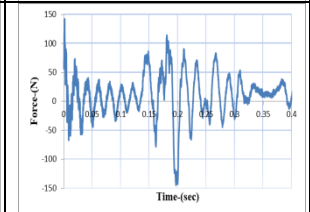
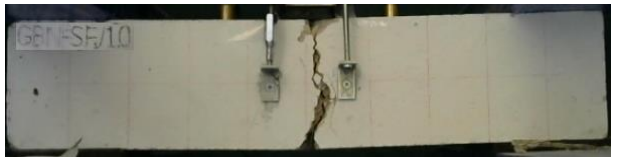
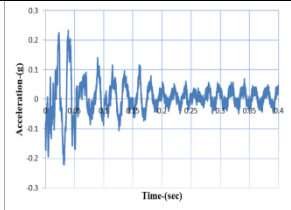
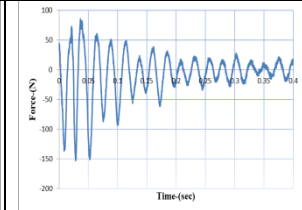
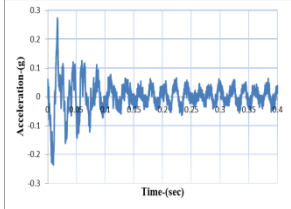
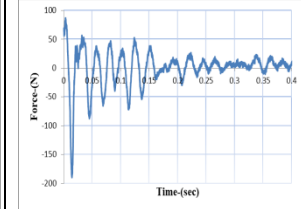
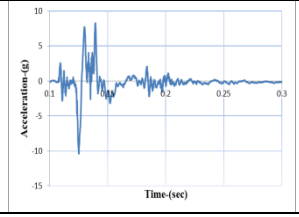
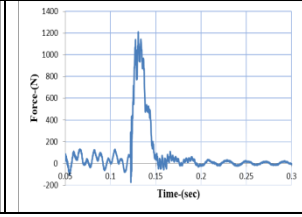
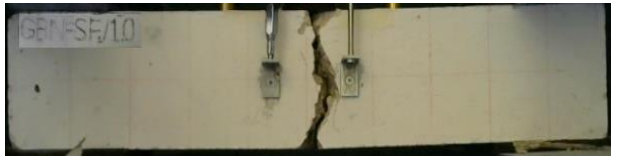
SAMPLE NAME	DROP NUMBER	DISPLACEMET (mm)	CRACK WIDTH (mm)	AVERAGE ACCELERATION(g)-TIME(sec)	FORCE(N)-TIME(sec)	
GBN	1	0.005	0.6			
	2	0.006	0.8			
	3	0.005	0.8			
	4	0.015	0.8			

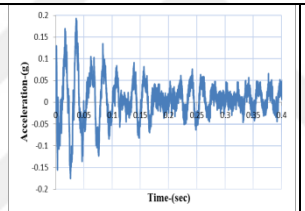
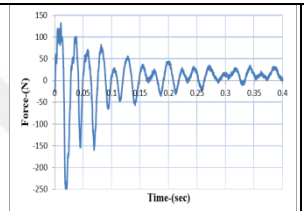
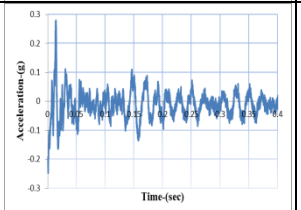
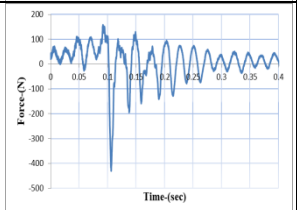
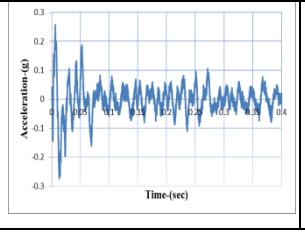
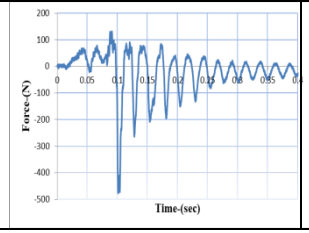
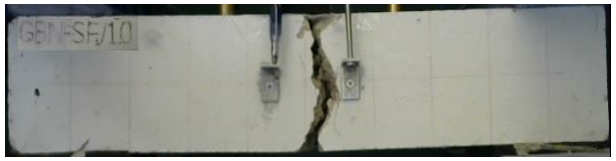
GBN	5	0.205	0.8			
	6	0.001	0.8			
	7	0.206	0.85			

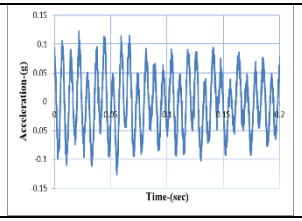
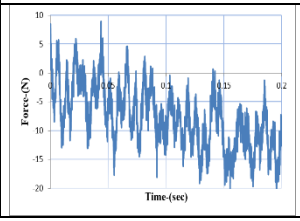
SAMPLE NAME	DROP NUMBER	DISPLACEMET (mm)	CRACK WIDTH (mm)	AVERAGE ACCELERATION(g)-TIME(sec)	FORCE(N)-TIME(sec)	
GBN-SF$_1$/0.5	1	0.085	0.50			
	6	0.077	10			
	13	0.0684	11			
	18	0.0719	12			

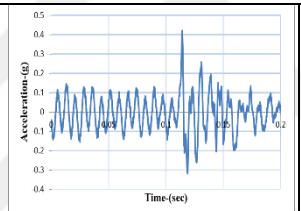
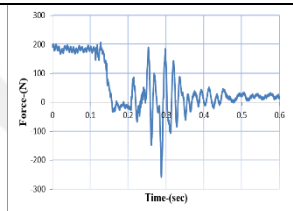
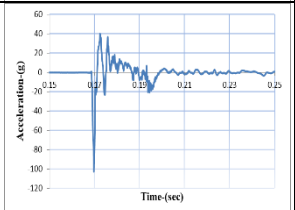
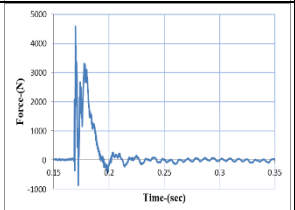
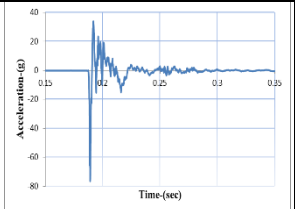
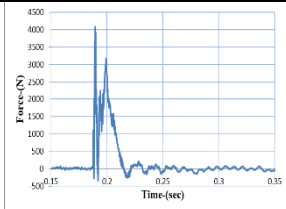
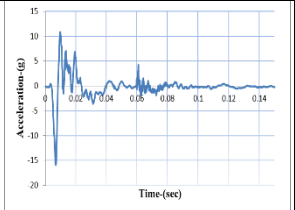
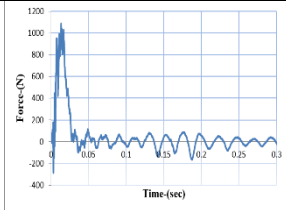
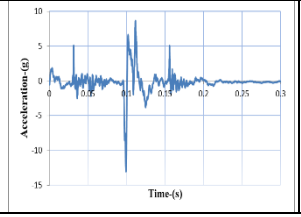
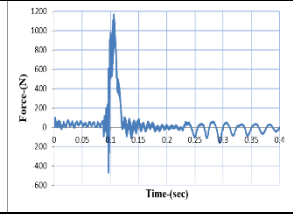
GBN-SF$_1$/0.5	25	0.0035	13			

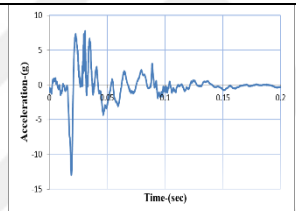
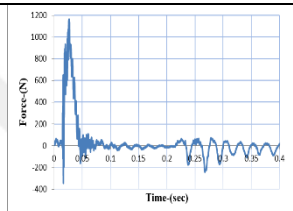
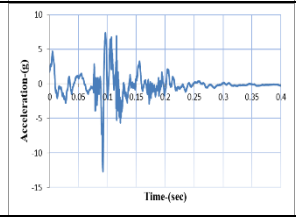
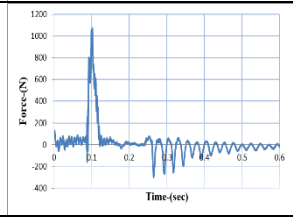
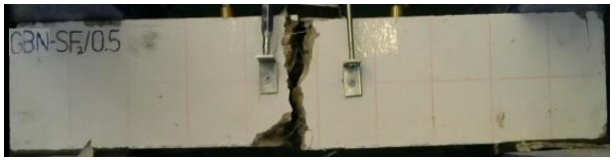
SAMPLE NAME	DROP NUMBER	DISPLACEMET (mm)	CRACK WIDTH (mm)	AVERAGE ACCELERATION(g)-TIME(sec)	FORCE(N)-TIME(sec)	
GBN-SF$_1$/1.0	1	0.1540	0.65			
	7	0.037	5			
	13	0.3817	9			

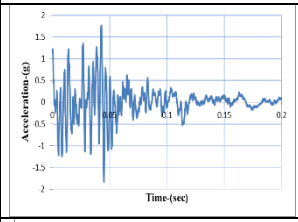
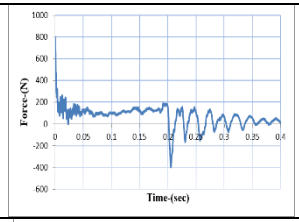
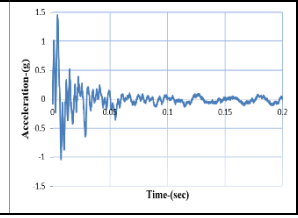
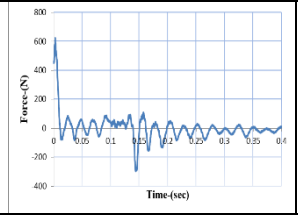
GBN-SF$_1$/1.0	20	0.015	19			
	28	0.003	21			
	45	0.015	22			
	52	0.0394	22			
	61	0.017	23			

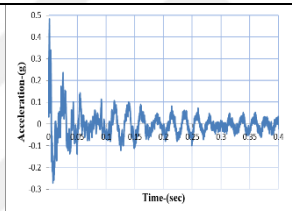
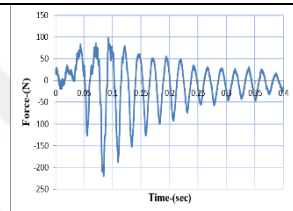
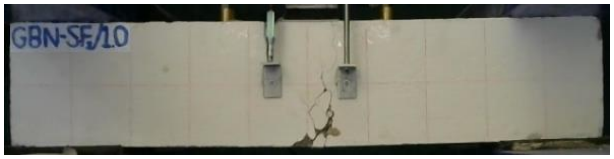
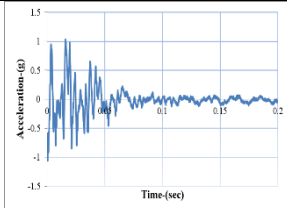
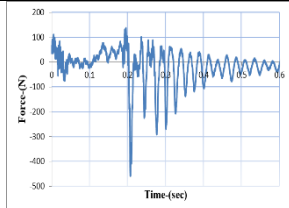
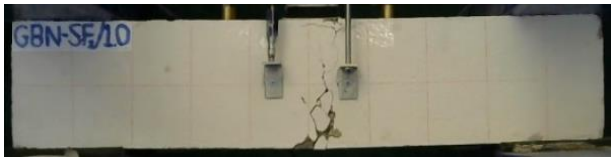
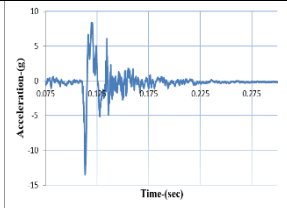
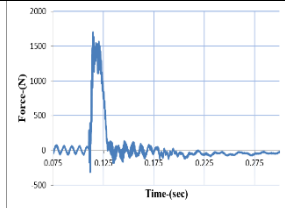
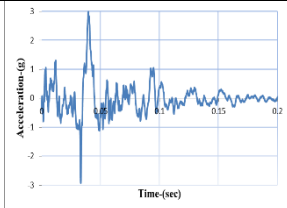
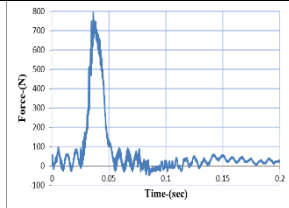
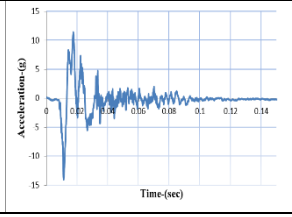
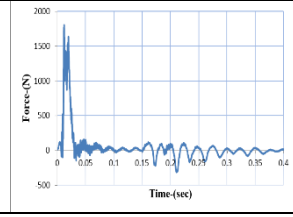
GBN-SF$_1$/1.0	73	0.006	23			
	81	0.022	23			
	89	0.053	25			

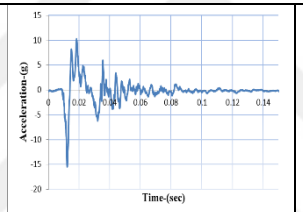
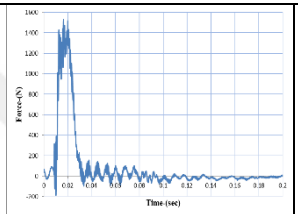
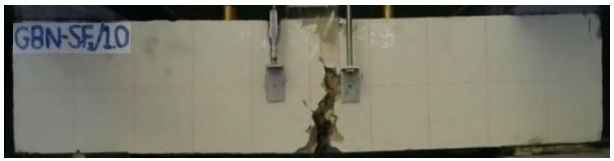
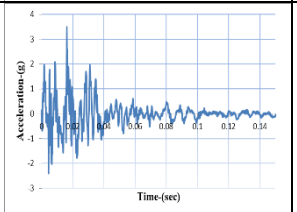
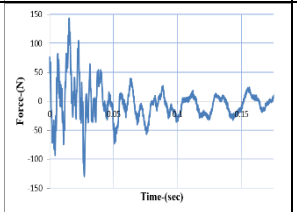
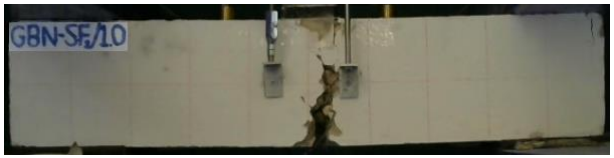
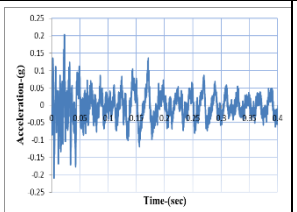
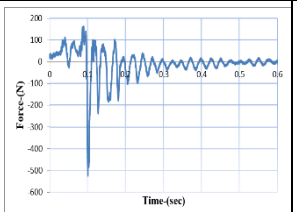
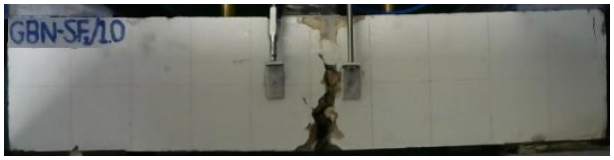
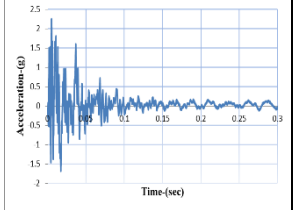
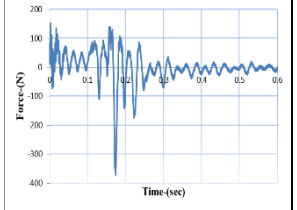
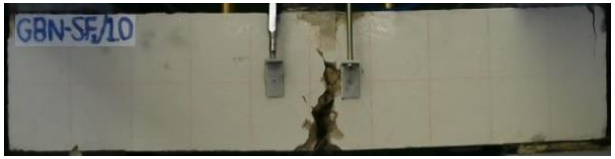
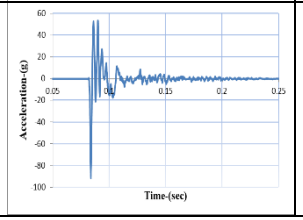
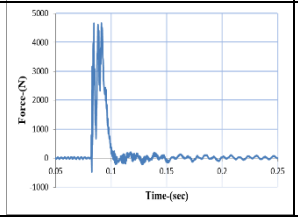
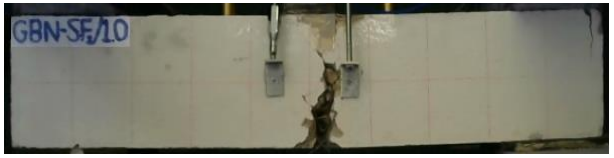
SAMPLE NAME	DROP NUMBER	DISPLACEMET (mm)	CRACK WIDTH (mm)	AVERAGE ACCELERATION(g)-TIME(sec)	FORCE(N)-TIME(sec)	
GBN-SF$_2$/0.5	1	69.5305	0.4			

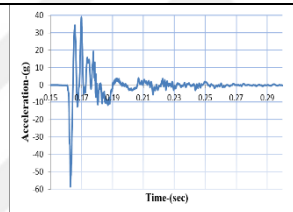
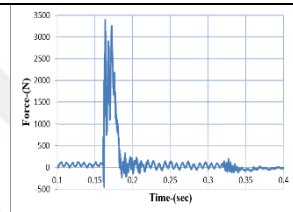
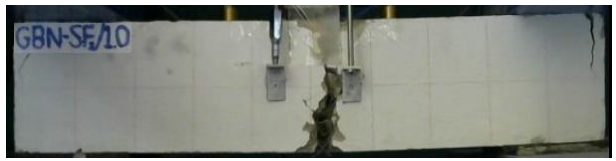
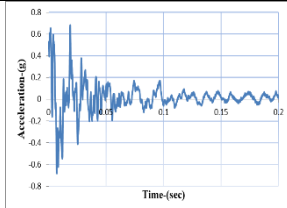
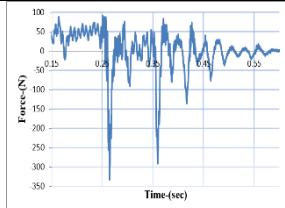
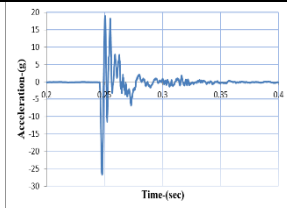
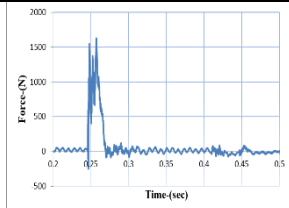
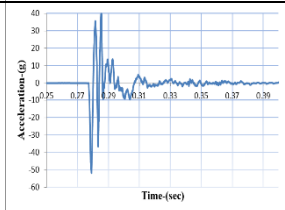
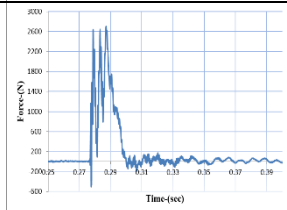
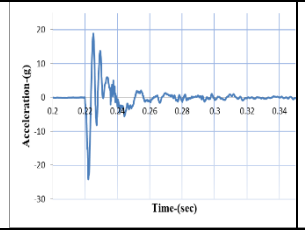
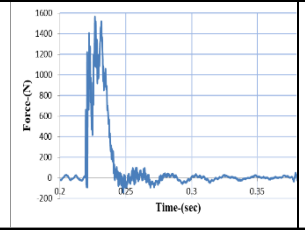
GBN-SF$_2$/0.5	12	0.060	36			
	20	10.291	36			
	29	0.053	36			
	43	0.013	38			
	51	0.0995	40			

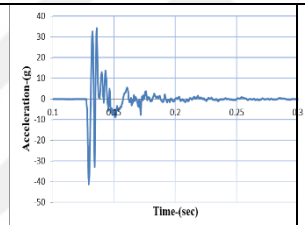
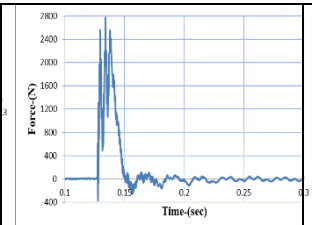
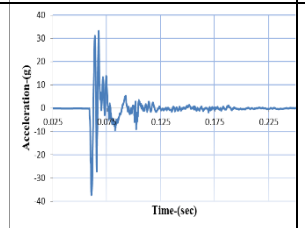
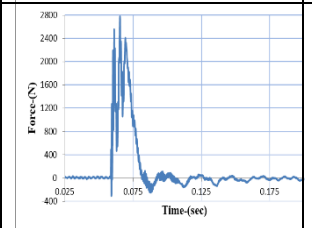
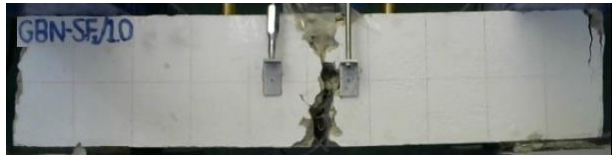
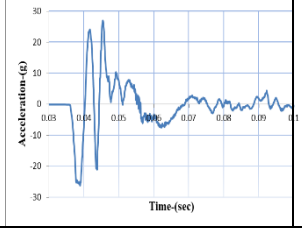
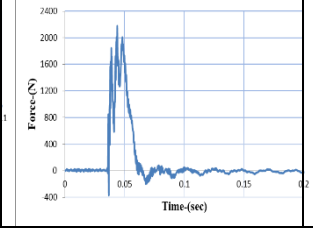
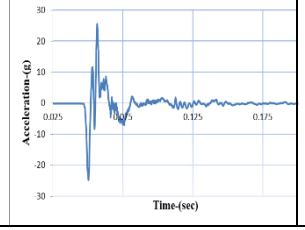
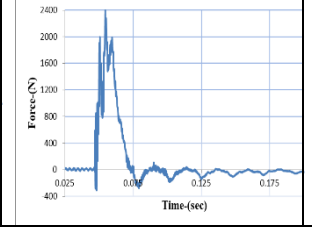
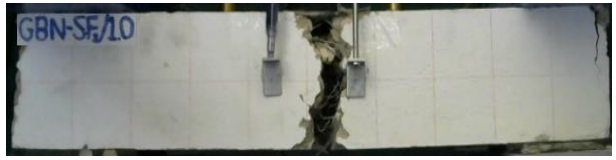
GBN-SF$_2$/0.5	58	0.0154	43			
	62	0.065	45			

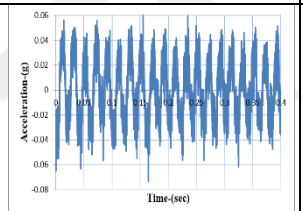
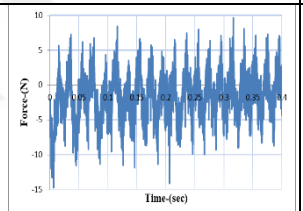
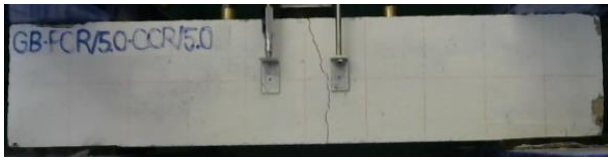
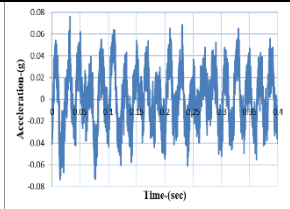
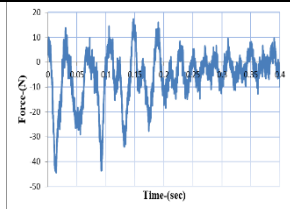
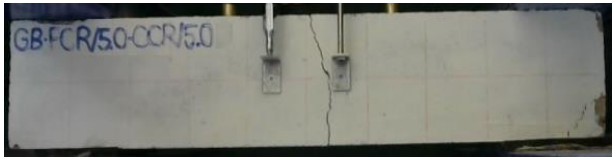
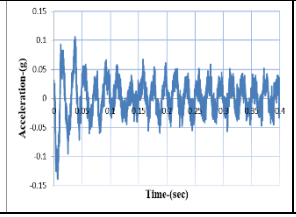
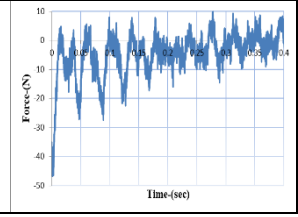
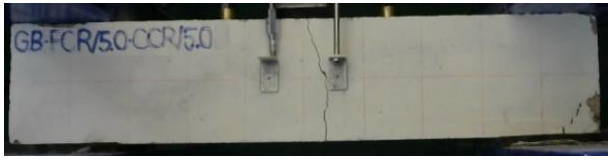
SAMPLE NAME	DROP NUMBER	DISPLACEMET (mm)	CRACK WIDTH (mm)	AVERAGE ACCELERATION(g)-TIME(sec)	FORCE(N)-TIME(sec)	
GBN-SF$_2$/1.0	1	0.003	0.06			
	12	0.0393	16			

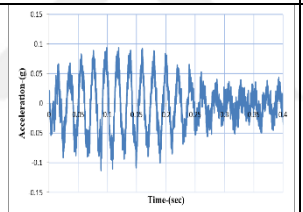
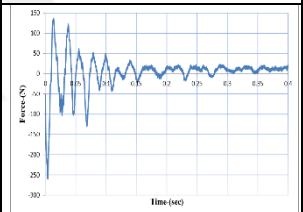
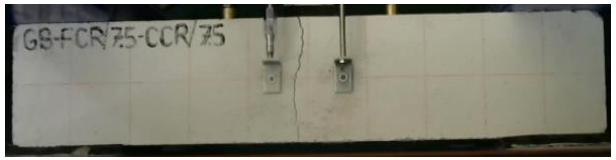
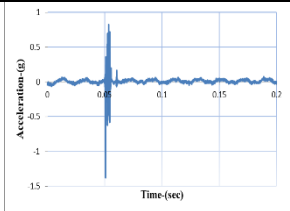
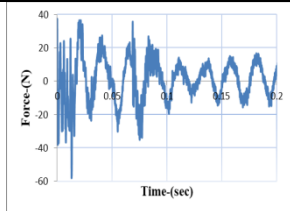
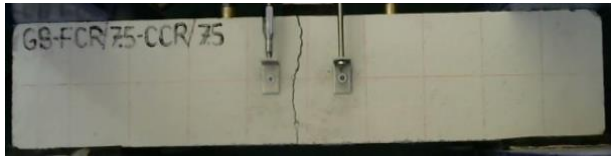
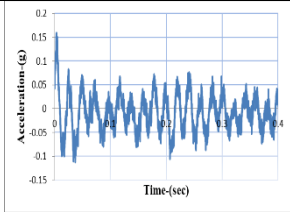
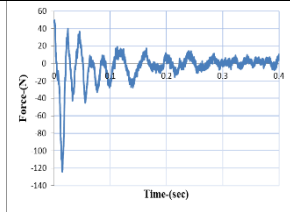
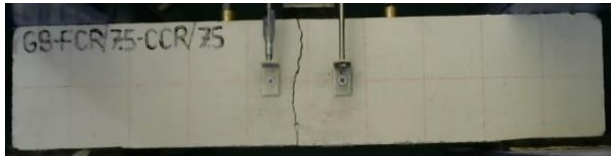
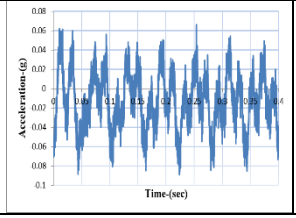
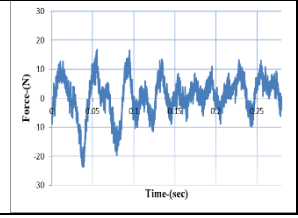
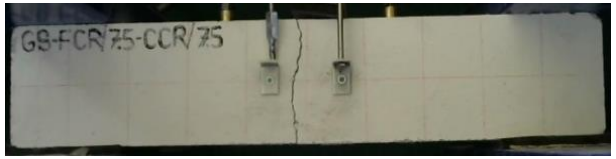
GBN-SF$_2$/1.0	23	0.0017	17			
	34	0.0086	18			
	43	0.001	18			
	57	0.003	39			
	68	0.005	39			

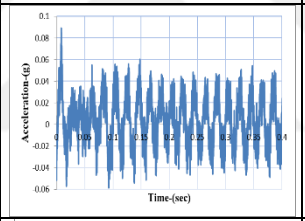
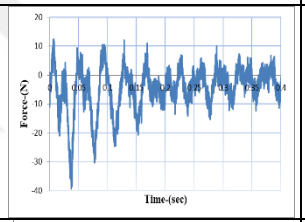
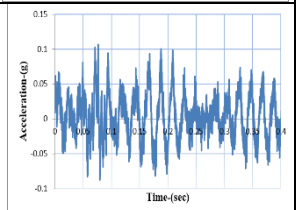
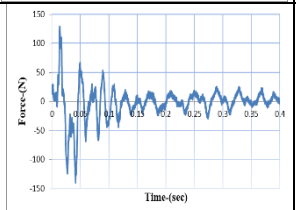
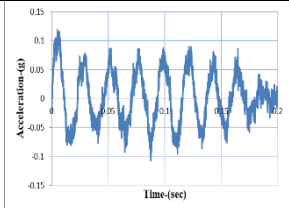
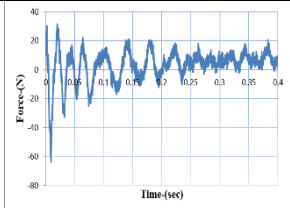
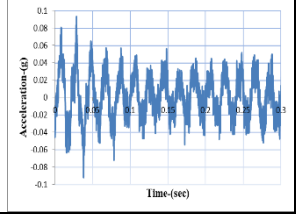
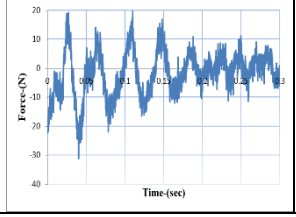
GBN-SF$_2$/1.0	79	0.0085	39			
	88	0.0325	39			
	98	0.008	39			
	110	0.0291	39.5			
	121	0.003	39.5			

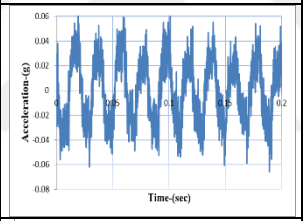
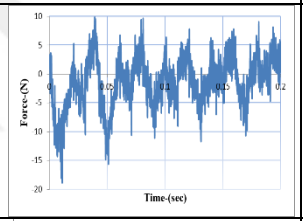
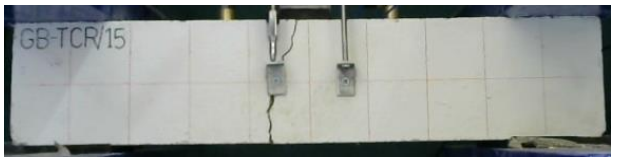
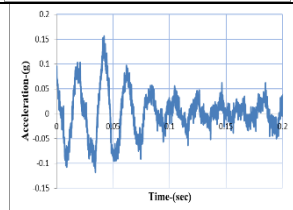
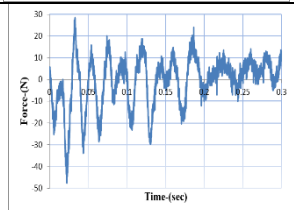
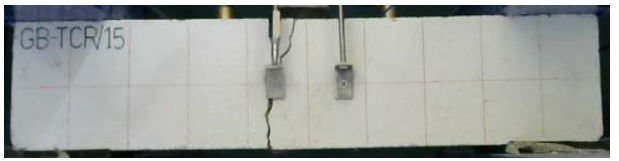
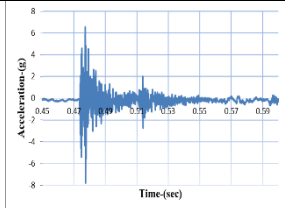
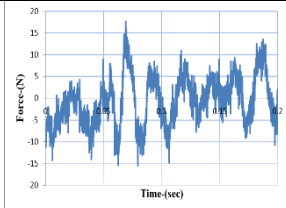
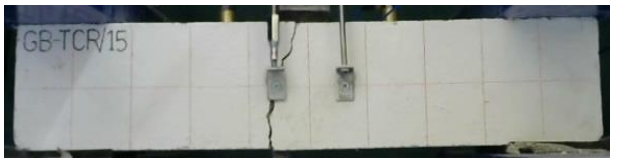
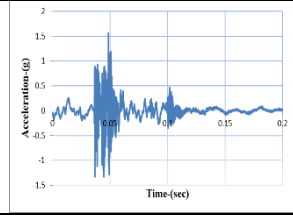
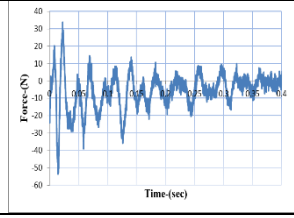
GBN-SF$_2$/1.0	167	0.001	41			
	177	0.020	41			
	193	0.025	41			
	207	0.0086	41			
	221	0.013	41			

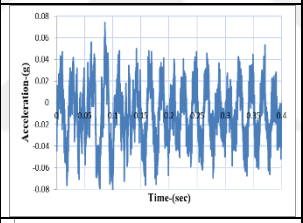
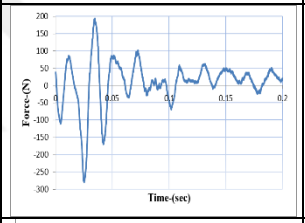
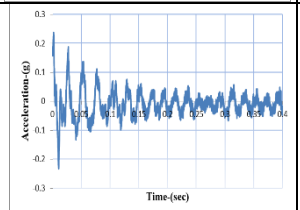
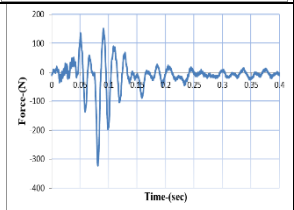
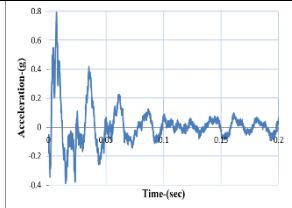
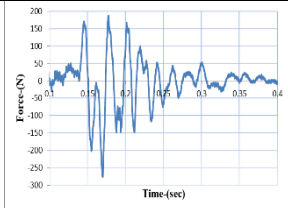
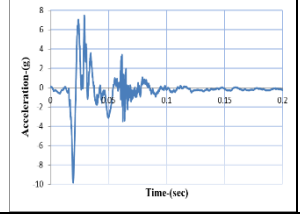
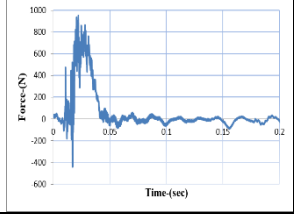
GBN-SF$_2$/1.0	237	0.020	41.5			
	253	0.0035	41.5			
	271	0.029	42			
	289	0.0069	48			

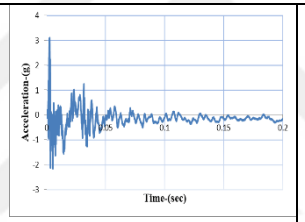
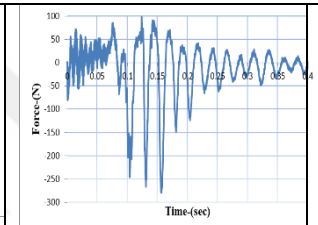
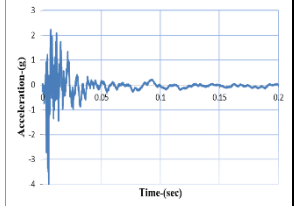
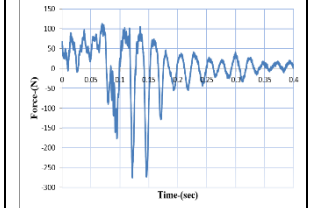
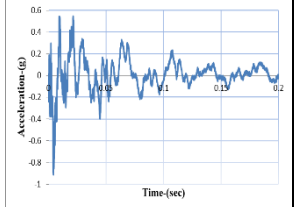
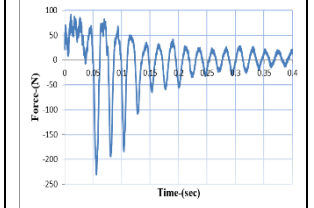
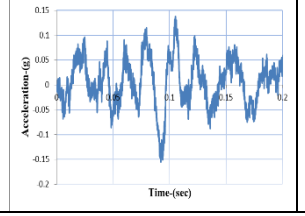
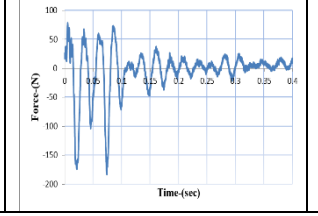
SAMPLE NAME	DROP NUMBER	DISPLACEMET (mm)	CRACK WIDTH (mm)	AVERAGE ACCELERATION(g)-TIME(sec)	FORCE(N)-TIME(sec)	
GB-FCR/5.0-CCR/5.0	1	0.005	0.30			
	2	0.001	0.50			
	3	0.001	0.50			

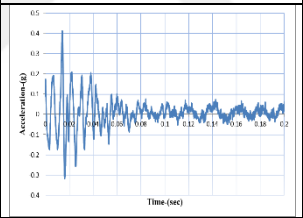
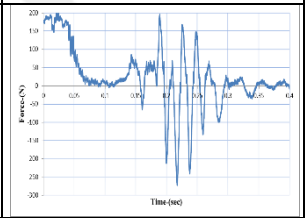
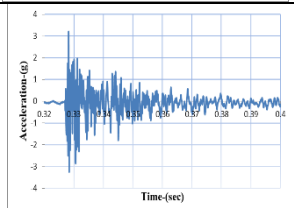
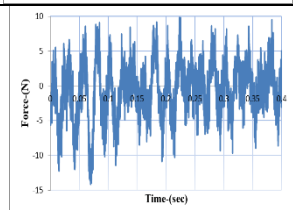
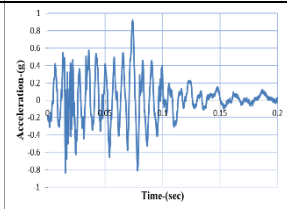
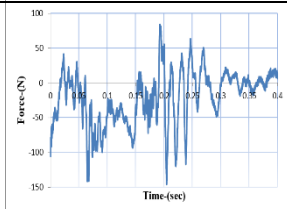
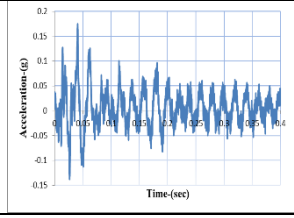
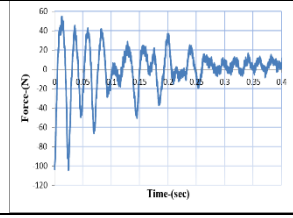
SAMPLE NAME	DROP NUMBER	DISPLACEMET (mm)	CRACK WIDTH (mm)	AVERAGE ACCELERATION(g)-TIME(sec)	FORCE(N)-TIME(sec)	
GB-FCR/7.5-CCR/7.5	1	0.0394	0.10			
	2	0.005	0.50			
	3	0.048	0.60			
	4	0.0034	0.65			

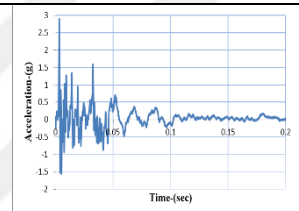
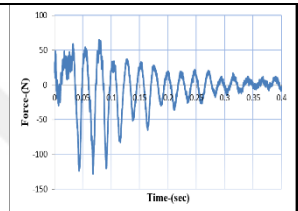
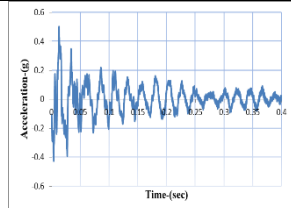
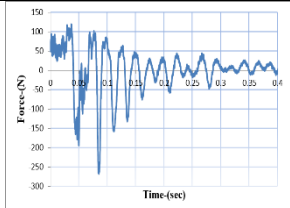
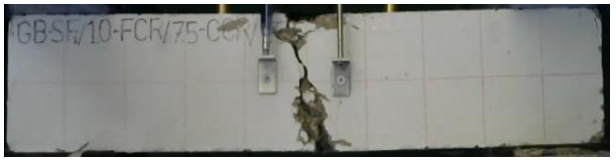
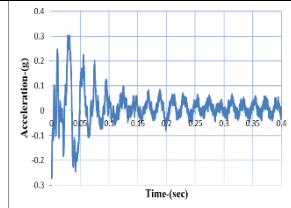
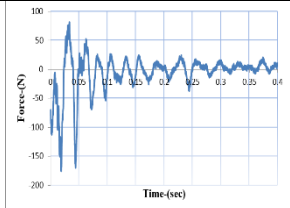
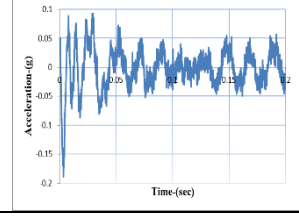
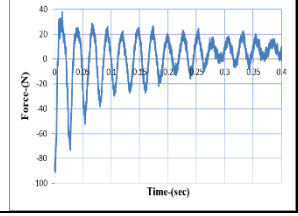
SAMPLE NAME	DROP NUMBER	DISPLACEMET (mm)	CRACK WIDTH (mm)	AVERAGE ACCELERATION(g)-TIME(sec)	FORCE(N)-TIME(sec)	
GB-TCR/10	1	0.0154	0.75			
	2	0.0594	0.85			
	3	0.001	0.90			
	5	0.0632	0.90			

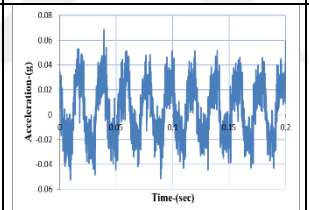
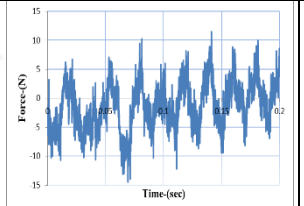
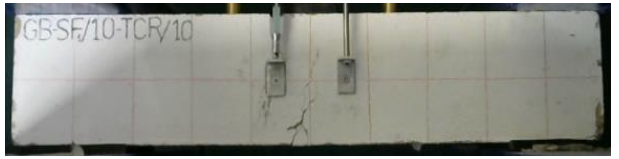
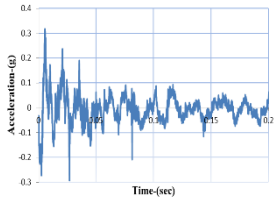
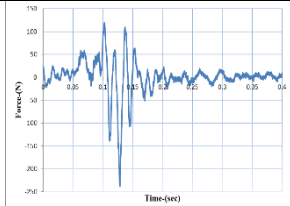
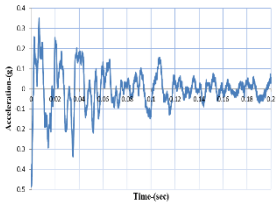
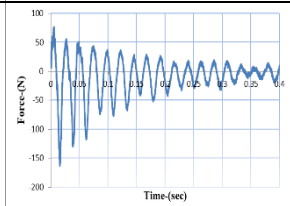
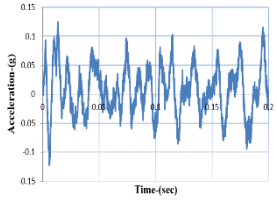
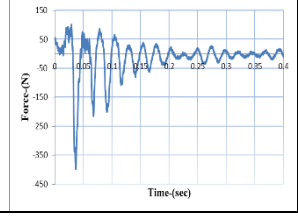
SAMPLE NAME	DROP NUMBER	DISPLACEMET (mm)	CRACK WIDTH (mm)	AVERAGE ACCELERATION(g)-TIME(sec)	FORCE(N)-TIME(sec)	
GB-TCR/15	1	0.020	2.5			
	2	0.0034	4.0			
	4	0.0051	5.0			
	6	0.0052	5.0			

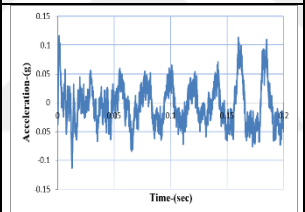
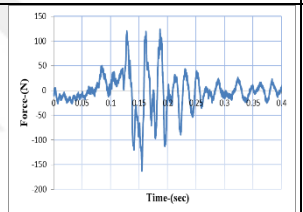
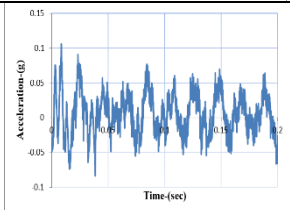
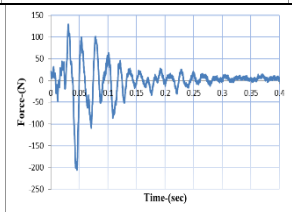
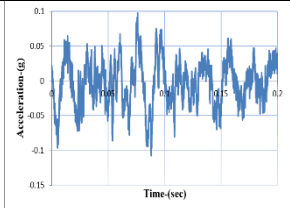
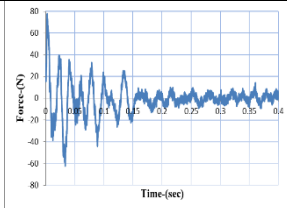
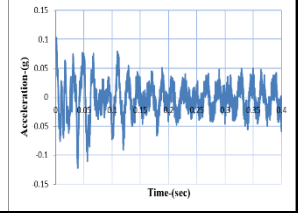
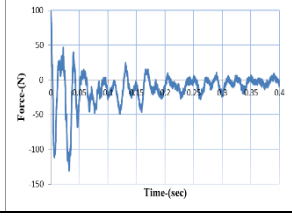
SAMPLE NAME	DROP NUMBER	DISPLACEMET (mm)	CRACK WIDTH (mm)	AVERAGE ACCELERATION(g)-TIME(sec)	FORCE(N)-TIME(sec)	
GB-SF$_1$/1.0-FCR/5.0-CCR/5.0	1	0.266	0.25			
	5	0.213	1.6			
	12	0.244	3.5			
	28	0.0034	28			

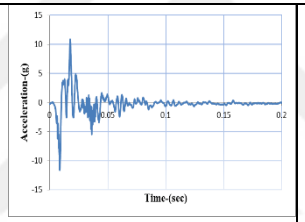
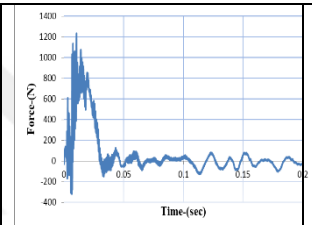
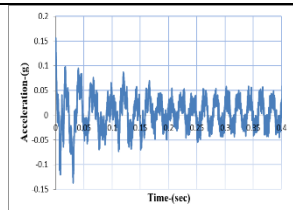
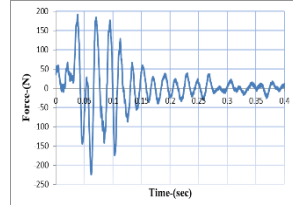
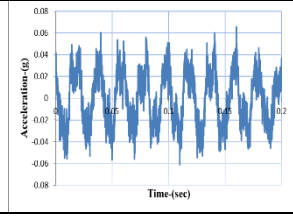
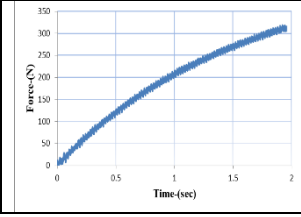
GB-SF$_1$/1.0-FCR/5.0-CCR/5.0	34	0.0667	28			
	41	0.0017	29			
	47	0.017	30			
	55	0.008	36			

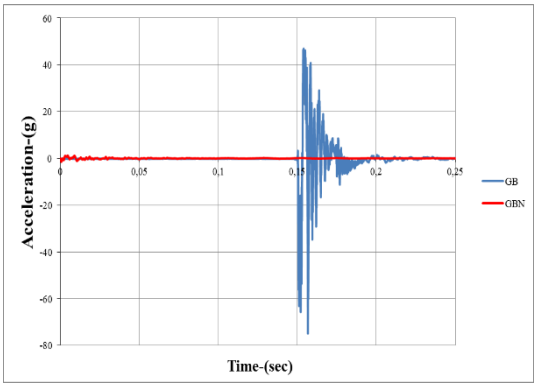
SAMPLE NAME	DROP NUMBER	DISPLACEMET (mm)	CRACK WIDTH (mm)	AVERAGE ACCELERATION(g)-TIME(sec)	FORCE(N)-TIME(sec)	
GB-SF$_1$/1.0-FCR/7.5-CCR/7.5	1	0.106	0.1			
	14	1.624	17			
	17	0.0137	17.5			
	27	0.034	18			

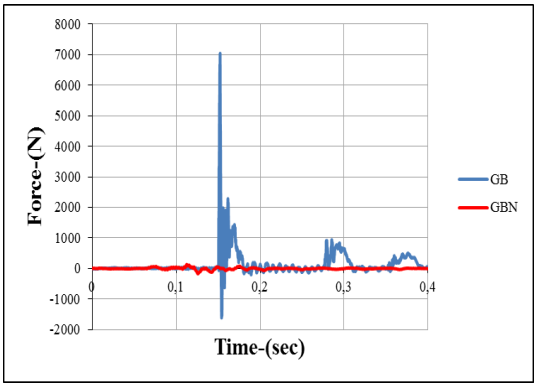
GB-SF$_1$/1.0-FCR/7.5-CCR/7.5	34	0.0017	18			
	40	0.0051	18			
	50	0.0171	30			
	59	0.010	32			

SAMPLE NAME	DROP NUMBER	DISPLACEMET (mm)	CRACK WIDTH (mm)	AVERAGE ACCELERATION(g)-TIME(sec)	FORCE(N)-TIME(sec)	
GB-SF$_1$/1.0-TCR/10	1	0.013	0.65			
	12	0.058	17.5			
	20	0.010	19			
	37	0.035	23			

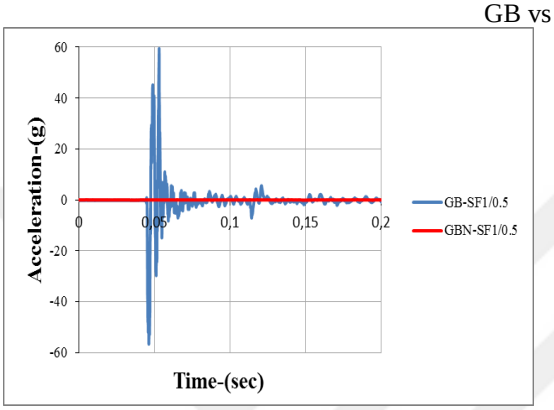
SAMPLE NAME	DROP NUMBER	DISPLACEMET (mm)	CRACK WIDTH (mm)	ACCELERATION(g)-TIME(sec)	FORCE(N)-TIME(sec)	
GB-SF$_1$/1.0-TCR/15	1	0.0171	5			
	11	0.0171	16			
	22	0.010	17			
	27	0.008	17			

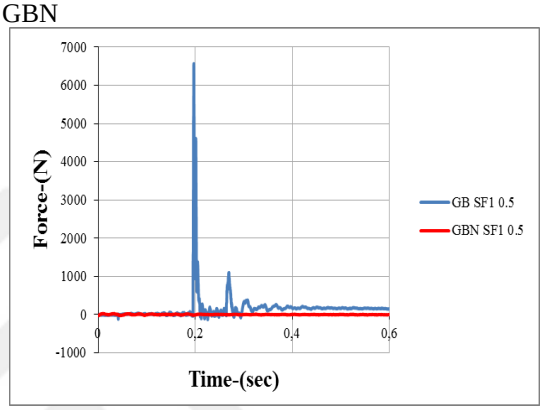
GB-SF$_1$/1.0-TCR/15	35	0.034	17			
	43	0.0188	17			
	52	0.0103	19			



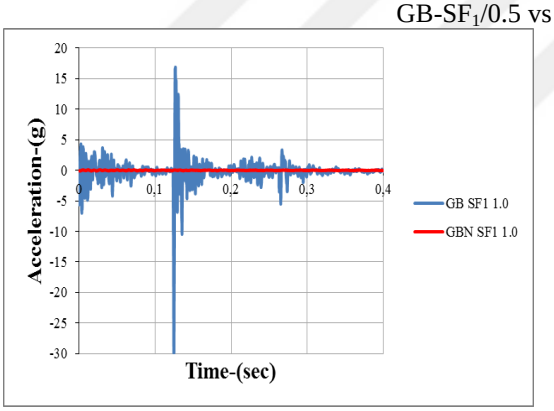


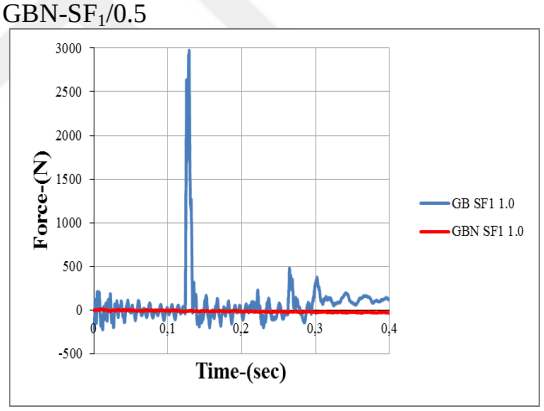
GB vs GBN



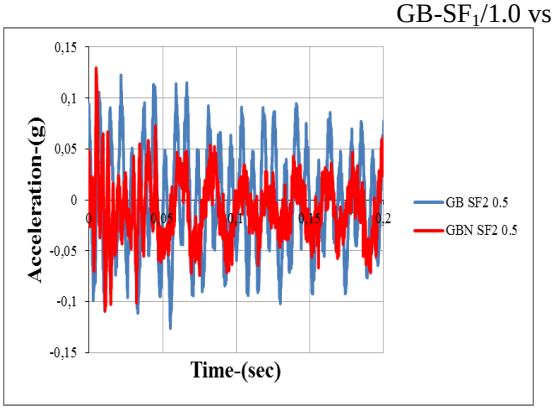


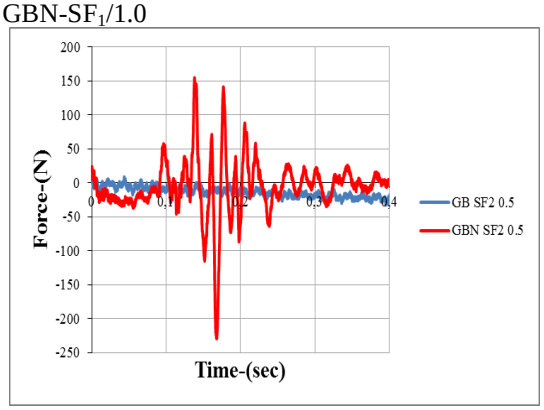
GB-SF_1/0.5 vs GBN-SF_1/0.5



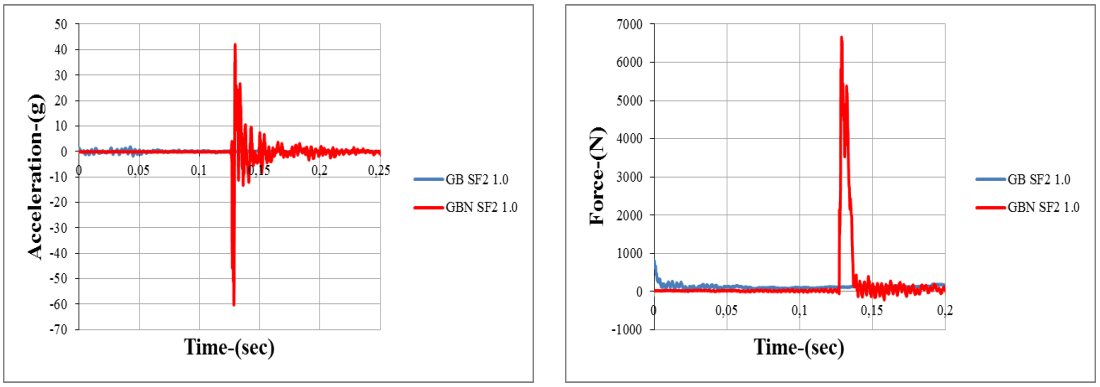


GB-SF_1/1.0 vs GBN-SF_1/1.0



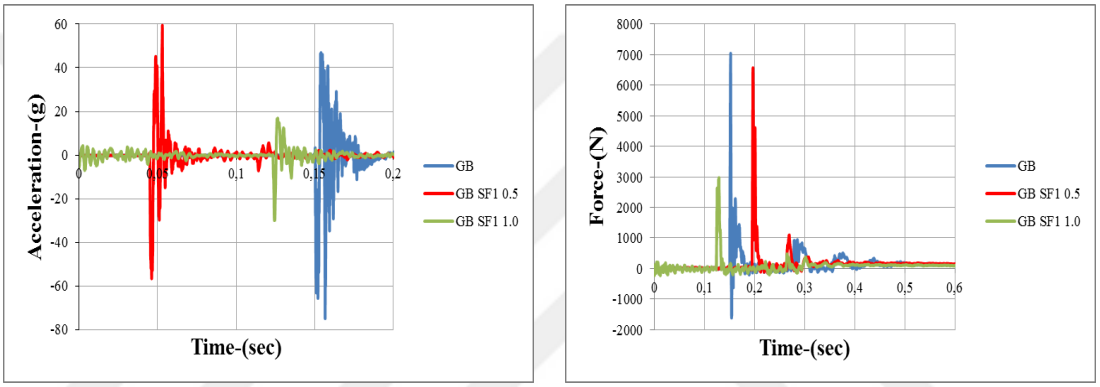


GB-SF_2/0.5 vs GBN-SF_2/0.5

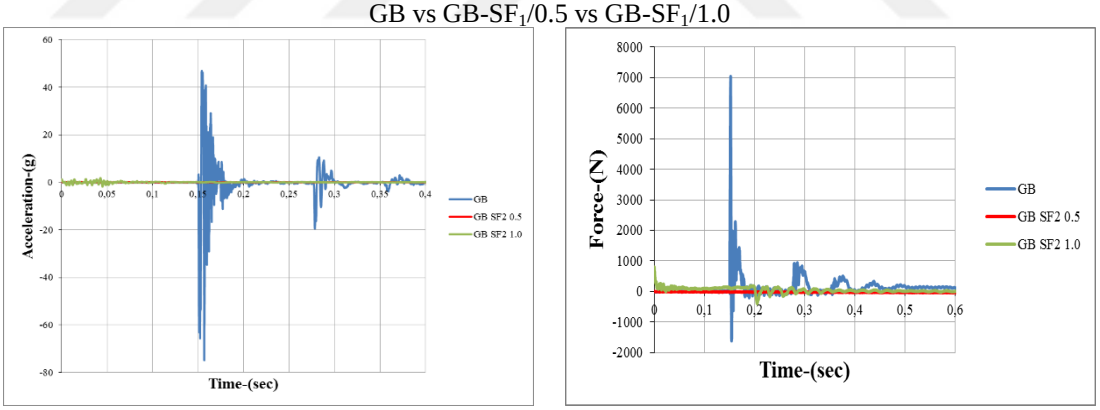


GB-SF_2/1.0 vs GBN-SF_2/1.0

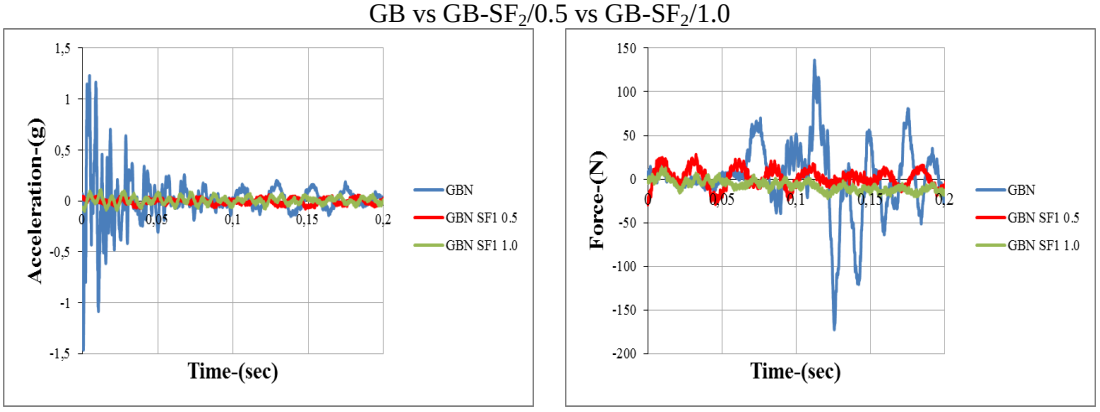
a) Effects of NS



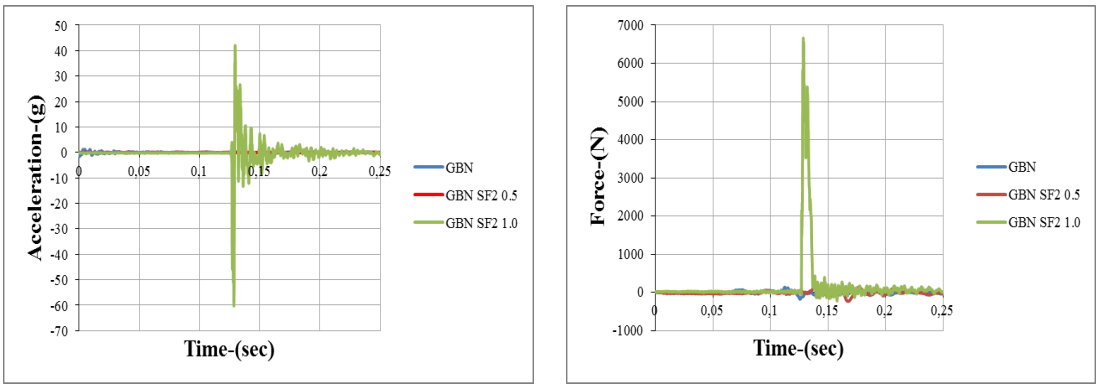
GB vs GB-SF_1/0.5 vs GB-SF_1/1.0



GB vs GB-SF_2/0.5 vs GB-SF_2/1.0

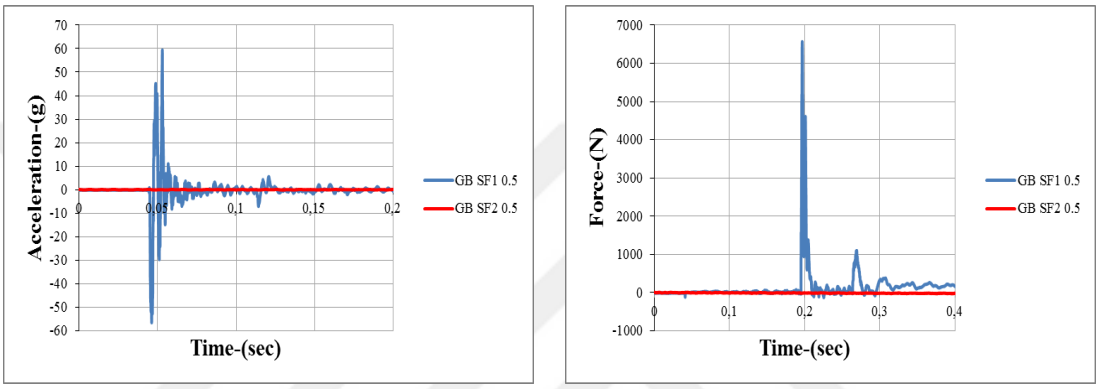


GBN vs GBN-SF_1/0.5 vs GBN-SF_1/1.0

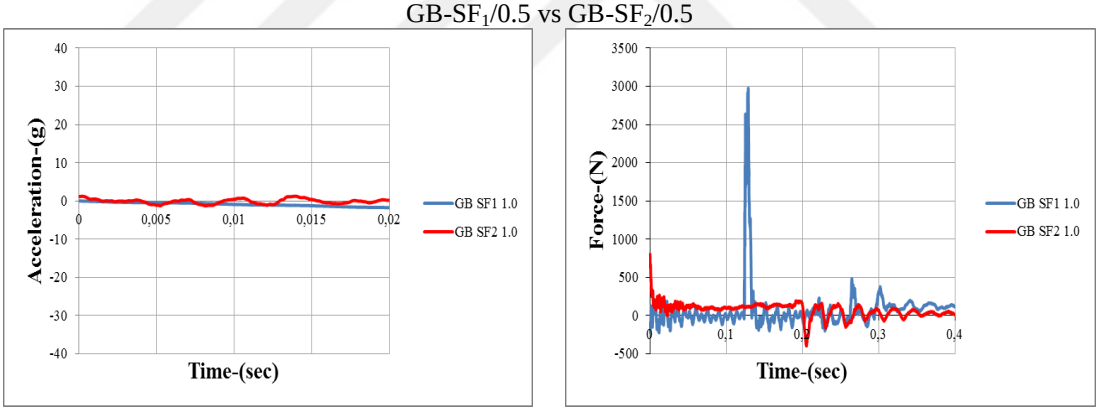


GBN vs GBN-SF_2/0.5 vs GBN-SF_2/1.0

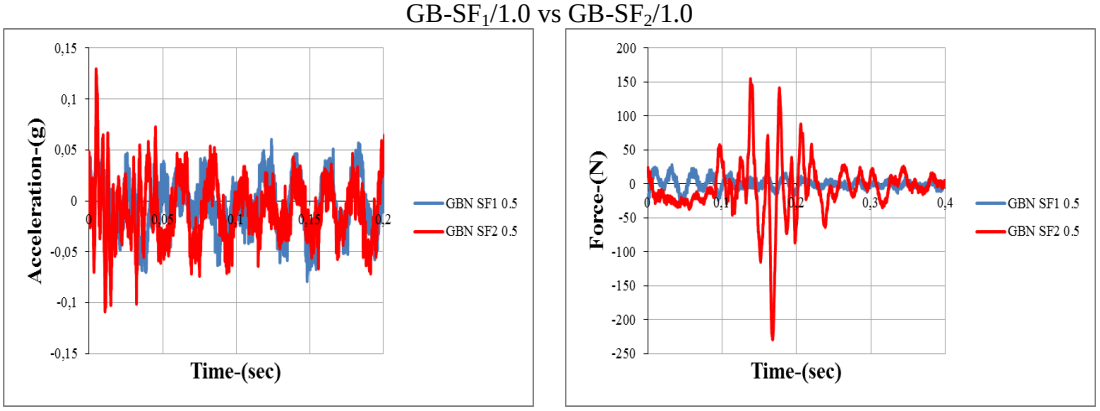
b) Effects of SFs volume fraction



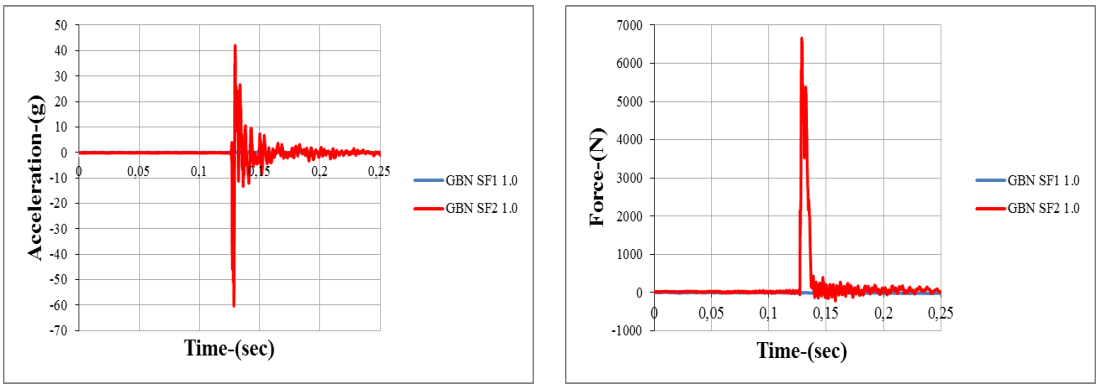
GB-SF_1/0.5 vs GB-SF_2/0.5



GB-SF_1/1.0 vs GB-SF_2/1.0



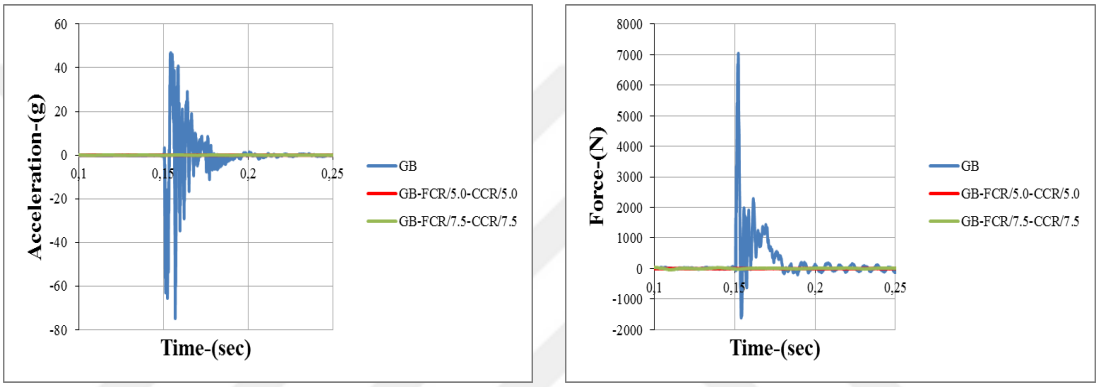
GBN-SF_1/0.5 vs GBN-SF_2/0.5



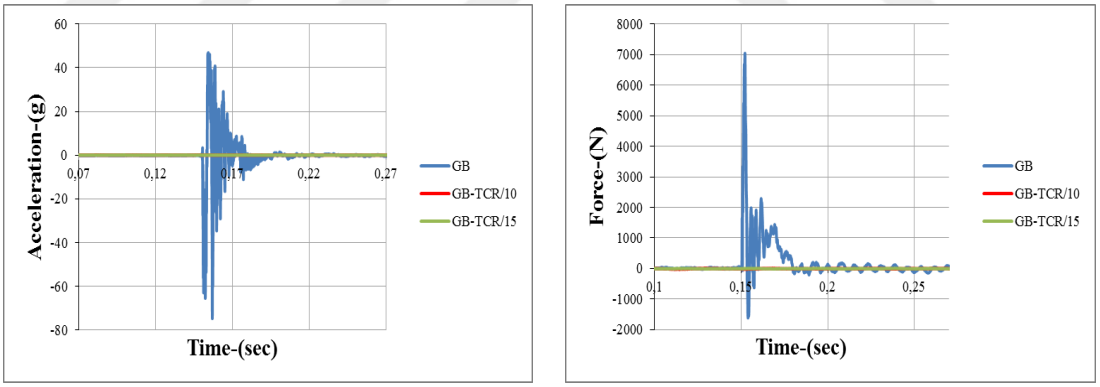
GBN-SF_1/1.0 vs GBN-SF_2/1.0

c) Effects of SFs aspect ratio

Figure 4.29 a) Effects of NS, **b)** Effects of SFs volume fraction and **c)** Effects of SFs aspect ratio

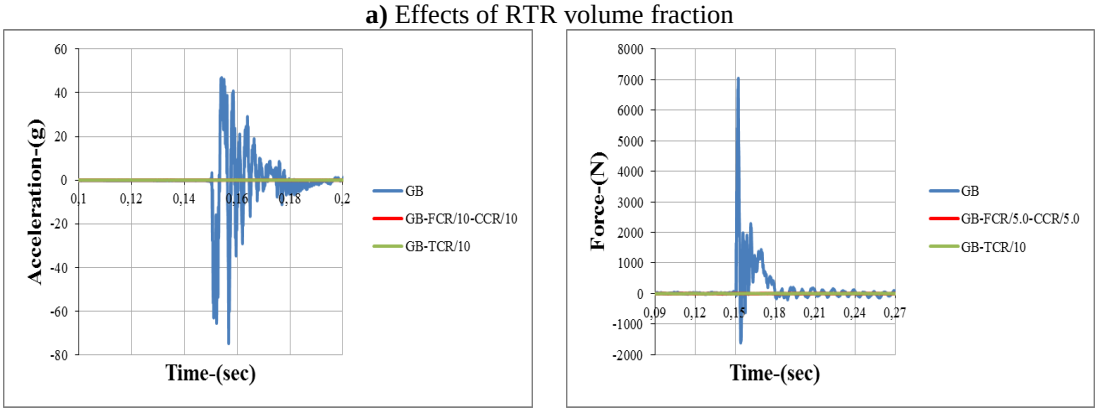


GB vs GB-FCR/5.0-CCR/5.0 vs GB-FCR/7.5-CCR/7.5

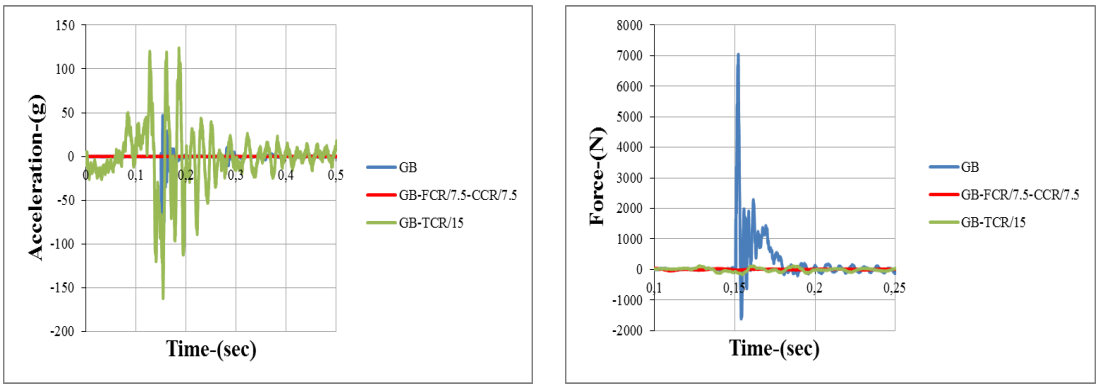


GB vs GB-TCR/10 vs GB-TCR/15

a) Effects of RTR volume fraction

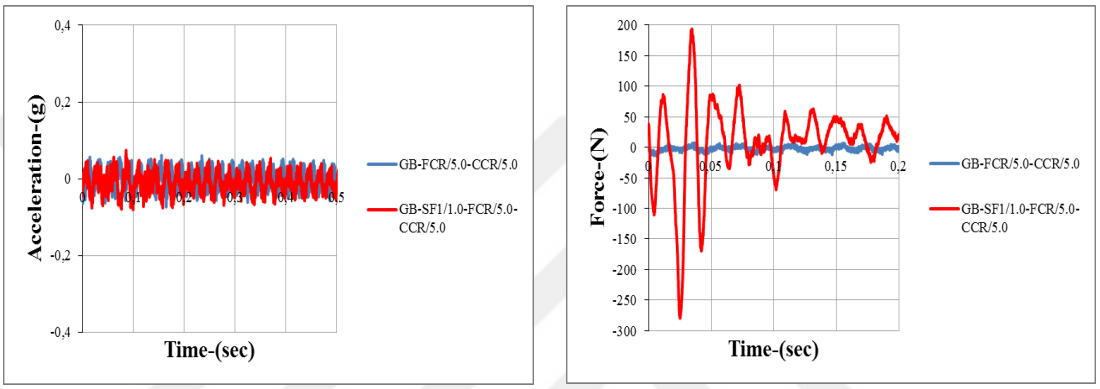


GB vs GB-FCR/5.0-CCR/5.0 vs GB-TCR/10

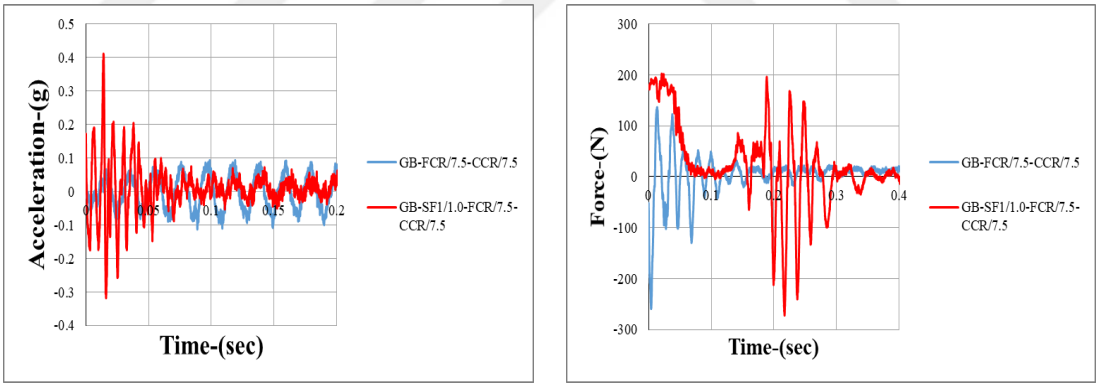


GB vs GB-FCR/7.5-CCR/7.5 vs GB-TCR/15

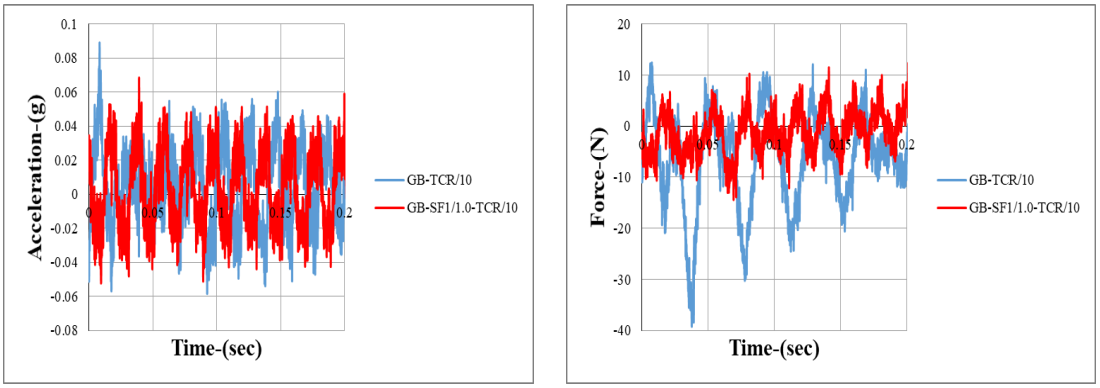
b) Effects of RTR aspect ratio



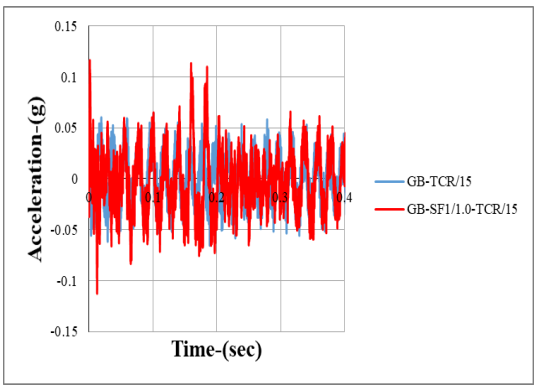
GB-FCR/5.0-CCR/5.0 vs GB-SF1/1.0-FCR/5.0-CCR/5.0

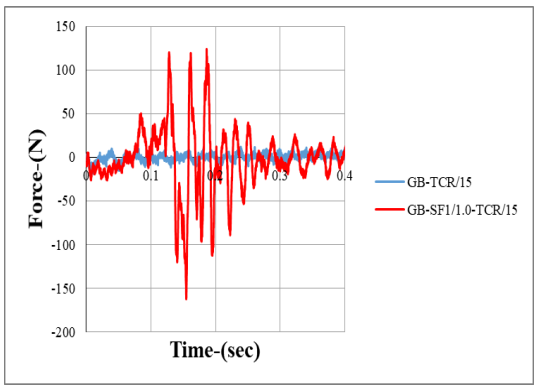


GB-FCR/7.5-CCR/7.5 vs GB-SF1/1.0-FCR/7.5-CCR/7.5



GB-TCR/10 vs GB-SF1/1.0-TCR/10

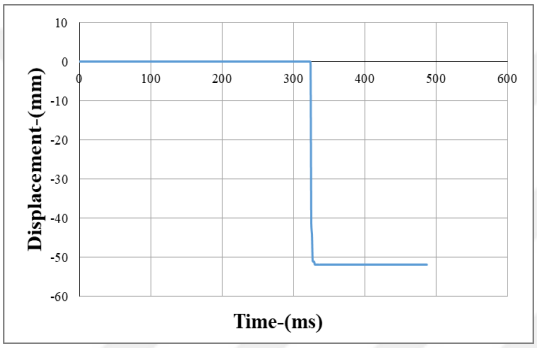




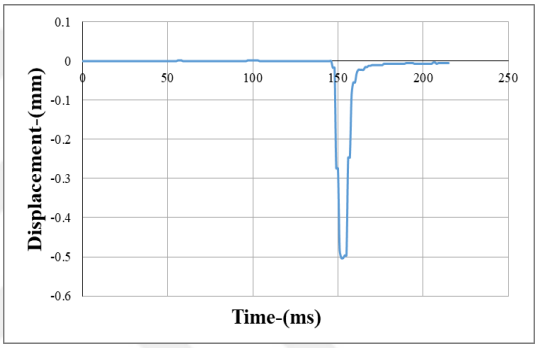
GB-TCR/15 vs GB-SF₁/1.0-TCR/15

c) Effects of SF_1

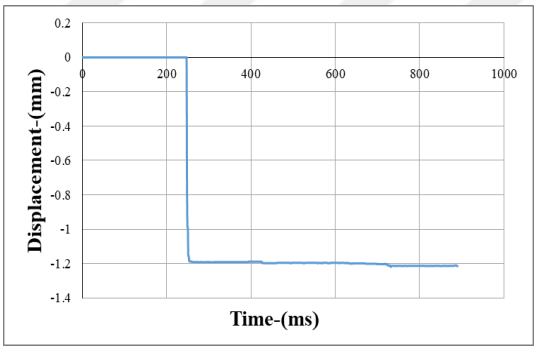
Figure 4.30 a) Effects of RTR volume fraction, **b)** Effects of RTR aspect ratio and **c)** Effects of SF_1



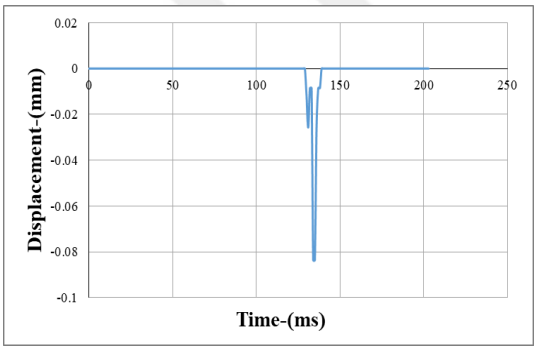
GB



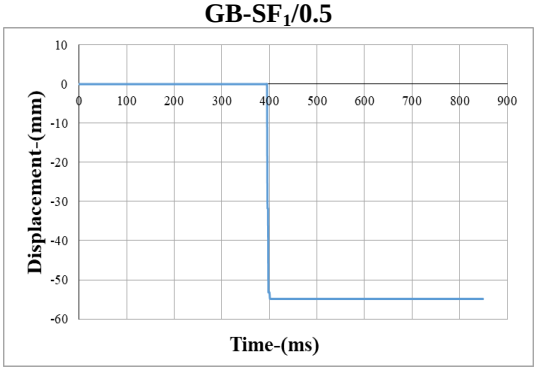
GBN



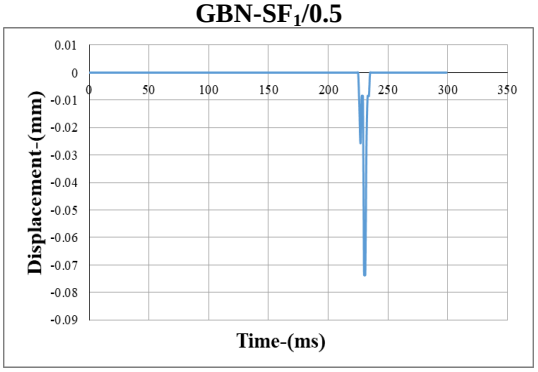
GB-SF_1/0.5



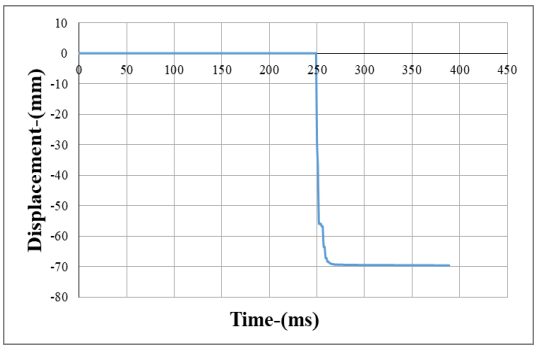
GBN-SF_1/0.5



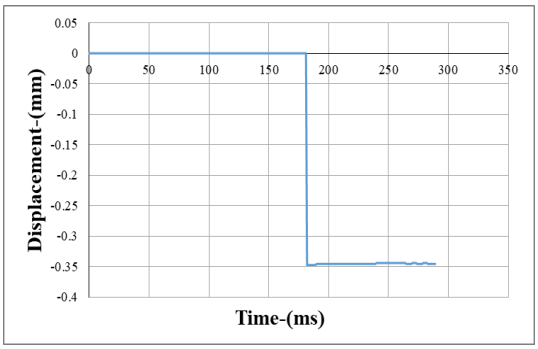
GB-SF_1/1.0



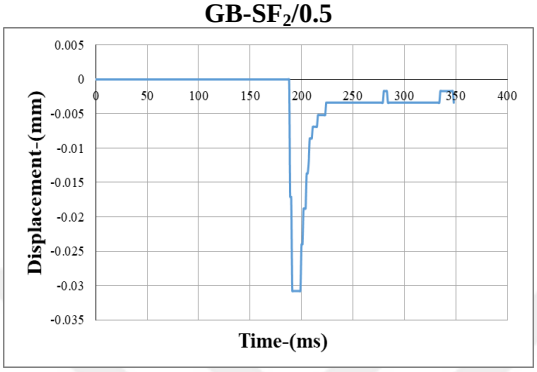
GBN-SF_1/1.0



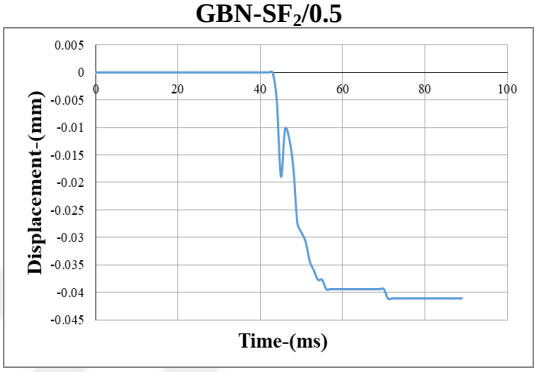
GB-SF$_2$/0.5



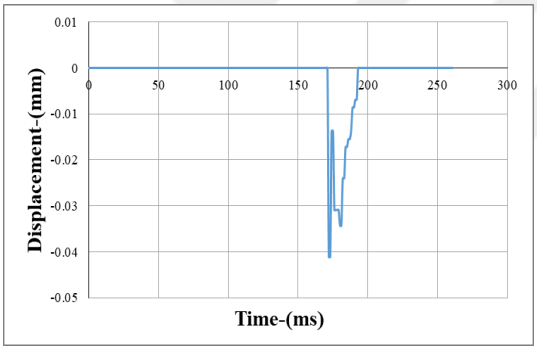
GBN-SF$_2$/0.5



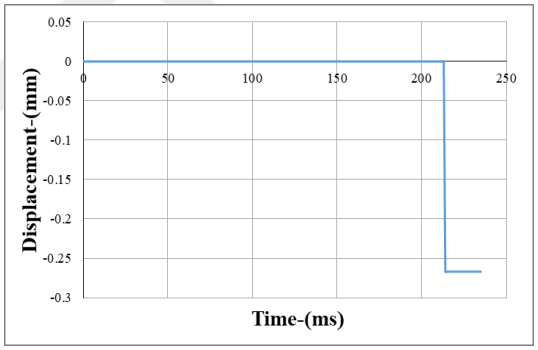
GB-SF$_2$/1.0



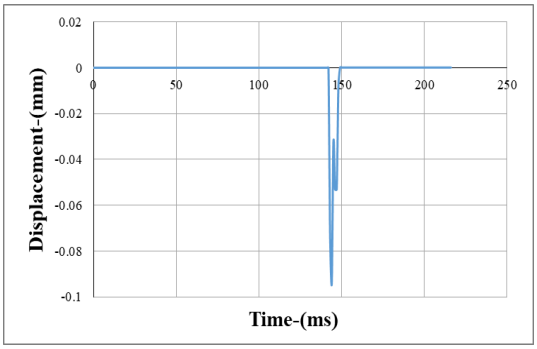
GBN-SF$_2$/1.0



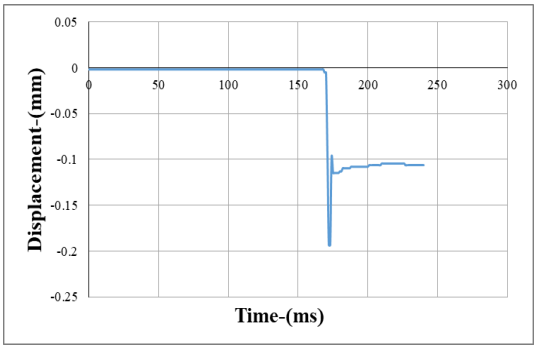
GB-FCR/5.0-CCR/5.0



GB-SF$_1$/1.0-FCR/5.0-CCR/5.0



GB-FCR/7.5-CCR/7.5



GB-SF$_1$/1.0-FCR/7.5-CCR/7.5

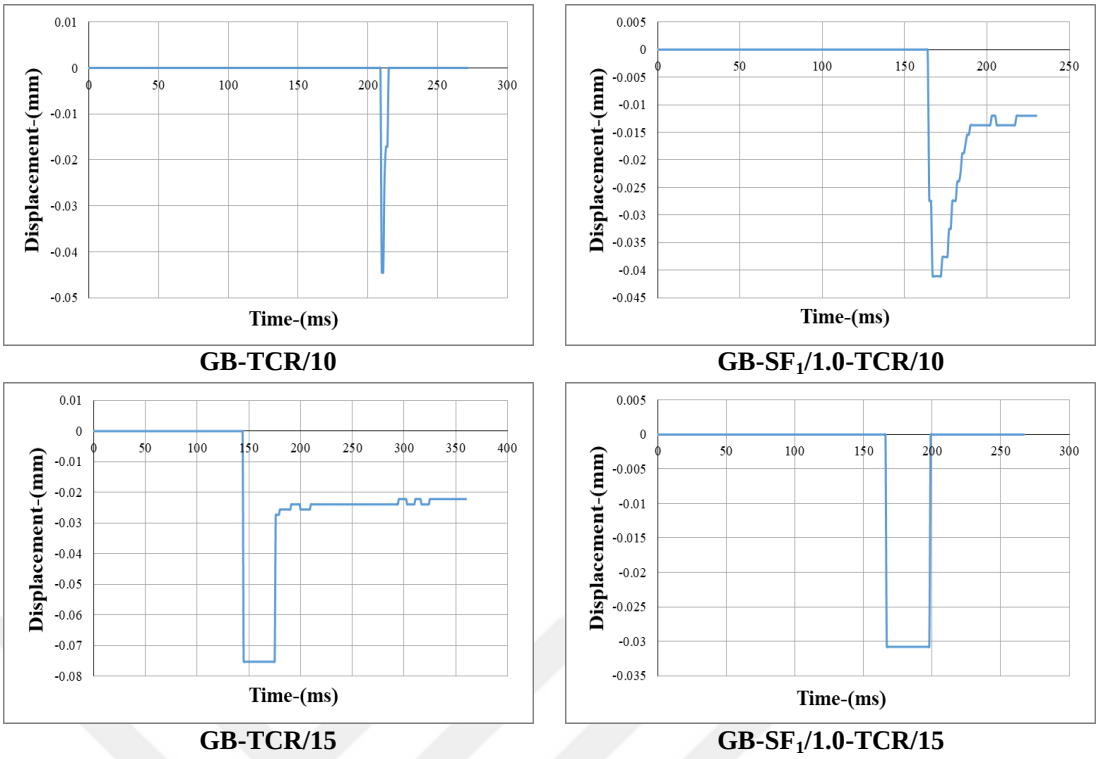


Figure 4.31 Displacement vs time relations of each SCGC beam specimen

4.3 Impact Energy

In this study, eighteen SCGC beams produced different each mixes were used for the drop-weight tests. Moreover, all beams had same sizes by 50x50x10cm and same drop height, and same weigth of impactor was 28.5 kg. The impact energy of all tested beam specimens are shown in the Table 4.4. According to the test results, it can be reached that the utilize of NS, SFs and RTR in the SCGC beam specimens improved the impact resistance (energy absoption capacity) of tested specimens in terms of the number of blows required to cause ultimate failure of the specimen. Among the tested samples, while GBN-SF_2/1.0 has the highest impact resistance, GB has the lowest impact resistance. In other words, whereas GBN-SF_2/1.0 has the most energy absorption capacity, GB has the lowest energy absorption capacity according to the drop numbers as shown in the Table 4.4. Moreover, the volume fractions of SFs in the SCGC beams sicnificantly affected the impact resistance of the beam specimens. According to the test results, it can be said that as SFs volume fraction in the SCGC beams incresed, impact resistance of the SCGC beams improved. While the drop number of ultimate failure of the beams was 10 for GB-SF_1/0.5%, it was 41 for GB-SF_1/1.0%. Furthermore, whereas the drop number of ultimate failure of the beams was 47 for GB-SF_2/0.5%, it was 128 for GB-SF_2/1.0%. So, the aspect ratio and length of SFs affected the impact resistance. It can be deductived that as the

aspect ratio and length of SFs increased, the impact resistance improved. While, the drop number of GB specimen was 2, GBN specimen was 7. Also, whereas the drop number of GB-SF_1/0.5 specimen was 10, GBN-SF_1/0.5 was 25 and while the drop number of GB-SF_1/1.0 specimen was 41, it was 89 for GBN-SF_1/1.0. Meanwhile, the drop number of GB-SF_2/0.5 was 47, it was 62 for GBN-SF_2/0.5 and while the drop number of GB-SF_2/1.0 was 128, it was 289 for GBN-SF_2/1.0. It can be deduced that the precence of NS in the beams sicnificantly improved the impact resistance of SCGC beams. Because, the specimens incorporation of NS improved the microstructure of specimens and enforced the bond strength between SFs and matrix, so the impact resistance of the beam specimens increased. The results clearly showed that the specimens incorporation of NS and SFs improved the impact resistence of SCGC specimens. Therefore, GBN-SF_2/1.0 has the highest impact resistance among the tested specimens. The impact energy ratio over GB of all tested specimens are shown in the Figure 4.32. Moreover, relations between SFs volume fraction & types and drop number & impact energy are shown in the Figure 4.33.

In the study, the impact resistance (energy absorption capacity) of the rubberized SCGC beam specimens were also determined by applied the drop-weight tests. Moreover, the drop-weight tests of the rubberized SCGC specimens are given in the Table 4.4. According to the tests results, it can be shown that the use of RTR generally improves the impact resistance of the tested mixtures in terms of the number of blows required to cause eventual failure of the specimens. As the amount and aspect ratio of the RTR in the specimens increased, the impact resistance increased. While the drop number of GB was 2, it was 3, 4, 5 and 6 for GB-FCR/5.0-CCR/5.0, GB-FCR/7.5-CCR/7.5, GB-TCR/10 and GB-TCR/15, respectively. The results indicated that increasing the amount and aspect ratio of RTR from 0 to 15% increased the drop number up to failure by 2.5 and 3 times. This increase can be attributed to the low stiffness of the rubber particles which this increased flexibility of the rubberized concrete and increased its energy absorption compared to GB. These findings point to a decrease in the brittleness of SCGC specimens with the addition of RTR to the mixes. Furthermore, the results indicated that the rubberized SCGC specimens with SF_1 showed the better impact resistance performance. In addition, the drop numbers of GB-SF_1/1.0-FCR/5.0-CCR/5.0, GB-SF_1/1.0-FCR/7.5-CCR/7.5, GB-SF_1/1.0-TCR/10 and GB-SF_1/1.0-TCR/15 were 55, 59, 37 and 52,

respectively. SF_1 significantly improved the impact resistance of the rubberized SCGC specimens. This increase was due to the positive effect of SFs on stopping cracks caused by impact loading. The difference in the drop number of the rubberized SCGC specimens with/out SF_1 showed higher increases with the inclusion of SF_1, indicating a significant increase in post-cracking strength and ductility performance of SCGC.

Table 4.4 Drop-weight tests results

Sample	Drop Number	Impactor Weight (kg)	Drop Height (cm)	Gravity (g) (m/s^2)	Impact Energy (J)	Ratio On Impact Energy Over GB
GB	2	28.5	10	9.81	55.917	1
GB-SF_1/0.5	10	28.5	10	9.81	279.585	5
GB-SF_1/1.0	41	28.5	10	9.81	1146.2985	20.5
GB-SF_2/0.5	47	28.5	10	9.81	1314.0495	23.5
GB-SF_2/1.0	128	28.5	10	9.81	3578.688	64
GBN	7	28.5	10	9.81	195.7095	3.5
GBN-SF_1/0.5	25	28.5	10	9.81	698.9625	12.5
GBN-SF_1/1.0	89	28.5	10	9.81	2488.3065	44.5
GBN-SF_2/0.5	62	28.5	10	9.81	1733.427	31
GBN-SF_2/1.0	289	28.5	10	9.81	8080.0065	144.5
GB-FCR/5.0-CCR/5.0	3	28.5	10	9.81	83,8755	1.5
GB-FCR/7.5-CCR/7.5	4	28.5	10	9.81	111,834	2
GB-TCR/10	5	28.5	10	9.81	139,7925	2.5
GB-TCR/15	6	28.5	10	9.81	167,751	3
GB-SF_1/1.0-FCR/5.0-CCR/5.0	55	28.5	10	9.81	1537,7175	27.5
GB-SF_1/1.0-FCR/7.5-CCR/7.5	59	28.5	10	9.81	1649,5515	29.5
GB-SF_1/1.0-TCR/10	37	28.5	10	9.81	1034,4645	18.5
GB-SF_1/1.0-TCR/15	52	28.5	10	9.81	1453,842	26

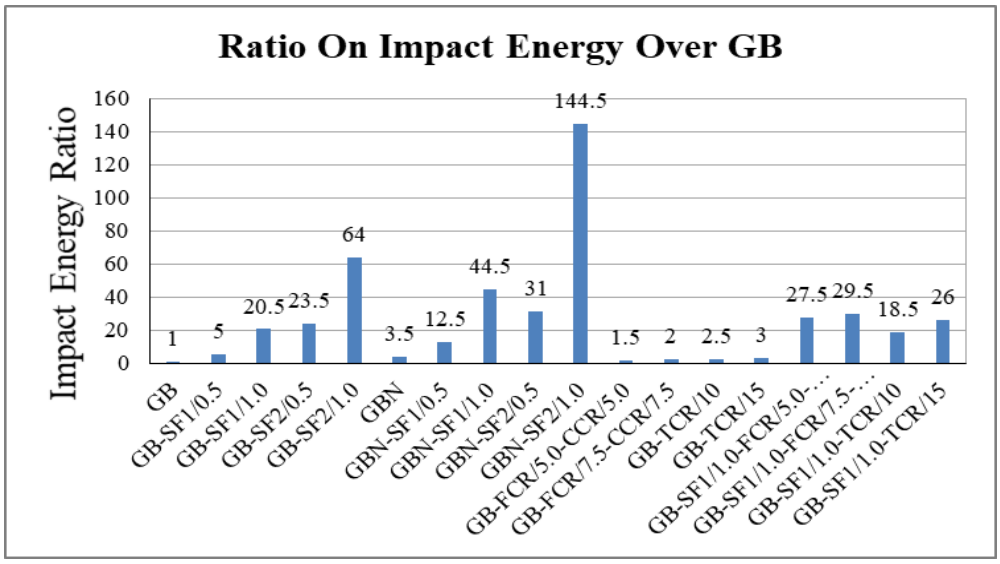


Figure 4.32 Ratio on impact energy over GB

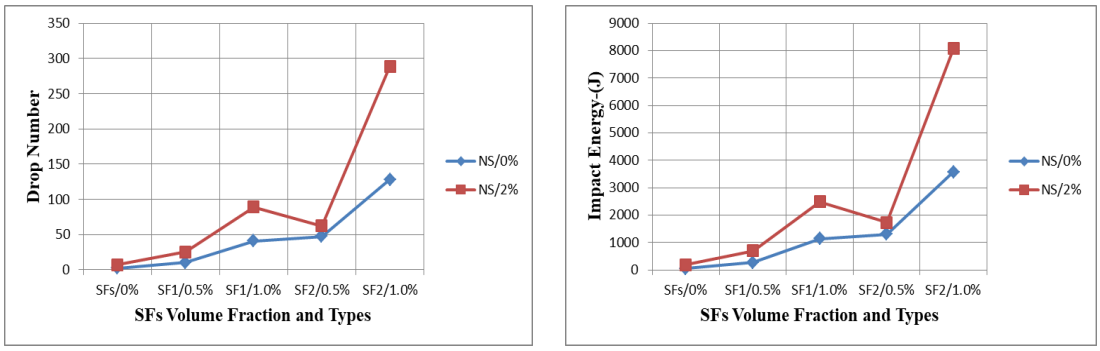


Figure 4.33 Relations between SFs volume fraction & types and drop number & impact energy

4.4 Conclusions

In the aim of the study, the fresh and hardened states performances of the slag based self-compacting geopolymer concrete (SCGC) specimens with/out nanosilica (NS) were investigated. Moreover, the effects of SFs with two different volumes fractions (0.5% and 1.0%) and aspect ratios (40 and 80) on both fresh and mechanical properties were determined. In addition, the effect of specimen thickness/SF length ratio (d/F_L) on the flexural tensile strength performance and failure modes of SCGC specimens were investigated. Meantime, fine and coarse crumb rubbers (FCR and CCR) were replaced with the fine aggregates of the SCGC mixes, and tyre crumb rubber chips (TCR) were replaced with the coarse aggregates with 10% and 15% recycled tyre rubber (RTR) replacement rates in the SCGC mixes. The SF_1 with 1.0% fiber volume ratio has also been used to investigate the possible use of rubberized SCGC for structural applications. As a result, the effects of SFs, NS and RTR on the hardened, fresh states properties and impact resistance of the slag based SCGC were studied. The following conclusions can be drawn according to the outcomes studied herein;

- The passing ability and flowability of the mixtures decreased as with the increase in SFs content, RTR content, SFs aspect ratio, and RTR particle size. The worst fresh state property was in the SCGC mix including only SF_2/1% (GB-SF_2/1.0%). Among RTR, TCR (large rubber particles) had more negative effect on fresh-state performance of the mixes than FCR and CCR(small rubber particles). The specimen containing SF_1/1.0% and TCR/15% (GB-TCR/15%) showed the worst fresh case performance. The flowability and passing ability tests showed that all mixtures with SF_1 and crumb rubbers (CCR, FCR and TCR) have adequate

flowability and passing ability requirements according to relevant guidelines/standards.The use of NS increased the flowability and passing ability performances of the mixes, and the together use of NS and SFs had negative effects on the fresh property of SCGC (L-Box passing ability, slump flow diameter, V-funnel flow time, and T50 flow time) compared to the only use of SFs. As the aspect ratio and volume fraction of SFs increased, the fresh properties of SCGC mixes adversely affected. Furthermore, the mixes incorparation of NS had better the fresh state properties of SCGC. The mixes including high amount and high aspect ratio of SFs (SF_2/1.0%) had lower flowability and passing-ability properties. However, the fresh properties were considerably affected by the incorporation of NS even for the mixes including SFs. Hence, all SCGC mixes fulfilled the specification requests of the SCGC mixes according to the EFNARC classification and TS-12350 standards. Moreover, it is recommended to utilize the NS to enhance the flowability and passing ability of slag based SCGC including SFs.

- The SCGC mixes including of NS had better fresh state properties than the mixes without NS. The quality and performance of the SCGC mixes regarding the resistance to segregation and bleeding were improved via NS incorporation and the mixes containing NS had better flow ability and passing ability.

- The outcomes deducted that all SCGC mixes were in the viscosity classification (VS2/VF2) through the relationship between V-funnel and slump flow. According to EFNARC specification, SCGC mixes exhibits good resistance to segregation and bleeding. Meanwhile, SCGC could be used for all reinforced structural applications.

- It was found that the addition of NS had no substantial influence on the modulus of elasticity and the compressive strength of SCGC specimens. However, the addition of SFs improved the modulus of elasticity and the compressive strength of SCGC specimens. The reduction of the modulus of elasticity and the compressive strength values due to the presence of NS can be compensated with the presence of SFs.

- The incorporation of SFs were improved the splitting tensile strength, compressive strength, flexural tensile strength, and modulus of elasticity of SCGC specimens due to the crack propagation characteristic of SFs. On the other hand, only use of NS doesn't have a substantial influence on mechanical performance, however, the mechanical properties of SCGC specimens significantly improved via combined use of SFs and NS incorporation. The highest mechanical properties achieved when the SCGC specimens includes both SFs and NS (GBN-SF2/1.0%). Improved performance may be due to improved ITZ and higher bond strength between NS particles and SFs, especially for higher SFs aspect ratios.

- The mechanical properties of SCGC specimens were positively affected by the aspect ratio and volume faction of SFs. The SCGC specimens including higher amount and longer SFs had less mechanical properties than the specimens containing less amount and shorter SFs. Finally, it can be deducted that the combined utilization of SFs and NS realized an excellent bending property; the maximum tensile strength was found for the GBN-SF_2/1.0 specimen.

- The effects of SFs and NS are also shown by correlation analysis results. It was indicated that the almost properties of SCGC were significantly affected by the utilization of both SFs and NS. The superior effect was found to be the addition of SFs/1% and NS. However, tensile strength (flexural and splitting) of SCGC specimen was considerably enhanced by the presence of SFs and NS much more than the modulus of elasticity and compressive strength of SCGC specimens.

- The specimens incorporation of NS and SFs had negative effect on the modulus of elasticity and the compressive strength of SCGC specimens compared to the mixes only including SFs; whereas the combination of NS and SFs have significant effects on tensile strength of SCGC specimens, because NS can be attributed to the bond strength improvement of SCGC specimens.

- The higher mechanical strengths were obtained in the rubberized specimens with SF_1/1.0%. For the non-fibrous specimens, RTR addition reduced overall mechanical strengths and modulus of elasticity and the degree of reduction was found more for higher RTR replacements. For the SF_1/1% rubberized specimens, all

mechanical strengths and modulus of elasticity were improved with the increase in the RTR ratio, with the exception of the compressive strength attributable to the ineffectiveness of the steel fibers due to their fiber orientations in the vertical loading direction.

- Under the flexural tensile strength test, the specimen thickness/SF length ratio (d/F_L) was found to be an important parameter in failure modes of SFs reinforced specimens. The specimens with a ratio of 3.33 d/F_L indicated the flexural cracks in the middle of samples, while the specimens with d/F_L ratio of 1.25 showed the flexural-shear cracks in the bending zone around supports, especially for SFs/1.0% volume. The SFs efficiency increased with decreasing d/F_L ratio, as crack prevention feature is improved with low d/F_L ratios. The NS also influenced failure modes by improving bond strength so that stress transfer is possible and the cracks can extend further into the shear zone without bending, depending on the d/F_L ratio and SFs content. The failure modes also showed that more and wider microcracks were observed in samples containing SFs/1.0% and higher RTR content explaining the highest post peak performance in GB-SF_1/1.0-TCR/15 specimen.

- The SEM photos prove the experimental obtained results; the SEM microstructure of specimens with NS showed less porosity and denser microstructure and increase the bond strength between the SFs and the matrix. In addition, more reaction products between SF and matrix at ITZ were observed in the microstructure, which may be attributed to improved bond strength between SFs and matrix, resulting in enhanced tensile and flexural performance. However, more micro cracks were observed in the microstructure of the specimens with NS, and this may be an explanation for the decrease in the compressive strength of specimens including NS. Also, the SEM results proved that a more dense and homogeneous microstructure was obtained in the rubberized specimens.

- The strong relationships were found between the fresh and hardened state tests, this may be due to increased fiber orientations along the casting direction resulting in improved mechanical performance. The rubberized SCGC specimens with SF_1 reinforced can be used for structural applications, especially for high ductility requirements in high seismic areas.

- It can be deduced that the prence of NS and SFs in the SCGC beam specimens increased the impact resistance (energy absoption capacity) of tested specimens in terms of the number of blows required to cause ultimate failure of the specimen.

- Among the tested samples, while the beam specimen had the highest impact resistance was GBN-SF2/1.0, the lowest impact resistance beam specimen was GB. In other words, according to the drop numbers of the tested beam specimens, as GBN-SF2/1.0 possesses the most energy absorption capacity and GB possesses the lowest energy absorption capacity

- The volume fractions of SFs in the SCGC beams considerably infulenced the impact resistance of the beam specimens. Moreover, as amount of SFs in the SCGC beams incresed, impact resistance of the SCGC beams enhanced.

- The precence of NS in the beams sicnificantly increased the impact resistance of SCGC beams. Because, the specimens including of NS enhanced the microstructure of specimens and powered the bond strength among SFs and matrix, so the impact resistance of the beam specimens improved.

- The results clearly showed that the specimens incorporation of NS and SFs improved the impact resistence of SCGC. Therefore, GBN-SF2/1.0 has the highest impact resistance among the tested specimens. The impact energy or energy apsorption capacity of all tested specimens are shown in the table-4.4.

- According to the drop-weight test results, it can be deduced that although the precense of RTR in the SCGC beam specimens negatively infulenced the compressive strength, the splitting tensile strength, the flexural tensile strength and the modulus of elasticity, the impact resistance (energy absoption capacity) of the specimens were improved.

- The test results clearly showed that as the amount and aspect ratio of the RTR in the rubberized specimens increased, the impact resistance of the specimens improved. Because, the rubber particles which this increased flexibility of the

rubberized concrete have the low stiffness. In addition, this indicated that the brittleness of rubberized SCGC specimens was reduced. Moreover, the drop number of GB-FCR/5.0-CCR/5.0, GB-FCR/7.5-CCR/7.5, GB-TCR/10 and GB-TCR/15 were 3, 4, 5 and 6, respectively. Furthermore, the increasing the amount and aspect ratio of RTR from 0 to 15% increased the drop number up to failure by 2.5 and 3 times.

- The results showed that the precense of SF1 in the rubberized SCGC specimens seriously enhanced the impact resistance of the specimens and the better impact resistance performance. In addition, the drop numbers of GB-SF1/1.0-FCR/5.0-CCR/5.0, GB-SF1/1.0-FCR/7.5-CCR/7.5, GB-SF1/1.0-TCR/10 and GB-SF1/1.0-TCR/15 were 55, 59, 37 and 52, respectively. This improvement was due to the positive effect of SF1 on stopping cracks caused by impact loading.

- The rubberized SCGC specimens with SF1 showed quite better performance than the rubberized speciemens without SF1. Because, the addition SF1 to the rubberized specimens indicated a significant increase in post-cracking strength and ductility performance of SCGC.
-

REFERENCES

[1] Javeed, M. A., Kumar, M. V., Narendra, H. (2015). *Studies on Mix Design of Sustainable Geo-Polymer Concrete*, International Journal of Innovative Research in Engineering & Management *(IJIREM)*, **2(4)** ISSN: 2350-0557.

[2] Hasanbeigi, Menke and Price (2010). *The CO_2 Abatement Cost Curve For The Thailand Cement Industry*, Journal of Cleaner Production **18(15)**, 1509-1518.

[3] Das, S. K., Mishra, J., Mustakim, S. M. (2018). An Overview of Current Research Trends In Geopolymer Concrete, *International Research Journal of Engineering and Technology (IRJET)*, **5(11)**, e-ISSN: 2395-0056, p-ISSN: 2395-0072.

[4] Karthik, A., Sudalaimani, K., Vijaya Kumar, C. T. (2017). Investigation on Mechanical Properties of Fly Ash-Ground Granulated Blast Furnace Slag Based Self Curing Bio-Geopolymer Concrete, *Construction and Building Materials*, **149**, 338-349.

[5] Narayanan, A., Shanmugasundaram, P. (2017). An Experimental Investigation On Flyash-based Geopolymer Mortar under Different Curing Regime For Thermal Analysis, *Energy and Buildings*, **138**, 539-545.

[6] Nuruddin, M. F., Qazi, S., Shafiq, N., Kusbiantoro, A. (2010). Compressive Strength and Microstructure of Polymeric Concrete Incorporating Fly Ash and Silica Fume, *Canadian Journal on Civil Engineering*, **1**, No. 1.

[7] Nuruddin, M. F., Demie, S., Shafiq, N. (2011). Effect of Mix Composition on Workability and Compressive Strength of Self-Compacting Geopolymer Concrete, *Can. J. Civ. Eng*., **38**, 1196–1203.

[8] Niş, A. (2019). The Compressive Strength Development of Alkali Activated Fly Ash/Slag Concretes with Different Alkali Activator Ratios, *IJET*, **5**, No.2.

[9] Hardjito, D., Wallah, S. E., Sumajouw, D. M. J., and Rangan, B. V. (2004). Factors Influencing The Compressive Strength of FlyAsh-Based Geopolymer Concrete, *Civil Engineering Dimension*, **6**, No. 2, 88–93.

[10] Davidovits, J. (1994). Properties of Geopolymer Cements, *Alkaline Cements and Concretes*, KIEV Ukraine.

[11] Wallah, S. E., Rangan, B. V. (2006). Low-Calcıum FlyAsh-Based Geopolymer Concrete: Long-Term Properties, *Research Report GC-2 Faculty of Engineering Curtin University of Technology Perth*, Australia.

[12] Ahmed, M. F., Nuruddin, M. F., Shafiq, N. (2011). Compressive Strength and Workability Characteristics of Low-Calcium Fly ash-based Self-Compacting Geopolymer Concrete, *World Academy of Science, Engineering and Technology International Journal of Civil and Environmental Engineering*, **5**, No:2.

[13] Najim, K. B. , Hall, M. R. (2010). A review of the fresh/hardened properties and applications for plain- (PRC) and self-compacting rubberised concrete (SCRC), *Construction and Building Materials*, **24**, 2043–2051.

[14] EFNARC, *The European Guidelines for Self-Compacting Concrete: Specification, Production and Use, Eur. Guidel. Self Compact. Concr*. (2005) 68.

[15] Demie, S., Nuruddin, M. F., Shafiq, N. (2013). Effects of micro-structure characteristics of interfacial transition zone on the compressive

strength of self-compacting geopolymer concrete, *Construction and Building Materials*, **41**, 91-98.

[16] Ibrahim, K. I. M., Al-Tersawy, S. H. (2017). The Hybrid Effect of Micro and Nano Silica on the Properties of Normal and High Strength Concrete, *IOSR Journal of Mechanical and Civil Engineering (IOSR-JMCE)*, **14**, Issue 4, 62-72.

[17] Tao, J. (2005). Preliminary Study on the Water Permeability and Microstructure of Concrete Incorporating Nano-SiO_2, *Cement and Concrete Research*, **35**, Issue 10, 1943-1947.

[18] Yu, R., Spiesz, P., Brouwers, H. J. H. (2014). Effect of nano-silica on the hydration and microstructure development of Ultra-High Performance Concrete (UHPC) with a low binder amount, *Construction and Building Materials*, **65**, 140–150.

[19] Tavakoli, H. R., Omran, O. L., Shiade, M. F., Kutanaei, S. S. (2014). Prediction of combined effects of fibers and nanosilica on the mechanical properties of self-compacting concrete using artificial neural network, *Latin American Journal of Solids and Structures*, **11(11)**, 1906-1923.

[20] Song, P. S., Hwang, S. (2004). Mechanical Properties of High-Strength Steel Fiber-Reinforced Concrete, *Construction and Building Materials*, **18**, 669–673.

[21] Topçu, I. B., Bilir, T. (2009). Experimental investigation of some fresh and hardened properties of rubberized self-compacting concrete, *Materials and Design*, **30**, 3056–3065.

[22] Yorgancı, M. A. (2016). *Çimento Bağlayıcılı Kompozit Beton Kirişlerin Çarpışma Davranışının Deneysel Olarak İncelenmesi*, Ph.D. Thesis, Gazi Üniversitesi (Turkey)**.**

[23] Yaşayanlar, S. (2015). *Impact Resistance of Steel Fiber Reinforced Concrete Slabs,* MSc Thesis, Graduate School of Engineering and Sciences of İzmir Institute of Technology (Turkey).

[24] Kantar, E., Arslan, A., Anil, Ö. (2011). Beton Dayanimindaki Değişimin Çarpma Davranişina Etkisi, *J. Fac. Eng. Arch. Gazi Univ.*, **26**, No 1, 115-123.

[25] Kantar E. (2009). *CFRP İle Güçlendirilmiş Beton Kirişlerin Çarpma Davranışının Deneysel Olarak İncelenmesi*, Ph.D. Tezi, Gazi Üniversitesi.

[26] Şahmaran, M. *Yeni Nesil Erken Yaş Yüksek Dayanımlı Çimento Bağlayıcılı Onarım Malzemesi*. https://docplayer.biz.tr/11706596-Yeni-nesil-erken-yas-yuksek-dayanimli-cimento-baglayicili-onarim-malzemesi.html

[27] Hasanbeig, A., Menke, C., Price, L. (2010). The CO_2 abatement cost curve for the Thailand cement industry, *Journal of Cleaner Production*, **18**, Issue 15, 1509-1518.

[28] Das, S. K., Mishra, J., Mustakim, S. M. (2018). An Overview of Current Research Trends in Geopolymer Concrete, *International Research Journal of Engineering and Technology (IRJET)*, **5**, Issue: 11, e-ISSN: 2395-0056, p-ISSN: 2395-0072.

[29] Karthik, A., Sudalaimani, K., Vijaya, K. C. T. (2017). Investigation on mechanical properties of fly ash-ground granulated blast furnace slag based self curing bio-geopolymer concrete, *Construction and Building Materials*, **149**, 338-349.

[30] Anuja, N., Shanmugasundaram, P. (2017). An Experimental Investigation on Flyash-based Geopolymer Mortar under different curing regime for Thermal Analysis, *Energy and Buildings*, **138**, 539-545.

[31] Nuruddin, M. F, Qazi, S., Shafiq, N., Kusbiantoro, A. (2010). Compressive strength and microstructure of polymeric concrete incorporating fly ash and silica fume, *Canadian Journal on Civil Engineering*, **1**, No. 1.

[32] Nuruddin, M. F., Demie, S., Shafiq, N. (2011). Effect of mix composition on workability andcompressive strength of self-compacting geopolymer concrete, *Canadian Journal of Civil Engineering,* **38**, No.11, 1196-1203.

[33] Davidovits, J. (2015). *Geopolymer Chemistry and Applications.* Institut Géopolymère: France, ISBN: 9782951482098.

[34] Pavithra, P., Reddy, M. S., Dinakar, P., Rao, B. H., Satpathy, B. K., Mohanty, A. N. (2016). A mix design procedure for geopolymer concrete with fly ash, *Journal of Cleaner Production*, **133**, 117-125.

[35] Hardjito, D., Rangan, B. V. (2005). *Development and properties of low-calcium fly ash-based geopolymer concrete*, Research Report GC 1 Faculty of Engineering Curtin University of Technology Perth: Australia.

[36] Kong, D. L. Y., Sanjayan, J. G. (2008). Damage Behavior of Geopolymer Composites Exposed to Elevated Temperatures, *Cement & Concrete Composites,* **30**, 986–991.

[37] Hardjito, D., Wallah, S. E., Sumajouw, D. M. J., Rangan, B. V. (2004). On The Development of Fly Ash-Based Geopolymer Concrete, *Materials Journal,* **101**, 467–472.

[38] https://docplayer.biz.tr/6402802-Dokuz-eylul-universitesi-insaat-muhendisligi-bolumu-alternatif-yapi-malzemeleri.html

[39] Hardjito D. (2005). *Studies on Fly Ash-Based Geopolymer Concrete*. Ph.D Thesis, Faculty of Engineering and Computing Department of Civil Engineering, Curtin University of Technology, Perth, Australia.

[40] Pavithra, P., Reddy, M. S., Dinakar, P., Rao, B. H., Satpathy, B. K., Mohanty, A. N. (2016). A mix design procedure for geopolymer concrete with fly ash, *Journal of Cleaner Production*, **133**, 117-125.

[41] Xie, J., Wang, J., Rao, R., Wang, C., Fang, C. (2019). Effects of Combined Usage of GGBS and Fly Ash on Workability and Mechanical Properties of Alkali Activated Geopolymer Concrete with Recycled Aggregate, *Compos. Part B Eng.*, **164**, 179–190.

[42] Noushini, A., Aslani, F., Castel, A., Gilbert, R. I., Uy, B., Foster, S. (2016). Compressive Stress-Strain Model For Low-Calcium Fly-Ash Based Geopolymer And Heat-Cured Portland Cement Concrete, *Cem. Concr. Compos.*, **73**, 136–146.

[43] Kurtoğlu, A. E., Alzeebaree, R., Aljumaili, O., Niş, A., Gülşan, M. E., Humur, G., Çevik, A. (2018). Mechanical and Durability Properties of Fly Ash and Slag Based Geopolymer Concrete, *Adv. Concr. Constr.*, **6**. https://doi.org/10.12989/acc.2018.6.4.345.

[44] Zhang, P., Zheng, Y., Wang, K., Zhang, J. (2018). A Review on Properties of Fresh and Hardened Geopolymer Mortar, *Compos. Part B Eng.*, **152**, 79–95.

[45] Khaloo, A., Raisi, E. M., Hosseini, P., Tahsiri, H. (2014). Mechanical Performance of Self-Compacting Concrete Reinforced with Steel Fibers, *Construction and Building Materials*, **51**, 179–186. https://doi.org/10.1016/j.conbuildmat.2013.10.054.

[46] Alzeebaree, R., Çevik, A., Nematollahi, B., Sanjayan, J., Mohammedameen, A., Gülşan, M. E. (2019). Mechanical Properties and Durability of Unconfined and Confined Geopolymer Concrete with Fiber Reinforced Polymers Exposed To Sulfuric Acid, *Construction and Building Materials*, **215**, https://doi.org/10.1016/j.conbuildmat.2019.04.165.

[47] Aleem, M. I. A., Arumairaj, P. D. (2012). Optimum Mix For The Geopolymer Concrete, *Indian Journal of Science and Technology*, **5**, No. 3, 2299-2301, DOI: 10.17485/ijst/2012/v5i3.8.

[48] Tuyan, M., Yılmaz, G., Çakır, Ö. A. Süper akışkanlaştırıcıların Kendiliğinden Yerleşen Betonun Taze Hal ve Sertleşmiş Özelikleri ile Maliyetine Etkisi, *Yapılarda Kimyasal Katkılar 4. Sempozyum ve Sergisi,* 24-25 Ekim 2013, Milli Kütüphane, Ankara, pp. 17-32.

[49] Çitoğlu, G. S., Bayraktar, O. Y., Çağlar, A., Çağlar, H. (2017). Süper Akışkanlaştırıcı Katkıların Beton Basınç Dayanımına Etkileri, *1st International Turkish World Engineering and Science Congress in Antalya.*

[50] Aydos Yapı Kimyasalları. *Süperakışkanlaştırıcı Beton Katkıları*, http://www.aydos.com.tr/sayfa/sektorel-cozumler-detay/7/superakiskanlastirici-beton-katkilari-en-934-2-cizelge-3_1-3_2

[51] Türkel, S., Felekoğlu, B. (2004). Aşırı Dozda Akışkanlaştırıcı Kimyasal Katkı Kullanımının Taze ve Sertleşmiş Betonun Bazı Özellikleri Üzerine Etkileri, *Dokuz Eylül Üniversitesi Mühendislik Fakültesi Fen ve Mühendislik Dergisi*, Cilt 6 , Sayı 1, 77-89.

[52] GN İnşaat, *Süper Akışkanlaştırıcılar*. https://www.gninsaat.com.tr/super-akiskanlastiricilar

[53] Cecel, R. T., Abrão, P. C. R. A., Cardoso, F. A., John, V. M. (2019). Consumption of Superplasticizer Admixture For Different Cements and Their Binder Efficiency, *IBRACON Structures and Materials Journal,* **12**, Number 6, 1260-1287.

[54] EFNARC (2005), *The European Guidelines for Self-Compacting Concrete: Specification, Production and Use, Eur. Guidel. Self Compact. Concr*.

[55] Demie, S., Nuruddin, M. F., Shafiq, N. (2013). Effects of Micro-Structure Characteristics of Interfacial Transition Zone on The Compressive Strength of Self-Compacting Geopolymer Concrete, *Construction and Building Materials,* **41**, 91-98.

[56] Yazıcı H., *Beton Katkıları*. https://docplayer.biz.tr/4238014-Doc-dr-halit-yazici.html

[57] Ghezal, A., Khayat, K. H. (2002). Optimizing Self-Consolidating Concrete with Limestone Filler by Using Statistical Factorial Design Methods, *ACI Materials Journal,* **99**, 264–272.

[58] Khayat, K. H. (2000). Optimization and Performance of Air-Entrained, Self-Consolidating Concrete, *ACI Materials Journal,* **97**, 526–535.

[59] Khayat, K. H., Paultre, P., Tremblay, S. (2001). Structural Performance and In-Place Properties of Self-Consolidating Concrete Used for Casting Highly Reinforced Columns, *ACI Materials Journal*, **98**, 371–378.

[60] Felekoglu, B., Turkel, S., Baradan, B. (2007). Effect of Water/Cement Ratio on The Fresh and Hardened Properties of Self-Compacting Concrete, *Building and Environment,* **42**, 1795–1802, https://doi.org/10.1016/j.buildenv.2006.01.012.

[61] Ferraris, C. F., Brower, L., Ozyildirim, C., Daczko, J. (2000). Workability of Self-Compacting Concrete, *The Economical Solution for Durable Bridges and Transportation Structures*, International Symposium on High Performance Concrete. PCI/FHWA/FIB. September 25-27, 2000, Orlando, Florida, 398-407, 2000.

[62] Selvi, M. T., Thandavamoorthy, T. S. (2014). Mechanical and durability properties of steel and polypropylene fibre reinforced concrete, *International Journal of Earth Sciences and Engineering*, **7**, 696–703.

[63] Gencel, O., Brostow, W., Datashvili, T. Thedford M., (2011). Workability and Mechanical Performance of Steel Fiber-Reinforced Self-Compacting Concrete with Fly Ash Workability and Mechanical Performance of Steel Concrete with Fly Ash, *Composite Interfaces*, **18**, 169–184. https://doi.org/10.1163/092764411X567567.

[64] Frazão, C., Camões, A., Barros, J., Gonçalves, D. (2015). Durability of Steel Fiber Reinforced Self-Compacting Concrete, *Construction and Building Materials*, **80**,155–166. https://doi.org/10.1016/j.conbuildmat.2015.01.061.

[65] Memon, F. A., Nuruddin, M. F., Demie, S., Shafiq, N. (2011). Effect of Curing Conditions on Strength of Fly Ash-Based Self-Compacting Geopolymer Concrete, *Int. J. Civ. Environ. Eng*., **3**, 183–186.

[66] Ahmed, M. F., Nuruddin, M. F., Shafiq, N. (2011). Compressive Strength and Workability Characteristics of Low-Calcium Fly ash-based Self-Compacting Geopolymer Concrete, *Int. J. Civil, Environ. Struct. Constr. Archit. Eng.*, **5**, 64–70.

[67] Noushini, A., Castel, A. (2016). The Effect of Heat-Curing on Transport Properties of Low-Calcium Fly Ash-Based Geopolymer Concrete, *Construction and Building Materials*, **112**, 464–477. https://doi.org/10.1016/j.conbuildmat.2016.02.210

[68] Prisco, M. D., Felicetti, R., Iorio, F., Gettu, R. (2001). On The Identification of SFRC Tensile Constitutive Behaviour, *Fract. Mech. Concr. Struct*. AA Balkema Publ. Rotterdam, 541–548.

[69] Arslan, K. M. (2014). *Sülfat Etkisine Maruz Kalmış Mineral ve Nano Katkılı Harçların Durabilitesi*, Yüksek Lisans Tezi, İstanbul Teknik Üniversitesi, Fen Bilimleri Enstitüsü, İnşaat Mühendisliği Anabilim Dalı, Yapı Mühendisliği Programı, İstanbul.

[70] Ibrahim, K. I. M., Al-Tersawy, S. H. (2019). The Hybrid Effect of Micro and Nano Silica on the Properties of Normal and High Strength Concrete,

IOSR Journal of Mechanical and Civil Engineering (IOSR-JMCE), **14**, Issue 4 Ver. VI, 62-72.

[71] Tao, J. (2005). Preliminary Study on the Water Permeability and Microstructure of Concrete Incorporating Nano-SiO_2, *Cement and Concrete Research*, **35**, Issue 10, 1943-1947.

[72] Yu, R., Spiesz, P., Brouwers, H. J. H. (2014). Effect of Nano-Silica on The Hydration and Microstructure Development of Ultra-High Performance Concrete (UHPC) with a Low Binder Amount, *Construction and Building Materials,* **65**, 140-150.

[73] Alibaba, https://www.exportersindia.com/sri-shakthi-minerals/nano-silica-4532342.htm

[74] Sobolev, K., Flores, I., Hermosill,o R., Martinez, L. M. T. (2006). Nanomaterials And Nanotechnology For High-Performance Cement Composites, *Proc. ACI Sess. Nanotechnol. Concr. Recent Dev. Futur. Perspect*. 91–118.

[75] Qing, Y., Zenan, Z., Deyu, K., Rongshen, C. (2007). Influence of Nano-SiO_2 Addition on Properties of Hardened Cement Paste as Compared with Silica Fume, *Constr. Build. Mater*., **21**, 539–545.

[76] Li, H., Xiao, H., Yuan, J., Ou, J. (2004). Microstructure of Cement Mortar with Nano-Particles, *Compos. Part B Eng.*, **35**, 185–189.

[77] Çevik, A., Alzeebaree, R., Humur, G., Niş, A., Gülşan, M. E. (2018). Effect of Nano-Silica on The Chemical Durability and Mechanical Performance of Fly Ash Based Geopolymer Concrete, *Ceram. Int.* https://doi.org/10.1016/j.ceramint.2018.04.009.

[78] Senff, L., Labrincha, J. A., Ferreira, V. M., Hotza, D., Repette, W .L. (2009). Effect of Nano-Silica on Rheology and Fresh Properties of Cement Pastes And Mortars, *Constr. Build. Mater.*, **23**, 2487–2491.

[79] Görhan, G., Aslaner, R., Sinik, O. (2016). The Effect of Curing on the Properties of Metakaolin and Fly Ash-Based Geopolymer Paste, *Compos. Part B Eng.*, **97**, 329–335.

[80] Alzeebaree, R., Gülşan, M. E., Niş, A., Mohammedameen, A., Çevik, A. (2018). Performance of FRP Confined and Unconfined Geopolymer Concrete Exposed To Sulfate Attacks, *Steel Compos. Struct.*, **29**. https://doi.org/10.12989/scs.2018.29.2.201.

[81] Belkowitz, J. S., Armentrout, D. (2009). An Investigation of Nano-Silica In The Cement Hydration Process, *Masters Abstr. Int.*

[82] Quercia, G., Brouwers, H. J. H. (2010). Application of Nano-Silica (NS) in Concrete Mixtures, *8th Fib PhD Symp. Kgs.*

[83] Alzeebaree, R., Çevik, A., Mohammedameen, A., Niş, A., Gülşan, M. E. (2019). Mechanical Performance of FRP Confined Geopolymer Concrete Under Seawater Attack, *Advances in Structural Engineering*. https://doi.org/10.1177/1369433219886964.

[84] Aydöner, T. (2002*). Çelik Tel Takviyeli Betonların Mekanik Davranışı*, İstanbul Teknik Üniversitesi, Fen Bilimleri Enstitüsü, İnşaat Mühendisliği Anabilim Dalı, Yapı Mühendisliği Programı, İstanbul.

[85] Arslan, M. H., Doğan, G., Dabanlı, K., Özdemir, M., Divarcı, H. (2015). Beton İçinde Çelik Tel Kullanarak Betonarme Binaların Deprem Performansının Artırılması, *S.Ü. Müh. Bilim ve Tekn. Derg*., c.3, s.1.

[86] Beton Fiber, *Çelik Fiber Donatılar*, https://www.yapikatalogu.com/Files/Products/2989/file-24700.pdf

[87] Gordion Beton, https://gordionbeton.com.tr/?page_id=465

[88] Tavakoli, H. R., Omran, O. L., Shiade, M. F., Kutanaei, S. S. (2014). Prediction of Combined Effects of Fibers And Nanosilica on The Mechanical Properties of Self-Compacting Concrete Using Artificial

Neural Network, *Latin American Journal of Solids and Structures,* **11**, 1906-1923.

[89] Marar, K., Eren, Ö., Çelik, T. (2001). Relationship Between Impact Energy and Compression Toughness Energy of High-Strength Fiber-Reinforced Concrete, *Mater. Lett.,* **47**, 297–304**.**

[90] Daniel, L., Loukili, A. (2002). Behavior of High Strength Fiber-Reinforced Concrete Beams Under Cyclic Loading, *Structural Journal*, **99**, 248-256.

[91] Song, P. S., Hwang, S. (2004). Mechanical Properties of High-Strength Steel Fiber-Reinforced Concrete, *Constr.Build. Mater.,* **18**, 669–673.

[92] Swamy, R. N., Stavrides, H. (1979). Influence of Fiber Reinforcement on Restrained Shrinkage and Cracking, *Journal Proceedings*, **76**, 443–460.

[93] Grzybowski, M., Shah, S. P. (1990). Shrinkage Cracking of Fiber Reinforced Concrete, *Materials Journal,* **87**, 138–148.

[94] Gencel, O., Brostow, W., Datashvili, T., Thedford, M. (2011). Workability and Mechanical Performance of Steel Fiber-Reinforced Self-Compacting Concrete With Fly Ash, *Composite Interfaces,* **18**, 169–184. https://doi.org/10.1163/092764411X567567.

[95] Gülşan, M. E., Alzeebaree, R., Rasheed, A. A., Niş, A., Kurtoğlu, A. E. (2019). Development of Fly Ash/Slag Based Self-Compacting Geopolymer Concrete Using Nano-Silica and Steel Fiber, *Constr. Build. Mater.,* **211**, 271-283. https://doi.org/10.1016/j.conbuildmat.2019.03.228

[96] Day, K. E., Holtze, K. E., Metcalfe-Smith, J. L., Bishop, C. T., Dutka, B. J. (1993). Toxicity of Leachate From Automobile Tires To Aquatic Biota. *Chemosphere,* **27(4)**, 665-675.

[97] Chen, S. J., Su, H. B., Chang, J. E., Lee, W. J., Huang, K. L., Hsieh, L. T., Lin, C. C. (2007). Emissions of Polycyclic Aromatic Hydrocarbons

(PAHs) From The Pyrolysis of Scrap Tires, *Atmospheric Environment*, **41(6)**, 1209-1220.

[98] Pacheco-Torgal, F., Ding, Y., Jalali, S. (2012). Properties and Durability of Concrete Containing Polymeric Wastes (Tyre Rubber And Polyethylene Terephthalate Bottles), *Construction and Building Materials*, **30**, 714-724.

[99] Wang, Q. Z., Wang, N. N., Tseng, M. L., Huang, Y. M., Li, N. L. (2020). Waste Tire Recycling Assessment: Road Application Potential and Carbon Emissions Reduction Analysis of Crumb Rubber Modified Asphalt in China, *Journal of Cleaner Production*, **249**, 119411.

[100] Chan, C. W., Yu, T., Zhang, S. S., Xu, Q. F. (2019). Compressive Behaviour of FRP-Confined Rubber Concrete, *Construction and Building Materials*, **211**, 416-426.

[101] Topçu, I. B., Avcular, N. (1997). Collision Behaviours of Rubberized Concrete, *Cement and Concrete Research*, **27(12)**, 1893-1898.

[102] Liu, F., Chen, G., Li, L., Guo, Y. (2012). Study of Impact Performance of Rubber Reinforced Concrete, *Construction and Building Materials*, **36**, 604-616.

[103] Gholampour, A., Ozbakkaloglu, T., Hassanl,i R. (2017). Behavior of Rubberized Concrete Under Active Confinement, *Construction and Building Materials*, **138**, 372-382.

[104] Aslani, F., Ma, G., Wan, D. L. Y., Le, V. X. T. (2018). Experimental Investigation into Rubber Granules and Their Effects on The Fresh and Hardened Properties of Self-Compacting Concrete, *Journal of Cleaner Production*, **172**, 1835-1847.

[105] Ganjian, E., Khorami, M., Maghsoudi, A.A. (2009). Scrap-Tyre-Rubber Replacement For Aggregate and Filler in Concrete. *Construction and Building Materials*, **23(5)**, 1828-1836.

[106] Emiroğlu M., (2006). *Atık Taşıt Lastiğin Beton İçerisinde Kullanımı ve Betonun Karakteristiklerine Etkisi,* Yüksek Lisans Tezi, T.C. Fırat Üniversitesi, Fen Bilimleri Enstitüsü, Yapı Eğitimi Anabilim Dalı, Elazığ.

[107] Najim K.B., Hall M.R.,(2010). A Review of The Fresh/Hardened Properties and Applications For Plain-(PRC) and Self-Compacting Rubberized Concrete (SCRC), *Construction and Building Materials* **24(11)**, 2043–2051.

[108] https://dir.indiamart.com/search.mp?ss=crumb+rubber&src=as-popular%3Akwd%3Dcrumb%3Apos%3D2%3Acat%3D-2%3Amcat%3D-2&prdsrc=1&countryiso=TR

[109] Engin Y., (2014). *Yüksek Fırın Curüfü,* http://www.betonvecimento.com/surdurulebilirlik/yuksek-firin-curufu-ozet

[110] https://insapedia.com/yuksek-firin-curufu/

[111] Ün, H. (2007). *Taze ve Sertleşmiş Beton Deneyleri*, https://www.yumpu.com/tr/document/read/6734883/taze-ve-sertlesmis-beton-deneyleri-yrd-doc-dr-hayri-

[112] Üç Nokta Eğme Testi Deneyi, (2017). http://cdn.hitit.edu.tr/mf/files/39932_1703231357926.pdf

[113] Çapik M., Kaya S., (2015). Eğilme (Bükülme) Dayanımı. http://www.ktu.edu.tr/dosyalar/maden_263ff.pdf

[114] https://theconstructor.org/concrete/determination-modulus-elasticity-concrete/2119/

[115] Yüce, İ., (2007). *Dairesel Kompozit Tabakalarda Düşük Hızlı Darbe Hasarının İncelenmesi*, Yüksek Lisans Tezi, T.C. Selçuk Üniversitesi Fen Bilimleri Enstitüsü, Makina Mühendisliği Anabilim Dalı.

[116] Ceyhun, V., Turan, M. (2003). Tabakalı Kompozit Malzemelerin Darbe Davranışı, *Mühendis ve Makine Dergisi***.**

[117] Oltulu, M., Altun, M. G. (2018). Betonun Darbe Dayanımının Tespitinde Ağırlık Düşürme Deney Yöntemi ve Yapılan Çalışmalar, *Gümüşhane Üniversitesi Fen Bilimleri Enstitüsü Dergisi,* Cilt 8, Sayı 1, 155-163.

[118] Düşen Ağırlık Darbe Testi Föyü, *Bursa Teknik Üniversitesi, Makine Müh.Böl*.http://depo.btu.edu.tr/dosyalar/makine/Dosyalar/Darbe%20Testi%20Deney%20F%C3%B6y%C3%BC%281%29.pdf

[119] Darbe Deney Cihazı, *Utest Malzeme Test Cihazları* http://www.utest.com.tr/tr/20824/Darbe-Deney-Cihazi

[120] Çeltik Darbe Deneyi, *Bartın Üniversitesi.* https://cdn.bartin.edu.tr/makine/68df7d9c9f6ecb4700d81de4ba2b2163/darbedeneyleri.pdf

[121] Xin-Hua, C., Zhen, H.,Wen, L. (2014). Experimental study on Impact Resistance of PVA Fiber Reinforced Cement-based Composite, *Applied Mechanics and Materials*, Vols. 584-586,1630-1634.

[122] Yük-Hücresi, *Vikipedi.* https://tr.wikipedia.org/wiki/Y%C3%BCk_h%C3%BCcresi

[123] İvme-Ölçer, *Elektirik Port.* https://www.elektrikport.com/teknik-kutuphane/ivmeolcer-nedir-nasil-calisir/12216#ad-image-0

[124] Beton İçin Yüksek Oranda Su Azaltıcı Katkı Maddesi, *Basf, MasterGlenium-RMC303*.https://assets.master-builders-solutions.com/en-tr/eng_masterglenium-rmc%20303-tds_r1.pdf

[125] Aleem, M. I. A. and Arumairaj, P. D. (2012). Optimum Mix For The Geopolymer Concrete, *Indian Journal of Science and Technology*, **5**, No. 3, ISSN: 0974- 6846, 2299-2301.

[126] Memon, F. A., Nuruddin, M. F., Khan, S., Shafiq, N., Ayub, T. (2013). Effect of Sodium Hydroxide Concentration on Fresh Properties and Compressive Strength of Self-Compacting Geopolymer Concrete, *Journal of Engineering Science and Technology,* **8(1)**, 44-56.

[127] Olivia, M., Nikraz, H. (2012). Properties of Fly Ash Geopolymer Concrete Designed By Taguchi Method, *Materials and Design,* **36**, 191-198.

[128] NaOH-Sodyum Hidroksit, *Aker Kimya.* https://akerkimya.com.tr/details/14/206/sodyum-hidroksit

[129] Akcay, B., Tasdemir, M. A. (2009). Optimisation of Using Lightweight Aggregates in Mitigating Autogenous Deformation of Concrete, *Construction and Building Materials,* **23(1)**, 353-363

[130] Islam, A., Alengaram, U. J., Jumaat, M. Z., Ghazali, N. B., Yusoff, S., Bashar, I. I. (2017). Influence of Steel Fibers on the Mechanical Properties and Impact Resistance of Lightweight Geopolymer Concrete, *Construction and Building Materials,* **152**, 964-977

[131] PCB Piezotronics, https://www.pcb.com/

[132] http://www.ateksensor.com/content/img/LTR/DS_LTR_002_LTR_Datasheet__EN_.pdf

[133] https://www.alfasanayi.com/content/img/EPA/EPA100_TechnicalDocument_ENG.pdf

[134] https://www.ni.com/pdf/manuals/374829a_02.pdf

[135] B. 12350-8 EN, (2010). Testing Self Compacting Concrete: Slump Flow Test, *Br. Stand. Int.*.

[136] B. 12350-9 EN, (2010). Testing Self Compacting Concrete: V-Funnel Test, *Br. Stand. Int.*

[137] B. 12350-10 EN, (2010). Testing Self Compacting Concrete: L-Box Test, *Br. Stand. Int.*

[138] Ismail, M. K., Hassan, A. A. (2016). Use of Metakaolin on Enhancing The Mechanical Properties of Self-Consolidating Concrete Containing High Percentages of Crumb Rubber, *Journal of Cleaner Production*, **125**, 282-295.

[139] Niş, A. (2018). Mechanical Properties of Steel Fiber Reinforced Self-Compacting Concrete. *International Journal of Engineering Technologies*, **4(1)**, 33-40.

[140] Niş, A., Özyurt, N., Özturan, T. (2020). Variation of Flexural Performance Parameters Depending on Specimen Size and Fiber Properties, *Journal of Materials in Civil Engineering*, **32(4)**, 04020054.

[141] Ghanbari, A., Karihaloo, B. L. (2009). Prediction of The Plastic Viscosity of Self-Compacting Steel Fibre Reinforced Concrete, *Cement and Concrete Research*, **39(12)**, 1209-1216.

[142] Belkowitz, J. S., Belkowitz, W. L. B., Nawrocki, K., Fisher, F. T. (2015). Impact of Nanosilica Size and Surface Area on Concrete Properties, *ACI Mater. J.*, **112**, 419–427, https://doi.org/10.14359/51687397

[143] Nili, M., Afroughsabet, V. (2010). Combined Effect of Silica Fume and Steel Fibers on The Impact Resistance and Mechanical Properties of Concrete, *Int. J. Impact Eng.*, **37**, 879–886.

[144] Bayramov, F., Tasdemir, C., Tasdemir, M. A. (2004). Optimisation of Steel Fibre Reinforced Concretes By Means of Statistical Response Surface Method, *Cem. Concr. Compos*., **26**, 665–675.

[145] Mohammadi, Y., Singh, S. P., Kaushik, S. K. (2008). Properties of Steel Fibrous Concrete Containing Mixed Fibres in Fresh and Hardened State, *Constr. Build. Mater.*, **22**, 956–965.

[146] Yazıcı, S., İnan, G., Tabak, V. (2007). Effect of Aspect Ratio and Volume Fraction of Steel Fiber on The Mechanical Properties of SFRC, *Constr. Build. Mater.*, **21**, 1250–1253.

[147] Wang, Y., Li, V. C., Backer, S. (1990). Experimental Determination of Tensile Behavior of Fiber, *ACI Mater. J.* 87.

[148] Campione, G., Cucchiara, C., La, Mendola L., Papia, M. (2005). Steel-Concrete Bond in Lightweight Fiber Reinforced Concrete Under Monotonic and Cyclic Actions, *Eng. Struct.*, **27**, 881–890.

[149] Chen, B., Liu, J. (2004). Properties of Lightweight Expanded Polystyrene Concrete Reinforced with Steel Fiber, *Cem. Concr. Res.*, **34**, 1259–1263.

[150] Somna, K., Bumrongjaroen, W. (2011). Effect of External and Internal Calcium in Fly Ash on Geopolymer Formation, *Dev. Strateg. Mater. Comput. Des. II Ceram. Eng. Sci. Proceedings*, **32**, 1–16.

[151] Kayalı, O., Haque, M. N., Zhu, B. (2003). Some Characteristics of High Strength Fiber Reinforced Lightweight Aggregate Concrete, *Cem. Concr. Compos.*, **25**, 207–213.

[152] Nanni, A. (1988). Splitting-Tension Test For Fiber Reinforced Concrete, *ACI Mater. J.*, **85**, 229–233.

[153] Wardhono, A., Gunasekara, C., Law, D. W., Setunge, S. (2017). Comparison of Long Term Performance Between Alkali Activated Slag and Fly Ash Geopolymer Concretes, *Construction and Building Materials*, **143**, 272-279.

[154] Lee, N. K., Jang, J. G., Lee, H. K. (2014). Shrinkage Characteristics of Alkali-Activated Fly Ash/Slag Paste and Mortar at Early Ages, *Cement and Concrete Composites*, **53**, 239-248.

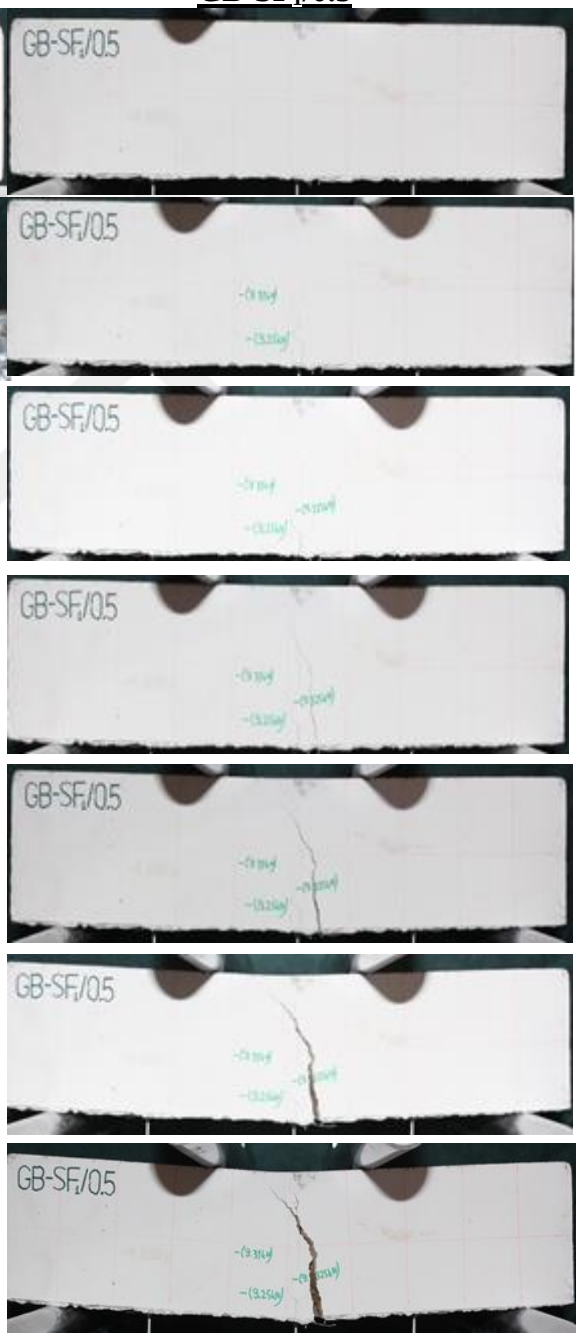
APPENDIX-1

CRACK PROPOGATION

1) CRACK PROPOGATION OF THE FLEXURAL STRENGTH TESTS

GB **GB-SF$_1$/0.5**





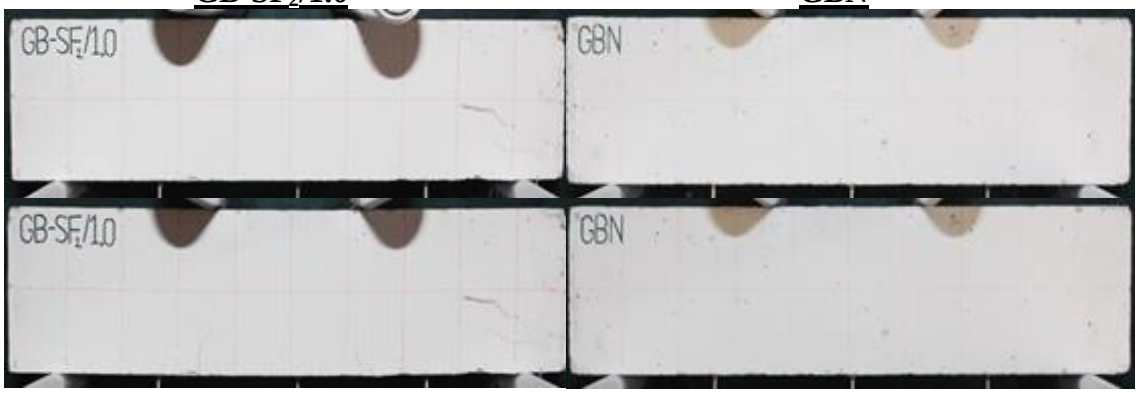


GB-SF$_1$/1.0 **GB-SF$_2$/0.5**




GB-SF1/1.0
GB-SF1/0.5
GB-SF1/1.0
GB-SF1/0.5
GB-SF1/1.0
GB-SF1/0.5
GB-SF1/1.0
GB-SF1/0.5
GB-SF1/1.0
GB-SF1/0.5
GB-SF1/1.0
GB-SF1/0.5
GB-SF1/1.0
GB-SF1/0.5

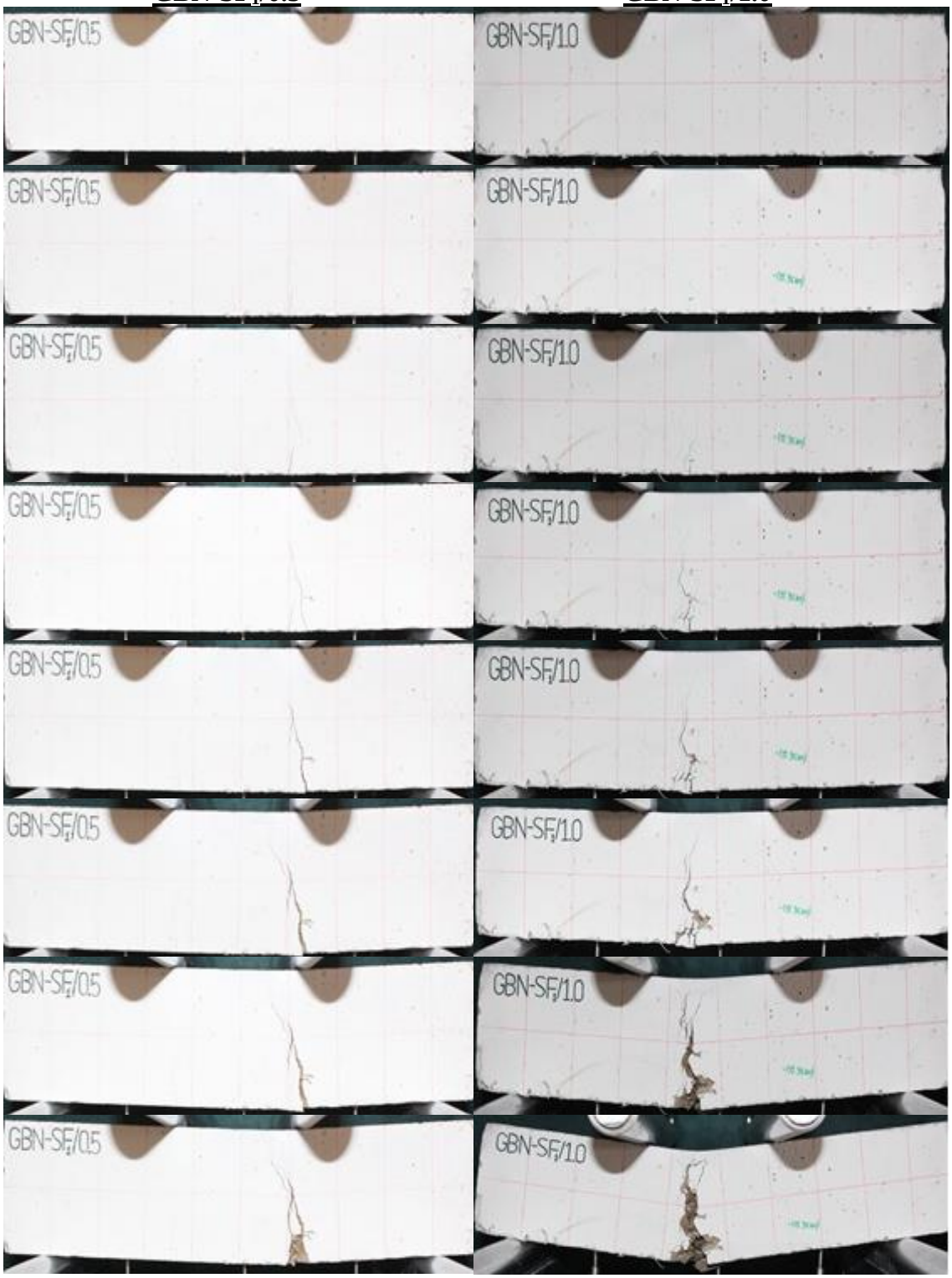
GB-SF$_2$/1.0 **GBN**

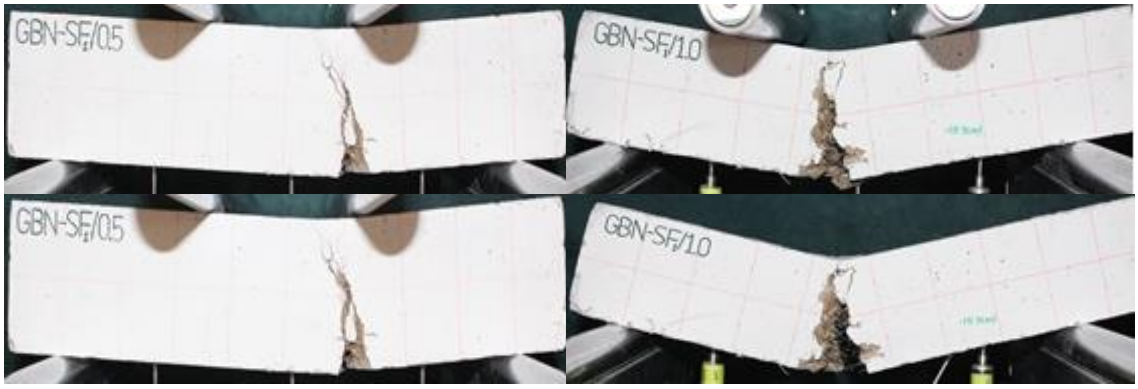

GB-SF1/1.0
GBN
GB-SF1/1.0
GBN


GB-SF2/1.0
GBN



GBN-SF$_1$/0.5 **GBN-SF$_1$/1.0**





GBN-SF$_2$/0.5 **GBN-SF$_2$/1.0**





GB-FCR/5.0-CCR/5.0 **GB-FCR/7.5-CCR/7.5**

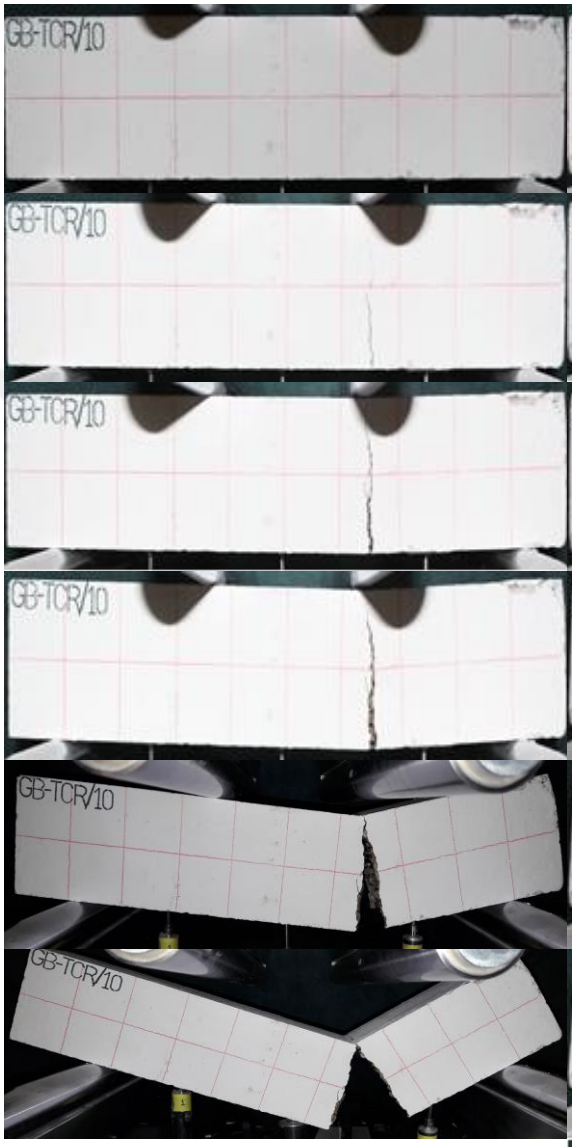


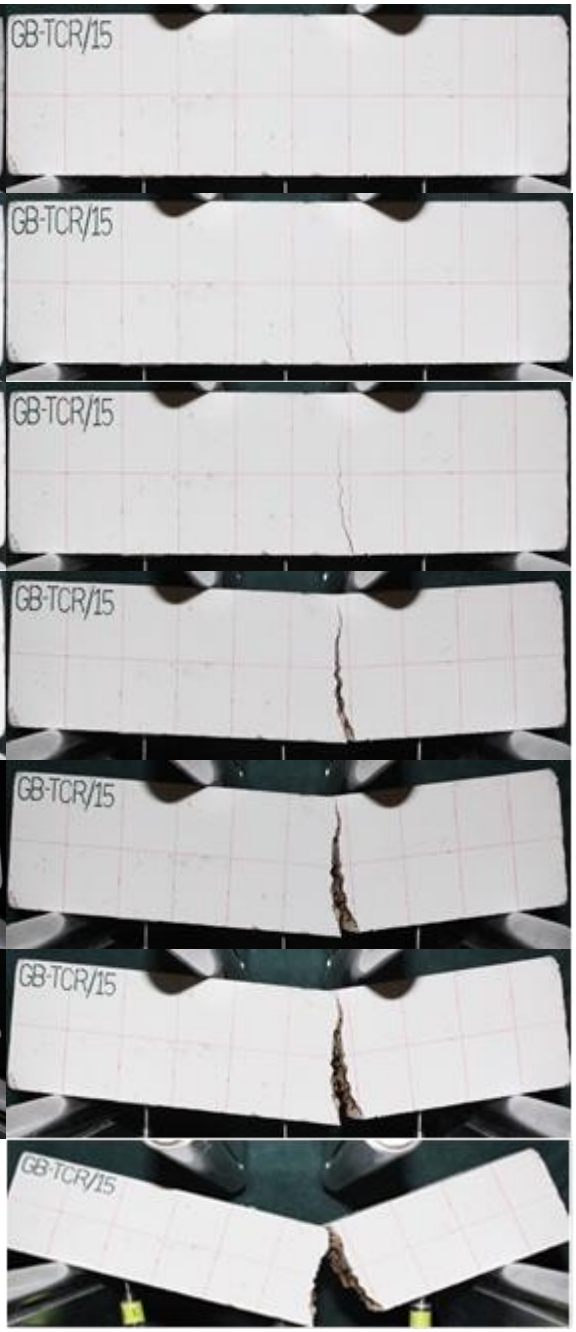


GB-TCR/10



GB-TCR/15





GB-SF$_1$/1.0-FCR/5.0-CCR/5.0

GB-SF$_1$/1.0-FCR/7.5-CCR/7.5









GB-SF$_1$/1.0-TCR/10 **GB-SF$_1$/1.0-TCR/15**



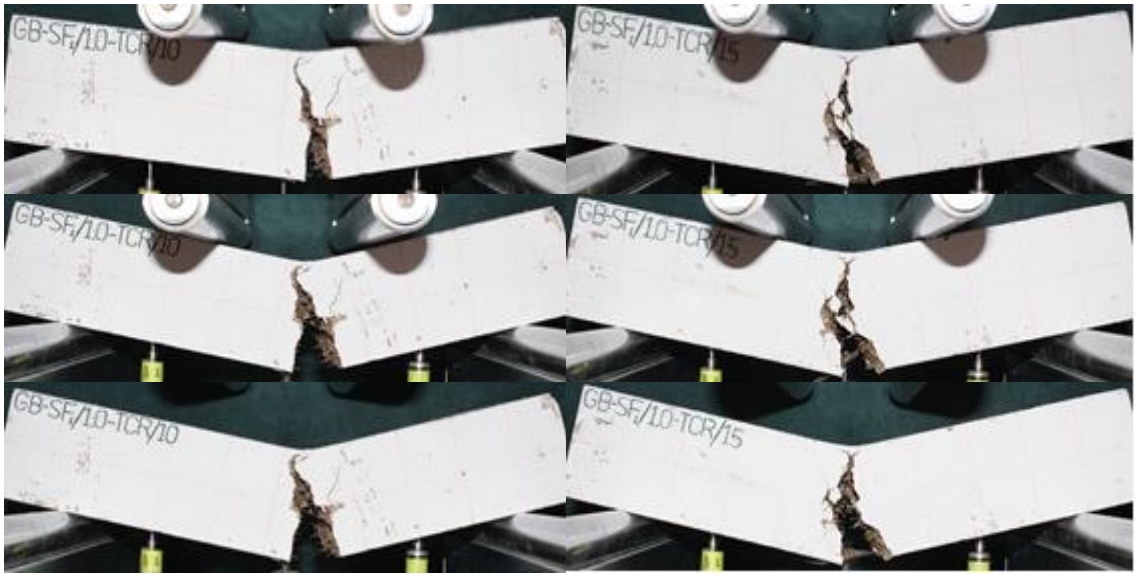
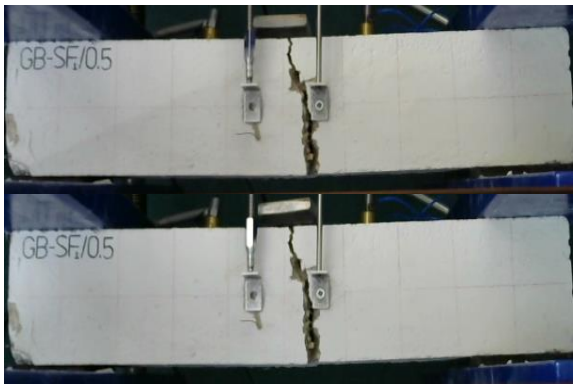


Figure A.1 Crack propogation of the flexural sstrength tests

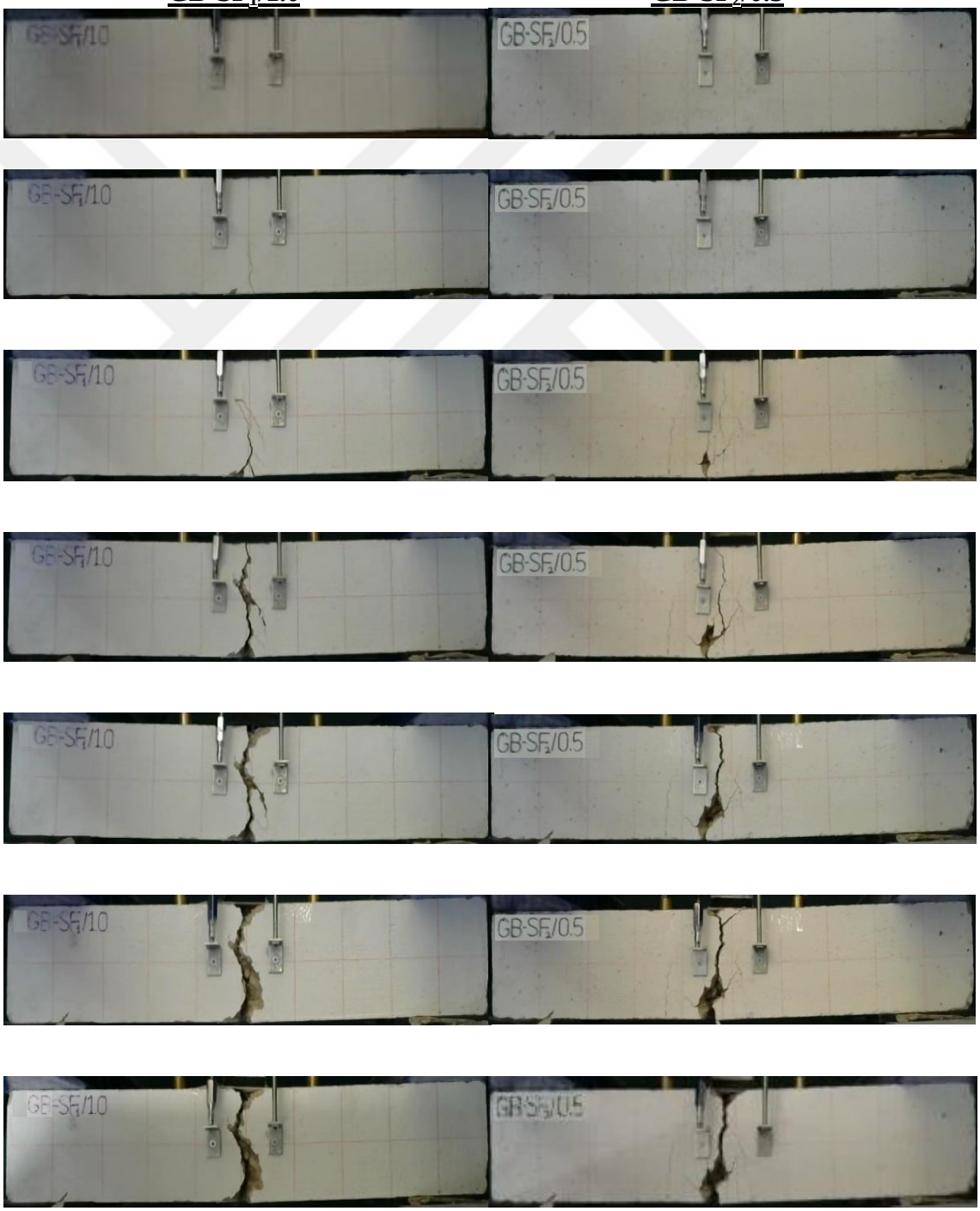
2) CRACK PROPOGATION DURING THE DROP-WEIGHT TESTS

GB **GB-SF_1/0.5**



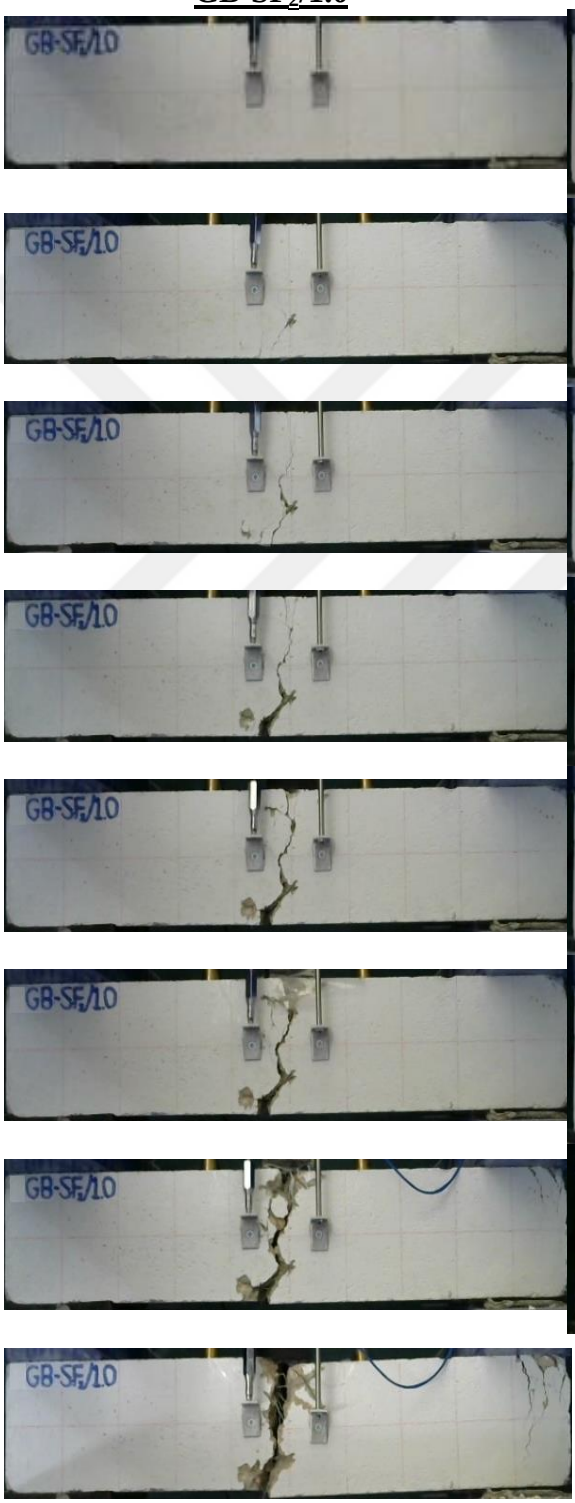


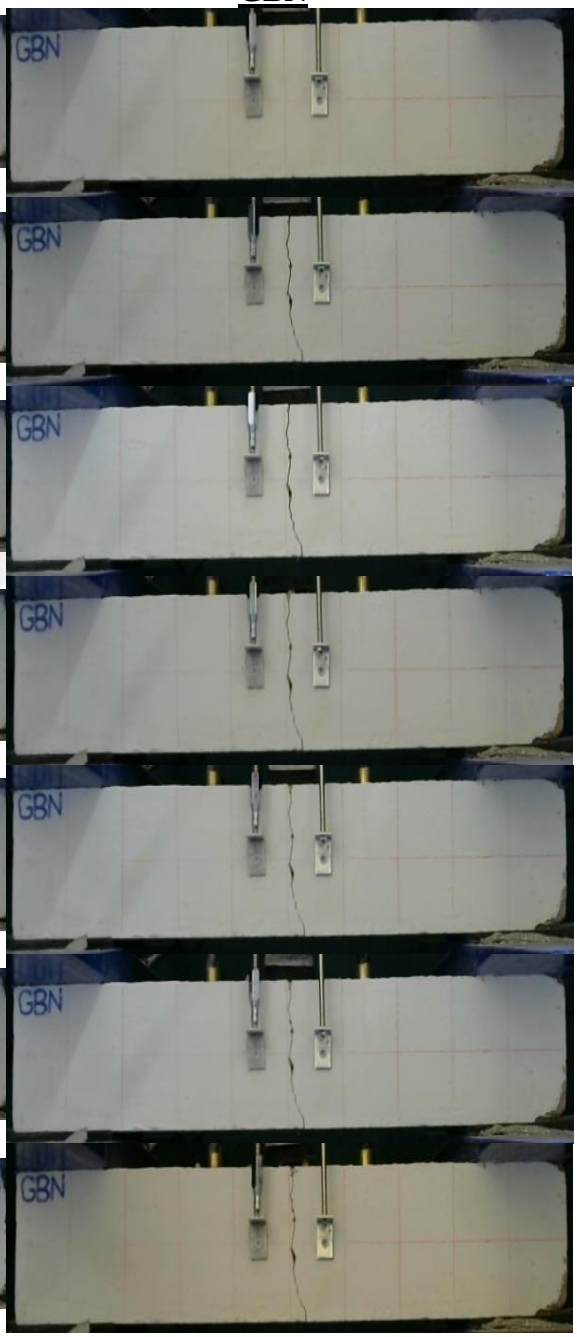
GB-SF$_1$/1.0 **GB-SF$_2$/0.5**



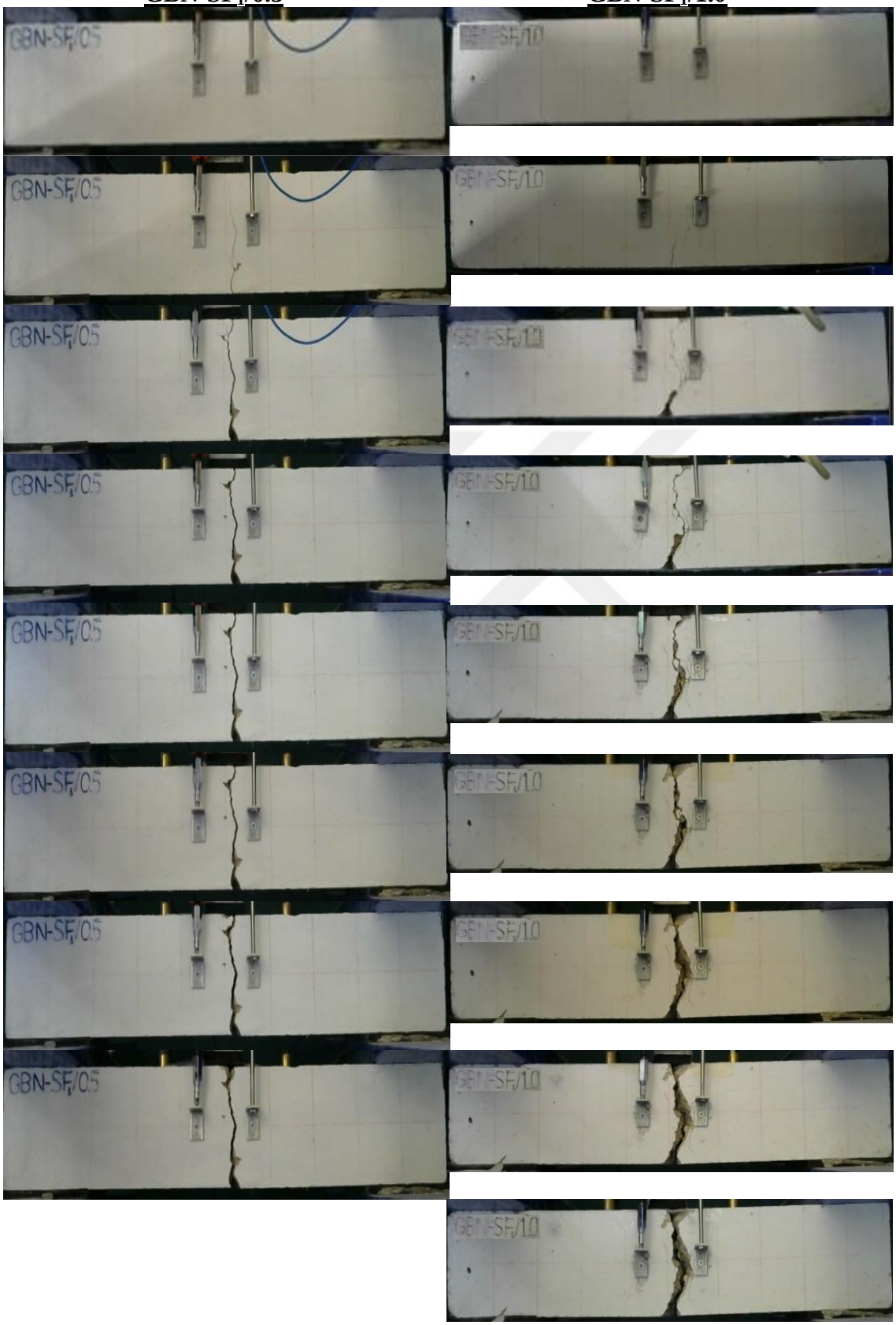


GB-SF$_2$/1.0 **GBN**

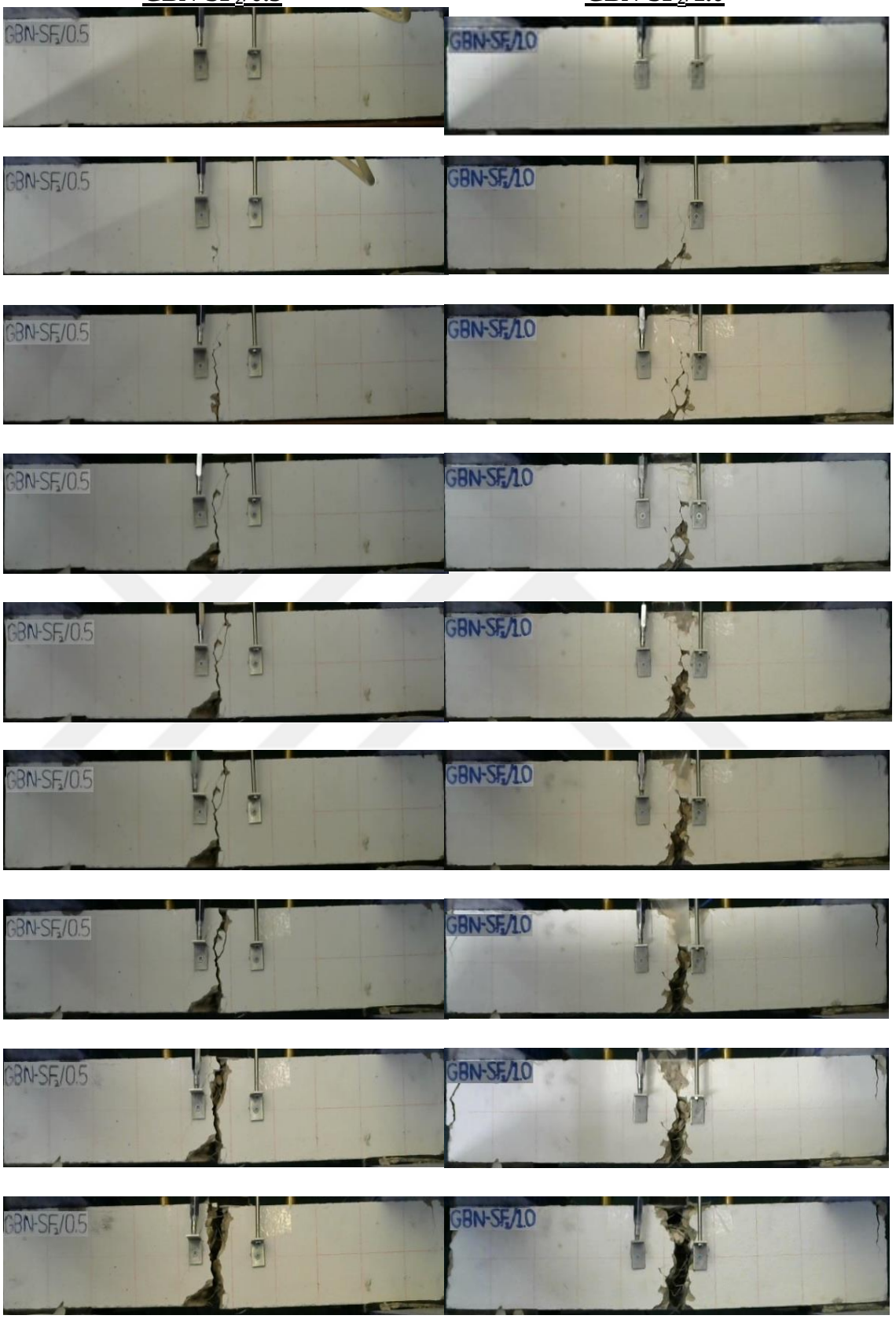




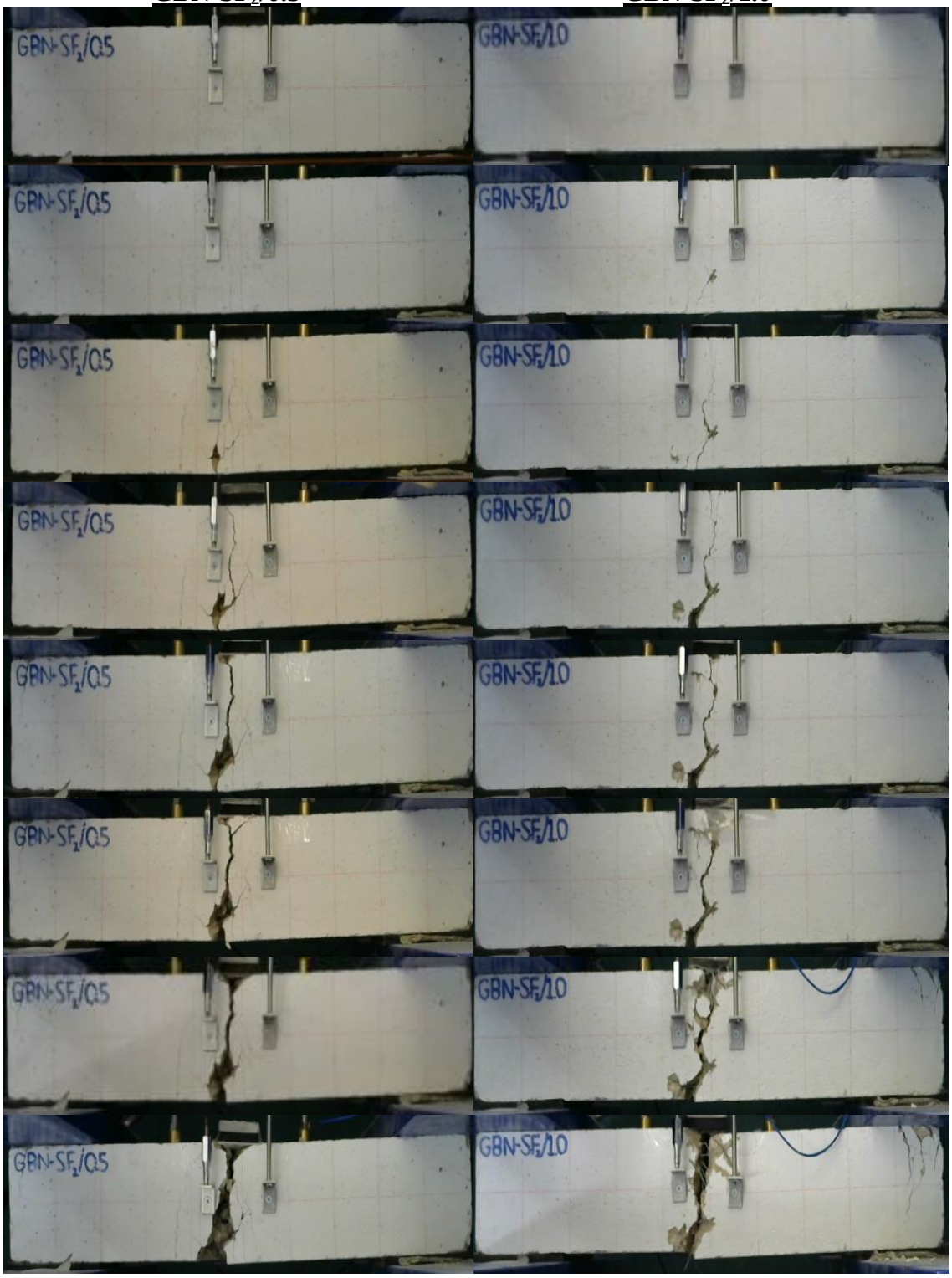
GBN-SF$_1$/0.5 **GBN-SF$_1$/1.0**



GBN-SF_2/0.5 **GBN-SF_2/1.0**

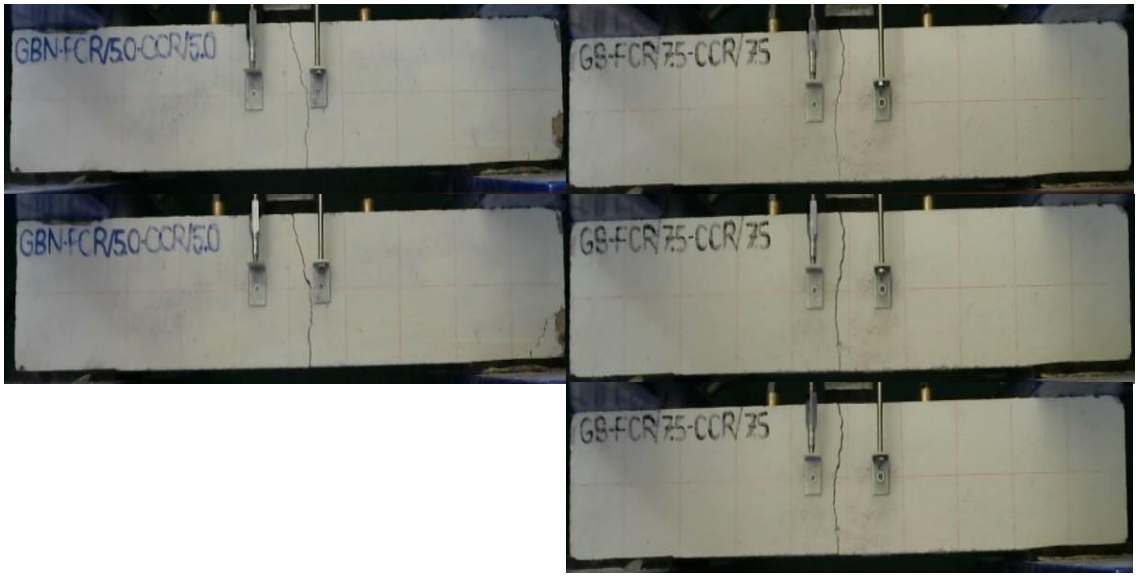


GBN-SF_2/0.5 **GBN-SF_2/1.0**

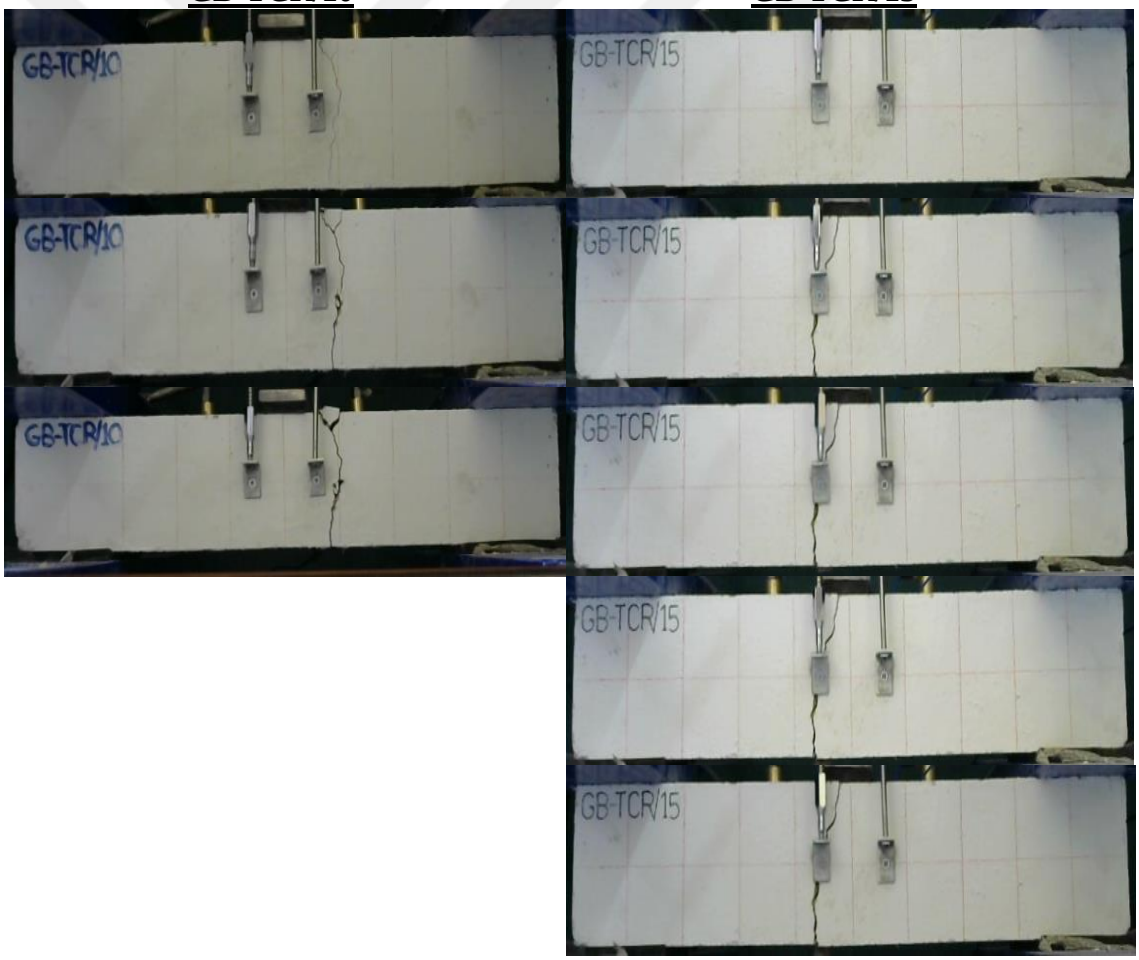


GB-FCR/5.0-CCR/5.0 **GB-FCR/7.5-CCR/7.5**

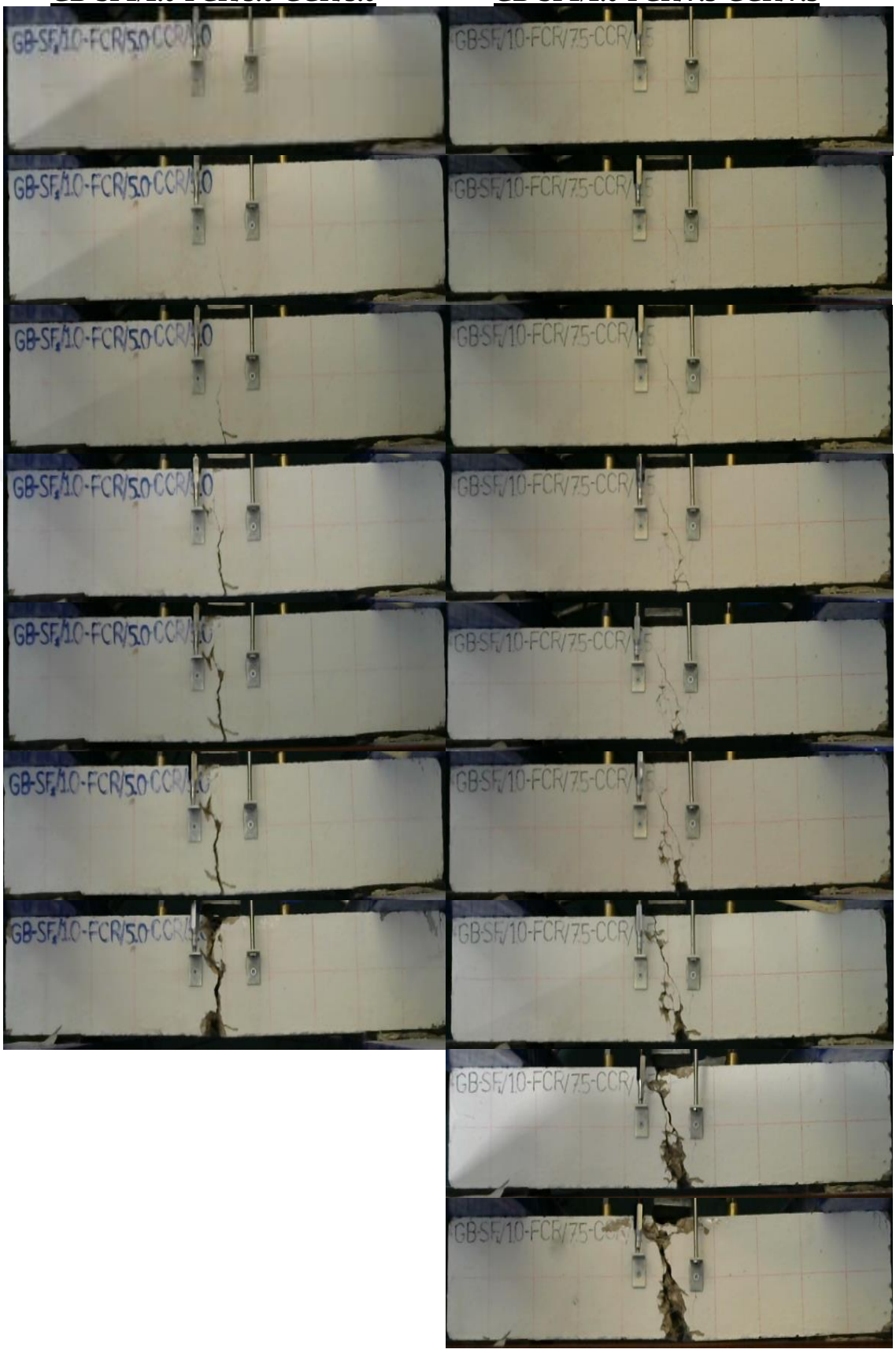




GB-TCR/10 **GB-TCR/15**



GB-SF1/1.0-FCR/5.0-CCR/5.0 **GB-SF1/1.0-FCR/7.5-CCR/7.5**



GB-SF1/1.0-TCR/10 **GB-SF1/1.0-TCR/15**

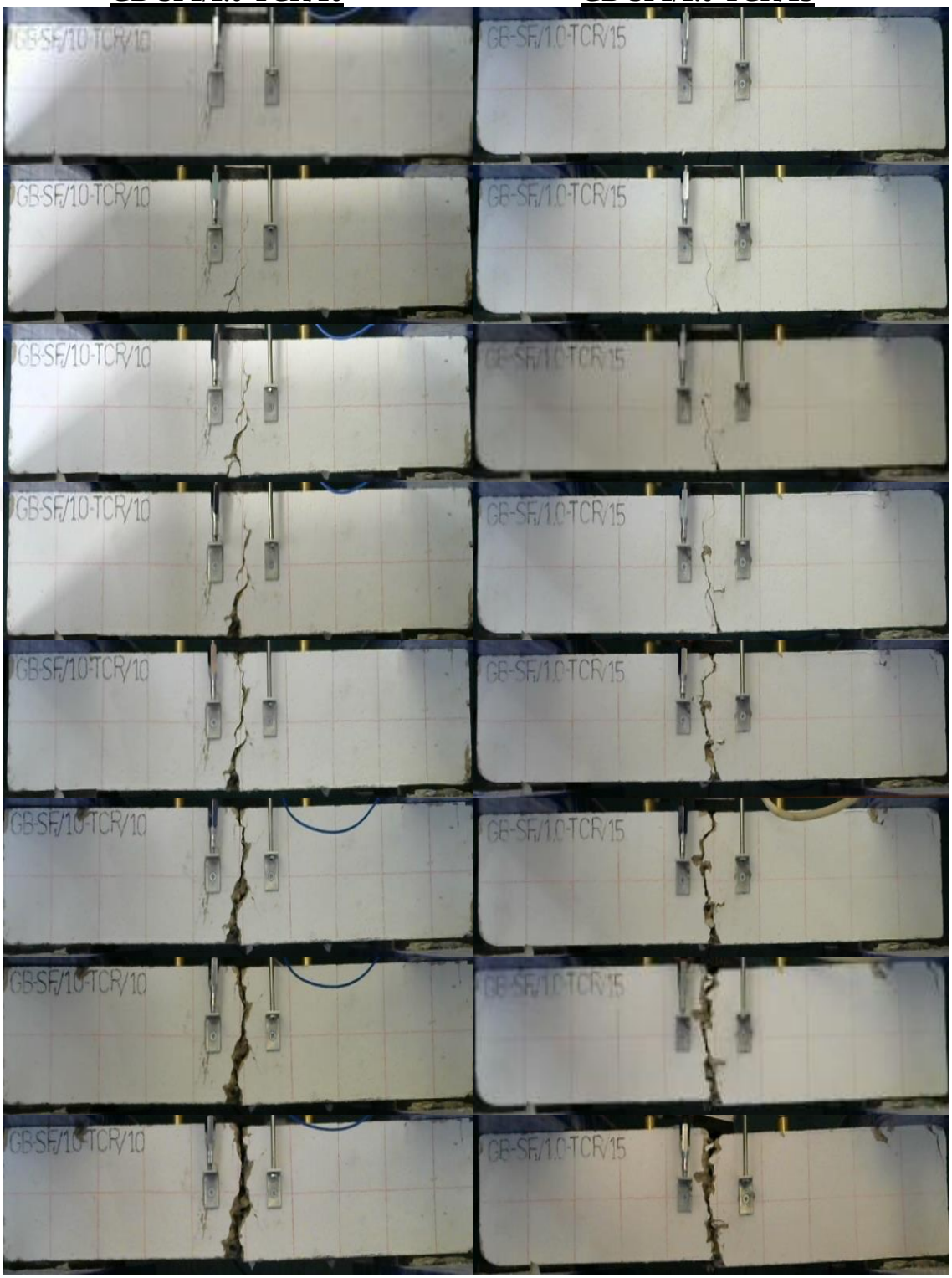


Figure A.2 Crack propogatıon durıng the drop-weıght tests

CURRICULUM VITAE
Necip Altay EREN

EDUCATION

PHD	**Civil Engineering, Gaziantep University**	
2016 – 2021	Thesis: Behavior of Geopolymer Concrete Under Impact	
Master	**Civil Engineering, University of Connecticut, USA**	2006 - 2008
University	**Civil Engineering, Gaziantep University**	1998 - 2002

WORK EXPERIENCE

Gaziantep University 02/2014 - Present

Academician

THESIS & PROJECTS

PHD Thesis: Behavior of Geopolymer Concrete Under Impact

PHD Project: Gaziantep University Scientific Research Project Goverining Unit (BAPYB).
Project Number: MF.DT.17.06
Geopolimer Betonların Çarpışma Davranışının İncelenmesi

PUBLICATIONS

The Effects of Recycled Tire Rubbers and Steel Fibers on the Performance of Self-compacting Alkali Activated Concrete, Periodica Polytechnica Civil Engineering, https://doi.org/10.3311/PPci.17601

PRESENTATIONS & CONFERENCES

- 4TH INTERNATIONAL ENERGY ENGINEERING CONGRESS, Gaziantep (2019)
- The International Conference of Materials and Engineering Technology (TICMET'20)

COMPUTER SKILLS

AutoCAD: Good
Word, Excel, Powerpoint: Excellent

LANGUAGE SKILLS

English Reading: Advanced, Writing: Advanced, Speaking: Good